# Charging and ion adsorption behaviour of different iron (hydr)oxides

Peter Venema

Promotor: dr. W.H. van Riemsdijk
hoogleraar in de bodemscheikunde en chemische grond en gewasanalyse

Peter Venema

# Charging and ion adsorption behaviour of different iron (hydr)oxides

**Proefschrift**
ter verkrijging van de graad van doctor
op gezag van de rector magnificus
van de Landbouwuniversiteit Wageningen
dr. C.M. Karssen
in het openbaar te verdedigen
op dinsdag 4 maart 1997
des namiddags te vier uur in de Aula

## Stellingen

1) Voor een veldsituatie kunnen verschillende ijzer (hydr)oxiden chemisch gezien op een hoop gegooid worden. (Dit proefschrift)

2) Het chemisch adsorptie gedrag van een mineraal kan in principe voorspeld worden op basis van zijn kristal struktuur en morfologie. (Dit proefschrift)

3) De waarde van 0.2 $F/m^2$ die wordt gebruikt voor de capaciteit van de buitenste Sternlaag van het Triple Layer Model is niet alleen fysisch onjuist, maar leidt ook tot onwaarschijnlijke waarden voor andere modelparameters. (Dit proefschrift)

4) Wageningers houden erg van natuur en milieu, mits het meer dan 3 uur vliegen is. (Naar Midas Dekkers, Fransen houden erg van de natuur mits goed klaargemaakt)

5) Van een AIO salaris kan men goed rondkomen, men zou zelfs kunnen concluderen dat niet AIO's worden onderbetaald maar dat anderen worden overbetaald.

6) Goede wetenschappelijk onderzoekers vertonen een gedrag dat sterk overeenkomt met dat van autisten.

7) De wereld gaat aan vlijt ten onder. (Titel boek Max Dendermonde)

8) Groen en links zijn moeilijk te verenigen. (Rijk van de schaarste, Hans Achterhuis).

9) Friezen ontdooien pas als het gaat vriezen. (Ruurd van der Made in een persoonlijk gesprek)

10) Ieder volk krijgt de milieuverontreiniging die het verdient

11) Het zou de verkeersveiligheid ten goede komen als auto's minder degelijk zouden zijn.

Stellingen behorende bij het proefschrift "Charging and adsorption behaviour of different iron (hydr)oxides". Peter Venema, 4 maart 1997.

## Abstract

Metal (hydr)oxides are of importance for many soil systems. All metal (hydr)oxides have a surface charge that varies with the pH. The variation in this surface charge is caused by adsorption and desorption of protons. The adsorption of cat- and anions on the metal (hydr)oxide surface is strongly influenced by their variable surface charge. The description of the charging behaviour of metal (hydr)oxides should therefore always be the starting point for modeling.

For the modeling of the chemical adsorption behaviour of metal (hydr)oxide surfaces, many different models are available. Five of these models were compared in their ability to describe an extended data set of cadmium adsorption on goethite (iron oxyhydroxide). None of the models could describe all data simultaneously. The best results were obtained with a surface complexation model, based on the MUlti SIte Complexation MUSIC approach of Hiemstra and van Riemsdijk.

A combination of a new interface model and the MUSIC model, the charge distribution (CD) MUSIC model is used for the description of cadmium adsorption on goethite. The CD-MUSIC model could give a good simultaneous description of an extended data set for cadmium adsorption on goethite. The same model, with adapted parameters, could describe extended adsorption data sets for adsorption on goethite in a system with only cadmium, phosphate and a mixture of these two ions.

The MUSIC model predicts proton affinities for individual surface groups of metal-(hydr)oxides. A refinement of the MUSIC model shows that the prediction of the proton affinities of both dissolved and surface groups can be understood in one theoretical framework. The application of the refined MUSIC model to different iron (hydr)oxides shows that the model can predict the charging behaviour very well. For a good prediction of the charging behaviour, the crystal structure and morphology of the oxide must be well known.

Finaly, a comparison is made of the charging behaviour and the cadmium and phosphate adsorption for three different goethites, lepidocrocite and hematite. The differences between the chemical behaviour of the different goethites could be modelled well with parameters which were consistent with the refined MUSIC model. The modelling of the behaviour of lepidocrocite and hematite was more problematic because the crystal morphologies were less well known.

## Voorwoord

Na langer afzien dan gepland (vijf in plaats van vier jaar) ligt hier dan het proefschrift. Het was een leuke tijd bij de vakgroep Bodemkunde en Plantenvoeding en ik heb er veel geleerd.

Via deze weg wil ik Debby Swinkels en Leonard Osté bedanken voor de prettige samenwerking met hen tijdens hun afstudeeropdracht. Leonard heeft zich later ontpopt tot een heel gezellige kamer/kantoorgenoot.

In het oude gebouw heb ik veel gewerkt op het lab met Theo Vens, van hem heb ik allerlei "oude analisten trucs" geleerd. In die tijd had ik een kantoortje in een donkere uithoek van het Scheikundegebouw, niet ver van Leon Vogels waar ik indertijd dus ook veel mee optrok. Ook dronk ik indertijd vaak koffie met Vic Houba, Ivo Novozamsky, Hans van der Lee en Johan Uittenbogaard.

Tijdens de verbouwing heb ik een tijdje "gehokt" met Egbert Nab. Egbert wist me niet alleen de fijne kneepjes van het laboratorium werk te vertellen, maar ook die van het schaatsen slijpen. Op het Staring gebouw heb ik vervolgens met Jeanine Geelhoed en Dirkje van Dijk een kamer gedeeld.

De laatste jaren heb ik gewerkt in het nieuwe gebouw op de beneden verdieping. De sfeer was daar erg collegiaal. Dat heeft me zeker geholpen om door het laatste en zwaarste jaar van deze promotie heen te komen.

Tenslotte wil ik bij deze mijn begeleiders Willem van Riemsdijk en Tjisse Hiemstra bedanken voor de prima begeleiding bij het schrijven van dit proefschrift.

## Contents

Venema, P., 1997. Charging and ion adsorption behaviour of different iron (hydr)oxides, Ph.D. thesis, Wageningen Agricultural University, Wageningen, The Netherlands.
ISBN 90-5485-658-0; 209 pages

Part of this work is financed by the European Community for a STEP (Science and Technology for Environmental Protection) project, through contract STEP-CT90-0031.
The work was done at the deparment of Soil Science and Plant Nutrition, Wageningen Agricultural University, P.O. Box 8005, 6700 EC Wageningen, The Netherlands

# 1

# Introduction

## Introduction

The bio-availability and mobility of nutrients and contaminants in soil systems is an important topic of soil research. The availability of ions is not only related to their total amounts in the soil system, but also to soil properties. A cat- or anion that is present in a soil, may not be available for plants or soil animals, because of specific adsorption to the solid fraction of the soil. Recently bio-availability has been interpreted in terms of relative competition between a bio-interface and soil component surfaces (1). The availability of heavy metals for the soil biota was shown to be dependent on pH, calcium concentration and soil type. The idea of competition between interfaces indicates that for a good prediction of bio-chemical behaviour of cat- and anions in soils, a thorough understanding of the important chemical processes is essential.

In natural soil systems, also physical transport of cat- and anions is of great influence on the bio-availability. A study to the influence of non-linear adsorption and soil heterogeneity on solute transport (2) showed that the chemical adsorption during transport is important. It was found that non-linear adsorption has a strong effect on solute movement and spreading in heterogeneous formations. This indicates the importance of knowledge of the chemical adsorption processes in soil systems. An important phenomenon, for example, is the exchange of protons upon ion adsorption. Recently, both Fluoride breakthrough curves and concomitant pH changes during a column experiment could be predicted very well using a chemical model that was calibrated independently (3). The data of the column experiment could not be described with a simple langmuir or freundlich isotherm. This indicates that combination of a simple chemical model with a sophisticated transport program may not lead to good predictions of solute transport in soils.

The dependence of the bio-availability on soil type can be explained by the different constituents of the soil. The main reactive constituents of soils comprise, clay, metal (hydr)oxides, organic matter and other important minerals like carbonates. The chemical behaviour of these constituents define the chemical behaviour of a soil. The effect of interaction between different constituents on the sorption behaviour is also subject of ongoing research.

In this thesis the chemical behaviour of one of the constituents of soil systems, me-

tal (hydr)oxides, in particular the behaviour of iron (hydr)oxides is studied in detail. The objectives of this research was to determine the chemical adsorption behaviour of different iron (hydr)oxides and explain these differences. The findings of this research have resulted in this thesis.

Iron (hydr)oxides are the most abundant metal (hydr)oxides in soil systems (4). Therefore iron (hydr)oxides are used as a model substance for a detailed study on the chemical behaviour of metal(hydr)oxides. Before giving a more detailed overview of the work described in the thesis, first some general explanation about the chemical behaviour of metal (hydr)oxides will be given.

The models that are used and extended in this thesis are quite complicated for outsiders. For this reason an introduction is chosen in which a brief explanation of the basic principles of the behaviour of metal (hydr)oxides is given. For the explanation of existing models we refer to chapter 2. Reviews of existing models are given by Davis and Kent 1990 (5), Goldberg 1990 (6) and Bolt 1982 (7). Before we focus on metal (hydr)oxide surfaces, first some common model concepts for chemical adsorption processes will be explained.

## The reactive surface of a solid

The importance of an soil constituent for the chemical behaviour of a soil is determined by its contribution to the total **reactive surface area** of the soil. A soil constituent may be dominant in a soil expressed on basis of mass, but its reactive surface can be very low. This has lead to the introduction of an important property of a solid, the **specific surface area**. This specific surface area $A$ is expressed as the surface of a solid in $m^2$ per kilogram of material. A soil constituent that may seem unimportant on mass basis in a soil, can be the main reactive constituent because of a high specific surface area.

The surface of an inorganic soil particle exists of surface atoms. In case of metal (hydr)oxides and clay minerals, the surface atoms are oxygens (5, 8, 9). Some of the surface oxygens can participate in the formation of chemical bonds with ions that are present in the soil solution. The differences between chemical behaviour of the different surface oxygens is related to the crystal structure. On a metal (hydr)-oxide surface, the oxygen can have one or more structural bonds with underlying

metal ions. Two surface oxygens which differ in their number of structural bonds will have a different chemical behaviour (10, 11). So the reactivity of a solid is not dependent on the number of surface groups, but on the number of reactive surface groups. The relation between the crystal structure of a metal (hydr)oxide and the chemical behaviour is an important topic of this thesis.

The total concentration of a reactive surface group S of a solid in a porous system is now dependent on its abundance at the surface of the solid ($N_S$) in mol/m$^2$ and the amount of reactive surface area which is in contact with the solution according to:

$$[S]_{Tot} = N_s \cdot \rho \cdot A \qquad [1]$$

in which $\rho$ is the amount of solid present in kg/l and $A$ is its specific surface area in m$^2$/kg

## Adsorption of ions to soil particles

In the previous section it was mentioned that a surface group of a soil particle can react with ions of the soil solution. Such a chemical reaction of a surface group is called **chemical adsorption**. Adsorption to a soil particle can be described with a chemical equilibrium. For the description of such an equilibrium, we consider the adsorption of A to a surface group of a soil particle S:

$$S + A \leftrightarrows S\text{–}A \qquad K_{S\text{-}A} \qquad [2]$$

the product S-A that is formed will be indicated as a **surface complex**. The activity of the adsorbing ion A will be influenced by the surface charge or potential of the soil particle. The overall affinity $K_{S\text{-}A}$ is dependent on the "intrinsic" chemical affinity of A for the surface group S and on the electrostatic interaction. The magnitude of the electrostatic interaction is normally calculated by means of a model. The affinity constant $K_{S\text{-}A}$ is thus split into an intrinsic constant and an electrostatic part:

$$K_{S\text{-}A} = K^{int}_{S\text{-}A} \cdot f \qquad [3]$$

in which $K_{S\text{-}A}$ is the affinity of A for the surface group S, $K^{int}_{S\text{-}A}$ is the intrinsic affinity of A for S, and $f$ is the influence of the electrostatic interaction. The magni-

tude of the electrostatic effect is thus dependent on the model chosen. In this thesis a new approach for an interface model, developed by Hiemstra and van Riemsdijk (12) will be used. In the following section, the interface model will be treated in some more detail.

The electrostatic term $f$ depends among other things on the salt concentration of the system and is thus dependent on the experimental conditions. The constant $K_{S\text{-}A}$ is thus a "conditioned constant". Models that treat ion binding as a combination of a chemical reaction with electrostatic interactions are normally referred to as **surface complexation models**.

## *Surface charging of metal (hydr)oxides*

The chemical equilibrium is the basis of surface complexation modelling. As discussed in the previous section, an important characteristic of metal (hydr)oxides, that influences the equilibrium very strongly is their charging behaviour. This will now be discussed.

The surface of metal (hydr)oxides has a charge that varies with the pH as was shown for silicium oxide by Bolt (13) (Fig. 1a) and for hematite by Parks and de Bruyn (14) (Fig. 1b). The origin of this variable charge is the adsorption and desorption of protons and/or hydroxyls to surface groups. The reaction of protons and hydroxyls can be measured by simply titrating a suspension with acid or base. The net amount of adsorbed protons and hydroxyls is then determined from a mass balance: $(H\text{-}OH)_{Adsorbed}=(H\text{-}OH)_{Added}-(H\text{-}OH_{Solution})$

The proton adsorption and desorption processes are sometimes modelled without considering individual surface groups (15, 16, 17). The first attempt to explain the origin of the surface charge has been to attribute it to a two step proton adsorption reaction (9, 14, 18):

$$MeO^{-1} + H^{+} \leftrightarrows MeOH^{0} \qquad K_{H1} \qquad [4a]$$

$$MeOH^{0} + H^{+} \leftrightarrows MeOH_2^{+1} \qquad K_{H2} \qquad [4b]$$

in which MeO represents a surface oxygen with underlying metal ion(s), $K_{H1}$ and $K_{H2}$ are the protonation constants of the first and second protonation step. These

surface complexation reactions provided a first physical chemical view on the surface charging behaviour. Based on this approach, different surface complexation models were developed that could describe the charging behaviour (19, 20, 21, 22, 23, 24, 25, 26).

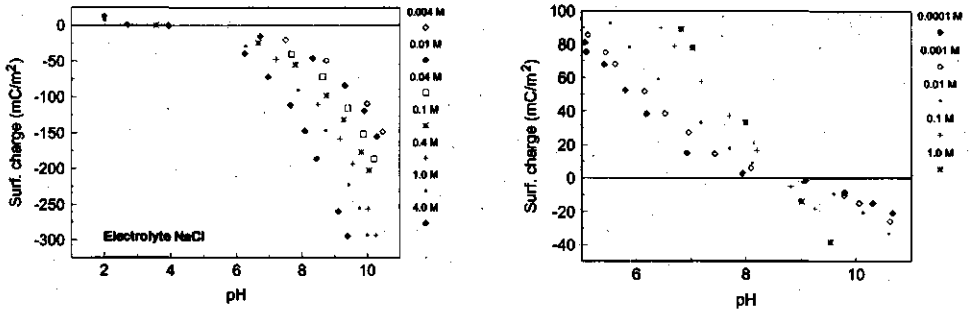


Fig. 1 Typical charging curves for a) silica (Bolt 1957) and b) goethite (Parks and de Bruyn 1962)

More recently Bolt and van Riemsdijk proposed another reaction for the surface protonation of iron and aluminium (hydr)oxides (27, 28):

$$\mathrm{MeOH}^{-\frac{1}{2}} + \mathrm{H}^{+} \leftrightarrows \mathrm{MeOH}_2^{+\frac{1}{2}} \qquad K_{\mathrm{H}} \qquad [5]$$

in which MeOH is a surface hydroxyl, H a proton and $K_{\mathrm{H}}$ the proton affinity constant. This surface complexation model was the basis of a more generalized multi-site approach developed by Hiemstra and van Riemsdijk (10, 11). This MUlti SIte Complexation (MUSIC) model forms the basis of the models used in this thesis to interpret the physical origin of the surface charge. The different behaviour of Silica (Fig. 1a) versus iron (hydr)oxides (Fig. 1b) can be explained and described with the MUSIC model. This model predicts that the protonation of the silica surface follows eq. [4a], in which log $K_{\mathrm{H1}}$ has a value of 7.5, while log $K_{\mathrm{H2}}$ is very low so eq. [4b] is of no importance at normal pH values (11). This implies that the silica surface charge at normal pH values is zero or negative, which is in accordance with the experimental data (Fig. 1a). For the protonation of iron (hydr)oxides, the MUSIC model predicts that eq. [5] is the major reaction. So the model predicts a goethite surface charge that can be positive, zero or negative at normal pH values. This is in accordance with the data of Parks and de Bruyn (14) (Fig. 1b). The different shape of the curves around the PZC is also in accordance with the insights obtained from the MUSIC model.

The surface charge does not only vary with the pH, but also with the ionic strength (Fig. 1a and Fig. 1b). This influence of the salt concentration is due to the **Diffuse Double Layer** (DDL, Fig. 2), which will be discussed later. In this layer ions are accumulated that compensate the charge of the surface. The binding of protons is influenced by this DDL, in the next section this will be explained in more detail.

## The solid/solution interface of charged particles

The concept of variable charging is of major importance for the understanding of cat- and anion adsorption (9, 13, 14). Gouy (29) and Chapman (30) developed a theory in which they could describe the distribution of ions, considered to be point charges, near a charged surface (5). In case the surface charge and the ion charge have the same sign (positive or negative), the ion will be repelled from the surface. This results in a lower ion concentration near the metal (hydr)oxide surface than the background concentration, these ions will be referred to as co-ions (Fig. 2). If, however, the ion charge and the surface charge have an opposite sign, the ion will be attracted and its concentration near the surface will be higher than the background concentration. Such ions will be referred to as counter-ions (Fig. 2). The charge of the surface is thus compensated by ions in a so called Diffuse Double Layer (DDL, Fig. 2) in which counter ions are concentrated and co-ions are excluded.

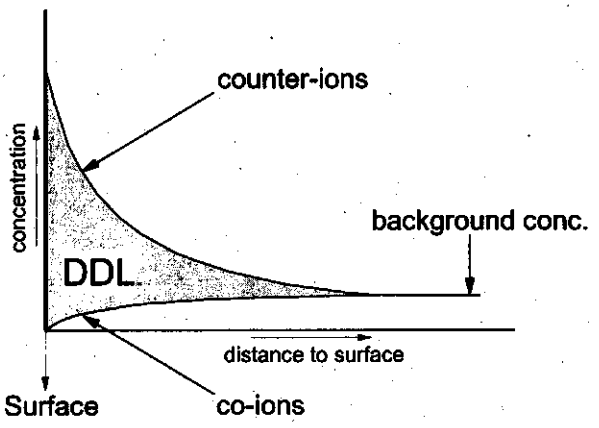


Fig. 2 The concentration profile near the charged surface of a metal (hydr)oxide. The concentration of the counter ions (charge has opposite sign as surface charge) increases on approaching the surface. The concentration of the co-ions (charge has the same sign as surface charge) decreases on approaching the surface. The overall charge of the Diffuse Double Layer is indicated as the hatched area.

Bolt (13) and Parks and de Bruyn (14) showed that the slope of the charging curves differs with the background salt concentration. The surface can charge higher at a higher background salt concentration (Fig. 1a, Fig. 1b). This can be explained as the result of a better neutralization of the surface charge by the salt ions in the solution which suppresses the effect of the electrostatic field on the adsorption. If the surface charge is zero, the electrostatic field is absent, so no salt effect is observed. The pH at this point is usually called the **Point of Zero Charge** (PZC, see Fig. 1b).

In the Gouy-Chapman theory, ions are considered to be point charges, which is a simplification. Stern (31) improved the model by introducing a charge-free Stern layer between the surface and the DDL, in which no background electrolyte ions can occur. The charge free layer has a thickness which correspondents with the radius of the partly hydrated background electrolyte ions. The use of a charge free Stern layer considerably improves the description of the charging behaviour.

A new vision on interface modelling is introduced by Hiemstra and van Riemsdijk (12). In their interface model, two charge free (Stern) layers are placed between the surface and the DDL (Fig. 3). The ligands of the adsorbed complex that are present in the surface are shared with the metal ions of the metal (hydr)oxide and form the chemical bond with the solid. The charge of the central cation of a surface complex (e.g. $Cd^{2+}$, $P^{5+}$) is in the model divided over the ligands which are present in the inner plane (surface plane) and the intermediate plane (1-plane) (Fig. 3). So, in the model, the charge of an adsorbed species is not treated as a point charge as is classically the case, but it is divided over two planes; the surface plane and the 1-plane. This so-called Charge Distribution (CD) approach is combined with the MUSIC approach in the CD-MUSIC model (12).

Resuming, it can be concluded that adsorption of cat- and anions on charged surfaces can be described well with a combination of an electrostatic interface model and an surface complexation model. With the electrostatic model the local concentrations of all ions near the surface can be calculated. These local ion concentrations near the surface are used to calculate the chemical equilibrium of the reaction with a surface group.

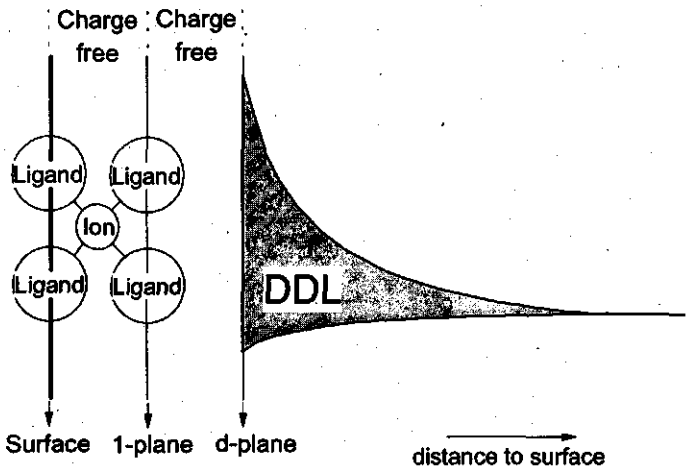


Fig. 3 The interface model that is used in the Charge Distribution (CD) model. The charge of an adsorbing ion (e.g. $Cd^{2+}$, $P^{5+}$) is in this model divided over its ligands which are placed in the surface and the 1-plane.

## Present thesis

Different types of iron(hydr)oxides occur in nature, differing in crystal structure. For this thesis, goethite, lepidocrocite and hematite are used. Attempts to measure on other iron (hydr)oxides (magnetite and akaganite) failed. A short overview of the most important iron (hydr)oxides will be given here (32):

-Goethite, α-FeOOH — This is the most important iron(hydr)oxide in soil systems in almost every soil type and climate region.

-Lepidocrocite, γ-FeOOH — This orange coloured hydroxyoxide is less common than goethite, it is formed from oxidation of precipitated $Fe^{2+}$hydroxy compounds. So it is formed under circumstances where oxygen is deficient

-Akaganite, β-FeOOH — This is a grey coloured hydroxooxide with the same composition as Goethite and Lepidocrocite but with a different crystal structure. It has been identified in mineral deposits.

-Hematite, $Fe_2O_3$ — This is the second most important iron(hydr)oxide, it colours the soil red. The soil pigmenting effect for hematite is higher than for goethite so that in a red coloured soil goethite still can be dominant.

-HFO — HFO (Hydrous Ferric Oxide) is often associated with goethite in bog iron ores. The structure of HFO is not well known and it is therefore not considered in this study.

It can be expected that the differences in crystal structure imply a difference in chemical behaviour (10, 11). It is therefore interesting to study the chemical behaviour of well defined metal(hydr)oxides. The most important iron (hydr)oxides in nature are goethite ($\alpha$-FeOOH) and hematite ($\gamma$-$Fe_2O_3$). Goethite is the most abundant iron(hydr)oxide in nature and it can be produced in the laboratory with well defined monodomainic crystals. Therefore the attention will be focused on Goethite first and later other iron (hydr)oxides will be considered.

The ions that are chosen for the work of this thesis are cadmium and phosphate. Cadmium is chosen because of its toxicity and abundance in many natural soil systems. In soils cadmium is, compared with other heavy metals, relatively mobile (33, 34). The chemical behaviour of cadmium in soils is therefore an interesting research topic. In soils, metal(hydr)oxides may play an important role for cadmium adsorption. Phosphate is a very important nutrient in many agricultural systems. In many phosphate fertilizers, cadmium is abundant (35) so the combination of these two ions is relevant. Iron (hydr)oxides have a high affinity for phosphate and they play an important role for the availability of phosphate in many soils (26, 36, 37, 38, 39, 40, 41).

In current modelling of reactions at the metal (hydr)oxide/solution interface, many parameters are used for fitting data. Some of these parameters, for example the number of reactive sites ($N_s$), should not be treated as an adjustable parameter because they are fixed by the crystal structure and morphology. Also different surface species, which are not based on a physical interpretation, are often assumed in order to be able to describe a chemical data set. The challenge in this thesis is to use a model that is as close as possible to the physical reality. In chapter 2, different electrostatic models are discussed and compared for the description of an extended data set. Using an extended data set implies restrictions to the model, i.e. a model should not only be able to describe the pH dependency of metal adsorption, but also the

salt dependency and metal/proton exchange. This approach means a severe test for the different surface complexation models.

With the aid of modern spectroscopic techniques, information about surface species can be obtained. The choice of surface species in chemical modelling should preferably be in accordance with spectroscopic data. Hayes et al. (42) were the first to use spectroscopic data for chemical modelling. Hiemstra and van Riemsdijk (12) were the first to describe both spectroscopic and chemical phosphate data with the CD-MUSIC model. Recently, extended x-ray adsorption fine spectra (EXAFS) measurements have been done for cadmium adsorption on goethite (43). In the third chapter, both chemical adsorption data and EXAFS data are used for the model description of cadmium adsorption with the CD-MUSIC model.

In many soil systems, phosphate and cadmium occur simultaneously. It can be expected that the presence of phosphate will have a large influence on cadmium adsorption (44). In the fourth chapter, the CD-MUSIC models that are calibrated on adsorption data for a system with only phosphate (12, 45) and with only cadmium (46) are combined. This combined model is tested on adsorption data for a system where both ions occur simultaneously. Whether the description is in accordance with the data sets, is a severe test for the CD-MUSIC model.

It was mentioned before in this introduction that different surface oxygens will have a different chemical behaviour. The differences in chemical behaviour between different surface oxygens are related to the crystal structure. Therefore, the crystal structure and morphology are of major importance to understand differences in chemical adsorption behaviour of different iron (hydr)oxides. In chapter 5, a further refined MUSIC model is developed and discussed for the prediction of proton affinity constants for surface groups of various metal (hydr)oxides. The main differences between this refined approach and the previous MUSIC model is that asymmetric distribution over the ligands of a central ion is taken into account and hydrogen bridges are explicitly used. This method is applied to three different iron (hydr)oxides in chapter 6.

For practical soil science problems, the question arises if different iron (hydr)oxides will show a significant difference in their chemical behaviour. In chapter 7, there-

fore, cadmium and phosphate adsorption for the three different iron (hydr)oxides are compared. In this chapter, it is tried to answer the question if different iron (hydr)-oxides can be considered as one and the same chemical adsorption component in soil systems.

## References


1. Plette A.C.C., Cadmium and zinc interactions with a Gram-positive soil bacterium, PhD. Thesis, Dept. Soil Science and Plant Nutrition, W.A.U., Wageningen (1996)
2. Bosma W.J.P. Transport of reactive solutes in heterogeneous porous formations, PhD. Thesis, Dept. Soil Science and Plant Nutrition, W.A.U., Wageningen (1994)
3. Meeussen, J.C.L, Scheidegger, A., Hiemstra, T., van Riemsdijk, W.H., and Borkovec, M. Predicting multicomponent adsorption and transport of fluoride at variable pH in a goethite-silica sand system, *Environ. sci. technol*, **30**, 481-489 (1996)
4. Schwertmann U., Cornell R. Iron Oxides in the laboratory., VCH Weinheim, New York, Basel, Cambridge (1991)
5. Davis, J.A., and Kent, D.B. "Mineral Water Interface Geochemistry" *in* "Reviews in Mineralogy Vol.23" (Hochella, M.F. and White, A.F. eds.), Mineralogical Soc. Am. (1990)
6. Goldberg, S. Use of surface complexation models in soil chemical systems, *Advances in Agronomy*, **47**, 233 (1992)
7. Bolt, G.H. Soil chemistry; B. physico chemical models, Elsevier scientific publishing comp., Amsterdam (1982)
8. Dixon J.B. and Weed S.B. Minerals in soil environments, (Dixon J.B. and Weed S.B. eds.), Soil Science Society of America, Madison, Wisconsin (1977)
9. Yates, D.E. The Structure of the Oxide/Aqueous Electrolyte Interface, PhD. thesis, University of Melbourne, Melbourne, Australia (1975)
10. Hiemstra, T, vanRiemsdijk, W.H., and Bolt, G.H. Multisite Proton Adsorption Modeling at the Solid/Solution Interface of (Hydr)oxides: A New Approach, I. Model Description and Evaluation of Intrinsic Reaction Constants, *J. Colloid Interface Sci.* **133**, 91-104 (1989a)
11. Hiemstra, T, de Wit J.C.M., and vanRiemsdijk W.H. Multisite Proton Adsorption Modeling at the Solid/Solution Interface of (Hydr)oxides: A New Approach, II. Application to various Important (Hydr)oxides, *J. Colloid Interface Sci.* **133**, 105-117 (1989b)
12. Hiemstra, T, and van Riemsdijk, W.H. A surface structural approach to ion adsorption: The Charge Distribution (CD) model, *J. Colloid Interface Sci.* **179**, 488-508 (1996)
13. Bolt, G.H. Determination of the charge density of silica sols, *J. Phys. Chem.*, **61**, 1166-1169 (1957)
14. Parks, G.A., and de Bruyn, P.L., The Zero Point of Charge of oxides, *J. Phys. Chem.*, **66**, 967-973 (1962)
15. Lyklema, J. *J. Electroanal. Chem.*, **18**, 341 (1968)
16. Fokkink, L.G.J. Ion adsorption on oxides, surface charge formation and cadmium binding on rutile and hematite, PhD. thesis, Dept. Soil Science and Plant Nutrition, W.A.U., Wageningen (1987)
17. Venema, P., Hiemstra, T., and van Riemsdijk, W.H. Comparison of different site binding models for cation sorption; Description of pH dependency, salt dependency, and cation -proton exchange, *J. Colloid Interface Sci.* **181**, 45-59 (1996)
18. Parks, G.A. The iso electric points of solid oxides, solid hydroxides and aqueous hydroxo complex systems, *Chem. rev.*, **65**, 177 (1965)
19. Yates, D.E., Levine, S., and Healy, T.W. Site binding model of the electrical double layer at the oxide/water interface, *J. Chem. Soc. Faraday Trans. I*, **70**, 1807-1818 (1974)

20. Davis J.A., Leckie J.O. Surface ionization and complexation of the oxide/water interface. II. Surface properties of amorphous iron oxyhydroxide and adsorption of metal ions, *J. Colloid Interface Sci.* **67**, 90-107 (1978)
21. Davis J.A., James R.O., Leckie J.O. Surface ionization and complexation of the oxide/water interface. I. Computation of the electrical double layer properties in simple electrolytes, *J. Colloid Interface Sci.* **63**, 480-499 (1978)
22. Dzombak D.A. and Morel F.M.M. Surface complexation modelling: Hydrous Ferric Oxide, John Wiley, New York (1990)
23. Schindler, P.W., and Gamsjäger, H. Acid base reactions of $TiO_2$ (Anatase)-water interface and the point of zero charge of $TiO_2$ suspension , *Kolloid-Z. u. Z. Polymere*, **250**, 759-763 (1972)
24. Stumm, W. (1987) Aquatic surface chemistry, John Wiley, New York
25. Bowden, J.W., Posner, A.M., Quirk, J.P. Ionic adsorption on variable charge mineral surfaces. Theoretical-charge development and titration curves, *Aust. J. Soil Res.*, **15**, 121-136 (1977)
26. Barrow, N.J. "Reactions with variable charge soils", Nijhoff, Dordrecht, The Netherlands (1987)
27. Bolt. G.H. and van Riemsdijk, W.H. The ionic distribution in the diffuse double layer; *In*: "Soil chemistry; B. physico chemical models", (Bolt G.H., Ed.), Elsevier scientific publishing comp., Amsterdam (1982)
28. vanRiemsdijk, W.H., Bolt, G.H., Koopal, L.K., Blaakmeer, J. Electrolyte adsorption on heterogeneous surfaces: Adsorption models, *J. Colloid Interace Sci.*, **109**, 219-228 (1986)
29. Gouy, G Sur la constitution de la charge electrique a la surface d'un electrolyte, *J. Phys.*, **9**, 457 (1910)
30. Chapman, D.L. A contribution to the theory of electrocapillarity, *Philos. Mag.*, **6 (25)**, 475 (1913)
31. Stern O. Zür theory der electrolytischen doppelschicht; *Z. Elektrochem.* **30**, 508-516 (1924)
32. Schwertmann U., and Taylor R. M. Iron Oxides, *in* "Minerals in soil environments", (Dixon J.B. and Weed S.B. eds.), Soil Science Society of America, Madison, Wisconsin (1977)
33. Boekholt A.E. Field scale behaviour of cadmium in soil, PhD thesis, Dept. Soil Science and Plant Nutrition, W.A.U., Wageningen (1992)
34. Wilkens B.J. Evidence for groundwater contamination by heavy metals through soil passage under acidifying conditions, PhD thesis, Dept. Geosciences, R.U.U., Utrecht (1995)
35. "Handboek voor milieubeheer, Deel IV, Bodembescherming", (Edelman Th., van der Gun, J.H.J, and Lexmond Th. eds.), Samson H.D. Tjeenk Willink, Alphen aan de Rijn (1991)
36. Torrent, J., Barrón, V., and Schwertmann, U., Phosphate adsorption and desorption by goethites differing in crystal morphology, *Soil Sci. Soc. Am. J.*, **54**, 1007-1012 (1990)
37. Torrent, J., Schwertmann, U., and Barron, V. Fast and slow phosphate sorption by goethite-rich natural materials, *Clays and clay minerals*, **40**, 14-21 (1992)
38. Torrent, J., Schwertmann, U., and Barron, V. Phosphate sorption by natural hematites, *European Journal of Soil Science*, 45, 45-51 (1994)
39. Pena, F., Torrent, J., Predicting phosphate sorption in soils of mediterranean regions, *Fertilizer research*, 23, 173-179 (1990)
40. Solis, P., and Torrent, J., Phosphate fractions in Calcareous Vertisols and Inceptisols of Spain, *Soil Sci. Soc. Am. J.*, **53**, 462-466 (1989)

41. Soltan, S., Römer, W., Adgo, E., Gerke, J., and Schilling G., Phosphate sorption by Egyptian, Ethiopian and German soils and P uptake by rye (Secale,cereale L.) seedlings, *Z. pflanzenernähr. Bodenk.*, **156**, 501-506 (1993)
42. Hayes, K.F., Lawrence, R.A., Brown, G.A., Hodgson K.O., Leckie J.O., Parks, G.A. In Situ X-ray adsorption study of Surface complexes: Selenium Oxyanions on α-FeOOH, *Science*, **238**, 783-786 (1987)
43. Spadini, L., Manceau, A., Schindler, P.W., and Charlet, L.C., Structure and stability of $Cd^{2+}$ surface complexes on Ferric Oxides, *J. Colloid Interface Sci.* **168**, 73-86 (1994)
44. Kuo S., and McNeal B.L., Effects of pH and Phosphate on Cadmium Sorption by a Hydrous Ferric Oxide, *Soil Sci. Soc. Am. J.*, 48, 1040-1044 (1984)
45. Geelhoed, J.S., Hiemstra, T., and van Riemsdijk, W.H., Phosphate and sulfate adsorption on goethite: single anion and competitive adsorption, submitted, *Geoch. et cosmoch. acta* (1996)
46. Venema, P., Hiemstra, T., and van Riemsdijk, W.H., Multisite adsorption of cadmium on goethite, *J. Colloid Interface Sci.* **183**, in press (1996)

# 2

# Comparison of different site binding models for cation sorption; Description of pH dependency, salt dependency and cation - proton exchange

Peter Venema, Tjisse Hiemstra, Willem H. van Riemsdijk
Journal of Colloid and Interface Science, vol 181, p. 45-59, 1996

# Comparison of different site binding models for cation sorption; Description of pH dependency, salt dependency and cation - proton exchange.


## Abstract

*Ion adsorption on metal (hydr)oxides has been described in the literature with many different surface complexation models. In the present study, five of these models were used to systematically compare their description of the basic charging behaviour and cation adsorption phenomena using an extended data set for proton and cadmium adsorption on goethite. The scope and limitations of the models are discussed. None of the models gave a completely satisfactory description of all of the data.*

*A 1 pK model in combination with three electrostatic planes yielded the best results. This model was able to describe the pristine charging behaviour, the pH dependency of cadmium adsorption and the salt dependency of cadmium adsorption, using 5 adjustable parameters. However, the H/Cd exchange ratio was significantly less than the observed ratio.*


## Introduction

Adsorption of cations on metal (hydr)oxides has been the subject of many studies. A number of different models has been used to describe the adsorption behaviour (1 - 11). Most of the models can satisfactorily describe one adsorption phenomenon, such as the pH dependency of metal ion binding for a limited data set, but none of the existing models can describe simultaneously all available data for a particular extended data set.

A systematic comparison between the various models, with an assessment of their scope and limitations, has not yet been made. Five different models (Fig. 1) will be compared, focusing on three important aspects of cation adsorption on metal hydroxides: pH dependency, salt dependency and the proton/cation exchange ratio.

Because protons are the primary potential determining ions for the metal (hydr)-oxide surface (12), the description of the charging curve (surface charge versus pH) should be a basic feature of any adsorption model. Therefore, a data set that con-

tains both charging curves and cation adsorption data is a prerequisite for the evaluation of the models.

| Interface Model | Complexation Model | | |
|---|---|---|---|
| | Without surface sites | With surface sites | |
| | Nernst $\Psi_0 = \frac{RT}{F(\mathrm{Log}(e))}(PZC - pH)$ | 1 pK $SOH^{-1/2} + H^+ \rightleftharpoons SOH_2^{+1/2}$ $pK_1$ | 2 pK $SO^- + H^+ \rightleftharpoons SOH^0$ $pK_{H1}$; $SOH^0 + H^+ \rightleftharpoons SOH_2^+$ $pK_{H2}$ |
| Only Diffuse Double Layer | | | 4) Purely Diffuse Model (PDM) |
| Diffuse Double Layer + one charge-free layer | 1) Nernstian Stern Model (NSM) | 2) Basic Stern Model (BSM) | |
| Diffuse Double Layer + two charge-free layers | | 3) Three Plane Model (TPM) | 5) Triple Layer Model (TLM) |

Fig. 1 The five different models that are evaluated, divided by their differences in surface complexation (columns) and electrostatical model (rows)

## Methodology

For the model evaluation, cadmium adsorption data for goethite were used. Details of the experimental methods are discussed elsewhere (13). For all experiments much attention was paid to avoid silica contamination and to exclude $CO_2$. The charging curves were measured for three different concentrations sodium nitrate background electrolyte. For the cadmium experiments, the goethite suspension was brought to the desired pH and salt level. If the pH was considered to be stable (drift < 0.05 mV/min), cadmium was added and the suspension was titrated to the desired pH again with NaOH. After 4 hours, a sample was taken, followed by a new cadmium dose and backtitration to the desired pH and sampling after four hours etc. A maximum of 7 samples were taken from one suspension. The samples were filtered and cadmium concentration was measured on a flame-AAS. The amount of hydrogen needed to keep the pH at the desired value was used to calculate the moles of protons released per mole of adsorbed cadmium.

The data set for the pH dependent cadmium adsorption, used in this study was based on five different adsorption isotherms, which were interpolated to a constant sum of total dissolved cadmium species ($Cd_{sol}$ (mol/l)). This gave a set of data of the cadmium adsorption as a function of pH at a constant $Cd_{sol}$ and fixed ionic

strength ($I$ = 0.1 mol/l). A similar procedure was used for the salt dependency. Three adsorption isotherms at different ionic strengths were used to give a set of data for cadmium adsorption as a function of ionic strength at a constant $Cd_{sol}$ and pH (pH = 7). The values of $Cd_{sol}$ used were $10^{-4}$ mol/l and $10^{-6}$ mol/l. The integral molar ratio of protons released to cadmium ions bound was derived directly by the experiment and no significant dependence of the pH and cadmium concentration was observed. The H/Cd exchange ratio is only given for data of which the quotient {Total adsorbed cadmium}/{Total dissolved cadmium} is larger than 1. The values, with their 95% reliability interval are: 1.4 ± 1.3 (pH 6), 1,63 ± 0.18 (pH 7), 1.59 ± 0.27 and 1.71 ± 0.63 (pH 9). The average H/Cd exchange ratio for all data equals 1.6 over a cadmium concentration range of about 1 to 500 µmol/l.

Optimization was carried out by trial-and-error fitting aided by plots of the charging curves and the cadmium adsorption data. The first step in the optimization was the description of the charging curve. For the optimization of the cadmium data description, only the parameters for the cadmium surface complex formation were varied.

The aim of this article is not to find the best fit of the data sets but to gain insight in the influence of the different model parameters on the description of the data sets. A model should not only be able to fit data sets, but it should also approach the physical reality as close as possible. Therefore some fit parameters have more restrictions than others. In this article, the site density is fixed on a value of 6 sites/nm$^2$, which is found to be a realistic value for goethite. Recently this value has been confirmed for modelling chemical and spectroscopic data of phosphate adsorption on goethite (14).

The calculations were carried out with ECOSAT, a computer code for the calculation of chemical equilibria and transport (15).

Activity coefficients for the ionic species were calculated using the Davis equation:

$$\gamma_i = -0.5\ z_i^2\ \left(\frac{\sqrt{I}}{1+\sqrt{I}} - 0.2\ I\right) \qquad [1]$$

in which $I$ is the ionic strength and $z_i$ the valence of ion i.

In the formulation of the adsorption equations, the activity of the ions in solution is multiplied by a Boltzmann factor to take into account the electrostatics on the ion binding. The overall reaction for the adsorption of X to a surface group S;

$$S + X = SX$$

can be separated into chemical (intrinsic) and electrostatic parts:

$$K_{X\,int} = (SX)\ (S)\ (X)_s = \frac{(SX)}{(S)\ (X)\ e^{-Z\frac{F\psi}{RT}}} = K_X\ e^{+Z\frac{F\psi}{RT}} \qquad [2]$$

in which $K_{X\,int}$ is the intrinsic overall equilibrium constant, $K_X$ is the overall equilibrium constant, subscript s indicates the plane of adsorption for X, $(X)_s$ is the activity of X at the position s in the interface and $\psi$ is the corresponding potential of the adsorption plane, $Z$ is the charge of the adsorbing ion, $T$ is the temperature, F is the Faraday constant, R the gas constant. Note that for an adsorbing ion, the bulk activity (not the concentration) is multiplied with a Boltzmann factor. In other studies, no activity coefficient is used for adsorbing ions (7,10,11).

There are different ways to describe the electrostatic potential profile of the metal (hydr)oxide.

## Interface models

The five models described in Fig. 1, are each used to describe the available data. The five models differ in their formulation of the surface reactions and in the description of the electrostatic potential profile. In this section, the electrostatic interface models and their relation to the five models will be discussed briefly.

The Nernstian Stern layer Model NSM (Fig. 1) is unique in that it has no surface sites. This surface composition model is combined with an interface model with a Basic Stern double layer, which includes a charge free layer (16) (Fig. 2). In all of the other models, surface sites are used. The 1 p$K$ Basic Stern Model (BSM) includes surface sites and a Basic Stern double layer, this model behaves in the same way as the NSM. The 1 p$K$ Basic Stern interface model can be extended with an extra charge free layer (Fig. 2). This model is termed the Three Plane Model (TPM). An alternative and commonly used way of modelling surface complexation

is based on the 2 p*K* approach (2,3,4). The most simple 2 p*K* model is the Purely Diffuse Model (PDM), in which the interface model is purely diffuse (Fig. 2). The final model discussed is the classical 2 p*K* model with two charge free layers, the so called Triple Layer Model (TLM).

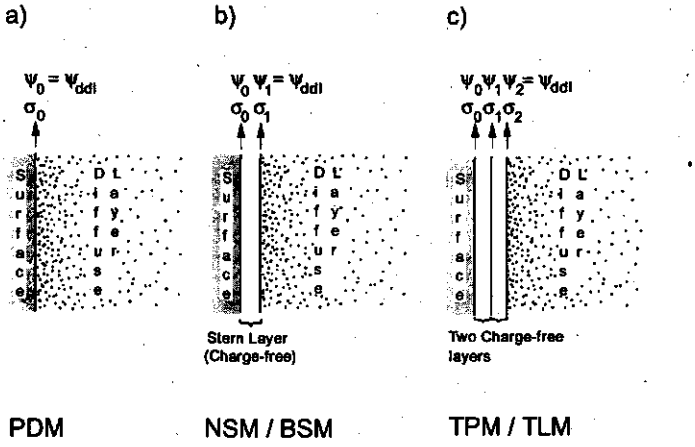


Fig. 2 a) Surface with only a diffuse double layer (PDM (see Fig 1.), one plane). In this model the potential ($\psi$) and charge ($\sigma$) in the surface plane are indicated with subscript 0. The potential at the surface ($\psi_0$) coincides with the potential at the end of the diffuse double layer ($\psi_{ddl}$). b) Surface with a Stern layer and a diffuse double layer (NSM, BSM (see Fig.1), two planes. In this model the subscript is 0 for the potential and charge at the surface; for the outer layer this subscript is 1. The potential in the outer layer ($\psi_1$) coincides with the potential at the end of the diffuse double layer ($\psi_{ddl}$). c) Surface with two charge-free layers and a diffuse double layer (TPM, TLM, (see Fig. 1.) three planes). In this model the subscript is 0 for the potential and charge at the surface, for the intermediate layer this subscript is 1 and for the outer layer it is 2. The potential in the outer layer ($\psi_2$) coincides with the potential at the end of the diffuse double layer ($\psi_{ddl}$).

All models have a Diffuse Double Layer (DDL) in common. For a DDL adjacent an infinite flat plate, the relation between the total charge of the DDL, $\sigma_{DDL}$ and the potential at the head end of the DDL, $\psi_{DDL}$ is (17,18):

$$\sigma_{ddl} = \pm \sqrt{2000\ \varepsilon_0\ \varepsilon_1\ R\ T}\ \sqrt{\sum C_i\ (e^{-\frac{z_i F}{R T}\psi_{dd}} - 1)} \qquad [3]$$

in which $\varepsilon_0$ is the dielectric constant for vacuum, $\varepsilon_1$ the relative dielectric constant for water, $c_i$ the bulk concentration for ion i, $z_i$ the valence of ion i, F the Faraday constant, R the gas constant and $T$ the temperature.

For the PDM (Fig. 2a), the surface charge ($\sigma_0$) is exactly compensated for by the charge of the diffuse double layer.

$$\sigma_0 = -\sigma_{ddl} \qquad [4]$$

Furthermore, the value of the DDL potential $\psi_{ddl}$ equals the surface potential $\psi_0$. For the NSM and the BSM, the interface model is extended with a charge free layer (Fig. 2b). In this Stern interface model no ions are present in the charge free Stern layer. The charge of potential determining ions (protons) is allocated to the surface ($\sigma_0$) whereas the charge of specifically adsorbing ions can be attributed either to the surface plane ($\sigma_0$) or to the outer plane ($\sigma_1$). Again based on the concept of electroneutrality, the sum of the charge in the two electrostatic planes ($\sigma_0 + \sigma_1$) is neutralized by the charge in the diffuse double layer, according to:

$$\sigma_0 + \sigma_1 = -\sigma_{ddl} \qquad [5]$$

The value of $\psi_{ddl}$ in the Stern model equals the potential at the outer plane ($\psi_1$) (Fig. 2). Because the Stern layer is free of charge, there is a linear relationship between $\psi_0$, $\psi_1$ and $\sigma_0$ according to:

$$\sigma_0 = C_{Stern} (\psi_0 - \psi_1) \qquad [6]$$

In this equation $C_{Stern}$ is the capacitance of the Stern layer, which is a measure of the thickness of the charge free layer according to:

$$C_{Stern} = \frac{\epsilon_0 \epsilon_r}{d} \qquad [7]$$

where $d$ is the thickness of the layer, $\epsilon_0$ is the dielectric constant in vacuum and $\epsilon_r$ is the relative dielectric constant. In several approaches, the Stern layer is split into two parts (Fig. 2c), resulting in three electrostatic planes. This interface model is used in the TPM and the TLM. The outer plane is given the subscript 2. Again applying the principle of electroneutrality, the total surface charge ($\sigma_0 + \sigma_1 + \sigma_2$) is compensated by the charge of the diffuse double layer according to:

$$\sigma_0 + \sigma_1 + \sigma_2 = -\sigma_{ddl} \qquad [8]$$

The value of $\psi_{ddl}$ is set equal to the potential of the outer plane $\psi_2$. The potentials

can again be related to the surface charge. For the inner charge free layer the relationship is:

$$\sigma_0 = C_1 (\psi_0 - \psi_1) \qquad [9]$$

where $C_1$ is the capacitance of the inner layer (between the physical surface and the intermediate plane). For the outer layer one may write:

$$\sigma_0 + \sigma_1 = C_2 (\psi_1 - \psi_2) \qquad [10]$$

here $C_2$ is the capacitance of the outer layer (between the intermediate plane (subscript 1) and the outer plane (subscript 2) ). It should be noted that the inner and outer layers are again free of charge.

The surface complexation models are discussed in more detail in the different sections for each model, starting with the Nernstian Stern layer model.

## Nernstian Stern layer Model (NSM)

The most striking feature of the Nernstian Stern model is that surface sites are not required for the description of the surface charge. The charge of the surface is thought to be evenly distributed. The Stern layer is required to obtain a proper description of the charging behaviour and metal ion adsorption. The NSM was recently used and described in detail by Fokkink and Lyklema (5, 6). The basis for this approach is the Nernstian relation in which the surface potential ($\psi_0$) is related to the pH:

$$\text{PPZC-pH} = \text{Log(e)} \frac{F}{R\,T} \psi_0 \qquad [11]$$

in which PPZC = the pH of the pristine point of zero charge, Log(e) ≈ 0.43 and $\psi_0$ is the potential near the surface.

In the NSM of Fokkink and Lyklema, adsorbed cadmium ions are placed in a plane separated from the surface by the Stern layer. The charge in the adsorption plane is related to the amount of cadmium adsorbed $\{Cd_{ads}\}$ according to:

$$\sigma_1 = F \{Cd_{ads}\} \qquad [12]$$

In the NSM an adsorption isotherm equation is required for the description of the adsorption of cations such as cadmium. Fokkink and Lyklema use the Frumkin-Fowler-Guggenheim model as the adsorption model. This approach includes a term to account for lateral interactions. Since the main lateral interactions will be of an electrostatic nature, and are also included in the model, other lateral interactions are ignored. In this case the Frumkin-Fowler-Guggenheim model simplifies to a Langmuir model:

$$\frac{\theta_{Cd}}{1 - \theta_{Cd}} = (Cd)_1 \, K_{Cd} \qquad [13]$$

in which $\theta_{Cd}$ represents the adsorbed cadmium surface complexes expressed as a fraction of the total number of sites and $(Cd)_1$ is the cadmium activity in the 1-plane.

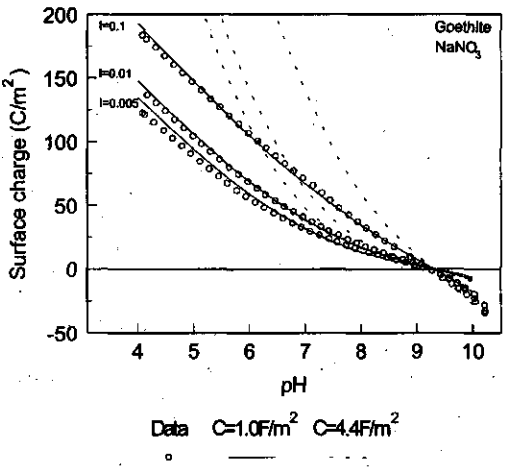


Fig. 3 Proton charging curve of goethite at three salt levels (data Venema 1995). The lines represent NSM calculations with different values of the capacitance; $C$ = 1.0 F/m$^2$ (Solid), $C$ = 4.4 F/m$^2$ (dashed)

The use of a Langmuir-type model implies that adsorption sites are involved. In Fokkink and Lyklema's approach these sites are related to the assumption that a partly hydrated cadmium ion replaces water molecules adsorbed at the surface. The adsorption maximum follows from the cross-section of a primary hydrated cadmium ion (0.2-0.3 nm$^2$) (5) and equals about 4.2 sites/nm$^2$, i.e. $\Gamma_{Cd,Max}$ is about 6.9 $\mu$mol/m$^2$.

The above described model can be applied to the experimental charging curves and the cadmium adsorption data. In Fig. 3, the experimental pristine proton charging curves for our goethite are shown with two sets of NSM parameters. The NSM with a Stern layer capacitance of 4.4 F/m$^2$, as used by Fokkink and Lyklema (5, 6) for hematite, describes the charging curve for goethite rather poorly. As will be shown later, however, this capacitance gives quite good results for the description of cadmium adsorption. The charging curves of our goethite can be described very well using a capacitance of 1.0 F/m$^2$.

The pH dependency of cadmium adsorption at two concentrations of the total sum of dissolved cadmium species (mol/l) is shown in Fig. 4. Cadmium adsorption has been plotted on a logarithmic scale because of the large variation in adsorption at different pH values. The data are described with the NSM using the same capacitance values as used in Fig. 3.

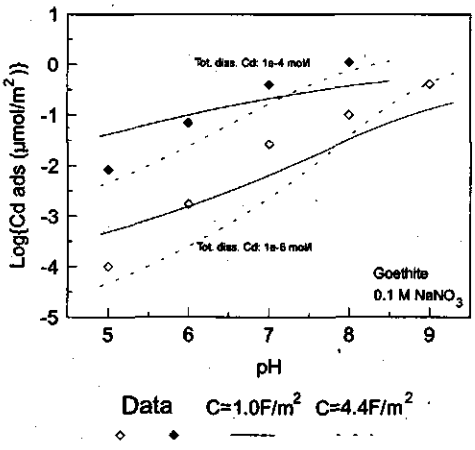


Fig. 4. The pH dependency of cadmium adsorption on goethite at ionic strength $I$ = 0.1 mol/l, ($NaNO_3$). The points indicate the adsorption for two amounts of cadmium species in solution. The lines represent the NSM calculations for two values of the capacitance, $C$ = 1.0 F/m$^2$ (solid) $C$ = 4.4 F/m$^2$ (dashed).

It follows from Fig. 4 that the predicted pH dependency for cadmium adsorption is influenced by the value of the Stern layer capacitance. The choice of the higher Stern layer capacitance (4.4 F/m$^2$) is equivalent with (for constant $\varepsilon_r$) a smaller distance between the Stern layer and the surface (Eq. [7]). Because the cadmium ions

are placed in the Stern layer, the influence of the surface potential on the cadmium adsorption will increase with increasing $C_{Stern}$. A greater influence of the surface potential implies a greater influence of pH (see Eq. [11]). A higher $C_{Stern}$, therefore, leads to a higher predicted pH dependency of cadmium adsorption. As shown in Fig. 4, the NSM with the higher capacitance gives the best description of the pH dependency of the cadmium adsorption. This high value of the capacitance, however, conflicts with the basic proton charging behaviour (Fig. 3). Representing both data sets with a consistent set of model parameters is apparently not possible with this model approach.

The values of the model parameters are given in Table 1. The fit value of the intrinsic $K_{Cd\ int.}$ varies as $C$ varies. This also can be explained by the difference in Stern layer thickness for the different capacitances. For an increasing capacitance, the Stern layer becomes thinner and the cadmium ion will approach the surface more closely. Because the goethite has a high PPZC, the surface is positively charged below a pH of 9.3. This means that the repulsion of the cadmium ion will increase as the capacitance increases. This higher repulsion is compensated for by a higher value of the (fitted) intrinsic affinity constant.

Table 1 Model parameters of the two considered options of the NSM for the description of the data set

| Parameter | Low $C$ | High $C$ |
|---|---|---|
| $C$ (F/m$^2$) | 1.0 | 4.4 |
| $\log(K_H)$ | 9.3 | 9.3 |
| $\log(K_{Cd})$ | 6.0 | 7.0 |

It is known that the experimental salt dependency for cadmium adsorption is low (7). This is confirmed by our own data shown in Fig. 5. A logarithmic scale was chosen for the adsorption of cadmium because the model description can show large effects of the background salt concentration on the cadmium adsorption. The solid lines in Fig. 5 represent the model description. The salt dependency predicted by the NSM is not high, but it is much higher than the observed dependency. The value of the capacitance does not have much influence on the salt dependency. The description using a low capacitance, however, is better.

The last important phenomenon of cation adsorption that will be discussed is the exchange of protons upon cation adsorption. The H/Cd exchange ratio that follows from this model, at pH = PPZC and at low metal adsorption densities, is given by Eq. [14] (5):

$$r_{H/Cd} = \frac{2\ C}{\varepsilon_0\ \varepsilon_r\ \kappa + C} \qquad [14]$$

In which $\kappa$ is the reciprocal Debije length $(= \sqrt{\{(2N_A e^2\ I\ )/(\varepsilon_r \varepsilon_0\ k\ T)\}})$. Calculations using Eq. [14] the influence of the Stern layer capacitance (reflecting the distance of the cadmium ion from the surface plane) on the H/Cd ratio. A general method for calculating the H/Cd ratio at different pH values and cadmium concentrations will be discussed later.

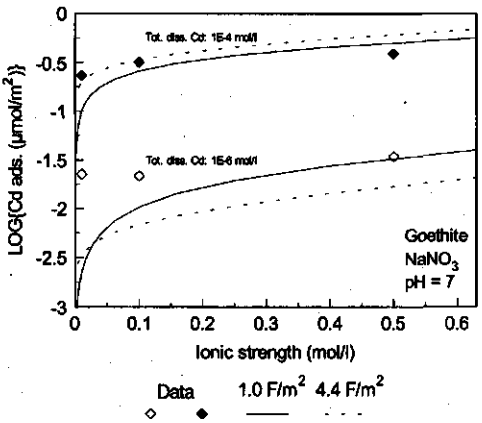


Fig. 5 The salt dependency ($NaNO_3$) of cadmium adsorption at pH = 7. The data points indicate the adsorption for two amounts of cadmium species in solution. The lines represent the NSM calculation for two values of the Stern layer capacitance, $C$ = 1.0 F/m² (solid) and $C$ = 4.4 F/m² (dashed)

The calculated H/Cd exchange ratio as a function of the capacitance, calculated using Eq. [14], for three salt levels is shown in Fig. 6. The capacitance has a large influence on the H/Cd exchange ratio. This can again be understood by interpreting the capacitance in terms of the Stern layer thickness. The closer the cadmium ion is to the surface, the higher will be the H/Cd exchange ratio. The predicted H/Cd exchange ratio for goethite at a salt level of 0.1 mol/l and a capacitance of 1.0 is 1.15.

This is much lower than the experimental value of 1.6. For the high capacitance the predicted value is better (1.71). The values calculated with Eq. [14] are only valid close to the PPZC and at very low cadmium concentrations. More information is needed to get a clear picture of the behaviour of the NSM with respect to the predicted values for the H/Cd exchange ratio.

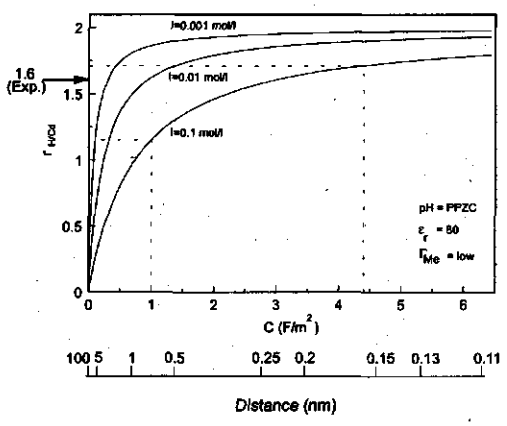


FIG. 6 The H/Cd exchange ratio as a function of the Stern capacitance, calculated with eq. [14]. The capacitance can be considered as a distance (Eq. [7]). The closer the cadmium is placed at the surface the higher the exchange ratio. The experimental value of r = 1.6 at a salt level of 0.1 mol/l. The dashed lines indicate the predicted values for the two different values of the capacitance that are considered in this text.

The general expression defining the H/Cd exchange ratio for the NSM follows from Eq. [15] (5).

$$r_{H/Cd} = \frac{\Delta\Gamma_H}{\Delta\Gamma_{Cd}} = \frac{\sigma_0 - \sigma_{0,Cd}}{\frac{1}{z_{Cd}}\sigma_{1,Cd}} = 2\,\frac{\sigma_0 - \sigma_{0,Cd}}{\sigma_{1,Cd}} \qquad [15]$$

in which $\Delta\Gamma_H$ is the change in the amount of adsorbed protons, $\Delta\Gamma_{Cd}$ is the change in the amount of adsorbed cadmium, $\sigma_0$ is the surface charge at fixed pH and no metal in the solution, $\sigma_{0,Cd}$ is the surface charge at the same pH at a given density of cadmium ion adsorption and $\sigma_{1,Cd}$ is the Stern plane charge at the same pH and cadmium ion adsorption density. The values for the different surface charges are

calculated with ECOSAT. In this way, a plot could be made of the cadmium concentration versus the H/Cd exchange at different values of the pH.

The calculated H/Cd exchange ratio (Fig. 7) shows a large pH dependency for the H/Cd exchange ratio which is not in accordance with the measured values. Moreover, the calculated ratio's are also much too low if the capacitance is assumed to be 1.0 F/m$^2$, and are not much improved by using a capacitance value of 4.4 F/m$^2$ (Fig. 7b).

We concluded, based on the analysis given above, that the Nernstian Stern model is of limited use for describing the adsorption of cations to metal (hydr)oxide surfaces. Firstly, the pH dependence of adsorption and the charging curve cannot be described with a simple set of parameters. In addition, the salt dependence and the H/Cd exchange ratio are poorly described. Finally, the absence of surface sites for protons is physically not very realistic. Examples of models with reactive surface sites will now be discussed.

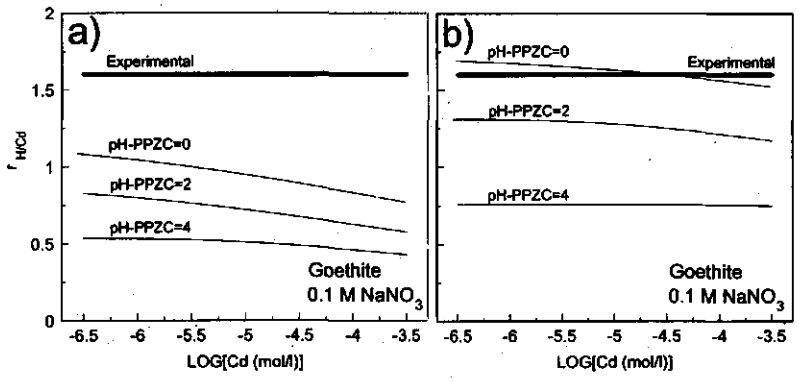


Fig. 7 The H/Cd exchange ratio of cadmium adsorption on goethite. The experimental value, represented by a bold solid line, is valid for a salt level of 0.1 mol/l ($NaNO_3$) and is independent of the pH. The model calculations, for three different values of the pH, as described with the NSM are represented by the solid lines. a) $C$= 1.0 F/m$^2$ b) $C$= 4.4 F/m$^2$

## 1 p*K* surface complexation models

Two different types of models with surface sites are commonly used, i.e., the 1 p*K* and 2 p*K* models (Fig. 1). The surface of a metal (hydr)oxide can be considered as

a combination of oxide, hydroxide and water groups. These surface O, OH, $OH_2$ groups can be coordinated to one or more metal ions in the solid. This leads to a kind of surface heterogeneity. The different surface groups will each have their own distinct proton affinity and charging characteristics (8,9). This complicated situation will be simplified here, by the use of only one charging reaction. For goethite, the basic protonation of the surface can thus be written as (17):

$$FeOH^{-½} + H^{+} \rightleftharpoons FeOH_2^{+½} \qquad K_H \qquad [16]$$

Because only one protonation step is involved, the model is called the 1 p$K$ model. The adsorption of cadmium at the goethite surface can be described by:

$$FeOH^{-½} + Cd^{+2} \rightleftharpoons FeOH^{-½}Cd^{+2} \qquad K_{Cd} \qquad [17]$$

Two different electrostatic models will be combined with this surface complexation model. First, a model with one charge free layer, the 1 p$K$ Basic Stern model (BSM) and then, a model with two charge free layers, the 1 p$K$ Three Plane model (TPM) will be discussed (Fig. 1, 2).

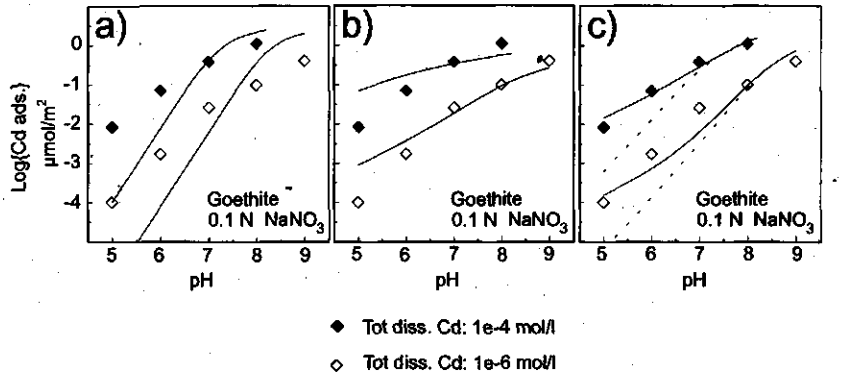


FIG. 8 The pH dependency of cadmium adsorption on goethite at ionic strength I = 0.1 mol/l, ($NaNO_3$). The points indicate the adsorption for two amounts of cadmium species in solution. The lines represent the BSM calculations; a) $Cd^{2+}$ placed in the 0-plane; b) $Cd^{2+}$ placed in the 1-plane; c) $Cd^{2+}$ and $CdOH^{+}$ placed in the 1-plane, the dashed line represents the model with only the CdOH in the 1-plane.

### *1 pK model with the Basic Stern approach (BSM)*

In the Basic Stern approach, two electrostatic planes are considered. These are separated from each other by an empty Stern layer with a capacitance $C_{Stern}$. The charge of the adsorbed protons is located in the surface plane. The $\sigma_0$ - pH curves can be described well, Using Eq. [16]. The optimal value of $C$ equals 1.1 F/m$^2$ (Table 2). In the BS approach, there are two options for placing specifically adsorbing cations: the charge of the adsorbing metal ion (Eq. [17]) can either be placed in the surface plane (0-plane) or in the Stern plane (1-plane).

Some workers prefer to place a strongly binding ion like cadmium in the 0-plane (Fig. 2). This can be interpreted as inner sphere complex formation (7). Using this assumption, the calculated pH dependency for cadmium sorption is much too high (Fig. 8). Therefore, this option is not very promising for the description of metal ion adsorption.

For the same reasons as mentioned in the discussion of the NSM, the placement of the cadmium ion close to the surface gives a high pH dependency. It could, therefore, be expected that placing the cadmium ion in the surface plane will also result in a too high a pH dependency. The pH dependency will decrease if the cadmium ion is placed in the outer electrostatic plane.

Table 2 Model parameters of the 1pK Basic Stern models for the description of the data set

| Parameters | $Cd_1$ | $(Cd+CdOH)_1$ | $Cd_0$ |
|---|---|---|---|
| $C$ (F/m$^2$) | 1.1 | 1.1 | 1.1 |
| $N_s$ (sites/nm$^2$) | 6 | 6 | 6 |
| $\log(K_H)$ | 9.3 | 9.3 | 9.3 |
| $\log(K_{Cd})$ | 6.5 | 5.7 | 7 |
| $\log(K_{CdOH})$ | Not used | -2.5 | Not used |

Placing the cadmium in the outer electrostatic plane, however, leads to too low a pH dependency (Fig. 8b). In general, a pH dependency that is too low can be increased by introducing a hydrolysed surface species (19). A feasible chemical reaction for the adsorption of the $CdOH^+$ species is given by Eq. [18];

$$FeOH^{-½} + Cd(H_2O)_n^{2+} \leftrightarrows FeOH^{-½}CdOH^{+1}(H_2O)_{n-1} + H^+ \qquad K_{CdOH} \qquad [18]$$

The presence of adsorbed cadmium as a $CdOH^+$ species in the outer Stern plane gives too high a pH dependency (Fig. 8c). The analysis given above suggests that the combination of $Cd^{2+}$ and $CdOH^+$ adsorption might yield better results. This is shown in Fig. 8c. The values of the equilibrium constants for the best fit are $\log K_{Cd} = 5.7$ and $\log K_{CdOH} = -2.5$. The difference between these two constants is not the same as the difference between these constants for solution species. The ratio (Cd)/(CdOH) in the solution is considerably smaller than the ratio (Cd)/(CdOH) on the surface.

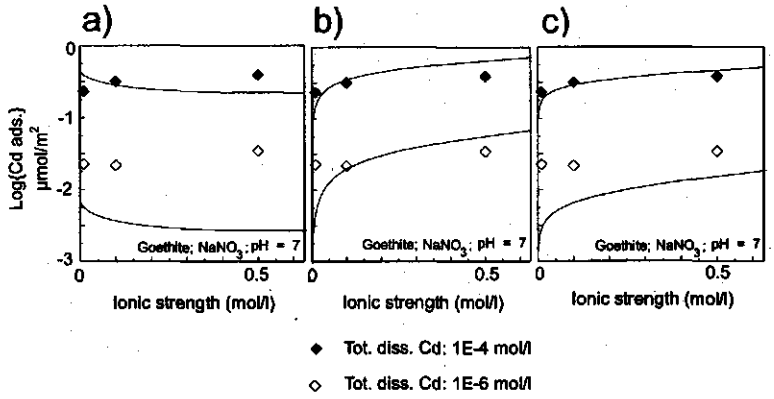


Fig. 9 The salt dependency ($NaNO_3$) of cadmium adsorption on goethite at pH = 7. The data points indicate the adsorption for two amounts of cadmium species in solution. The lines represent the BSM calculation; For the differences between a, b and c see the legend of Fig. 8.

The salt dependency of cadmium adsorption shows that adsorption of $Cd^{2+}$ in the 1-plane best describes adsorption at the two cadmium levels (Fig. 9). The H/Cd exchange ratio will first be considered for binding of Cd in the 1-plane. The H/Cd exchange ratio calculated for the model assuming binding of Cd in the 1-plane and using Eq. [15] shows that differences between the outer sphere BSM and the NSM (Fig. 7a) are small. This may be expected from the similarity of the models.

If both $Cd^{2+}$ and $CdOH^+$ are placed in the outer plane, then Eq. [15] cannot be used any more because these species have a different charge. A more general expression

to calculate the H/Cd ratio is needed. The calculation is, therefore, made on the basis of adsorbed amounts: the ratio of the change in adsorbed protons to the change in adsorbed cadmium. So Eq. [15] is rewritten as:

$$r_{H/Cd} = \frac{\theta_{H,Cd} - \theta_H}{\theta_{Cd}} \qquad [19]$$

in which $\theta_{H,Cd}$ is the fraction of protonated sites when metal is adsorbed, $\theta_H$ is the fraction of protonated sites at the same pH and salt level when no metal is present, and $\theta_{Cd}$ is the fraction of metal surface complexes at the same pH and salt level. The calculated H/Cd exchange ratio when both $Cd^{2+}$ and $CdOH^+$ are placed in the 1-plane is shown with dashed lines in Fig. 10. The introduction of the $CdOH^+$ species increases the H/Cd exchange ratio, but the model prediction is still not satisfactory.

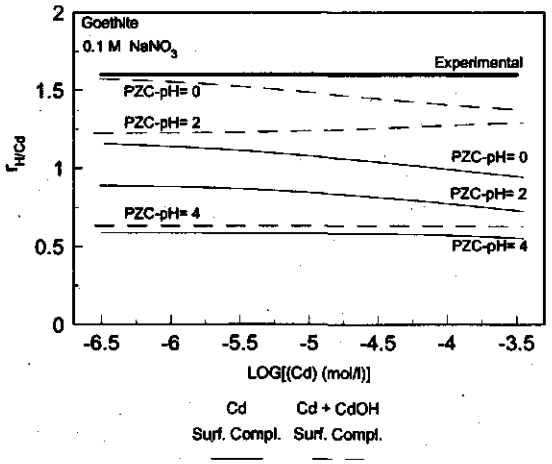


Fig. 10 The H/Cd exchange ratio of cadmium adsorption on goethite. The experimental value, represented by a bold solid line, is valid for a salt level of 0.1 mol/l ($NaNO_3$) and is independent of the pH. The thin lines refer to the model calculations for three values of the pH, assuming binding in the 1-plane of the BS model with two options; only surface Cd complexation (solid), both Cd and CdOH surface complexation (dashed).

In the case of binding in the 0-plane, the charge in the outer layer ($\sigma_1$) remains zero, so that Eq. [19] must be used for the calculation of the H/Cd exchange ratio. The calculated H/Cd exchange ratio is much higher than for the 1-plane approach,

but it is too high compared with the experimental value (Fig. 11). A high value for the H/Cd exchange ratio is to be expected when both cadmium and hydrogen ions are placed in the same electrostatic plane because the maximum electrostatic interaction is then possible.

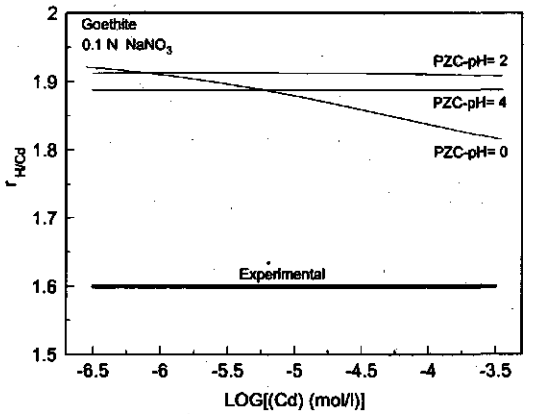


Fig. 11 The H/Cd exchange ratio of cadmium adsorption on goethite. The experimental value, represented by a bold solid line, is valid for a salt level of 0.1 mol/l ($NaNO_3$) and is independent of the pH. The model calculations, for three different values of the pH, as described with 0-plane approach of the BSM are represented by the solid lines.

It can be concluded that an electrostatic model with only one Stern layer does not result in a satisfactory description of all the observed adsorption phenomena. The 0-plane approach results in too high a pH dependency and the 1-plane approach in too low a pH dependency. The 1-plane approach using both the $Cd^{2+}$ and the $CdOH^{+}$ surface species improves the description.

These results can be compared with a physical-chemical interpretation of the BS model, in particular, the location of adsorbed ions in the double layer. In the BS approach, two options for the placement of the adsorbed $Cd^{2+}$ ions are possible. In the case of inner sphere complex formation, the $Cd^{2+}$ ion is treated as a point charge and it is placed in the surface plane. However, this does not lead to a satisfying description of the data because the $Cd^{2+}$ ion is too close to the adsorbing protons. The second option is placement of the adsorbing $Cd^{2+}$ ion in the 1-plane. According to the Stern concept (16), this is identical with the assumption that a $Cd^{2+}$ ion re-

mains hydrated at the head end of the DDL and conflicts with recent spectroscopic evidence of inner sphere complex formation on iron (hydr)oxides (20).

The results suggest that the cadmium ion should neither be placed in the surface plane nor in the outer plane. It seems logical to place the ion somewhere between these two planes since the cadmium ion is larger than a proton and smaller than the distance of closest approach of the hydrated counter ions. In the next section, the 1 p*K* model will be extended with an extra electrostatic plane in which the cadmium ion can be placed.

### *1 pK model with two Stern layers: the Three Plane Model (TPM)*

In the previous discussion, it was concluded that cadmium should be placed within the Stern layer, between the electrostatic planes. The introduction of an extra electrostatic plane in the Basic Stern model offers the possibility of placing the cadmium ion between the inner and outer planes (Fig. 12). We call this the Three Plane Model (TPM) since this makes clear that this model differs from the classical Triple Layer Model (TLM) in which three electrostatic planes are also used. The main differences between the TLM and the TPM are:

- In the TPM, the outer layer capacitance is not fixed on a value of 0.2 F/m$^2$ as in the TLM.
- In the TPM, pair forming ions (if considered), are placed in the 2-plane, in the TLM they are placed in the 1-plane.
- In the TPM, surface protonation is described with the 1 p*K* approach, in the TLM this is done with the 2 p*K* approach.

The fact that $C_2$ is not fixed on a value of 0.2 F/m$^2$ implies that the overall capacitance ($C_{TOT}$) can have a much higher value. The choice for a low capacitance is based on the idea that the overall capacitance of the compact part of the diffuse double layer should be comparable with the capacitance found for surfaces like AgI. As shown by Hiemstra and van Riemsdijk (21), this assumption is based on a misinterpretation of the compact part of the double layer of metal (hydr)oxides in relation to that of AgI. The low value of the capacitance of AgI is especially due to the presence of primary hydration water molecules fixed by the $Ag^+$ and $I^-$ ions, resulting in a very low dielectric constant. In the metal (hydr)oxide interface, only a layer with secondary hydration water is present. This layer has a much higher dielectric

constant. As a result, the capacitance of metal (hydr)oxides is much higher than that of AgI. For more details we refer to Hiemstra and van Riemsdijk 1991 (21).

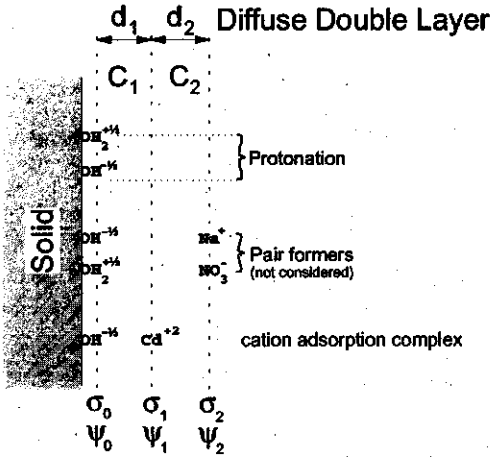


Fig. 12 Position of adsorbed ions in the interface, according to the 1pK Three Plane model. In the surface or the 0-plane, protons are located, the protonation is modelled as a 1 p$K$ model. Adsorbing Me ions are present in the 1-plane (intermediate plane). The 2-plane (outer plane) corresponds with the head end of the DDL, in this plane normally pair formers are placed.

The TPM approach is similar to the BSM for the description of the proton charging curve because the intermediate plane is empty. Hence, in order to obtain the same description of the charging behaviour, the overall capacitance of the two charge free layers in the TPM must equal the capacitance of the Stern layer in the BSM. This overall capacitance ($C_{TOT}$) for the compact part of the DDL is related to the capacitances of the two charge free layers according to:

$$C_{TOT} = \frac{C_1 C_2}{C_1 + C_2} \qquad [20]$$

in which $C_1$ is the capacitance of the inner layer and $C_2$ the capacitance of the outer layer. The description of the pH dependence of cadmium adsorption can be varied by varying the position of the plane in which the cadmium ion is placed. The position of the intermediate plane can be changed by varying the values of $C_1$ and $C_2$ under the condition that the overall capacitance remains constant, (Eq. [20]). The

TPM simplifies to the BSM when either $C_1$ or $C_2$ goes to infinity. In the case where $C_1 = \infty$, which is equivalent to $d_1 = 0$ (Eq. [7]), the intermediate plane coincides with the surface and the cadmium will be located in the 0-plane. For $C_2 = \infty$, the TPM results in the BSM with the cadmium ion located in the 1-plane. The optimized values of the model parameters are given in Table 3.

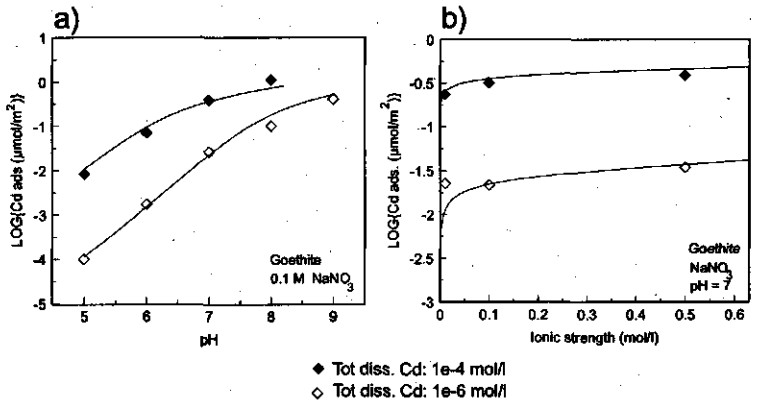


Fig. 13 The pH dependency of cadmium adsorption on goethite at ionic strength I = 0.1 mol/l, ($NaNO_3$). The points indicate the adsorption for two amounts of cadmium species in solution. The lines represent the TPM calculations (a), and the salt dependency ($NaNO_3$) of cadmium adsorption at pH = 7 (b). The data points indicate the adsorption for two amounts of cadmium species in solution. The lines represent the TPM calculation.

Table 3 Model parameters of the 1pK Three Plane model for the description of the data set

| Parameter | Value |
|---|---|
| $C_1$ (F/m$^2$) | 1.85 |
| $C_2$ (F/m$^2$) | 2.71 |
| $N_s$ (sites./nm$^2$) | 6 |
| $\log(K_H)$ | 9.3 |
| $\log(K_{Cd})$ | 7.4 |

The TPM description of both the pH dependency and the concentration dependence of cadmium adsorption is very good as can be seen in Fig. 13a. The salt dependence is also described very well (Fig. 13b). The TPM approach thus appears to be the most successful for the description of $Cd^{2+}$ adsorption on goethite.

The calculated H/Cd exchange ratio based on the TPM shows that it is still not optimal, as shown in Fig. 14. The calculated exchange ratio varies too much with pH and the values are all somewhat low. The calculated exchange ratio can be increased if the cadmium ions, present in the intermediate plane, are moved to the surface plane, but this will negatively affect the description of the pH dependency.

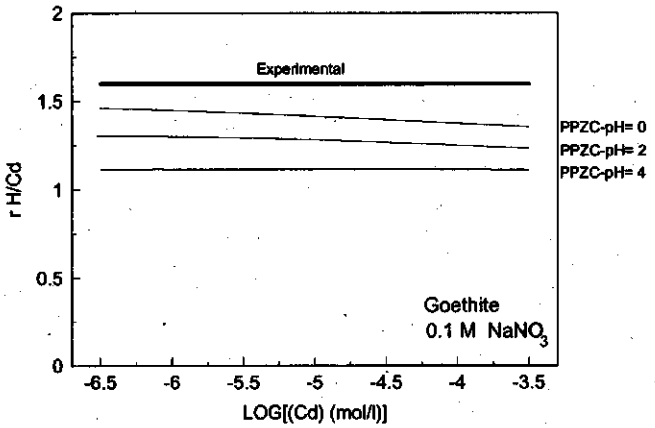


Fig. 14 The H/Cd exchange ratio of cadmium adsorption on goethite. The experimental value, represented by a bold solid line, is valid for a salt level of 0.1 mol/l ($NaNO_3$) and is independent of the pH. The model calculations, for three different values of the pH, as described with the TPM are represented by the solid lines.

## 2 p*K* surface complexation models

We are now at the point to discuss the last series of surface complexation models shown in Fig. 1, namely the models based on a 2 p*K* surface protonation approach. Models with a two step surface protonation are widely used (4,10,11,22). In these models, the charge of the surface groups can vary from -1 for a surface O, to 0 for OH and +1 for surface $OH_2$. The surface protonation is described with the following equilibria (2, 4, 18):

$$\begin{aligned} FeO^- + H^+ &\leftrightarrows FeOH^0 \qquad K_{a1} \\ FeOH^0 + H^+ &\leftrightarrows FeOH_2^+ \qquad K_{a2} \end{aligned} \qquad [21]$$

The difference in log *K* values is given by $\Delta$ p*K* ( = $\log(K_{a1}) - \log(K_{a2})$). The PPZC for the equilibria shown in Eq. [21] can be calculated as:

$$PPZC = \tfrac{1}{2} (\log(K_{a1}) + \log(K_{a2})) \qquad [22]$$

The 2 p$K$ approach must be combined with an electrostatic model. Two popular options are used in the literature: a purely diffuse model (4) and a triple layer model (2, 3). In both models, the adsorption of cadmium has been described by:

$$FeOH^0 + Cd^{2+} \leftrightarrows FeO^- Cd^{2+} + H^+ \qquad K_{b1} \qquad [23]$$

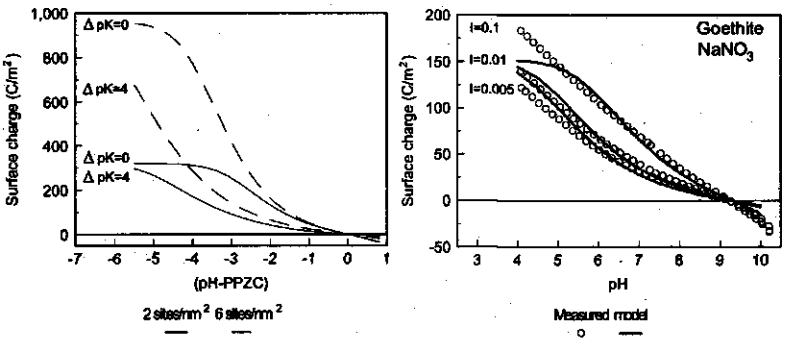


Fig. 15 Charging curves, calculated with the PDM for two site densities (2 sites/nm$^2$, solid lines and 6 sites/nm$^2$, dashed lines). For each site density two values of $\Delta pK$ are calculated (a). Experimental charging curves of goethite in $NaNO_3$ (circles) and the PDM description (lines) (b).

## *Purely diffuse 2 pK model (PDM)*

The 2 p$K$ PDM is described in detail by Dzombak and Morel (4). Various charging curves are shown for different sets of model parameters (Fig. 15). The purely diffuse double layer can lead to very high surface charging. Two factors can be used to prevent this extreme charging:

- The value of $\Delta$ p$K$ influences the slope of the titration curve; smaller values of $\Delta$ p$K$ reduce the charging (23).
- The site density determines the maximum surface charge; lower site densities reduce the charging.

In a recent evaluation it was concluded that the PDM description of titration curves (pH versus added acid) is relatively insensitive to variations in the site density (24). The contrary can be concluded for charging curves (pH versus surface charge) (Fig.

15); the PDM description of the charging curve is very sensitive to variations in the site density.

A site density of 0.95 sites/nm$^2$ and a $\Delta$ p$K$ of 2.5 (Table 4) leads to a reasonable description of our experimental surface charging data (Fig. 15b). Note the poor fit at low pH, corresponding with a high surface coverage of protons. This is related to the choice of a low site density. The model appears to be physically unrealistic, as the site density needed for a good description of the charging curves is much lower than the density which is derived from the surface structure of goethite, combined with adsorption data (14).

Table 4 Model parameters of the 2 pK diffuse double layer model for the description of the data set

| Parameter | Value |
|---|---|
| $N_s$ (sites/nm$^2$) | 0.95 |
| log($K_{a1}$) | 10.55 |
| log($K_{a2}$) | 8.05 |
| log($K_{b1H}$) | 1.6 |
| log($K_{b1L}$) | -1.6 |

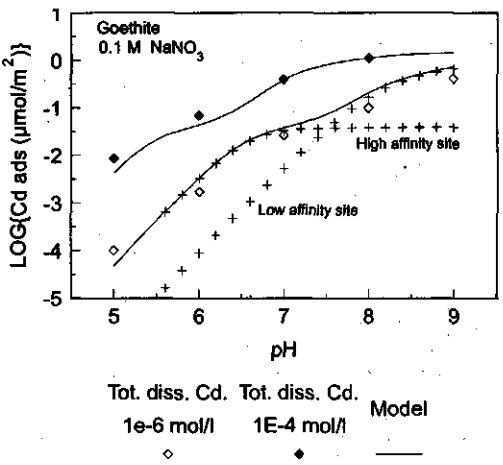


Fig. 16 The pH dependency of cadmium adsorption on goethite at ionic strength I = 0.1 mol/l, ($NaNO_3$). The points indicate the adsorption for two amounts of cadmium species in solution. The lines represent the PDM calculations. For the low Cd concentration the contributions of the high and the low affinity site to the calculation are indicated with markers (+).

In the PDM, the specifically adsorbed ions can only be placed at the surface, i.e., in the same electrostatic plane as the protons. It has been shown in the previous sections that this leads to a pH dependency that is greater than that observed. In order to improve the fit, Dzombak and Morel (4), used 2 types of surface sites, a high affinity site and a low affinity site. The pH dependence shown by the model (Fig. 16) when there is only one type of surface site is much higher than the model with two types of surface sites. Two sites with a log $K$ value of +1.6 and -1.6, respectively, give a reasonable description of the cadmium adsorption data.

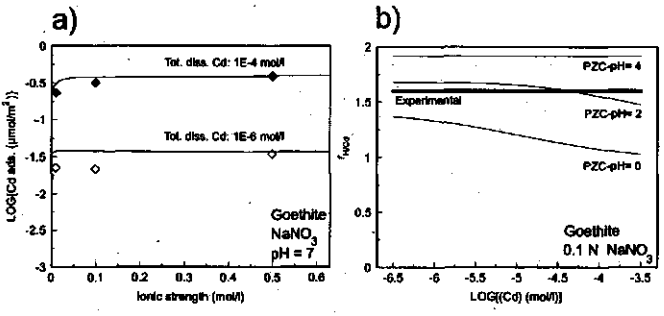


Fig. 17 The salt dependency ($NaNO_3$) of cadmium adsorption at pH = 7. The data points indicate the adsorption for two amounts of cadmium species in solution. The lines represent the PDM calculation (a), and the H/Cd exchange ratio of cadmium adsorption on goethite. The experimental value, represented by a bold solid line, is valid for a salt level of 0.1 mol/l ($NaNO_3$) and is independent of the pH. The model calculations, for three different values of the pH, as described with the PDM are represented by the solid lines (b).

The salt dependency of cadmium adsorption is also described well by this model (Fig. 17). The 2 p$K$ DDL model has a very low salt dependency. This is caused by the balance between the decrease in the activity coefficient for $Cd^{2+}$ in solution and the increase in the number of deprotonated sites with increasing salt concentration (4).

Like the other models, the PDM describes the H/Cd exchange ratio for cadmium on goethite rather poorly (Fig. 17). The model suggests that the exchange ratio is strongly pH dependent compared with the models with a charge free layer in the

interface. It predicts too high an exchange ratio at low pH's (PPZC-pH=4) and too low a ratio at high pH's (PPZC-pH=0).

For the description of cadmium on goethite, the absence of a charge free layer in the PDM has two consequences: 1) a low site density is required to describe the charging behaviour; and 2) a high affinity site is needed for cation adsorption in order to obtain a reasonable pH dependency. The low site density is especially problematic and physically unrealistic. In the earlier sections, it was concluded that two charge free layers are needed to obtain a physically realistic and flexible model. In the next section, a 2 p$K$ model with two charge free layers and a diffuse double layer will be discussed: the Triple Layer Model.

## *The Triple Layer Model (TLM)*

The Triple Layer Model has frequently been used for the description of ion adsorption on metal(hydr)oxides (10,11,22). The model is described in detail by Davis et al. (2,3). This model combines the 2 p$K$ surface protonation model with a three layer electrostatic model. The TLM as used in the literature is characterized by two important features: the low fixed capacitance of the outer charge free layer ($C_2$= 0.2 F/m$^2$), and the position and presence of ion pairs. Both aspects will be discussed briefly.

Table 5 Different model parameters for the TLM that give the same description of the charging behaviour.

| Parameter | $\Delta$ p$K$ = 0.0 | $\Delta$ p$K$ = 2.0 | $\Delta$ p$K$ = 4.0 | $\Delta$ p$K$ = 8.9 |
|---|---|---|---|---|
| $C_1$ (F/m$^2$) | 0.80 | 0.80 | 0.80 | 0.77 |
| $C_2$ (F/m$^2$) | 0.20 | 0.20 | 0.20 | 0.20 |
| $N_s$ (sites/nm$^2$) | 6 | 6 | 6 | 6 |
| log($K_{a1}$) | 9.3 | 10.3 | 11.3 | 14.0 |
| log($K_{a2}$) | 9.3 | 8.3 | 7.3 | 5.1 |
| log($K_{Na}$) | -0.5 | 0.1 | 1.0 | 4.0 |
| log($K_{NO3}$) | -0.5 | 0.1 | 1.0 | 3.15 |

While the outer layer capacitance ($C_2$) is normally fixed at 0.2 F/m$^2$, the inner layer capacitance can be adjusted, usually to values between about 1.0 and 1.4 F/m$^2$ (3).

As discussed in the section of the TPM, the low value of the outer layer capacitance was based on a misinterpretation of the compact part of the double layer of metal (hydr)oxides in relation to that of AgI (21).

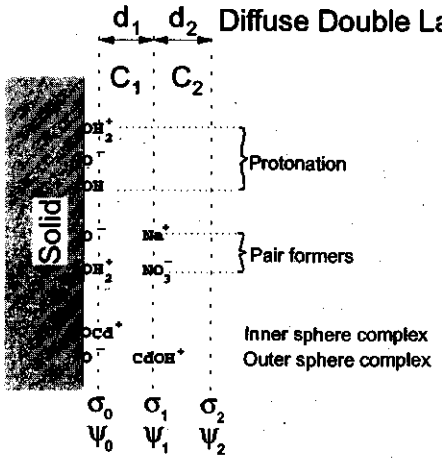


Fig. 18 Position of adsorbed ions in the interface, according to the Triple Layer model. Protons are located in the surface or the 0-plane, protonation is modelled with a 2 p$K$ model. The Me ions can be placed in the 0-plane (Cd complex) or the 1-plane (CdOH complex). Counter ions like Na and $NO_3$ are placed in the 1-plane. The 2-plane corresponds with the head end of the DDL.

The choice of a low fixed outer layer capacitance has two important consequences: 1) Pair formers are needed to give a proper description of the charging behaviour; and 2) these pair formers must be placed in the intermediate electrostatic plane. The ion pair reactions for the pair formers are (2):

$$\begin{aligned} FeO^- + Na^+ &\leftrightarrows FeO^- Na^+ & K_{Na} \\ FeOH_2^+ + NO_3^- &\leftrightarrows FeOH_2^+ NO_3^- & K_{NO_3} \end{aligned} \qquad [24]$$

One of the difficulties with the 2 p$K$ TLM is to determine the parameters that are responsible for the basic charging behaviour (25, 26). The single proton affinity constant in the 1 p$K$ approach follows directly from the value of the PPZC. In the TLM, the value of $\Delta$ p$K$ is an important parameter that is difficult to derive from the experimental information. It is known that a good description of the charging behaviour can be obtained with different values of $\Delta$ p$K$ (27). This is because an in-

crease in the value of Δ p$K$ can be compensated for by increasing the log $K$ values of the pair formers. Some different combinations of the model parameters are given that give a good description of the charging behaviour (Table 5). Note that for the highest value of Δ p$K$, the pair formation constants are "asymmetric".

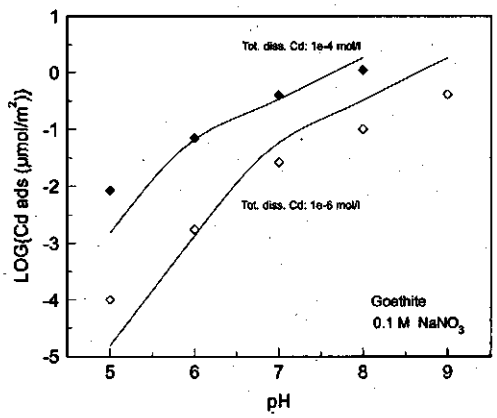


FIG. 19 The pH dependency of cadmium adsorption on goethite at ionic strength I = 0.1 mol/l. The points indicate the adsorption for two amounts of cadmium species in solution. The lines represent the TLM calculations using Δ p$K$=5.7.

The reason for the asymmetric pair formation can be explained from the influence of Δ p$K$ on the charging curve. The influence of Δ p$K$ on the charging behaviour for the TLM is similar to that for the PDM (Fig. 15). For large values of Δ p$K$, the slope of the described charging curve close to the PPZC will be too low. This slope can be increased by introducing asymmetric pair formers. However, when asymmetric pair formers are used, the intersection point no longer coincides with the point ½ ($\mathrm{Log}K_{a1}$+ $\mathrm{Log}K_{a2}$). The influence of these basic charging parameters on the description of the cadmium data will be discussed below.

From the previous discussions, it is clear that both the surface complexation constants and the position of the adsorbing ion in the interface have large influence on the description of cation adsorption. The possible location of the ions in the TLM are shown in Fig. 18. In a study by Hayes et al. (7), it was found that placing the cadmium ion in the intermediate plane leads to too high a salt dependency. A better result was obtained when the cadmium ion was placed in the surface plane. Accor-

ding to Hayes, this approach resulted in a good description of both the pH and salt dependency. In this study, therefore only this option will be considered.

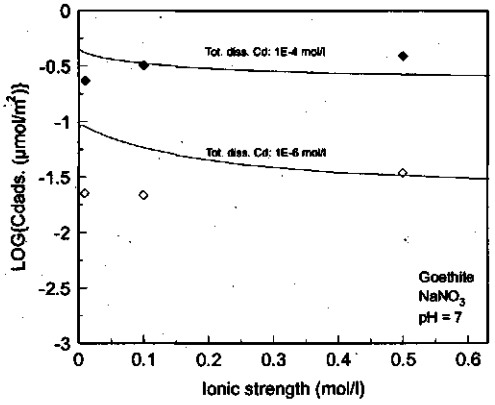


Fig. 20 The salt dependency ($NaNO_3$) of cadmium adsorption at pH = 7. The data points indicate the adsorption for two amounts of cadmium species in solution. The lines represent the TLM calculation

Table 6 Model parameters of the TLM for the description of the cadmium adsorption data

| Parameter | Value |
|---|---|
| $C_1$ (F/m$^2$) | 0.8 |
| $C_2$ (F/m$^2$) | 0.2 |
| $N_s$ (sites/nm$^2$) | 6.0 |
| log($K_{a1}$) | 12.4 |
| log($K_{a2}$) | 6.7 |
| log($K_{Na}$) | 2.3 |
| log($K_{NO3}$) | 1.7 |
| log($K_{Cd}$) | -1.0 |

The description of the pH dependence of cadmium adsorption, as given by the TLM with binding at the 0-plane, is strongly dependent on the value of $\Delta$ p$K$. For low values of $\Delta$ p$K$, the description resembles the 1 p$K$ inner sphere description (BSM),

i.e., a very high pH dependency. The pH dependence decreases with increasing Δ p$K$ (27). The decrease in the pH dependence is only significant, however, for values of Δ p$K$ that are larger than 4. This improves the possibilities for fitting the data, since the charging data can be described with a wide range of Δ p$K$ values. The model description is shown for Δ p$K$ = 5.7 in Fig. 19 (see Table 6). Although the cadmium and hydrogen ions are placed in the same plane, the result is much better than for the 1 p$K$ BSM with binding in the 0 plane. The description is, however, far from satisfactory, especially at low metal ion concentrations.

The salt dependence described by the TLM is shown in Fig. 20. The description is reasonable, but is still far from optimal, and predicts the opposite trend to that observed. The calculated H/Cd exchange ratio is too high for all pH values (see Fig. 21). Positioning cadmium in the 0-plane leads to too large a pH dependency and too high a value for the H/Cd exchange ratio. The description for both aspects can be improved by placing the cadmium ion in the intermediate plane, but this will result in too high a salt dependency (7). The analysis shows that the TLM cannot give a satisfactory description of all of the major adsorption phenomena simultaneously (charging curves, pH and salt dependency of cadmium sorption, hydrogen cadmium exchange).

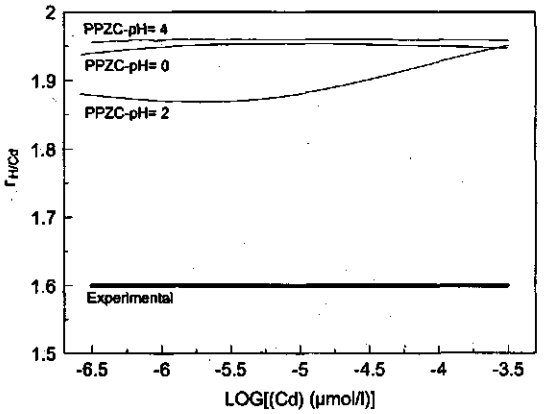


Fig. 21 The H/Cd exchange ratio of cadmium adsorption on goethite. The experimental value, represented by a bold solid line, is valid for a salt level of 0.1 mol/l ($NaNO_3$) and is independent of the pH. The model calculations, for three different values of the pH, as described with the TLM are represented by the solid lines.

## Conclusions

An evaluation of the model behaviour for Cd ion adsorption leads to the following conclusions:

None of the models discussed can describe all of the data satisfactorily. The release of protons upon $Cd^{2+}$ adsorption of cations seems to be the most difficult phenomenon to describe.

The behaviour of the Nernstian Stern Model (NSM) in terms of the charging behaviour and cadmium adsorption, is very similar to that of the 1 p$K$ Basic Stern Model (BSM). In fact, the NSM can be considered as a 1 p$K$ BSM with $N_s = \infty$.

The 1 p$K$ Basic Stern model can describe the charging behaviour of the metal (hydr)oxide surface very well. The pH dependence of Cd adsorption is controlled by the location of the ion in the interface either as an inner or outer sphere adsorption complex. The presence of both a Cd and a CdOH complex in the 1-plane gives a reasonable description of the cadmium adsorption data. In this case, however, neither the salt dependency, nor the H/Cd exchange ratio are described satisfactorily. The presence of specifically adsorbed Cd ions at the head end of the DDL, separated from the surface by the Stern layer, is in conflict with spectroscopic evidence for inner sphere complex formation.

The 1 p$K$ model in combination with three electrostatic planes (the Three Plane Model) seems a physically logical model that leads to a good description of most adsorption phenomena: the charging behaviour, pH and salt dependence of cation adsorption. The predicted H/Cd exchange ratio, however, is somewhat too low compared to the experimental value.

The 2 p$K$ DDL model can only describe the charging data reasonably well by invoking a very low total site density. The charging data at low pH, compared with the model description, indicate that the approach may not be physically realistic. By assuming a combination of high and low affinity sites for cadmium, a reasonable description of most phenomena can be obtained apart from the H/Cd exchange ratio.

The 2 p$K$ triple layer model can describe the basic charging behaviour by using a

wide range of model parameters.
The description of the pH dependency of cadmium binding is far from optimal. The best description for adsorption in the 0-plane necessitates a large value of $\Delta$ p$K$ and asymmetric pair formation with electrolyte ions. The prediction of the H/Cd exchange ratio is very poor.

**Acknowledgement:**
Part of this work is financed by the European Community through contract STEP-CT90-0031.

## References


1. Benjamin M. M., and Leckie J. O., Multiple-site adsorption of Cd, Cu, Zn and Pb on amorphous iron oxyhydroxide, *J. Colloid Interface Sci.* **79**, 209-221 (1981)
2. Davis J.A., James R.O., and Leckie J.O., Surface ionization and complexation at the oxide/water interface. I. Computation of electrical double layer properties in simple electrolytes, *J. Colloid Interface Sci.* **63**, 480-499 (1978)
3. Davis J.A., and Leckie J.O., Surface ionization and complexation at the oxide/water interface. II. Surface properties of amorphous iron oxyhydroxides and adsorption of metal ions, *J. Colloid Interface Sci.* **67**, 90-107 (1978)
4. Dzombak. D.A., and Morel F.M.M., Surface complexation modelling, Hydrous Ferric Oxide, (D.A. Dzombak, F.MM. Morel, Eds.), John Wiley and Sons, New York, 1990
5. Fokkink, L.G.J., Ion adsorption on oxides; surface charge formation and cadmium binding on rutile and hematite, PhD. thesis W.A.U. dept. Fys. and Coll. Chemistry, 1987
6. Fokkink L.G.J., Keizer A. de, and Lyklema J., Temperature dependance of cadmium adsorption on oxides, *J Colloid Interface Sci.* **135**, 118-131 (1990)
7. Hayes K.F., and Leckie J.O., Modeling ionic strength effects on cation adsorption at hydrous oxide/solution interfaces, *J. Colloid Interface Sci.* **115**, 564-572 (1987)
8. Hiemstra, T, Riemsdijk, W.H. van, and Bolt, G.H., Multisite Proton Adsorption Modeling at the Solid/Solution Interface of (Hydr)oxides: A New Approach, I. Model Description and Evaluation of Intrinsic Reaction Constants, *J. Colloid Interface Sci.* **133**, 91-104 (1989)
9. Hiemstra, T, de Wit J.C.M., and van Riemsdijk W.H., Multisite Proton Adsorption Modeling at the Solid/Solution Interface of (Hydr)oxides: A New Approach, II. Application to various Important (Hydr)oxides, *J. Colloid Interface Sci.* **133**, 105-117 (1989)
10. Davis J.A., and Kent D.B., *in* "Mineral-Water Interface Geochemistry, Reviews in Mineralogy" (M.F. Hochella and A.F. White eds.) , Vol. 23, 177-260, Mineralogical Society of America, Washington D.C. (1990)
11. Goldberg S., Use of surface complexation models in soil chemical systems, *Advances in Agronomy*, Vol. 47, 233-329 (1992)
12. Atkinson R.J., Posner A.M., and Quirk J.P., Adsorption of potential-determining ions at the ferric oxide-aqueous electrolyte interface, *J. Phys. Chem.* **71**, 550-558 (1967)
13. Venema P., Hiemstra T., and van Riemsdijk W.H., Multi site modelling of cadmium adsorption on Goethite, *J. Colloid Interface Sci.* **183**, in press (1996)
14. Hiemstra T.and van Riemsdijk W.H., A surface structural approach to ion adsorption: The charge distribution (CD) model, *J. Colloid Interface Sci.* **179**, 488-508 (1996)
15. Keizer M.G., and van Riemsdijk W.H., ECOSAT; Technical Report of the Departments Soil Science and Plant Nutrition; Wageningen Agricultural University; Wageningen 1994
16. Bolt G.H., and van Riemsdijk W.H., The ionic distribution in the diffuse double layer; *In*: "Soil chemistry; B. physico chemical models", (Bolt G.H., Ed.), Elsevier scientific publishing comp. Amsterdam, 1982
17. Stumm W., and Morgan J.J., *in* "Aquatic chemistry; An introduction emphasizing chemical equilibria in Natural Waters ", (W. Stumm, Ed.), John Wiley and Sons, New York, 1981
18. Stern O., Zur theorie der elektrolitischen doppelschicht, *Z. Elektrochem.* **30**, 508-516 (1924)

19. van Riemsdijk W.H., de Wit J.C.M., Koopal L.K., and Bolt G.H., Metal ion adsorption on heterogeneous surfaces: Adsorption models, *J. Colloid Interface Sci.* **116**, 511-522 (1987)
20. Spadini L., Manceau A, Schindler P.W., and Charlett L., Structure and stability of $Cd^{2+}$ surface complexes on Ferric Oxides, *J. Colloid Interface Sci.* **168**, 73-86 (1994)
21. Hiemstra T., and van Riemsdijk W.H., Physical-chemical interpretation of primary charging behaviour of metal (hydr)oxides, *Colloids and Surfaces* **59**, 7-25 (1991)
22. Smith R.W., and Jenne E.A., Compilation, Evaluation and Prediction of Triple-Layer Model constants for ions on Fe(III) and Mn(IV) oxides; Report U.S. Dept. of Energy contract DE-AC06-76RLO 1830; November 1988
23. Bolt G.H., and van Riemsdijk W.H., Ion adsorption on inorganic variable charge constituents; *In*: "Soil chemistry; B. physico chemical models", (Bolt G.H. Ed.), Elsevier scientific publishing comp., Amsterdam, 1982
24. Hayes K.F., Redden G.W., Wendell E. and Leckie J.O., Surface complexation models: An evaluation of model parameter estimation using FITEQL and oxide mineral titration data, *J. Colloid Interface Sci.* **142**, 448-469 (1991)
25. Lützenkirchen J., Magnico P., and Behra P. (1995) Constraints upon electrolyte binding constants in Triple-Layer Model calculations and consequences of the choice of the thermodynamic framework, *J. Colloid Interface Sci.* **170**, 326-334 (1995)
26. Righetto L., Azimonti G., Missana T., and Bidoglio G., The Triple Layer Model revised, *Colloids and Surfaces A*. **95**, 141-157 (1995)
27. Katz L.E., and Hayes K.F., Surface complexation modeling I. Strategy for modeling monomer complex formation at moderate surface coverage, *J. Colloid Interface Sci.* **170**, 477-490 (1995)

# 3

# Multi site adsorption of cadmium on goethite

Peter Venema, Tjisse Hiemstra, Willem H. van Riemsdijk
Journal of Colloid and Interface Science, Vol. 183, p. 515-527, 1996

# Multi site adsorption of cadmium on goethite


## Abstract

*Recently a new general ion adsorption model has been developed for ion binding to mineral surfaces (Hiemstra and van Riemsdijk 1996). The model uses the Pauling concept of Charge distribution (CD) and is an extension of the MUltiple SIte Complexation (MUSIC) approach. In the CD-MUSIC model the charge of an adsorbing ion that forms an inner sphere complex is distributed over its ligands which are present in two different electrostatic planes.*

*In this paper we have applied the CD-MUSIC model to the adsorption of metal cations, using an extended data set for cadmium adsorbing on goethite. The adsorption of cadmium and the cadmium-proton exchange ratio were measured as function of metal ion concentration, pH and ionic strength. The data could be described well, taking into account the surface heterogeneity resulting from the presence of two different crystal planes (the dominant 110 face and the minor 021 face). The surface species used in the model are consistent with recent EXAFS data. In accordance with the EXAFS results, high affinity complexes at the 021 face were used in the model.*


## Introduction

The adsorption of cations on metal (hydr)oxide surfaces has been studied extensively. The chemical behaviour of metal (hydr)oxides is strongly determined by their charging behaviour and so the modelling of ion adsorption behaviour is most successful when an electrostatic model is combined with a surface complexation model (1). Although a large number of such models exist, none can simultaneously describe satisfactory all of the various adsorption phenomena shown by an extended data set (2). The proton/metal ion exchange ratio, i.e. the number of protons that desorb per adsorbed cadmium ($r_{H/Cd}$), is particulary difficult to describe with these models. This ratio is important for predicting metal ion transport through poorly buffered media containing metal (hydr)oxides (3).

A new adsorption model, referred to as the CD-MUSIC model, has been developed (4) to describe ion adsorption at metal (hydr)oxide surfaces. The model emphasizes the importance of the surface structure and of the charge distribution at the interfaces. In this paper, we apply this charge distribution model to an extensive set of

cadmium adsorption data on goethite.

The surface structure of the dominant crystal faces of goethite is derived from the crystallographic structure and from information found from electron microscopy and Atomic Force Microscopy (5, 6, 7). A schematic view of the different features of the model is shown in Fig. 1 .

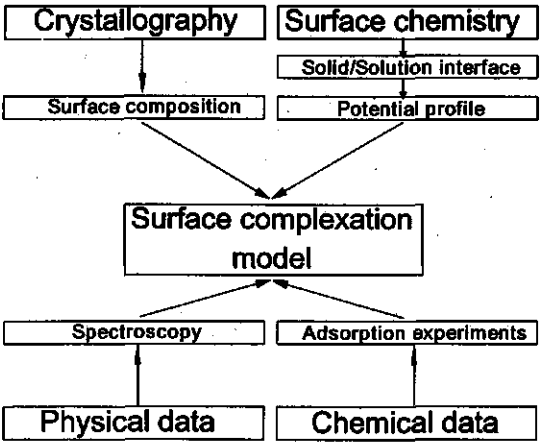


Fig. 1 Summary of the important features for the charge distribution model. Information about the surface composition is obtained from crystallography. The model of the surface/solution interface should be in accordance with surface chemistry. The character of adsorption complexes can be specified with spectroscopic data. The model is calibrated with data from adsorption experiments.

Considering the crystal structure of a metal (hydr)oxide, a wide variety of ion surface complexes may exist. The choice for a surface complex can influence the description of the chemical data considerably. It is therefore necessary to constrain the number of possible surface complexes. Recent advances in surface spectroscopy give the possibility to obtain information about the nature of surface complexes. Recent spectroscopic EXAFS data (8) are used to define the type of surface species.

## Model description

### *MUlti SIte Complexation (MUSIC)*

Metal (hydr)oxide surfaces show a variable charging behaviour. The surface charge of metal (hydr)oxides strongly influences their adsorption behaviour and vice versa.

Therefore, a thorough understanding of the charging behaviour on the surface provides a sound basis for modelling chemical adsorption.

A popular approach for the description of surface charging behaviour is a complexation model with a single site which protonates in two consecutive protonation steps (1,9). Surfaces are, however, heterogeneous due to a different number ($n$) of metal ions of the solid, coordinating with the surface oxygens (10,11). The two corresponding protonation reactions can be written as for iron oxide:

$$Fe_nO^{-2+n\cdot\frac{1}{2}} + 2\ H^+ \overset{K_{n,1}}{\rightleftharpoons} Fe_nOH^{-1+n\cdot\frac{1}{2}} + H^+ \overset{K_{n,2}}{\rightleftharpoons} Fe_nOH_2^{n\cdot\frac{1}{2}} \qquad [1]$$

in which $n$ is the number of underlying iron ions for the surface (hydr)oxide. The value ½ is the so called bond valence that follows from the Pauling's principle of charge distribution (12), defined as the charge of the central ion (+3 for Fe) is divided over its surrounding ligands (6 for Fe).

It has been shown that the log $K_H$ of both consecutive reactions differs strongly. This implies that only one of the both steps is of relevance for the charging behaviour (10). For singly coordinated surface groups, the relevant reaction is:

$$FeOH^{-\frac{1}{2}} + H^+ \rightleftharpoons FeOH_2^{+\frac{1}{2}} \qquad K_{1,2}$$

Protonation and deprotonation of the doubly coordinated surface group $FeOH^0$ is not important in the normal pH range, which implies that the $Fe_2OH^0$ species is dominant (10,11). Therefore the doubly coordinated surface groups are assumed to be inert under normal conditions.

The triply coordinated $Fe_3O^{-\frac{1}{2}}$ groups show only one protonation step because in the $Fe_3OH^{+\frac{1}{2}}$ groups, all oxygen orbitals are occupied. The relevant reaction is:

$$Fe_3O^{-\frac{1}{2}} + H^+ \rightleftharpoons Fe_3OH^{+\frac{1}{2}} \qquad K_{3,1}$$

### *The CD-MUSIC approach*

The above concept of Pauling charge distribution has recently been extended to surface complex formation and is called the CD-MUSIC model (4).

In the CD-MUSIC model, a part of the charge of a specific adsorbed cation is attributed to the common ligands present in an electrostatic plane called the 0 plane (Fig. 2). The other part of the charge of the adsorbed cation is attributed to the solution-oriented ligands present in a second electrostatic plane, the 1-plane (Fig. 2). In the model the fraction of the charge of the central ion that is placed in the 0-plane is defined with a factor $f$ (see appendix). Besides the two electrostatic planes mentioned a third plane is distinguished, indicated as the d-plane (Fig. 2), in which the ion pairs are positioned.

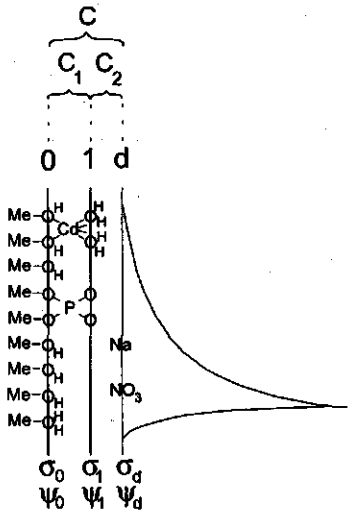


Fig. 2 Schematic representation of the solid / solution interface. The charge free layer is divided into two parts in case of specific adsorption of ions. Adsorbed protons and surface-oriented ligands of adsorbed ions are placed in the surface plane (subscript 0). The intermediate plane (subscript 1) is necessary for the solution-directed ligands of adsorbed ions. Pair forming ions are placed in the outer plane (subscript d).

In the case of absence of surface complex formation, the compact part of the double layer between the surface and the diffuse double layer does not contain any ions and the model becomes identical with the Basic Stern layer approach. The capacitance of this Stern layer ($C$) can be derived from basic charging experiments. The presence of adsorbed complexes with corresponding ligands separates the Stern layer into two parts. The values for $C_1$ and $C_2$ should be in accordance with the previously determined overall capacitance $C$. In this study, the capacitance of the outer layer ($C_2$) has been set to 5 F/m$^2$, based on physical-chemical interpretation of the interface region (13) and anion adsorption data (4). So, the value of $C_2$ is not a variable parameter. The above sketched electrostatic approach (Fig. 2) will be referred to as the Three Plane Model (TPM).

The affinity constant of a reaction can be split into an intrinsic part ($K_{int}$) in which no electrostatic influence is considered, and an electrostatic contribution (1, 4, 9):

$$K = K_{int} \cdot e^{-\frac{\Delta G_{el}}{RT}} \qquad [4]$$

The change in the electrostatic energy ($\Delta G_{el,i}$) upon ion adsorption, in an electrostatic plane $i$ with potential $\psi_i$, is directly related to the change in charge $\Delta z_i$ in that plane according to:

$$\Delta G_{el,i} = \frac{\Delta z_i \cdot F}{R \cdot T} \cdot \psi_i \qquad [5]$$

The total change in electrostatic energy due to the adsorption of an ion is given by the summation of changes in the different electrostatic planes:

$$\Delta G_{el} = \sum_i \frac{\Delta z_i \cdot F}{R \cdot T} \cdot \psi_i \qquad [6]$$

Application of eq. [6] and details of the calculation method are discussed in the appendix.

### *Comparison of the CD-MUSIC model with other models*

In a previous study (2), five different surface complexation models for cadmium adsorption on goethite were compared. All these models treat ions as point charges. It was concluded that only three of these models could give a reasonable description of the pH and salt dependency of cadmium adsorption simultaneously. None of these models could give a satisfactory description of the proton/metal exchange. Two widely used models that gave reasonable results in the study were the so called Triple Layer Model (TLM) (14,15,16) and the Purely Diffuse double layer Model (PDM) (17). The PDM, however, cannot give a satisfying description of the charging curves of a metal(hydr)oxide (2). The TLM may be confused with the previous mentioned Three Plane Model (Fig. 2) used in the CD-MUSIC approach, but there are three important differences:

- In the TLM the outer layer capacitance is fixed on a value of 0.2 F/m$^2$, in the TPM the value is 5 F/m$^2$.
- In the TLM pair forming ions are placed in the 1-plane, in the CD-MUSIC approach they are placed in the d-plane.
- In the TLM, an specifically adsorbing cation is considered as a point charge posi-

tioned in one electrostatic-plane, in the CD-MUSIC approach, the charge of the cation is divided over two electrostatic planes (0-plane and 1-plane).

The choice for a low value of $C_2$ in the TLM is based on the idea that the overall capacitance of the compact part of the diffuse double layer should be comparable with the capacitance found for surfaces like AgI. As shown by Hiemstra and van Riemsdijk (13), this assumption is based on a misinterpretation of the compact part of the double layer of metal (hydr)oxides in relation to that of AgI.

### *The surface composition of goethite*

The dominant crystal planes of goethite are the 110 and the 021 plane (5,6). Electron micrographs have shown that the goethite crystals used in this study are needle shaped. The cross sections of the needles are diamond shaped which indicates that the 110 crystal faces predominate. The head faces of the crystal are 021 faces. Based on the length of the crystals, we estimate that for our goethite, the surface consists of about 90% 110 face and 10% 021 face. A schematic representation of the goethite crystal is shown in Fig. 3.

In the crystal structure of goethite the oxygens are all triply coordinated with respect to Fe. Two types of oxygens can be distinguished in goethite (αFeOOH), unprotonated $Fe_3O$ (indicated as $Fe_3O(l)$) and protonated $Fe_3OH$ (indicated as $Fe_3O(h)H$), suggesting respectively a low (l) and a high (h) proton affinity (Fig. 4). At the surface, the coordination of these two types of oxygen can differ from three.

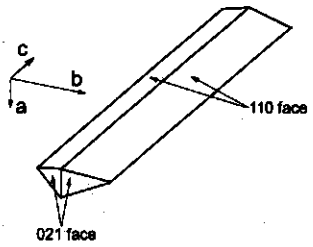


Fig. 3 Schematic presentation of the goethite crystal morphology

In crystallography, the chemical composition of a crystal face is usually found by cutting the crystal in the plane with the highest metal density (18). For the 110 plane, this leads to the surface composition shown in Fig. 4a. The triply coordinated surface groups are dominant and are ordered in rows parallel to the c-axis. Each row of surface oxygens represents a site density of 3 sites/nm$^2$. In a unit "cell", there are three rows of triply coordinated groups, one row of doubly co-

ordinated groups and one row of singly coordinated groups. It has been suggested that the triply coordinated O(l) has a low proton affinity and the triply coordinated O(h) surface group has a high proton affinity (4). One triply coordinated group with a low proton affinity in combination with one triply coordinated group with a high proton affinity will together result in a relatively inert combination (11). According to Hiemstra and van Riemsdijk (4) the remaining groups will determine the charging of the 110 face. The proton affinities for these two different types of surface groups is high but we do not know the exact log $K$ values of these groups and therefore both their proton affinities are set equal to the value of the pristine point of zero charge (*PPZC*).

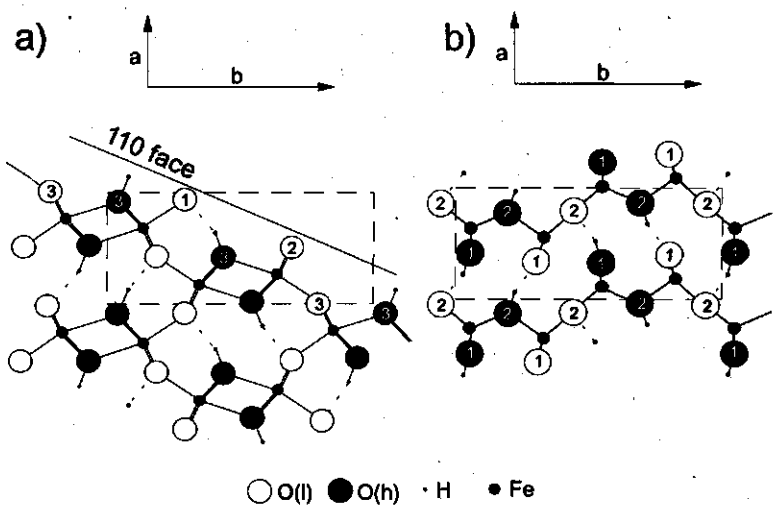


Fig. 4 Schematic picture of the cross section of the goethite crystal, perpendicular to the c-axis, showing the surface composition of the 110 face (a) and the 021 face (b). The large circles represent oxygens, the smaller circles represent underlying iron ($Fe^{3+}$) ions; protons are represented by black dots. The oxygens are protonated (O(h), black circles) or unprotonated (O(l), gray circles). The surface oxygens have a number, refering to their coordination number with iron of the solid. The chemical bond between two atoms is represent with lines. Fig. 4a shows that at the 110 face different triply coordinated surface groups will exist ($Fe_3O(h)H$ and $Fe_3O(l)$). The 021 face (b) has rows of singly and doubly coordinated surface groups that are connected by a hydrogen bridge. The singly and doubly coordinated groups are alternatingly protonated and deprotonated. The dashed box indicates the unity cell.

The chemical composition of the 021 face is quite different from that of the 110 face (Fig. 4b). On this face, rows of singly and doubly coordinated groups alternate. At the surface all surface groups share a proton with a neighbouring surface group

(see Fig. 4b). Half of the singly and half of the doubly coordinated surface groups is initially protonated (O(h)), the other half not (O(l)). Hence, two different kinds of singly and doubly coordinated groups occur at the surface. For reasons of simplicity, however, these differences will not be considered here in terms of proton binding. The surface groups on this crystal face are assumed to have the same proton affinity as the surface groups with the same coordination number on the 110 face. However, the affinity of cadmium will differ for the surface groups at the different crystal faces, as will be explained later.

Using the above surface structure for goethite, many aspects of the phosphate adsorption behaviour have been described very well (4). The same approach will now be used for the description of cadmium adsorption data by goethite.

### *Cadmium surface complexes on goethite*

The crystal structure of goethite, as discussed above, leads to a limited number of possible positions for adsorbed cadmium ions. EXAFS measurements done by Spadini et al. (8) suggest that adsorbed cadmium has the same structural environment as iron and that the cadmium ion can substitute for iron in the goethite crystal. This implied that cadmium will adsorb at growth positions for iron (8). Furthermore it was found that two different cadmium-iron distances predominate at the goethite interface. The two different cadmium-iron distances have been interpreted in terms of specific surface complex structures, namely an edge and a corner linkage (8). Both the cadmium and the iron are considered to have a sixfold coordination i.e. forming octahedra with oxygen ligands (O, OH, $OH_2$) (8). In a corner linkage, the cadmium octahedron shares a corner with one or more iron octahedra (8). This is illustrated in Fig. 5 in which an example is given for monodentate (Fig. 5a) and bidentate (Fig. 5b) complexes. With the edge linkage, the cadmium octahedron shares an edge with one or more iron octahedra (8). Examples for this linkage are shown in Fig. 6. Edge linkages can never occur in a monodentate complex because always two surface groups are involved.

Based on the assumption that adsorbed cadmium ions have the same structural environment as iron, triply coordinated surface groups will not be involved in the cadmium adsorption proces (8).

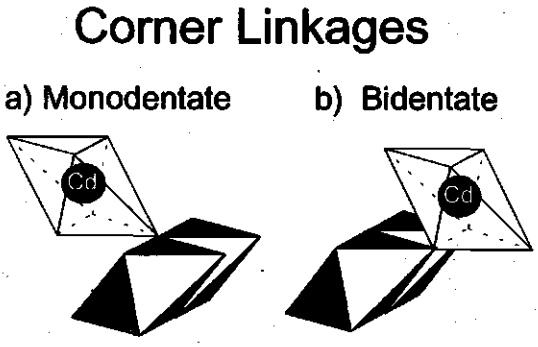


Fig. 5 Structural positions of adsorption Cd, linked to Fe-filled octahedra via corners forming a monodentate (a) or a bidentate (b).

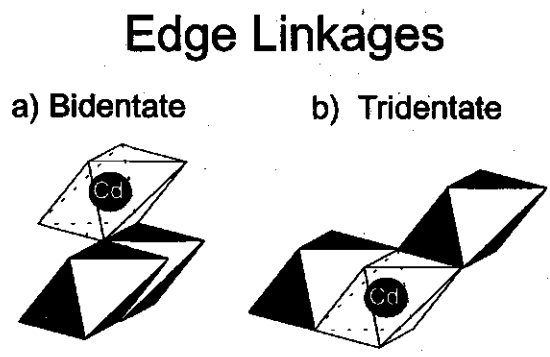


Fig. 6 Structural positions of adsorption Cd, linked to Fe-filled octahedra via edges forming a bidentate (a) or a tridentate (b).

In principle, cadmium may form at the 110 face monodentate and bidentate complexes with doubly and singly coordinated oxygens respectively, leading to two possible configurations (Fig. 7). For both options, it can be seen that the adsorbing octahedra and the crystal octahedra share only corners (C-linkage) (8). It is not possible to estimate individual log $K$ values for these complexes with the available data. Further it has been suggested that the singly coordinated surface groups are the most important reactive surface groups for specific adsorption (19). Therefore in the current model, only cadmium bidentate species are assumed to form on the 110 face. The corner linkage, leading to bidentate surface complexation with the singly coordinated surface groups can be represented by:

$$2\ FeOH^{-½} + Cd^{+2} \leftrightarrows [(FeOH)_2^{+a}Cd^{+b}]^{+} \qquad K_{Cd\text{-}bi} \qquad [7]$$

where $a$ and $b$ represent charge ($a+b=1$), as discussed in the appendix.The reactions of $Fe_2OH$ with Cd will be discussed later.

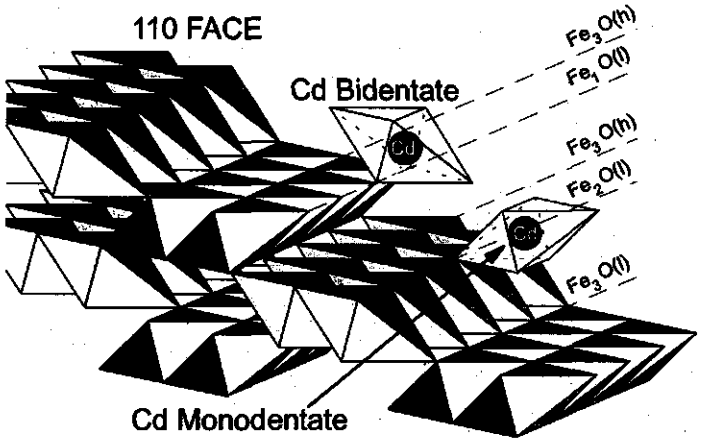


Fig. 7 A schematic representation of the 110 crystal face of goethite using Fe-filled octahedra. It is shown that an adsorbing cadmium ion can form two different surface complexes in a growth position (8): a bidentate with the singly coordinated surface groups and a monodentate with the doubly coordinated surface groups. In both options the adsorbing octahedra and the crystal octahedra only share corners (C-linkage).

The cadmium binding on the 021 face is different from the 110 face (8). With the assumptions discussed above, the only possible surface complexes that can be formed on this face are tridentate complexes with two singly coordinated and one doubly coordinated surface group. The reaction for the surface complexation of such complexes is given by:

$$2\ FeOH^{-½} + Fe_2OH^{0} + Cd^{2+} \leftrightarrows \left[\left[(FeOH)_2Fe_2OH\right]^{+c}Cd^{+d}\right]^{+} \qquad K_{Cd\text{-}tri} \qquad [8]$$

where $c+d=1$. Two types of cadmium tridentate complexes, located at crystal growth positions, can be distinguished. These complexes differ with respect to the numbers of shared edges and corners (Fig. 8). For each type of complex, two different growth positions occur for a unit cell. In Fig. 8, only one position per type of complex is shown for reasons of simplicity. The ratio of the two types of complexes

is 1:1. The two configurations are different in terms of EXAFS measurements and it is very probable that their affinity for cadmium differs. Based on EXAFS measurements (8), it has been shown that edge linkages are most abundant at low Cd coverage where Cd is bond with high affinity. We therefore assume that the configuration with two edges (Tridentate A) has the highest affinity for cadmium. This complex is considered in the calculations as high affinity complex, which implies that only half of the doubly coordinated surface groups at the 021 face is reactive for cadmium.

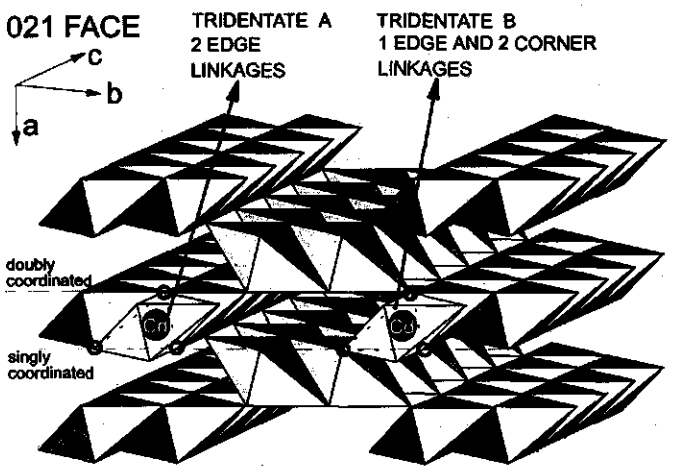


Fig. 8 A schematic representation of goethite showing the 021 crystal face from the front. The octahedra represent a central Fe ion with surrounding O, OH or $OH_2$ groups. Two different cadmium surface complexes are shown. Both complexes are tridentate complexes with two singly coordinated and one doubly coordinated surface group. The tridentate-A cadmium surface complex has an edge linkage with the two neighbouring iron octahedra. The tridentate-B cadmium surface complex shares an edge with a neighbouring iron octahedron (c-direction) and a corner with the two other iron octahedra. The open circles indicate surface groups that are a part of the cadmium complex.

The site densities that follow from the goethite crystal morphology and the assumed cadmium complexes can be found in Table 1. The site densities of the different surface groups can be calculated from crystallographic data and correspond to the total number of reactive groups. On the 110 face, two types of the triply coordinated surface groups and the doubly coordinated surface groups are assumed to be unreactive. The remaining singly and triply groups have each a density of 3 sites/nm$^2$. At the 021 face the singly coordinated surface groups have a density of 7.5 sites/nm$^2$. Half of the doubly coordinated surface groups are assumed to be reactive in terms of cadmium binding, so the site density of these groups is 3.75 sites/nm$^2$.

Table 1 Parameters values, used to describe the extended data set. The site densities and site fractions are based on the number of reactive sites (upper part of the table). The capacitances for the interface are based on the primary charging curves and modelling phosphate data (4). All log $K$ values are based on dimensionless surface fractions. Lines in the cell (----) mean that this surface site is not present.

| Part of the model | Parameter | 110 face | 021 face |
|---|---|---|---|
| Site densities (crystal surface) | Plane fraction | 0.9 | 0.1 |
| | $N_s$ (sites/nm$^2$) | 6 | 11.25 |
| | fraction singly c. | 0.5 | 0.667 |
| | fraction doubly c. | ---- | 0.333 |
| | fraction triply c. | 0.5 | ---- |
| Stern layer Capacitance (Interface) | $C_1$ (F/m$^2$) | 1.02 | 1.02 |
| | $C_2$ (F/m$^2$) | 5.00 | 5.00 |
| Protonation constants | $\log(K_{1,2})$ | 9.3 | 9.3 |
| | $\log(K_{3,1})$ | 9.3 | ---- |
| Pair formation | $\log(K_{p,f})$ | -1.0 | -1.0 |
| Metal binding: constants and charge distribution | $\log(K_{Cd\text{-}Bi})$ | 6.9 | ---- |
| | $f_{Cd\text{-}Bi}$ | 0.30 | ---- |
| | $\log(K_{Cd\text{-}Tri})$ | ---- | 9.0 |
| | $f_{Cd\text{-}Tri}$ | ---- | 0.58 |

## Predicting the total number of linkages with the CD-MUSIC model

The EXAFS analysis of Spadini et al. (8) showed two different cadmium - iron distances at the goethite surface. The abundance of these two linkages can be represented as the mean number of edge and corner linkages, $N_E$ and $N_C$ respectively (Table 2). Spadini et al. (8) found that the relative abundance of surface complexes having an E-linkage decreases on increasing cadmium surface loading. Therefore they concluded that at least two different cadmium surface complexes occur at the goethite surface (8). From the decrease of the relative abundance of the E-linkages with increasing cadmium surface loading Spadini et al. concluded that surface complexes having an E-linkage have a higher cadmium affinity than surface complexes with only C-linkages (8).

The cadmium surface speciation, calculated with the above given approach, can be related to the mean number of edge and corner linkages per adsorbed cadmium, $N_E$ and $N_C$, observed with EXAFS. The relation between the total number of edge and corner linkages and the number of edge and corner linkages per individual cadmium surface species $i$ ($N_{E,i}$ and $N_{C,i}$ respectively) is found by summation over all species:

$$\overline{N}_E = \frac{\sum_{i=1}^{n} (N_{E,i}\ \Theta_{Cd,i})}{\Theta_{Cd,T}} \qquad [6a]$$

$$\overline{N}_C = \frac{\sum_{i=1}^{n} (N_{C,i}\ \Theta_{Cd,i})}{\Theta_{Cd,T}} \qquad [6b]$$

in which $\theta_{Cd,i}$ is the adsorbed fraction of cadmium as surface complex $i$ and $\theta_{Cd,T}$ is the total fraction of adsorbed cadmium and $n$ is the number of different types of surface complexes.

Table 2 Average number of edge ($\overline{N}_E$) and corner linkages ($\overline{N}_C$) based on EXAFS data of Spadini et al. (8), measured at pH = 7.5 in [$NaClO_4$] = 0.3 mol/l. The relative number of edge linkages decreases on increasing surface loading

| Sample | Ads. Cd (μmol/m²) | $\overline{N}_E$ | $\overline{N}_C$ |
|---|---|---|---|
| #Gt-11% | 0.22 | 0.7 | 0.9 |
| #Gt-65% | 1.35 | 0.6 | 1.2 |
| #Gt-100% | 2.02 | 0.2 | 0.6 |

The values of $N_{E,i}$ and $N_{C,i}$ can be derived from the structural analysis given before (see Table 3). In case of a bidentate complex of the 110 face, where a Cd is bound by two singly coordinated surface groups, $N_{C,i}$ is 2. In case of a monodentate complex (Fig. 5), $N_{C,i}$ is 1. The value of $N_{E,i}$ is 0 for both complexes because no edge linkages occur on the 110 face. According to the crystal structure, the complexes with edge linkages can only be formed at the end of the goethite needles, like the 021 face.

Table 3 Actual values for number of edge ($N_{E,i}$) and corner ($N_{C,i}$) linkages of the various surface complexes and for the chosen surface species (mono, bi or tridentate).

| Surface complex | $N_{E,i}$ | $N_{C,i}$ | Face |
|---|---|---|---|
| bidentate | 0 | 2 | 110 |
| monodentate | 0 | 1 | 110 |
| tridentate - A | 2 | 0 | 021 |

## Experimental

All chemicals were stored in plastic bottles and all experiments were carried out in plastic vessels in order to avoid silica contamination. Demineralized, distilled (DD) water was used to prepare all solutions.

Goethite was prepared according to the procedure of Hiemstra et al. (11). A solution of 1 kg (2.47 mol) $Fe(NO_3)_3.9H_2O$ in 5 l DD water was titrated (10 ml base/min) with 2.5 M NaOH to a pH of 12 while rigorously stirring. The suspension was aged for 3 days at 60°C and subsequently dialysed with DD water. This results in a suspension containing fine, long needles of goethite with an average length of 150 nm and a width of 15 nm. The BET surface area, measured by $N_2$ gas adsorption was 95 $m^2/g$ (courtesy of P.Weidler).

For the adsorption experiments, general stock solutions were prepared. A NaOH stock solution was made by dissolving 25 g NaOH (Merck p.a.) in 25 ml DD water. This superconcentrated solution was cooled to room temperature, centrifuged in order to remove any solid $Na_2CO_3$ and 7.5 ml of the supernatant was pipetted into 1 l pre-boiled DD water. The stock solution was standardized by titration with 0.1000 M HCl (Titrisol) and phenolphthalein as indicator.

A $HNO_3$ stock was prepared by diluting 12 ml of $HNO_3$ in 1 l DD water. The acid was calibrated with the standard base using phenolphthalein as indicator. The background electrolyte solution was prepared by adding 255 g $NaNO_3$ to 1 l DD water. The cadmium stock solution was prepared by adding 61.694 g of $Cd(NO_3)_2.4H_2O$ (Merck p.a.) to 1 l DD water. The precise concentration was later standardized by titration with EDTA using eriochrome black as indicator.

Subsamples of the goethite suspension were titrated at three concentrations of background electrolyte (0.005 M, 0.01 M and 0.1 M $NaNO_3$). The reversibility was checked by titrating at each salt concentration both with base and with acid. The

working base (NaOH), acid ($HNO_3$) and salt ($NaNO_3$) solutions were freshly prepared from their stock solutions. To prepare the base and the salt solutions, pre-boiled, DD water was used in order to prevent carbonate contamination.
For the titration, 0.658 g goethite (62.5 $m^2$) was put in 45.6 ml DD water. The suspension was then brought to a salt concentration of 0.005 M and left overnight at pH 5 in a nitrogen atmosphere to remove any carbonate. The titration was carried out in a nitrogen atmosphere using a computer-controlled titrator (20). Using this titrator, three salt levels could be titrated automatically in one suspension. The outer junction of the reference electrode (a double-junction saturated KCl electrode) was filled with a mixture of $NaNO_3$ (0.125 M) and $KNO_3$ (0.875 M) (21). The mobility of the positive and negative ions in this solution is about the same, so that the diffusion potential over the outer junction is independent of the salt concentration (22). A check was made on salt leakage with the reference electrode in 50 ml pure water, after 1.5 day the salt concentration increase from 0 to 0.002 M. This is of no influence on the experiments because the titration at the lowest salt level (0.005 M) lasted only six hours.

The surface charge of the goethite was calculated from the ($H^+$ - $OH^-$) balance of the experiment. The intersection point for the three salt concentrations gave the Pristine Point of Zero Charge (*PPZC*). Cadmium adsorption isotherms were measured at 5 different pH's in 0.1 M $NaNO_3$. The goethite suspension concentration used depended on the pH of the experiment. For example at low pH, a large suspension density was required in order to get an accurately measurable amount of adsorption. The starting goethite densities varied from 39 (pH 5) to 4.4 (pH 9) g/l. The goethite suspension was brought to the appropriate salt level of the experiment with $NaNO_3$ and left overnight at pH 5 in a nitrogen atmosphere. This was followed by titration to the desired pH with NaOH, cadmium was then added and the pH was kept at the target value (± 0.05 pH units) by adding NaOH. The number of protons released was calculated from the amount of added NaOH that was needed to restore the pH to its stat value. Calculations showed that dissolved Cd-hydroxide species did not affect these proton exchange measurements. After equilibrating for 4 hours, a sample was taken and the next cadmium dose was added. Six or seven samples were taken for each experiment. Each experiment lasted 2.5 days. Duplicate experiments at pH 7 in a salt concentration of 0.1 M showed good agreement.

Cadmium analysis was performed for solution samples which had been filtered through 0.025 µm micropore membrane filters (PH70, Schleicher & Schuell). The first 1 to 2 ml of filtered solution were always discarded to prevent loss of cadmium by adsorption on the filter. The loss of cadmium by the filter was not detected for a concentration of $10^{-5}$ mol/l solution. The filtered solution was analyzed for cadmium by flame AAS and/or GFAAS. The use of an Orion ISE cadmium electrode for direct measurement in the suspension was tested but could not be used due to the interference of goethite with the electrode. A similar experience was reported by Gunneriusson (23).
Preliminary experiments showed that 4 hours after adding a dose of cadmium, the amount of $Cd^{2+}$ adsorbed was constant. This time might be considered too short in view of the kinetic studies of cadmium adsorption on goethite (24 ,25) which showed equilibration times up to 42 days. In three tested samples, the amount of cadmium adsorbed after 100 hours was larger than after 4 hours but the increase was generally small. The percentage cadmium removed from solution increased from 83.8% to 86.1% (pH 8); 65.7% to 67.8% (pH 7); 25.9% to 28.2% (pH 6). These increases were much smaller than those reported by Bruemmer et al. (25). Therefore we suggest that our data represent the behaviour of the relatively fast interfacial adsorption reaction.

All calculations were carried out with the computer code ECOSAT (26). ECOSAT is able to handle the non-integral charges of the CD-MUSIC model (4). The Davies equation (eq. [10]) was used to estimate ion activity coefficients ($f_k$) at 20°C.

$$Log(f_k) = -0.51 z_k^2 \cdot \left[ \frac{\sqrt{I}}{1+\sqrt{I}} - 0.2 \cdot I \right] \qquad [7]$$

in which $I$ is the ionic strength and $z_k$ is the valence of ion $k$. The values of log $K$ are based on dimensionless surface fractions of the species (4).

The description of the data with the CD-MUSIC model was optimized by trial and error, aided by plots of the data. First the description of the charging curve was optimized (overall capacitance, log $K_H$). Then the description of the cadmium data was optimized (log $K_{Cd}$ , $f$ values) while the parameters of the charging behaviour were fixed. During the optimization, the site densities of the two crystal planes were fixed on the values that were derived from the crystal structure and shape.

## Results

The primary charging data for goethite at three electrolyte concentrations show a *PPZC* of 9.3 (± 0.2) (Fig. 9). In Table 1, the model parameters for the description of the data can be found. For a good description of the data the overall Stern layer capacitance is 0.85 F/m$^2$. The overall capacitance is split over two charge-free layers ($C_1$ and $C_2$).

The protonation constants for both the triply and singly coordinated groups ($K_{3,1}$ and $K_{1,2}$ resp.) are set equal to the experimentally found *PPZC*. The pair formation constants for $Na^+$ and $NO_3^-$ are taken from Hiemstra and van Riemsdijk 1996 (4). The charging curves are described well for pH values below the *PPZC* by the model with the parameters shown in Table 1. For pH values above the *PPZC* the description is poor.

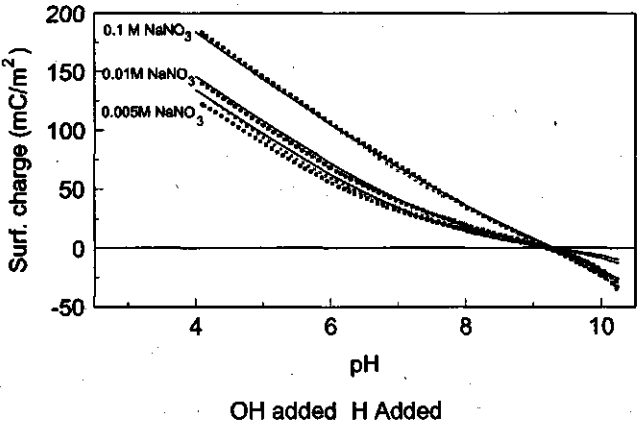


Fig. 9 Experimental charging curves of goethite for three electrolyte levels. The *PPZC* is 9.3 (± 0.2). The lines represent the model calculations. Parameter values are given in Table 1.

The experimental results and the model description for the pH dependent cadmium adsorption are shown in Fig. 10 and the salt dependency at pH 7 is shown in Fig. 11. The model descriptions are very good for both the pH dependency and the salt dependency. The cadmium model parameters that were used are also given in Table 1.

The data for the proton/cadmium ion exchange ratio ($r_{H/Cd}$) (Fig. 12), are cumulative values starting from zero cadmium. In order to obtain reliable estimates for $r_{H/Cd}$, only data for which $\{Cd_{Adsorbed} / Cd_{Solution}\}$ is larger than 1 are considered, for pH 5 none of the data met this criterion. Calculated values of $r_{H/Cd}$ are given by the slopes of the lines in Fig. 12. These values were extracted for each pH value (Table 4). The model calculations show a low pH dependency of the proton/cadmium exchange, which is in accordance with the experiments. The predicted proton/cadmium exchange ratios are, especially for higher cadmium concentrations, too low compared with the data (Fig. 12). The data show a near-constant value for the proton/cadmium exchange ratio which is independent of the cadmium concentration and pH within the experimental error.

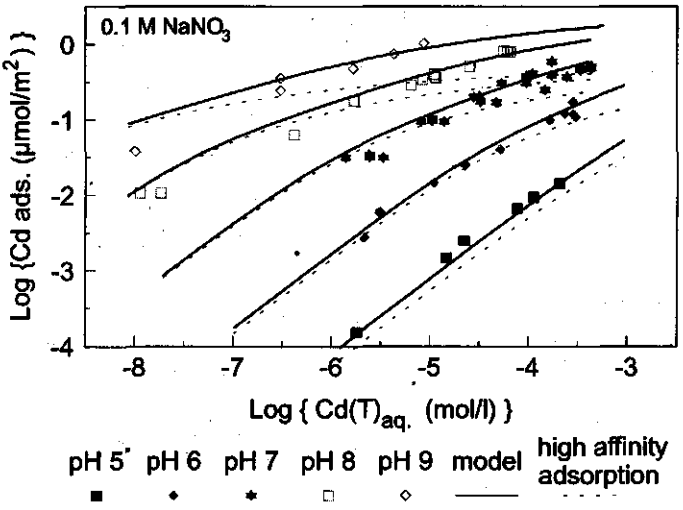


Fig. 10 pH dependency of cadmium adsorption on goethite at a fixed $NaNO_3$ salt level of 0.1 mol/l. The solid lines represent the model description, the dashed lines represent the contribution of the high affinity complex.

The number of edge and corner linkages as a fraction of the total number of linkages for cadmium, according to the EXAFS measurements of Spadini et al. (Table 2), are shown in Fig. 13. The model description is presented by the solid lines. The description is good except the predicted number of corner linkages is slightly too high for the highest cadmium adsorption.

Table 4 The proton/cadmium exchange ratios ($r_{H/Cd}$) found from linear regressions of the total amount of released protons (µmol) versus the total amount of adsorbed cadmium (µmol).

| pH | slope ($r_{H/Cd}$) (± 2σ) | intercept | $r^2$ |
|---|---|---|---|
| 5[a] | 3.4 ± 3.5 | -2.15 | 0.522 |
| 6 | 1.4 ± 1.3 | -0.34 | 0.948 |
| 7 | 1.63 ± 0.18 | 1.79 | 0.978 |
| 8 | 1.59 ± 0.27 | -1.69 | 0.992 |
| 9 | 1.71 ± 0.63 | 5.15 | 0.935 |
| Overall | 1.54 ± 0.11 | 3.74 | 0.971 |

(a) These data are unreliable due to the fact that the adsorption of cadmium is very low at this pH.

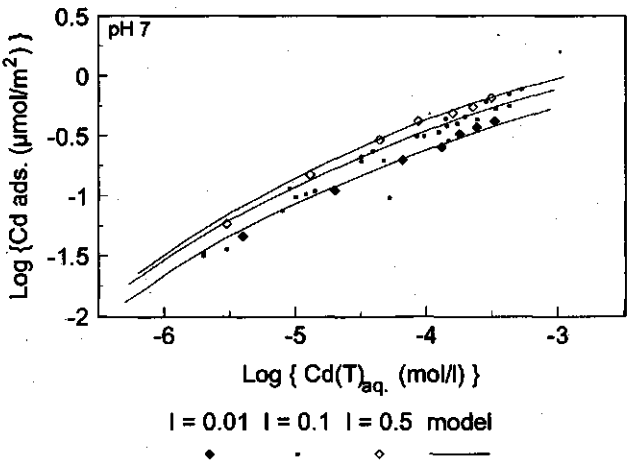


Fig. 11 Salt dependency of cadmium adsorption on goethite at different $NaNO_3$ levels with fixed pH 7. The lines represent the model calculation.

## Discussion

The experimental *PPZC* is in good agreement with values reported earlier for goethite (4, 27, 28, 29, 30, 31). The shape of the experimental charging curve is slightly asymmetric around the *PPZC* (Fig. 9). This asymmetry can be explained if the doubly coordinated surface groups have a lower log $K_{2,1}$ so that at pH 10 a significant part of these groups is negatively charged.

The pH dependency of cadmium adsorption on goethite found in this study is in agreement with other data (23, 27, 28, 32). The low salt dependency of cadmium adsorption on goethite that was found here is in accordance with data of Hayes and Leckie (32).

Calculations of the charging behaviour and Cd adsorption without the use of pair forming ions (Na and $NO_3$) gave practically the same results as the calculations with pair forming ions. This indicates that for the data set discussed in this study the use of pair forming ions is of minor importance for a good description of the data. However, for the description of anion adsorption, pair forming ions are of more importance (4), so in this study pair formers are used for reasons of consistency.

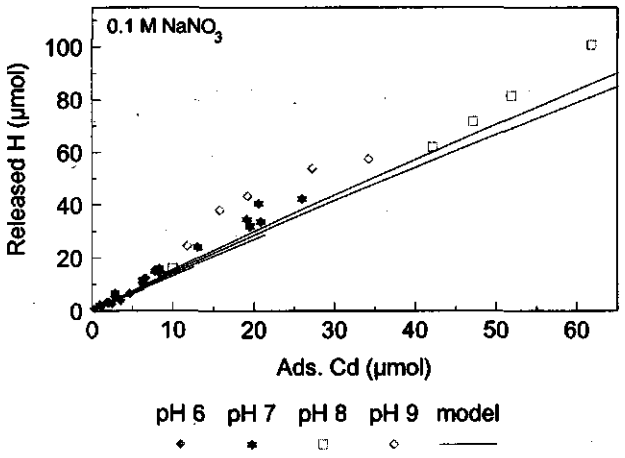


Fig. 12 Release of protons as a result of cadmium adsorption on goethite at various fixed pH values. The lines indicate the model calculations for different pH values.

Also the value of $C_2$ is consistent with the value used by Hiemstra and van Riemsdijk (4). The high capacitance of the outer layer ($C_2$ = 5 F/m$^2$) corresponds with a layer thickness of about half a water molecule (1.4 Å) if the dielectric constant for water is used ($\varepsilon_r$=78).

The fraction of 10% for the 021 plane is also used for the description of phosphate adsorption (4) and is considered to be a material property of our preparates. So the

adjustable parameters for the CD-MUSIC modeling in this study are the inner layer capacitance ($C_1$), two cadmium surface complexation constants with corresponding charge distribution factors $f$ for cadmium.

The charge distribution factors $f$ can be compared with the theoretical value that results from applying the Pauling concept of equal charge distribution over the surrounding ligands. For a bidentate and tridentate surface complex, respectively two and three ligands are placed in the 0-plane. Cadmium has six ligands so the theoretical charge distribution factors $f$ for the bi- and tridentate surface species are respectively 0.333 (=2/6) and 0.5 (=3/6). The fitted charge distribution factors $f$ for the bi- and tridentate surface complex are respectively 0.3 and 0.58 (Table 1). So the fitted charge distribution factors $f$ are in very good agreement with the values estimated from applying the Pauling concept.

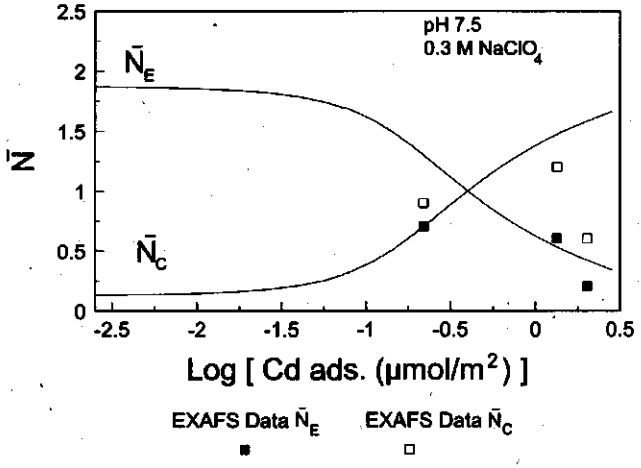


Fig. 13 Calculated and observed number of edge linkages ($\bar{N}_E$) and corner linkages ($\bar{N}_C$) at a salt level of 0.3 mol/l ($NaClO_4$) and a pH of 7.5. The experimental results are taken from Spadini et al. (8), they are based on the number of Fe linked to an adsorbed Cd, measured by EXAFS. The lines indicate the model calculations for the model in which only half of the sites at the 021 face are reactive for cadmium (tridentate-A).

The low pH dependency that was found for experimental $r_{H/Cd}$ is in accordance with earlier observations of the proton/zinc ion exchange on hydrous ferric oxide (33). Within the uncertainty, the values of $r_{H/Cd}$ for pH 8 and 9 are in reasonable agreement with the value of 1.5 found by Gunneriusson (23) for cadmium adsorption on goethite at pH 8.5. The predicted values of $r_{H/Cd}$ are about 1.45 for low cadmium

adsorption, which is slightly too low. For higher adsorption densities, the model description of $r_{H/Cd}$ decreases to about 1.25 but this decrease of $r_{H/Cd}$ is not observed in the data. This decrease in the model prediction for $r_{H/Cd}$ at increasing cadmium concentrations is caused by the decreasing importance of the high affinity cadmium surface complex (021 face, tridentate) at high cadmium concentrations. In the high affinity cadmium surface complex at the 021 face a relatively larger part of the charge of the adsorbing cadmium is placed in the surface plane (high charge distribution factor *f*, see Table 1). Placing a greater fraction of the charge of the cadmium in the surface plane will cause an increasing interaction with surface protons and therefore a higher predicted $r_{H/Cd}$ (2, 34).

The question arises whether other complexes than the ones used here, are able to improve the description, especially of the $r_{H/Cd}$ value. The predicted value of $r_{H/Cd}$ is nearly the same using a model in which the doubly-coordinated surface groups ($Fe_2OHCd$) were taken as the reactive groups for cadmium adsorption on the 110 face. Considering deprotonation of this complex ($Fe_2OCd$) did not increase the $r_{H/Cd}$ significantly. This confirms the idea that the model prediction of the value of $r_{H/Cd}$ is mainly defined by the position of the adsorbing cadmium in the interface (the charge distribution factor *f*), which also determines the pH dependency.

The description of the EXAFS data is quite good, but not perfect. The use of two different surface complexes is in accordance with the EXAFS data of Spadini et al. (5). Although the trend of the description is correct, the highest values of $N_C$ seem somewhat overestimated. It should be kept in mind that, according to Spadini et al., the experimental values of $N_C$ and in a lower extend of $N_E$ may be underestimated for high surface loading (8). The model description for the EXAFS data can be improved if it is assumed that cadmium forms only monodentate complexes at the 110 face which means that the doubly coordinated groups are the reactive groups for cadmium. In this case, the predicted value for $N_E$ remains almost unchanged while the predicted value of $N_C$ becomes lower. Such a model prediction would be in excellent agreement with the EXAFS data. The same result would be obtained if it is assumed that the singly coordinated surface groups form monodentate surface complexes in stead of bidentate surface complexes. However, this is in disagreement with the assumption that cadmium forms surface complexes at growth positions for iron as was proposed by Spadini et al. (8).

The assumption that high affinity complexes occur on the 021 face was investigated with a goethite having a different geometry, namely shorter needles compared to our goethite (sample courtesy to S. Glasauer). The 021 face is expected to be more important for this goethite (about 20% of the surface), hence it might be expected that this goethite would have a relatively high affinity for cadmium. However, in adsorption experiments at pH 6, no significant difference in cadmium adsorption, compared to our goethite was found. The reason why this result was not found may be the presence of imperfections at the 110 face (6, 7), which results in a higher relative abundance of the edge binding groups than expected from the idealized crystal morphology. The fact that both goethite preparates show similar chemical behaviour suggests that a model with only one electrostatic plane should be sufficient to describe the data. To test this hypothesis, calculations were done with the high and the low cadmium affinity surface complex present on the same face. This model showed no significant difference from the model in which the high and the low cadmium surface complex were placed on separate electrostatic planes.

**Acknowledgement**

The authors thank Dr. Peter Weidler for the physical characterisation of the goethite used in this study and for the fruitful discussions about the morphology of goethite. Also we acknowledge Dr. Susan Glasauer for the preparation of the short needle goethites.

Part of this work is financed by the European Community through contract STEP-CT90-0031.

## Appendix

The speciation tables for the surface species are shown in Table A-1 (110 face) and table A-2 (021 face). The first column of each table indicates the name of the surface complexes (surface species). These surface species consist of one or more surface component(s) (surface group(s)) and one or more dissolved component(s). The boltzmann factors have the subscript of the plane (0, 1 or d) to which they are related. The site densities of the surface groups have the subscripts (singly), d (doubly) and t (triply). For the 021 face an asterix is added to the surface components, the total amounts of all components and the electrostatic variables.

The concentrations of the surface species (in mol/l) can be calculated reading the table horizontally. The concentration of a species is then calculated according to:

$$[S] = 10^{\log K} \prod_{k} [C_k]^{n_k} \qquad [A\text{-}1]$$

in which $C_k$ is the concentration of component k in mol/l, the component can be a dissolved or a surface component. The coefficients in the table ($n_k$) indicate if component $k$ is involved in the species.

The total amount of a surface component $x$ in mol/m$^2$ ($N_{s,x}$) can be recalculated to a solution concentration in mol/l ($S_{s,x}$) according to:

$$S_{s,x} = \rho\, A_f\, N_{s,x} \qquad [A\text{-}2]$$

in which ρ is the suspension density in kg/l, $A_f$ the specific surface area of the crystal face on which the species occurs in m$^2$/kg ($f$ = 110 or 021). The surface fraction of a surface species $y$ ($\Theta_y$) is defined as its total surface coverage $S_y$ in mol/l divided by the summation of the total amounts (in mol/l) of all surface components ($S_{s,x}$) that are involved in the surface species:

$$\Theta_y = \frac{S_y}{\sum_{x=1}^{k} S_{s,x}} \qquad [A\text{-}3]$$

in which $k$ indicates the number of different surface components of which the surface species consists. For the cadmium tridentate surface complex, $k$=2, because in this complex two different surface groups are involved.

Table A-1 The Table of species for the 110 face of goethite. For explanation of the symbols, see the tekst.

| | Dissolved comp. | | | | Surface comp. | | Boltzmann factors | | | |
|---|---|---|---|---|---|---|---|---|---|---|
| Surface species | H | Na | $NO_3$ | Cd | FeOH | $Fe_3O$ | $e^{-F\psi_0/RT}$ | $e^{-F\psi_1/RT}$ | $e^{-F\psi_d/RT}$ | |
| FeOH | 0 | 0 | 0 | 0 | 1 | 0 | 0 | 0 | 0 | 0 |
| $FeOH_2$ | 1 | 0 | 0 | 0 | 1 | 0 | 1 | 0 | 0 | $\log K_H = \log K_{1,2}$ |
| FeOHNa | 0 | 1 | 0 | 0 | 1 | 0 | 0 | 0 | 1 | $\log K_{p,t}$ |
| $FeOHHNO_3$ | 1 | 0 | 1 | 0 | 1 | 0 | 1 | 0 | -1 | $\log K_H + \log K_{p,t}$ |
| $(FeOH)_2Cd$ | 0 | 0 | 0 | 1 | 2 | 0 | $2f$ | $2(1-f)$ | 0 | $\log K_{Cd} - \log S_s$ |
| $Fe_3O$ | 0 | 0 | 0 | 0 | 0 | 1 | 0 | 0 | 0 | 0 |
| $Fe_3OH$ | 1 | 0 | 0 | 0 | 0 | 1 | 1 | 0 | 0 | $\log K_H = \log K_{3,1}$ |
| $Fe_3ONa$ | 0 | 1 | 0 | 0 | 0 | 1 | 0 | 0 | 1 | $\log K_{p,t}$ |
| $Fe_3OHNO_3$ | 1 | 0 | 1 | 0 | 0 | 1 | 1 | 0 | -1 | $\log K_H + \log K_{p,t}$ |
| Sum: | H(t)-OH(t) | Na(t) | $NO_3$(t) | Cd(t) | $S_s$[a] | $S_t$[a] | $\Sigma_0$[b] | $\Sigma_1$[b] | $\Sigma_d$[b] | |

(a) $S_s = \rho A_{110} N_{s,s}$ , $S_t = \rho A_{110} N_{s,t}$

(b) $\Sigma_0 = \frac{\rho A_{110}}{F}(\sigma_0 - \sum_i z_i F N_{s,i})$, $\Sigma_1 = \frac{\rho A_{110}}{F}\sigma_1$ , $\Sigma_d = \frac{\rho A_{110}}{F}\sigma_d$

Table A-2 The Table of species for the 021 face of goethite. For explanation of the symbols, see the tekst.

| | Dissolved comp. | | | | Surface comp. | | Boltzmann factors | | | |
|---|---|---|---|---|---|---|---|---|---|---|
| Surface species | H | Na | $NO_3$ | Cd | FeOH* | $Fe_2OH^*$ | $e^{-F\psi_0^*/RT}$ | $e^{-F\psi_1^*/RT}$ | $e^{-F\psi_d^*/RT}$ | |
| FeOH* | 0 | 0 | 0 | 0 | 1 | 0 | 0 | 0 | 0 | 0 |
| $FeOH^*_2$ | 1 | 0 | 0 | 0 | 1 | 0 | 1 | 0 | 0 | $\log K_H = \log K_{1,2}$ |
| FeOH*Na | 0 | 1 | 0 | 0 | 1 | 0 | 0 | 0 | 1 | $\log K_{p,t}$ |
| $FeOH^*HNO_3$ | 1 | 0 | 1 | 0 | 1 | 0 | 1 | 0 | -1 | $\log K_H + \log K_{p,t}$ |
| $Fe_2OH^*$ | 0 | 0 | 0 | 0 | 0 | 1 | 0 | 0 | 0 | 0 |
| $(FeOH^*)_2Fe_2OH^*Cd$ | 0 | 0 | 0 | 1 | 2 | 1 | $2f^*$ | $2(1-f^*)$ | 0 | $\log K_{Cd\text{-}ht} + \log (S_s^* + S_d^*) - 2\log S_s^* - \log S_d^*$ |
| Sum: | (H(t)-OH(t))* | Na(t)* | $NO_3$(t)* | Cd(t)* | $S_s^{*c}$ | $S_d^{*c}$ | $\Sigma_0^{*d}$ | $\Sigma_t^{*d}$ | $\Sigma_d^{*d}$ | |

(c) $S_s^* = \rho A_{021} N_{s,s}^*$ , $S_d^* = \rho A_{021} N_{s,d}^*$

(d) $\Sigma_0^* = \frac{\rho A_{021}}{F}(\sigma_0^* - \sum_k z_k F N_{s,k})$ , $\Sigma_1^* = \frac{\rho A_{021}}{F}\sigma_1^*$ , $\Sigma_d^* = \frac{\rho A_{021}}{F}\sigma_d^*$

The log $K$ values are all calculated with surface fractions of the surface species, while in the tables all values are expressed in mol/l. From the definition of the surface fractions (eq. [A-3]) it follows that for bi- and tridentate species a recalculation factor is needed for a log $K$ on mol/l basis. In the newest version of ECOSAT this recalculation is done automatically according to the following description. The log $K$ for a bidentate surface species with total amount $S_{ads}$ and one type of reference group with total amount $S_{ref}$ can be recalculated according to:

$$K_{in} = \frac{\dfrac{S_{ads}}{\rho A_f N_{s,i}}}{\left(\dfrac{S_{ref}}{\rho A_f N_{s,i}}\right)^2 \prod C^{n_k}_{k,sur}} = (\rho A_f N_{s,i}) \frac{S_{ads}}{S^2_{ref} \prod C^{n_k}_{k,sur}} = (\rho A_f N_{s,i})\, K_{diss} \qquad [A\text{-}10]$$

$K_{in}$ is the equilibrium constant based on the surface fraction of the surface species and $K_{diss}$ based on concentrations in mol/l, $N_{s,i}$ is the total site density (in mol per $m^2$) of the involved surface component $i$ and $C_{k,sur}$ is the concentration of component $k$ at the surface while $A_f$ is the specific surface area of the crystal face on which the complex occurs.

For a tridentate species with total amount $S_{ads}$, that forms a bidentate with reference group $h$ (total amount $S_{ref,h}$) and a monodentate with reference group $i$ (total amount $S_{ref,i}$), this recalculation is:

$$K_{in} = \frac{\dfrac{S_{ads}}{\rho A_f (N_{s,h}+N_{s,i})}}{\left(\dfrac{S_{ref,h}}{\rho A_f N_{s,h}}\right)^2 \dfrac{S_{ref,i}}{\rho A_f N_{s,i}} \prod C^{n_k}_{k,sur}} = \frac{(\rho A_f N_{s,h})^2 \rho A_f N_{s,i}}{\rho A_f (N_{s,h}+N_{s,i})} \frac{S_{ads}}{S^2_{ref,h} S_{ref,i} \prod C^{n_k}_{k,sur}} = \frac{(\rho A_f N_{s,h})^2 \rho A_f N_{s,i}}{\rho A_f (N_{s,h}+N_{s,i})} K_{diss} \qquad [A\text{-}11]$$

Note that the fraction of the adsorption complex is calculated with the total site density of both reference groups ($N_{s,h}+N_{s,i}$) which is in accordance with eq. [A-3].

The columns of the table are the mass balances of the components. For the total adsorbed amounts of the dissolved components, the total amounts for the 110 face (Table A-1) and the 021 face (Table A-2) have to be added. The total dissolved amounts of the dissolved components are not considered here. The mass balance for the different surface components is straightforward. The summation in the columns of the Boltzmann factors, needs more explanation. First the coefficients $n_k$ in this

column indicate the change of charge in the surface plane for the involved component, expressed in mol/l. The charge of an adsorbing cation can be divided over the 0-plane and the 1-plane. The part that is placed in the 0-plane, $\Delta z_0$, can be calculated from the stoichiometric change of the number of protons in this plane upon cation adsorption, $\Delta n_H$, (positive, negative or zero) in combination with the fraction ($f$) of the charge of the specifically adsorbing cation ($z_{Me}$) that is attributed to the surface plane:

$$\Delta z_0 = n_H z_H + f z_{Me} \qquad [A\text{-}12]$$

For the 1-plane, $\Delta z_1$ results from the summation of the fraction 1-$f$ of the charge of the central ion ($z_{Me}$) and the summation of the charge of the coordinating ligands that are placed in this plane:

$$\Delta z_1 = (1-f) z_{Me} + \sum_j m_j z_j \qquad [A\text{-}13]$$

in which $m_j$ represents the number of ligands with charge $z_j$ placed in the 1-plane. In the formation of cadmium surface complexes, no protons desorb or adsorb (i.e. $n_H = 0$) and uncharged ligands ($H_2O$) are present in the 1-plane (i.e. $z_j = 0$). So the coefficients for the cadmium species are: $f \cdot z_{Cd}$ for the 0-plane and $(1-f) \cdot z_{Cd}$ for the 1-plane. Now the values of $\{+a, +b\}$ and $\{+c, +d\}$ in respectively eq. [3] and eq.[4] are easy to calculate. The charges in the 1-plane ($+b$ and $+d$) equal the value of $(1-f) \cdot z_{Cd}$, while the charges in the 0-plane ($+a$ and $+c$) equal the value of $f \cdot z_{Cd}$ increased with the formal charges of the involved surface components.

The summation of the Boltzmann columns is the total change of the charge (in eq/l) in that plane (see eq. [9]). For the 0-plane this leads to the summation of all attributed charge of the adsorbed ions ($\sigma_0$) minus the summation of the charge of all surface components ($\Sigma z_i$ F $N_i$ ). The factor ($\rho$ $A$)/F recalculates the surface charge from C/m$^2$ to eq./l. In the other two electrostatic planes only the charge resulting from adsorbing ions is present ($\sigma_1$ and $\sigma_2$). The electrostatics for a model with three planes is described in detail elsewhere (1,9).

## Literature


1. Bolt, G.H., The ionic distribution in the diffuse double layer; *In*: "Soil chemistry; B. physico chemical models", (Bolt G.H., Ed.). Elsevier scientific publishing comp. Amsterdam, 1982
2. Venema, P., Hiemstra, T., and van Riemsdijk, W.H., Comparison of different site binding models for cation sorption; Description of pH dependency, salt dependency, and cation -proton exchange, *J. Colloid Interface Sci.* **181**, 45-59 (1996)
3. Meeussen, J.C.L, Scheidegger, A., Hiemstra, T., van Riemsdijk, W.H., and Borkovec, M., Predicting multicomponent adsorption and transport of fluoride at variable pH in a goethite-silica sand system, *Environ. sci. technol*, **30**, 481-489 (1996)
4. Hiemstra, T, and van Riemsdijk, W.H., A surface structural approach to ion adsorption: The charge distribution (CD) model, *J. Colloid Interface Sci.* **179**, 488-508 (1996)
5. Schwertmann U., and Cornell R., Iron Oxides in the laboratory., VCH, Weinheim, 1991
6. Weidler, P.G., Schwinn, T. and Gaub, H.E., Vicinal faces on synthetic goethite observed by atomic force microscopy, *Clays and Clay Minerals*, **44**, in press (1996)
7. Weidler, P.G., Oberflächen und Porositäten synthetischer Eisenoxide, Phd. thesis dept. Soil Science T.U. München, Munich, (1994)
8. Spadini, L., Manceau, A., Schindler, P.W., and Charlet, L., Structure and stability of $Cd^{2+}$ surface complexes on Ferric Oxides, *J. Colloid Interface Sci.* **168**, 73-86 (1994)
9. Stumm, W., and Morgan, J.J., *in* "Aquatic chemistry; An introduction emphasizing chemical equilibria in Natural Waters ", (W. Stumm, Ed.), John Wiley and Sons, New York, 1981
10. Hiemstra, T.; Riemsdijk, W.H. van, and Bolt, G.H., Multisite Proton Adsorption Modeling at the Solid/Solution Interface of (Hydr)oxides: A New Approach, I. Model Description and Evaluation of Intrinsic Reaction Constants, *J. Colloid Interface Sci.* **133**, 91-104 (1989)
11. Hiemstra, T., de Wit, J.C.M., and van Riemsdijk, W.H., Multisite Proton Adsorption Modeling at the Solid/Solution Interface of (Hydr)oxides: A New Approach, II. Application to various Important (Hydr)oxides, *J. Colloid Interface Sci.* **133**, 105-117 (1989)
12. Pauling, L., The principals determining the structure of complex ionic crystals, *J. Am. Chem. Soc.* **51**, 1010-1026 (1929)
13. Hiemstra, T., and van Riemsdijk, W.H., Physical-chemical interpretation of primary charging behaviour of metal (hydr)oxides, *Colloids and Surfaces* **59**, 7-25 (1991)
14. Yates, D.E., Levine, S., and Healy, T.W., Site binding model of the electrical double layer at the oxide/water interface, *J. Chem. Soc. Faraday Trans. I* **70**, 1807-1818 (1974)
15. Davis, J.A., James, R.O., and Leckie, J.O., Surface ionization and complexation at the oxide/water interface. I. Computation of electrical double layer properties in simple electrolytes, *J. Colloid Interface Sci.* **63**, 480-499 (1978)
16. Davis, J.A., and Leckie, J.O., Surface ionization and complexation at the oxide/water interface. II. Surface properties of amorphous iron oxyhydroxides and adsorption of metal ions, *J. Colloid Interface Sci.* **67**, 90-107 (1978)
17. Dzombak, D.A., and Morel, F.M.M., Surface complexation modelling, hydrous ferric oxide, (D.A. Dzombak and F.M.M. Morel, Eds.), John Wiley and Sons, New York 1990
18. Barrón, V. and Torrent, J., Surface hydroxyl configuration of various crystal faces of hematite and goethite, *J. Colloid Interface Sci.* **177**, 407-410 (1996)

19. Parfitt, R.L., Atkinson, R.J. and Smart, R. St. C., The mechanism of phosphate fixation by iron oxides, *Soil Sci. Am. Proc.* **39**, 837-841 (1975)
20 Kinniburgh, D.G., Milne, C.J., Venema, P., Design and construction of a Personal-Computer based automatic titrator, *Soil Sci. Soc. Am. J.* **59** (2), 417-422 (1995)
21. de Keizer, A., Electrosorption of tetraalkylammonium ions on silver iodide, PhD. thesis dept. Fys. and Coll. Chemistry W.A.U., Wageningen, 1981
22. Mc Innes, D.A., *in* "The principles of electrochemistry", Dover publications Inc., New York, 1961
23. Gunneriusson, L., Composition and stability of Cd(II)-Chloro and -Hydroxo complexes at the goethite (α-FeOOH)/Water interface, *J. Colloid Interface Sci.* **163**, 484-492 (1994)
24. Gerth, J., and Bruemmer, G.W., Adsorption und Festlegung von Nickel, Zink und Cadmium durch Goethit (α-FeOOH), *Fresenius Z. Anal. Chem.* **316** (6), 616-620 (1983)
25. Bruemmer, G.W., Gerth, J., and Tiller, K.G., Reaction kinetics of the adsorption and desorption of nickel, zinc and cadmium by goethite. I. Adsorption and diffusion of metals, *J. Soil Sci.* **39**, 37-51 (1988)
26 Keizer, M.G., and van Riemsdijk, W.H., "ECOSAT: Technical Report of the Departments Soil Science and Plant Nutrition", W.A.U, Wageningen, 1994
27. Johnson, B.B., Effect of pH, temperature, and concentration on the adsorption of cadmium on goethite, *Environ. Sci. Technol.* **24**, 112-118 (1990)
28. Spark, K.M., Johnson, B.B., and Wells, J.D., Characterizing heavy-metal adsorption on oxides and oxyhydroxides, *Europ. J. of Soil Sci.* **46**, 621-631 (1995)
29. Lumdson, L.G., and Evans, L.J., Surface complexation model parameters for goethite (α-FeOOH), *J. Colloid Interface Sci.* **164**, 119-125 (1994)
30. vanGeen, A., Robertson, A.P., and Leckie, J.O., *Geochimica et cosmochimica Acta*, **58**(9), 2073 (1994)
31. Mesuere, K, and Fish, W, Chromate and oxalate adsorption on goethite 1. Calibration of Surface complexation models, *Environ. Sci. Technol.* **26**, 2357-2370 (1992)
32. Hayes K.F., and Leckie J.O., Modeling ionic strength effects on cation adsorption at hydrous oxide/solution interfaces, *J. Colloid Interface Sci.* **115**, 564-572 (1987)
33. Kinniburgh D.G., The $H^+/M^{2+}$ exchange stoichiometry of calcium and zinc adsorption by ferrihydrite, *J. Soil Sci.* **33**, 759-768 (1983)
34. Fokkink, L.G.J., Ion adsorption on oxides; surface charge formation and cadmium binding on rutile and hematite, PhD. thesis dept. Fys. and Coll. Chemistry W.A.U., Wageningen, 1987

# 4

# The interaction of cadmium with phosphate on goethite

P. Venema, T. Hiemstra, W.H. van Riemsdijk
Journal of Colloid and Interface Science, submitted 1996

# The interaction of cadmium with phosphate on goethite


## Abstract

*Interactions between different ions are of importance for understanding chemical processes in natural systems. In this study simultaneous adsorption of phosphate and cadmium on goethite is studied in detail.*

*The Charge Distribution (CD) -MUlti SIte Complexation (MUSIC) model has been successful in describing extended data sets of cadmium adsorption and phosphate adsorption on goethite. In this study, the parameters of these two models were combined in order to describe a new data set of simultaneous adsorption of cadmium and phosphate on goethite. The attention is focussed on the surface speciation of cadmium. With the extra information that can be obtained from the interaction experiments, the cadmium adsorption model is refined. For a perfect description of the data, the singly coordinated surface groups at the 110 face of goethite were assumed to form both monodentate and bidentate surface species with cadmium.*

*The CD-MUSIC model is able to describe data sets of both simultaneous and single adsorption of cadmium and phosphate with the same parameters. The model calculations confirmed the idea that only singly coordinated surface groups are reactive for specific ion binding.*


## Introduction

Interactions between different cat- or anions for adsorption on metal (hydr)oxides are of importance for understanding chemical processes in natural sytems. The mutual influence of different ions at adsorption to a variable charged surface is caused by site competition and/or electrostatic effects. For ions with the same charge these two effects will have a negative mutual influence on the adsorption (1, 2). For ions with opposite charge, however, the electrostatic effect will have a positive mutual influence on the adorption (3,4). So for simultaneous adsorption of a cat- and anion an interesting combination exists between synergy and competition. In this study this mechanism will be studied in detail.

Goethite is chosen as the adsorbing metal oxyhydroxide because a lot is known of its crystal structure and chemical behaviour. Moreover goethite is the most abundant

metal (hydr)oxide in natural systems. Recently the adsorption of cadmium on goethite is described in detail (5) and modeled with the Charge Distribution (CD) MUlti SIte Complexation (MUSIC) model of Hiemstra and van Riemsdijk (6). In soil systems there are many other ions that may influence the adsorption of cadmium on goethite. In this study phosphate was chosen as an interfering ion because in most soil systems phosphate is present as a nutrient adsorbed in relatively large quantities by oxides because of its high affinty for these minerals. The adsorption of phosphate on goethite and the CD-MUSIC model have been described in detail elsewhere (6).

Phosphate has a high affinity for iron-hydroxide surfaces (6, 7, 8, 9, 10). The interaction of phosphate and cadmium was studied before by Kuo et al. (3) and Kuo (11) using Hydrous Ferric Oxide (HFO). Also the zinc-phosphate interactions have been studied (12, 4). In these studies, however, no mechanistic model is presented that can describe both extended data sets of single ion adsorption and data sets of simulataneous adsorption. From these studies it is clear that phosphate adsorption on iron oxides has a positive influence on cation adsorption.

In previous work it has been found that the goethite surface mainly consists of the 110 crystal face (80-90%) with a minor contribution of the 021 crystal face (13, 14). These crystal faces have different adsorption sites for cadmium as shown for the interpretation of Extended Adsorption Fine Spectra (EXAFS) data by Spadini et al. (15). In the study of Venema et al. (5) the cadmium adsorption is described using sites with a high affinity for cadmium at the 021 crystal face in combination with low affinity sites at the dominant 110 face. This model is consistent with the interpretation of Spadini et al. With this model it has been shown that the 021 face is relatively important at low cadmium surface loading while the 110 face dominates the adsorption at high cadmium surface loading. In the present study, the Cd-$PO_4$ interaction has been studied for both situations, low and high cadmium loading, equivalent with a 021 and 110 dominated adsorption behaviour respectively. The information that is obtained with these experiments is used to refine the model of Venema et al. in order to describe both the cadmium data and the interaction data perfectly.

For the description of the phosphate adsorption, the model parameters are taken

from Geelhoed et al. (16), who studied the phosphate-sulfate interaction on goethite.

## The CD-MUSIC approach

### *Introduction*

In the MUSIC (Multi Site Complexation) approach different surface oxygens are distinguished on a metal (hydr)oxide surface. The various types of surface oxygens differ in their coordination to underlying metal ions. The charge of a central metal ion can be distributed over its bonds, resulting in a Pauling bond valence per bond. Application of this concept to iron (hydr)oxides, having a central iron (III) surrounded by six ligands, results in a bond valence of 3/6 = ½. The formal charge of a surface group is now found by the sum of its valence (-2 for O, -1 for OH and 0 for $OH_2$) and the bond valences of all coordinating iron ions. For example the charge of a singly coordinated hydroxo group (FeOH) is then: -1+½ = -½. An extended description of the MUSIC model can be found elsewhere (6, 17, 18).

In the CD-MUSIC approach, the principle of Charge Distribution (CD) has been applied to surface complex formation. The charge of a central ion in a surface complex is distributed over its ligands resulting in a new interface model.

### *The interface model*

For the application of the CD-MUSIC approach, an electrostatic model with two charge free layers, with a capacitance of resp. $C_1$ and $C_2$ is needed (Fig. 1). The presence of two charge free layers imply the existence of three electrostatic planes in which ligands of adsorbing ions can be placed. Adsorbing protons and surface ligands of adsorbed ions are placed in the surface plane (0 plane). Solution directed ligands of adsorbed ions are placed in the intermediate plane, (1 plane). The outer plane, indicated with d, is used for pair forming ions that do not form common ligands with the surface. A more extended description of the interface model can be found elsewhere (6).

If no specific adsorbing ions are present, the 1-plane is considered to be charge free. This means that the model for the description of proton adsorption transforms to a simple Basic Stern model with only one charge free layer. The overall capacitance can then be found from fitting the charging curves. The capacitances of the two layers are the same as used by Venema et al. (5) because the same material has

been used in this study (Table 1). The capacitance of the outer layer ($C_2$) is fixed on a value of 5 F/m$^2$ (6). This value of the outer layer capacitance corresponds with a layer thickness of about half a water molecule for the dielectric constant of water (=80).

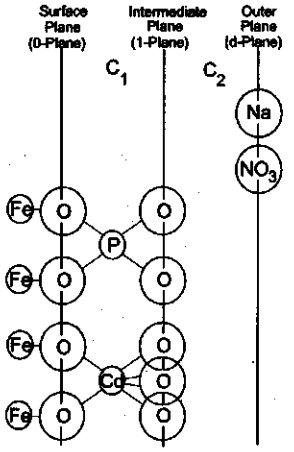


Fig. 1 The interface in the CD-MUSIC approach in case of bidentate inner sphere complex formation. Three electrostatic planes are used. The two inner planes (0-plane and 1-plane) are used for locating the charge of the specific adsorbing ions and the outer plane (d-plane) are used for the charge of pair forming ions.

## *Charge distribution in surface complexes*

The method of charge distribution in adsorption complexes will be explained briefly. A more extended treatment can be found elsewhere (6). In the previous section it is explained that the charge of the surface ligands is placed in the 0-plane while the charge of the solution oriented ligands is placed in the 1-plane. In the model this means that a fraction $f$ of the charge of a central ion ($z_{ion}$) is placed in the 0-plane and the remaining fraction (1-$f$) is placed in the 1-plane. The change in charge in the 0-plane upon ion adsorption is now given by the addition of the fraction of charge of the central ion that is placed in the surface ($z_{ion}\,f$) and the charge of co-adsorbed or de-adsorbed protons ($n_p$):

$$\Delta\sigma_0 = n_p + z_{ion} f \qquad [1]$$

in which $z_{ion}$ equals +5 for phosphate and +2 for cadmium. The change in charge in the 1-plane caused by ion adsorption is determined by the fraction of the charge that is placed in the 1-plane ((1-$f$) $z_{ion}$) plus the summation of the charges of all so-

lution oriented ligands ($\sum z_{L,i}$ ):

$$\Delta\sigma_1 = (1-f)z_{ion} + \sum_i z_{L,i} \qquad [2]$$

In the next section, the surface complexes that are used will be discussed.

## *Surface complexes*

The surface composition in terms of surface sites for the 110 and 021 face of goethite are deduced from the crystal structure. It has been shown (5, 6, 17) that some types of surface groups are not reactive with respect to protons and cadmium.

Table 1 Parameter values, used to describe the charging behaviour of goethite. The site densities and site fractions are based on the number of reactive sites (upper part of the table). It is assumed that the surface consists of 10% 021 face and 90% 110 face. The capacitances for the interface are based on the primary charging curves and modelling phosphate data (6). All log K values are based on dimensionless surface fractions. Lines in the cell (----) mean that this surface site is not present.

| Site densities | Parameter | 110 face | 021 face |
|---|---|---|---|
| | $N_s$ (sites/nm$^2$) | 6 | 11.25 |
| | fraction singly c. | 0.5 | 0.6666 |
| | fraction doubly c. | ---- | 0.3333 |
| | fraction triply c. | 0.5 | ---- |
| Stern layer Capacitance | $C_1$ (F/m$^2$) | 1.02 | 1.02 |
| | $C_2$ (F/m$^2$) | 5.0 | 5.0 |
| Protonation constants | $\log(K_{1,2})$ | 9.3 | 9.3 |
| | $\log(K_{3,1})$ | 9.3 | ---- |
| Pair formation | $\log(K_{p.f.})$ | -1.0 | -1.0 |

The start of the modeling is the desciption of the charging behaviour because protons are the potential determining ions (19, 20, 21). The site densities presented in table 1 are those that are assumed to be reactive according to the MUSIC approach (5, 6). The site densities have not been used as a fitting parameter. The proton affinity constants and Stern layer capacitances given in table 1 are taken from Vene-

ma et al. (5). The combination of these constants gives a good description of the charging behaviour of the goethite used in this study.

In the phosphate model of Hiemstra and van Riemsdijk (6) and Geelhoed et al. (16) only the singly coordinated surface groups are reactive for phosphate. In this model phosphate can form a monodentate:

$$FeOH^{-½} + H^{+} + PO_4^{-3} \rightleftharpoons FeO^{p}\,PO_3^{q} + H_2O \qquad K_{P\,1} \qquad [3]$$

in which $p+q$ = -2½. Phosphate may also form a (protonated) bidentate:

$$2\,FeOH^{-½} + 2\,H^{+} + PO_4^{-3} \rightleftharpoons (FeO)_2^{p}\,PO_2^{q} + 2\,H_2O \qquad K_{P\,2} \qquad [4]$$

$$2\,FeOH^{-½} + 3\,H^{+} + PO_4^{-3} \rightleftharpoons (FeO)_2^{p}\,POOH^{q} + 2\,H_2O \qquad K_{P\,3}$$

in which $p+q$ = -1½ and -2½ respectively. The surface species for phosphate that are used in the model are based on IR spectroscopic data of P adsorption (22, 23, 24).

Table 2 CD-MUSIC model parameters for the description of phosphate adsorption on goethite. The log $K$ and $f$ values are taken over from Geelhoed et al. 1996 (16).

| | Parameter | 110 face | 021 face |
|---|---|---|---|
| $PO_4$ binding: constants and charge distribution (Geelhoed et al. 1996) | $\log(K_{P\,1})$ | 20.5 | 20.5 |
| | $f_{P\,1}$ | 0.24 | 0.24 |
| | $\log(K_{P\,2})$ | 30.0 | 30.0 |
| | $f_{P\,2}$ | 0.55 | 0.55 |
| | $\log(K_{P\,3})$ | 35.5 | 35.5 |
| | $f_{P\,3}$ | 0.60 | 0.60 |

In the phosphate model as presented by Hiemstra and van Riemsdijk (6) and Geelhoed et al. (16) one face is used with an site density that is the weighted average of the two crystal faces mentioned above. They calculated a weighted average of the site densities assuming that the goethite surface consists of 10% 021 face and 90% 110 face. The crystal faces are assumed to have the same phosphate affinity. In this study, the phosphate model parameters for the description of phosphate-sulphate interaction on goethite (16) are used but the crystal faces are considered separately

as by Venema et al. (5) (Table 2).

Spadini et al. (15) showed that cadmium can replace iron in goethite crystals that were grown in a cadmium solution. According to this experiment it seems to be probable that cadmium adsorbs at crystal growth positions on the goethite surface. With this assumption, a model was developed by Venema et al. (5) that could describe the adsorption of cadmium very well. In the model, a bidentate surface complex was formed at the 110 face with the singly coordinated surface groups:

$$2\ FeOH^{-\frac{1}{2}} + Cd^{2+} \leftharpoondown (FeOH)_2^p\ Cd^q \qquad K_{Cd\,2} \qquad [5]$$

in which $p+q = +1$ and $K_{Cd\,2}$ is the intrinsic affinity constant for the cadmium bidentate complex. A crystal growth position at the 021 face lead to the use of a high affinity cadmium tridentate surface complex with two singly and one doubly coordinated surface group:

$$2\ FeOH^{-\frac{1}{2}} + Fe_2OH^0 + Cd^{2+} \leftharpoondown [(FeOH)_2Fe_2O]^p\ Cd^q \qquad K_{Cd\,3} \qquad [6]$$

in which $p+q = +1$ and $K_{Cd\,3}$ is the intrinsic affinity constant for the cadmium tridentate complex. In this study the cadmium parameters of Venema et al. (5) are used (Table 3).

Table 3 CD-MUSIC model parameters for the description of cadmium adsorption on goethite as used by Venema et al. (5).

| Cd binding: | Parameter | 110 face | 021 face |
|---|---|---|---|
| constants and charge distribution (Venema et al. 1996) | $\log(K_{Cd\,2})$ | 6.9 | ---- |
| | $f_{Cd\,2}$ | 0.30 | ---- |
| | $\log(K_{Cd\,3})$ | ---- | 9.0 |
| | $f_{Cd\,3}$ | ---- | 0.58 |

Venema et al. found that the description of the EXAFS data of Spadini et al. (15) improved if a cadmium monodentate surface complex was used at the 110 face. In this study, the speciation of the 110 face can be examined in more detail because of the extra information obtained from the cadmium-phosphate interaction. At this crystal face such a complex can form on a crystal growth position with the doubly

coordinated surface groups. It seems unlikely, however, to assume that the doubly coordinated groups are more reactive than the singly coordinated surface groups. A model in which both the singly and doubly coordinated surface groups are reactive for cadmium will not be discussed in detail here. The possibility for a monodentate cadmium surface complex with the singly coordinated surface groups is used as an option for reasons mentioned later. The monodentate surface complex, however, is not a crystal growth position. The formation of this monodentate surface complex can be written as:

$$FeOH^{-½} + Cd^{2+} \leftrightharpoons FeOH^{p}\ Cd^{q} \qquad K_{Cd\,1} \qquad [7]$$

in which $p+q=1½$ . The affinity constant $K_{Cd\,1}$ for this surface complex is treated as a fit parameter. According to the $f$ factor of 0.3 for the bidentate complex (Table 3), the $f$ factor of the cadmium monodentate surface complex should be 0.15.

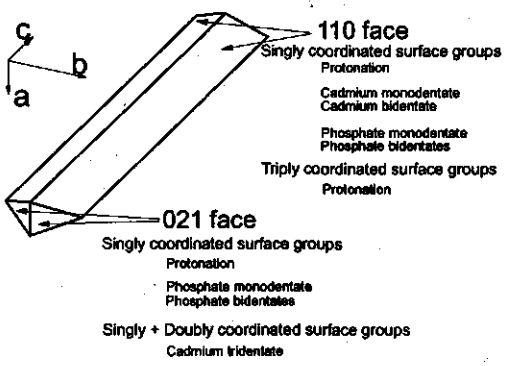


Fig. 2 Overview of the surface complexes that are used in this study and their position on the goethite crystal. At the 110 face the reactive sites are singly and triply coordinated surface groups. At the 021 face, singly and doubly coordinated surface groups are reactive.

Resuming, the singly coordinated surface groups at the 110 face are reactive for cadmium according to eq. [5] and eq. [7] and for phosphate according to eq. [3] and eq. [4]. At the 021 face, the singly coordinated surface groups can complexate with cadmium according to eq. [6] and with phosphate according to eq. [3] and eq. [4]. An overview of the surface complexes that are used in this study is shown in Fig. 2.

For all calculations, equilibrium constants for the important dissolved species and

minerals from Lindsay (25) and Smith and Martell (26) are used. The activitiy coefficients are calculated with an adapted Davis equation (27). All calculations are done with the calculation program ECOSAT (27).

## Experimental

Adsorption edges were measured at different phosphate and cadmium concentrations. Distilled, demineralized water was used in all experiments. The experiments were done with plastic bottles and a total volume of 60 ml with a suspension density of 6 g goethite per liter was used. The goethite had a specific surface area of 95 $m^2/g$ measured with BET $N_2$ adsorption. The background salt concentration ($NaNO_3$) was 0.1 mol/l in all cases. The same procedure was used for all experiments. No $CO_2$ was excluded. The estimated amount of $(H_2O)CO_2$ and $HCO_3$ in a bottle is about $10^{-4}$ mol/l. This amount is calculated as the sum of the total amount of carbonate present in the solutions and present in the goethite suspension that had a pH of 8.0 (dilution factor about 1:10) assuming equilibrium with air ($P_{CO_2} = 3 \cdot 10^{-4}$ bar). The experimental conditions were chosen so that no cadmium phosphates could precipitate.

First the suspensions were brought to the appropriate pH before the appropriate amounts of phosphate and/or cadmium were added. Next, the bottles were shaken in an end-over-end shaker for 24-36 hours. After shaking, the suspension pH was measured and a sample was centrifuged at 18000 rpm. In the supernatant the $PO_4$ concentrations were measured colorimetrically after colouring with molybdate. The cadmium concentrations were measured on flame AAS using the Smith-Hieftje background correction.

Adsorption edges of phosphate ($Na_2HPO_4$) were measured at different initial total amounts of phosphate (0.54, 1.61 and 2.14 mmol $PO_4$/l).

Cadmium was measured without phosphate at initial total amounts of 0.05, 0.25, 0.50, 1.00 mmol/l. The high cadmium amounts (0.25, 0.50 and 1.00 mmol/l) were also measured with an initial amount of 0.54 mmol/l phosphate. Additional cadmium measurements were done at a low total amount cadmium (0.05 mmol/l) with different amounts of phosphate (0.54, 1.61, 2.14 mmol/l). For these low cadmium experiments, the adsorption of phosphate was measured too.

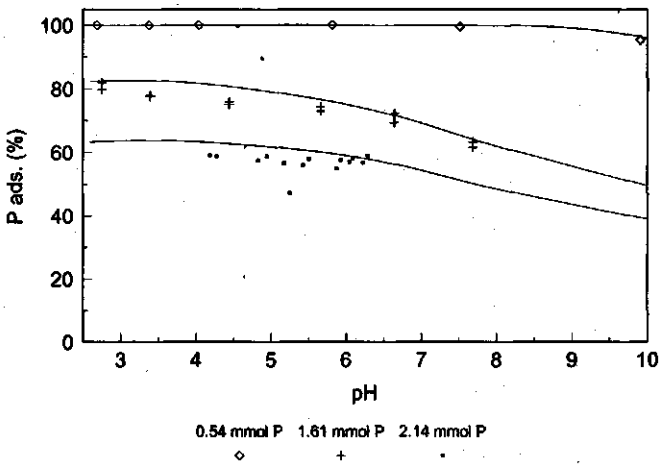


Fig. 3 Phosphate adsorption data for goethite (570 $m^2/l$) at a background salt concentration ($NaNO_3$) of 0.1 mol/l. The solid lines represent the model calculations with the parameters of Geelhoed et al. (1996) (16).

## Results and discussion

### *Phosphate adsorption*

The phosphate adsorption edges as measured in this study show a low pH dependency (Fig. 3). The adsorption is shown in % because otherwise the differences between the two high phosphate amounts would be too small. The phosphate data (Fig. 3) are in agreement with literature data (Bowden et al., Hiemstra and van Riemsdijk 1996, Geelhoed et al., Torrent et al. 1990). The model description of the phosphate data is shown by the lines. The model, with the parameters of Geelhoed et al. (16), slightly overestimates (up to 5%) the adsorption of phosphate for the high amounts of phosphate. This can be caused by an error in the BET surface of about 5%. This error is too small to adapt model parameters for it.

### *Cadmium adsorption*

The adsorption of cadmium (Fig. 4) shows a large pH dependency. The adsorption is indicated in $\mu mol/m^2$ because the differences between the different amounts of cadmium are then more pronounced and because the surface loading can thus be read directly from the graph. The cadmium adsorption data are in good accordance with data measured before (5, 29, 30).

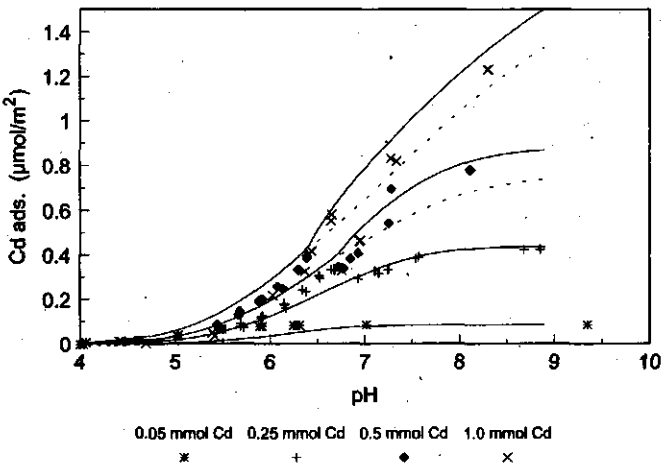


Fig. 4 Cadmium adsorption data for goethite (570 $m^2/l$) in 0.1 mol/l $NaNO_3$. The solid lines represent the model calculations with $CO_3$. The dashed lines are the calculations without $CO_3$, the higher "adsorption" is caused by precipitation of $CdCO_3$.

The only change in the cadmium model of Venema et al. (5) that is made in this study is the assumption of an extra monodentate surface species (eq. [7]). The values for log $K_{Cd\,1}$ and $f_{Cd\,1}$ of this monodentate species are shown in Table 4, so the cadmium model parameters comprise Table 3 and Table 4. The extra monodentate cadmium surface species is not needed for the description of the data for cadmium without phosphate. With only the model parameters of Venema et al. (5) (Table 3) the data of Fig. 4 can be described very well too. If phosphate is added, however, the extra surface species is very important as will be discussed in the following sections.

With the extended model (Table 3 +Table 4) the cadmium data are described well (lines in Fig. 4). In Fig. 4, the calculations without carbonate are indicated with a dashed line. According to the model, $CdCO_3$ precipitates only for the two highest amounts of cadmium. For these data, the predicted cadmium adsorption is improved if the precipitation of cadmium is taken into account. The maximum relative contribution of precipitated $CdCO_3$ is about 17% at pH 7 for the highest two cadmium amounts (0.5 mmol/l and 1 mmol/l). So the presence of $CO_3$ in the solution can have significant influence on the measured amount of total adsorbed cadmium.

Table 4 The CD-MUSIC model parameters for the extra cadmium surface complex, the monodentate at the 110 face. It must be stressed here that the parameters for the bi- and tridentate as used by Venema et al. 1996 (5) (Table 3) are unchanged.

| Cd binding: | Parameter | 110 face | 021 face |
|---|---|---|---|
| Extra constants and charge distribution | $\log(K_{Cd\,1})$ | 5.5 | ---- |
| | $f_{Cd\,1}$ | 0.15 | ---- |

In the description of the data of Venema et al. (5), the new introduced cadmium monodentate species is most important at pH 5 and 6, for the higher pH values its contribution is very small. The relative importance of the monodentate at low pH values is directly related to the number of available FeOH groups. At low pH values, less FeOH groups are available because they are protonated to $FeOH_2$. A decrease in the number of FeOH groups results in a shift to the left in the chemical equillibria for the cadmium mono- (eq. [7]) and bidentate (eq. [5]) species. This shift in the equillibrium for the bidentate will be larger because here two FeOH groups occur per cadmium species. So a decrease in pH will result in an increasing importance of the cadmium monodentate surface groups.

At the 021 face too, the number of FeOH will decrease with decreasing pH. For the reaction for the cadmium tridentate surface species, also two FeOH groups occur. So, the number of cadmium tridentate species will also decrease faster with decreasing pH than the number of cadmium monodentate species. This amplifies the increase of the relative importance of the cadmium monodentate with decreasing pH.

The introduction of the extra surface species has minor influence on the description of the data of Venema et al. 1996. The major change in the description is a very slight decrease in the pH dependency in the lower pH range. This is caused by the fact that the cadmium monodentate species is relatively important in the low pH range. The cadmium monodentate complex is more outer sphere than the bidentate complex (lower $f$ value). An outer sphere complex shows a smaller pH dependency than an inner sphere complex (5).

It was mentioned before that the doubly coordinated surface groups at the 110 face could also be assumed to be reactive for cadmium. This assumption would be in

better accordance with the vision of Spadini et al. (15). It was found in this study that the data with cadmium only could be described well with this option. However, it appeared to be impossible to describe the effect of phosphate on cadmium well with this option. This is the reason why at the 110 face the doubly coordinated surface groups are assumed not to be reactive for cadmium.

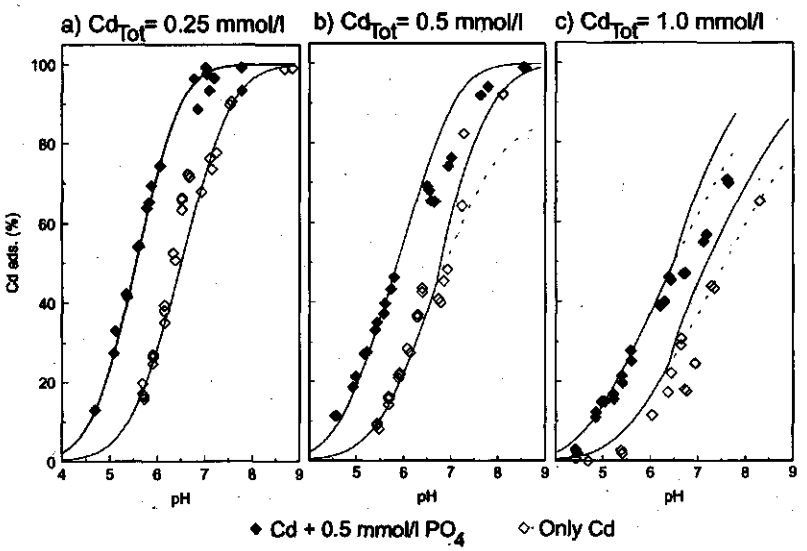


Fig. 5 Cadmium adsorption data for goethite (570 $m^2/l$) in 0.1 mol/l $NaNO_3$ with 0.25 mmol/l Cd (a), 0.5 mmol/l Cd (b) and 1.0 mmol/l Cd (c). The closed symbols represent data with 0.5 mmol/l P in the system while the open symbols represent a system without phosphate. The solid lines represent the model calculations with $CO_3$. The dashed lines show the model calculation without $CO_3$. In the model calculations, the cadmium monodentate surface complex (110 face) becomes more important when phosphate is present in the system (Fig. 6).

### *High amounts of Cadmium with phosphate*

The presence of phosphate has a positive influence on the cadmium adsorption (Fig. 5) as could be expected from the data of Kuo. The open symbols in Fig. 5 are the same data as shown in Fig. 4, the closed symbols are the data with phosphate. In Fig. 5 the same scale is used for all total amounts of cadmium in order to compare the three different data sets, the adsorption is therefore indicated in %.

The model describes both the data of cadmium with and without phosphate very well. The adsorption is slightly overestimated for the high amounts of cadmium at

high pH values. For the highest cadmium amount (Fig. 5c), this overestimation may be caused by the fact that oversaturation occurs so that no precipitate is formed. In Fig. 5, the model calculations without phosphate are shown as dashed lines. In Fig. 5c, the dashed lines describe the cadmium data with phosphate very well.

The importance of $CdCO_3$ precipitation is smaller if phosphate is present in the system (upper solid lines Fig. 5) compared to the data without phosphate (lower solid lines Fig. 5c). This is caused by the higher cadmium adsorption in the presence of phosphate and therefore the lower amount of free cadmium in the solution. The maximum relative contribution of the precipitate to the adsorption is about 8% at a pH of 7, so the predicted cadmium adsorption increases slightly at the high cadmium concentrations because of the presence of $CO_3$.

The cadmium monodentate surface complex (110 face) becomes more important if phosphate is present in the system (Fig. 6). It can be concluded that, according to the model, the increase in cadmium adsorption is mainly caused by the increase of the monodentate surface complex. It is not surprising that the 110 face will become more important for cadmium adsorption if phosphate is present in the system. Adding phosphate gives a similar effect as adding $OH^-$: decreasing the electrostatic potential near the surface. This causes an increase in the overall cadmium concentration near the surface so that the cadmium surface loading will increase. For higher surface loading, the 021 face becomes saturated so that the 110 face will become relatively important. The reason why the cadmium monodentate becomes dominant if phosphate is present in the system will be discussed in the following paragraph.

The relative increase of cadmium monodentate surface species upon phosphate adsorption has two causes. The first cause is a decrease in the number of the singly coordinated hydroxo surface groups (FeOH) upon adsorption of phosphate. This decrease is caused by the fact that more protons will adsorb because of the lower surface potential. As explained in the previous section, this results in a increase of the relative number of cadmium monodentates at the 110 face. The second cause is the decrease of the potential in the intermediate plane upon phosphate adsorption. The potential of the surface remains nearly constant because of co-adsorption of protons. The cadmium monodentate has a smaller $f$ factor than the cadmium

bidentate so that for the monodentate a larger part of the cadmium charge is placed in the intermediate plane. Therefore a decrease in the potential in this intermediate plane will have a stronger positive effect on the abundance of the cadmium monodentate surface species.

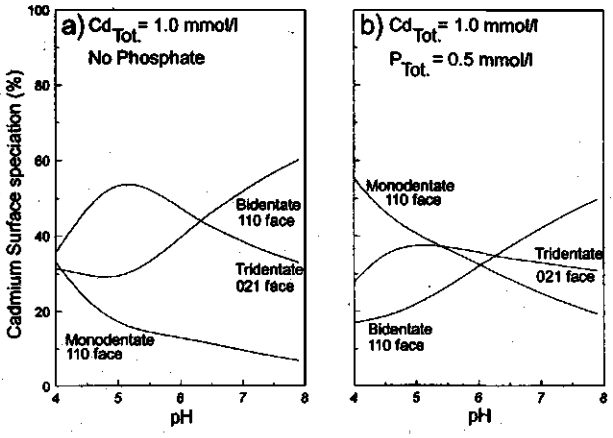


Fig. 6 The surface speciation of cadmium on the goethite surface according to the model calculations. The calculations have been done for a system with an ionic strength ($NaNO_3$) of 0.1 mol/l, 570 $m^2$/l goethite and 1.0 mmol/l Cd. A situation without (a) and with 0.5 mmol/l phosphate (b) is considered.

According to the model, site competition between phosphate and cadmium is not of importance for this data set. The competition seems to be indirect via the co-adsorption of protons with phosphate, which causes the shift from the cadmium bidentate to the monodentate. The surface coverage of all cadmium surface species, for the highest cadmium concentrations, is positively influenced by the presence of phosphate.

### *Low amount of Cadmium with phosphate*

For the low amount of cadmium it is possible to add higher amounts of phosphate without the risk of formation of cadmium phosphate precipitates. Therefore, three different phosphate amounts are considered (Fig. 7). For the two highest amounts of phosphate no difference is seen in the adsorption of cadmium. This is caused by the fact that for these two data sets, the phosphate adsorption is almost equal (about 2.3-2.4 µmol/$m^2$). Precipitates of carbonate are of no importance for this data set.

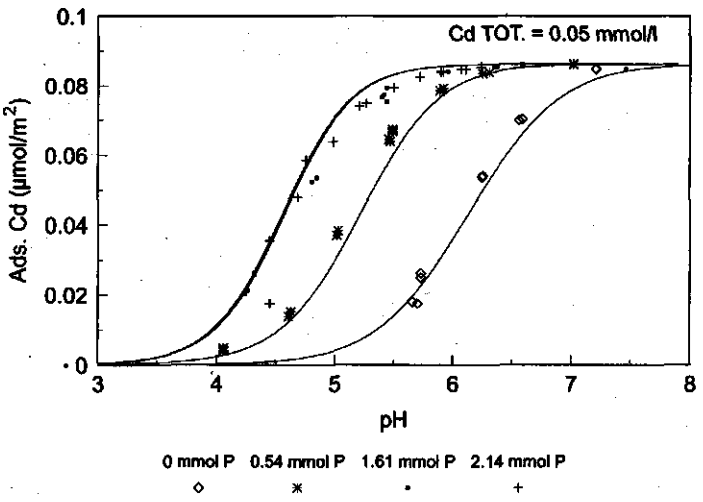


Fig. 7 Cadmium adsorption data for goethite (570 $m^2/l$) in 0.1 mol/l $NaNO_3$ and 0.05 mmol/l Cd in the system. The symbols represent data with different amounts of phosphate in the system. The solid lines represent the model calculations. At these low cadmium concentrations, $CO_3$ has no influence. According to the model, most cadmium is adsorbed to the 021 face for the low phosphate concentrations. For the two highest phosphate concentrations, the cadmium monodentate surface complex (110 face) is far dominant.

As discussed in the introduction, the 021 face is of major importace at low surface loading. For the cadmium data without phosphate, the 021 face appears indeed to be dominant (Fig. 8a). As for the data discussed before, the 110 face, especially the cadmium monodentate complex, becomes more important if phosphate is added (Fig. 8b). For the highest amounts of phosphate, the cadmium monodentate complex becomes even far dominant. At these two high phosphate concentrations, the contribution of the cadmium bidentate decreases to below 10% for all pH values. For these high amounts of phosphate, the dominance of the monodentate surface groups is mainly caused by the decrease in the number of FeOH groups.

The influence of cadmium on phosphate has been measured for this data set. It was found that cadmium did not have influence on the phosphate adsorption within the experimental error. This could be expected because the surface loading with cadmium is very low (below 0.1 $\mu mol/m^2$).

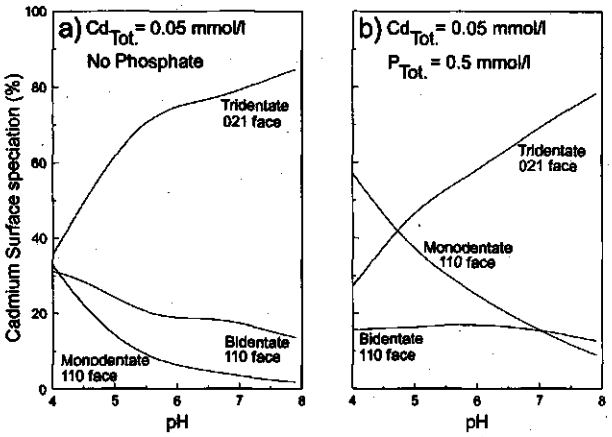


Fig. 8 The surface speciation of cadmium on the goethite surface according to the model calculations. The calculations have been done for a system with an ionic strength ($NaNO_3$) of 0.1 mol/l, 570 $m^2$/l goethite and 0.05 mmol/l Cd. A situation without (a) and with 0.5 mmol/l phosphate is considered.

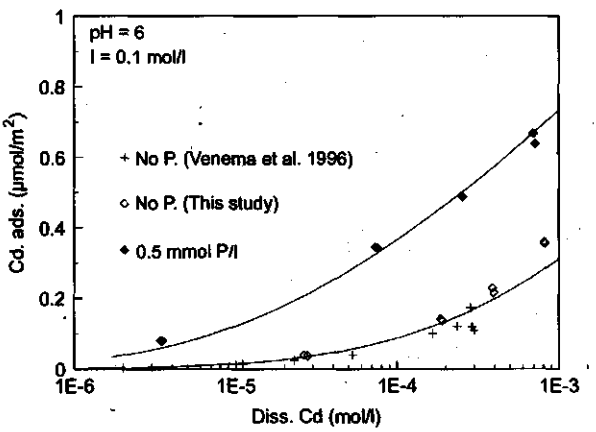


Fig. 9 Adsorption isotherms for cadmium adsorption at pH 6 in no phosphate is present (filled diamonds) and if phosphate is present (open diamonds). The isotherms are obtained from a cross-section of the adsorption edges for cadmium adsorption at pH 6. The filled squares represent a cadmium adsorption isotherm at pH 6 measured by Venema et al. (V&a). The lines represent the model calculation.

In Fig. 9, adsorption isotherms for cadmium are shown that are obtained from a cross section at pH 6 of the data shown in Fig. 4 and Fig. 5. The data for cadmium adsorption without phosphate are compared with the data of Venema et al. (5). The

data set measured in this study is in accordance with the data of Venema et al. within the experimental error.

The lines in Fig. 9 represent the model prediction of the data. It can be seen that the model describes the data well.

## Conclusions

Multicomponent adsorption studies can give more insight in the speciation than can be derived from simpler systems. The CD-MUSIC model can describe multi component adsorption to metal (hydr)oxides.

The newly introduced cadmium monodentate surface species is important for data with phosphate because of a combination of two effects. An electrostatic effects and the effect it has on the competition between protons and cadmium ions for binding sites.

From these data it cannot be concluded that the doubly coordinated surface groups at the 110 face are reactive. The model in which these surface groups are assumed to be reactive gives poorer results than the model in which only the singly coordinated surface groups are reactive.

The presence of carbonate has especially a large influence on the data with only cadmium in the system. In the presence of phosphate, the cadmium concentrations are so low that the influence is negligible. In soil systems in which cadmium concentrations are very low and phosphate concentrations may be high, the influence of carbonate may be negligible.

**Acknowledgement**

The authors thank Dr. Peter Weidler for the physical characterisation of the goethite used in this study and for the fruitful discussions about the morphology of goethite. Also we thank Debby Swinkels for her experimental work, of which the results are used for this publication.

Part of this work is financed by the European Community through contract STEP-CT90-0031.

## Literature


1 Benjamin, M.M., and Leckie, J.O., Multiple-site adsorption of Cd, Cu, Zn, and Pb, on amorphous iron oxyhydroxide, *J. Colloid Interface Sci.*, **79**, 209-221, (1981)

2 Cowan, Christina. E., Zachara, John. M, and Resch, Charles. T., Cadmium Adsorption on Iron Oxides in the Presence of Alkaline-Earth Elements, *Environ. Sci. Technol.*, **25**, 437-446, (1991)

3 Kuo S., and McNeal B.L., Effects of pH and Phosphate on Cadmium Sorption by a Hydrous Ferric Oxide, *Soil Sci. Soc. Am. J.*, **48**, 1040-1044, (1984)

4 Diaz-Barrientos E., Madrid L., Contreras M.C., and Morillo E., Simultaneaous adsorption of zinc and phosphate on synthetic Lepidocrocite, *Aust. J. Soil Res.*, **28**, 549-557, (1990)

5 Venema, P., Hiemstra, T., and van Riemsdijk, W.H., Multisite adsorption of cadmium on goethite, *J. Colloid Interface Sci.* **183**, in press (1996)

6 Hiemstra, T, and van Riemsdijk, W.H., A surface structural approach to ion adsorption: The Charge Distribution (CD) model, *J. Colloid Interface Sci.* **179**, 488-508 (1996)

7 Barrow, N.J., Brummer, G.W., and Strauss, R., Effects of Surface Heterogeneity on Ion Adsorption by Metal Oxides and by Soils, *Langmuir*, 9(10), 2606-2611, (1993)

8 Colombo C., Barron V., and Torrent J., Phosphate adsorption and desorption in relation to morphology and crystal properties of synthetic hematites, *Geochim. Cosmochim. Acta*, 38(4), 1261-1269, (1993)

9 Torrent, J., Barron, V., and Schwertmann, U., Phosphate Adsorption and Desorption by Goethites Differing in Crystal Morphology, *Soil Sci. Soc. Am. J.*, 54, 1007-1012, (1990)

10 Torrent J., Schwertmann U., and Barron V., Phosphate sorption by natural hematites, *Europ. J. Soil Sci.*, 45, 45-51, (1994)

11 Kuo S., Concurrent Sorption of Phosphate and Zinc, Cadmium, or Calcium by a Hydrous Ferric Oxide, *Soil Sci. Soc. Am. J.*, **50**, 1412-1419, (1986)

12 Bolland M.D.A., Posner A.M., and Quirk J.P., Zinc Adsorption by Goethite in the Absence and Presence of Phosphate, *Aust. J. Soil Res.*, 15, 279-286, (1977)

13 Schwertmann U., Cornell R., Iron Oxides in the laboratory., VCH Weinheim, New York, Basel, Cambridge, 1991

14 Weidler P.G., Schwinn T. and Gaub H.E., Vicinal Faces on Synthetic Goethite Observed by Atomic Force Microscopy, *Clays and Clay Minerals*, **44**, 437-442, (1996)

15 Spadini, L., Manceau, A., Schindler, P.W., and Charlet, L.C. (1994) Structure and stability of $Cd^{2+}$ surface complexes on Ferric Oxides, *J. Colloid Interface Sci.* **168**, 73-86

16 Geelhoed, J.S., Hiemstra, T., and van Riemsdijk, W.H. (1996) Phosphate and sulfate adsorption on goethite: single anion and competitive adsorption, accepted, *Geochim. Cosmochim. Acta*, (1997)

17 Hiemstra, T, vanRiemsdijk, W.H., and Bolt, G.H. (1989a) Multisite Proton Adsorption Modeling at the Solid/Solution Interface of (Hydr)oxides: A New Approach, I. Model Description and Evaluation of Intrinsic Reaction Constants, *J. Colloid Interface Sci.* **133**, 91-104

18 Hiemstra, T, de Wit J.C.M., and vanRiemsdijk W.H. (1989b) Multisite Proton Adsorption Modeling at the Solid/Solution Interface of (Hydr)oxides: A New Approach, II. Application to various Important (Hydr)oxides, *J. Colloid Interface Sci.* **133**, 105-117

19 Parks, G.A., and de Bruyn, P.L., The zero point of charge of oxides, *J. Phys. Chem.*, **66**, 967, (1962)

20 Hingston, F.J., Posner, A.M., and Quirk, J.P., Anion adsorption by goethite and gibbsite I. the role of the proton in determining adsorption envelopes, *J. Soil Sci.* **23**, 177-192 (1970)

21 Yates, D.E., "The Structure of the Oxide/Aqueous Electrolyte Interface", PhD. Thesis, University of Melbourne, Melbourne, Australia 1975

22 Russel, J.D., Parfitt, R.L., Fraser, A.R., and Farmer V.C., Surface structures of gibbsite goethite and phosphated goethite, *Nature* **248**, 220-221 (1974)

23 Parfitt, R.L., Atkinson, R.J., and Smart, R.St.C., The mechanism of phosphate fixation by iron oxides, *Soil Sci. Soc. Am. Proc.*, **39**, 837-841 (1975)

24 Tejedor-Tejedor, M.I., and Anderson, M.A., Protonation of phosphate on the surface of goethite as studied by CIR-FTIR and electrophoretic mobility, *Langmuir*, **6** 602-611 (1990)

25 Lindsay, W.L., Chemical equilibria in Soils, John Wiley, New York 1979.

26 Smith, R.M., and Martell, A.E., "Critical Stability Constants" Vol. 4, Plenum, New York, 1981

27 Keizer, M.G., and van Riemsdijk W.H., ECOSAT; Technical report of the Department Soil Science and Plant Nutrition, Wageningen Agricultural University, (1994)

28 Bowden J.W., Nagarajah S., Barrow N.J., Posner A.M., and Quirk J.P. (1980) Describing the adsorption of phosphate, citrate and selenite on a variable -charge mineral surface, *Aust. J. Soil Res.*, **18**, 49-60

29 Hayes K.F., and Leckie J.O., Modeling Ionic Strength Effects on Cation Adsorption at Hydrous Oxide/Solution Interfaces, *J. Colloid Interface Sci.*, **115**, 564-572, (1987)

30 Johnson Bruce B., Effect of pH, Temperature, and Concentration on the Adsorption of Cadmium on Goethite, *Environ. Sci. Technol.*, **24**, 112-118, (1990)

31 Gunneriusson Lars, Composition and stability of Cd(II)-Chloro and -Hydroxo Complexes at the Goethite (α-FeOOH)/Water interface, *J. Colloid Interface Sci.*, **163**, 484-492, (1994)

# 5

# Intrinsic proton affinity of reactive surface groups of Metal (hydr)oxides: The bond valence principle

T. Hiemstra, P. Venema and W.H. Van Riemsdijk
Journal of Colloid and Interface Science, Vol. 184, p. 680-692, 1996

# Intrinsic proton affinity of reactive surface groups of Metal (hydr)-oxides: The bond valence principle


## Abstract

*The proton affinity of individual surface groups has been calculated with a redefined version of the MUlti Site Complexation (MUSIC) model. In the new approach the proton affinity of an oxygen originates from the undersaturation of the oxygens valence. The factors valence and coordination number, which are the basis of Pauling definition of bond valence, in combination with the number of coordinating (Me and H) ions, are dominant in determining the proton affinity. The neutralization of an oxygen by Me ion(s) is calculated on the basis of the actual bond valence, which accounts for structural details, resulting from an asymmetrical distribution of charge in the coordination environment. An important role in the new version of the MUSIC model is given to the H bonds. The model shows that the proton affinity is not only determined by the number of donating H bonds but also by the number of accepting H bonds. The proton affinity of surface groups and that of solution complexes can be understood in one theoretical framework, on the basis of a different number of donating and accepting H bonds.*

*The MUSIC model predicts the variation in proton affinity constants for surface groups in particular also those with the same number of coordinating Me ions but with a different structural position. The model is able to predict on the basis of the proton affinity of the individual groups, the correct PZC of Me hydroxides, oxohydroxides and oxides, and explains previous exceptions. The model can also be applied in general to other minerals.*


## Introduction

Metal (hydr)oxides play an important role in many fields of chemistry. The interfacial chemistry is of practical and theoretical importance. The proton affinity of surface groups is of special interest because acidity and basicity is of direct concern in many chemical processes like catalysis and it determines the pristine charging and with it the binding behaviour of important chemical elements. The Point of Zero Charge (PZC) has been considered as a basic characteristic of metal (hydr)oxides and various attempts have been made (1, 2, 3, 4) to relate this overall chemical feature to the general characteristics of the metal (hydr)oxide, treating the interface as

chemically homogeneous. The surfaces of metal (hydr)oxides are however generally heterogeneous, i.e. several types of metal (hydr)oxides groups are present, and the PZC is only the resultant of a combined action of several types of surface groups. It implies that in general from the PZC value no direct information can be found about the proton affinity of individual types of surface groups. Also the charging curve as a whole will not give this important information a priori, in particular because it is very strongly influenced by the electrostatic field of the double layer, masking the individual contributions. With the development of the MUlti SIte Complexation model (MUSIC) a first attempt has been made to estimate the proton affinity for individual types of surface groups (5), resulting in a predicted PZC value once the chemical composition of the interface is known. In the MUSIC model the proton affinity of the individual groups was calculated on the basis of the Pauling bond valence (6) in which the charge of the central ion is equally distributed over its surrounding ligands. The MUSIC model predicts that one of the main differences in intrinsic proton affinity of surface groups is due to the number of metal ions coordinating to the surface oxygens. Another important prediction of the MUSIC model is that the difference in affinity between the first and second proton that binds to the same type of surface oxygen is very large, about 14 log $K$ units. The MUSIC model was calibrated using the oxo and hydroxo protonation reactions in solution. The MUSIC model has improved the understanding of the difference in charging behaviour of metal (hydr)oxides and various authors claim to have been successful in the application of the model (7, 8, 9, 10). Recently the MUSIC model has been extended applying the Pauling concept of Charge Distribution (CD) to the formation of surface complexes with cations and anions (11, 12) and is referred to as the CD-MUSIC model.

The MUSIC model for prediction of the proton affinity has been applied to an important metal oxohydroxide, namely α-FeOOH (goethite). Early electron microscopy work on goethite (13) suggested the presence of the 100, 010 and 001 crystal faces, which we have used in our previous applications of the MUSIC model (7, 14). However gradually, it has become clear that the main crystal plane of goethite is the 110 face (15). This face is dominated by triply coordinated surface $Fe_3O(H)$ groups (11, 16), which implies that the proton affinity of these predominant groups will strongly determine the value of the PZC. The PZC of goethite is high (9±0.5) indicating that one expects a high value for the log $K$ of the protonation reaction of

triply coordinated surface oxygens. This contrasts with the low log $K$ value for $Fe_3O$ groups, predicted by the MUSIC model. For this discrepancy a first qualitative explanation has been formulated (11) which is based on structural details of the solid.

The crystal structure of goethite is characterized by $Fe^{3+}$ ions in hexa-coordination with O and OH. Each O or OH coordinates with three $Fe^{3+}$ ions. In the bulk of the FeOOH mineral two types of triply coordinated oxygen groups are found, one protonated ($Fe_3OH$) and one non-protonated ($Fe_3O$) group. The protonated $Fe_3OH$ group forms a hydrogen bond with the non protonated one ($Fe_3O$). It suggests that a proton-oxygen bond of the $Fe_3OH^{+½}$ group is stronger than a proton-oxygen bond with the non-protonated $Fe_3O^{-½}$ group in the solid. It has been hypothesized that the difference in the proton-oxygen bond strength in the solid will also lead to different proton affinities in the interface (11). This illustrates that there can be different types of triply coordinated oxygens in the interface with different proton affinities. The first version of the MUSIC model does not take these differences into account.

The presence of a strong difference in proton affinity of triply coordinated groups is also supported by results of ion adsorption modelling with the previous mentioned CD-MUSIC approach. In the modelling we could only describe simultaneously a full range of adsorption phenomena (primary charging, concentration, pH and salt dependency, shift in zeta potentials and iso electric points (IEP), and ion/proton exchange ratios, *in situ* IR spectroscopy data) within one concept if a large difference in proton affinity for the different types of $Fe_3O$ groups exists on the 110 face of goethite. For details we refer to Hiemstra and VanRiemsdijk (11).

The MUSIC model has also been applied to the charging behaviour of silica. The shape of the charging curves is quite different from that of many other oxides. Similar observations have been made with respect to the experimentally measured pH dependent surface potential, where silica behaves quite non-Nernstian in contrast to other metal (hydr)oxides, which may react near-Nernstian (17, 18, 19). All these observations can be understood within one theoretical framework, the MUSIC model, on the basis of the difference in charge attribution of metal ions to surface groups (5, 7). Evaluation of the charging behaviour of silica however also showed that the MUSIC model was unable to predict the correct value for the proton af-

finity constant (7).

In the present paper we will describe a refined version of the MUSIC model which copes with the above discrepancies and predicts the variation in proton affinity constants of surface groups, in particular the variation for surface groups, which have the same number of coordinating Me ions, but different structural positions.

## Pauling bond valence

The charge of ions in the solid of Me (hydr)oxides is internally fully compensated. The principle of electroneutrality implies that the charge of a cation is compensated by the charge of the surrounding oxygens and vice versa. For neutralization, the charge is distributed over the surrounding ligands, which can be expressed per bond, leading to the concept of a bond valence $\nu$ as introduced by Pauling (6). The bond valence defined as the charge $z$ of a cation divided by its coordination number $CN$, i.e. the mean charge per bond:

$$\nu = \frac{z}{CN} \qquad [1]$$

In the MUSIC model we applied the bond valence concept to hydroxylated surfaces, assuming a symmetrical distribution of charge in metal (hydr)oxides. The bond valence expresses the effective repulsive force between the Me centre and protons present on the surrounding ligands. The interaction depends not only on the valence of the Me ion, but also on the number of surrounding oxygens able to screen the charge of the Me centre. The total amount of effective charge available for Me-H interaction will determine the proton affinity. This implies that the number of Me cations coordinating to the oxygen is important for the proton affinity of a surface group. In addition the affinity is also strongly determined by the number of protons present at the surface ligand. The affinity of an oxo group is considerably larger than the affinity of the corresponding hydroxo group, because of the presence of a H-H interaction at the latter one.

## Actual bond valence

For the prediction of the log $K$ in the first version of the MUSIC model, it was assumed that the charge is equally distributed over the ligands, according to Pauling's definition (eq.[1]). This is equivalent with assuming equal distances between the

central metal (Me) ion and the surrounding oxygens (20). However within one mineral the Me-O distances may be quite different, like for instance in goethite (α--FeOOH). As mentioned, in this mineral the oxygen charge is neutralized by three Fe3+ ions and in addition by a contribution of an asymmetric H bond, leading to a $Fe_3OH$--$OFe_3$ configuration (Fig. 1).

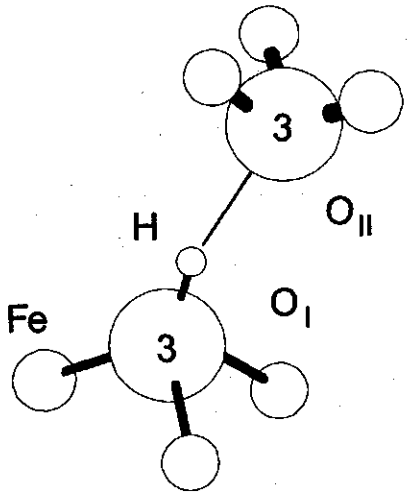


Fig. 1 The schematic basic structural unit of goethite, comprising two types of oxygens $O_I$ and $O_{II}$, both being triply coordinated to Fe. In the oxygens the coordination number 3 is indicated. Between both types of oxygens a H bond exists, which distributes its charge asymmetrically. The oxygen ion with the largest H contribution in the neutralization, receives from the coordinating Fe ions a smaller charge contribution for the neutralization. This leads to a larger FeO distance ($R$ = 2.09-2.10 Å) in the $Fe_3OH$ configuration. The opposite holds for the $Fe_3O$ groups ($R$ = 1.95-1.96 Å).

The asymmetric contribution of H in the neutralization implies that the coordinating Fe ions in the $Fe_3O$ part have to contribute more to the neutralization of the oxygen whereas the Fe ions in the $Fe_3OH$ part contribute less than is expected on the basis of the Pauling bond valences. This difference in neutralization finds its expression in the crystal lattice in different FeO distances for both units. It illustrates that charge distribution and neutralization are related to Me-O lengths, i.e. the actual bond valence is different from the Pauling bond valence based on equal charge distribution. Different distances can also be found in the oxides without hydrogen bonds in the structure, for instance in the isostructural minerals hematite ( $\alpha$-$Fe_2O_3$) and corundum ($\alpha$-$Al_2O_3$). In this structure close packed oxygen layers are bound to-

gether by $Me^{3+}$ ions, filling two out of three octahedral positions in the lattice (Fig. 2). Due to electrostatic Me-Me repulsion, the Me ions are displaced in the octahedrons towards the empty octahedral positions, resulting in an asymmetry within the octahedron and in different Me-O distances (21, 22). A bond with a smaller Me-O distance will contribute more to the neutralisation of charge than a bond with a large Me-O distance. Smaller distances in an octahedron lead to higher charge attributions, i.e. higher actual bond valences than conform to Pauling's bond valence rule.

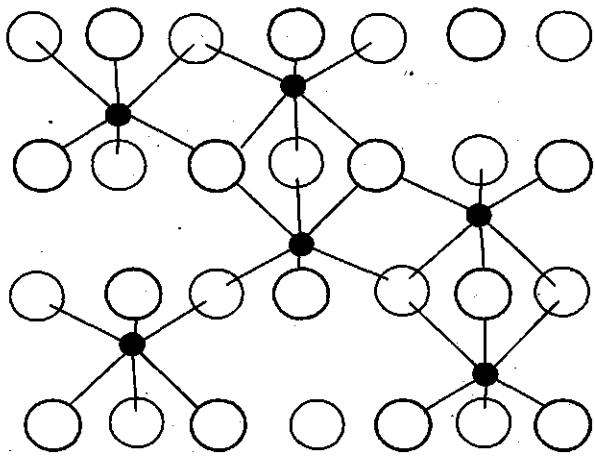

Fig. 2 The schematic bulk structure of hematite and corundum, comprising closed packed layers of oxygens (open circles) in which two out of three octahedral positions are filled with Me ions (filled circles). The oxygens are below (dashed line) or above (full line) the plane of the Me ions. Electrostatic repulsion between the Me ions leads to an asymmetric position of the Me ion an octahedron, i.e. a different length and a different actual bond valence.

The actual bond valence ($s$), based on differences in Me-O distances, can be interpreted as correction on the Pauling bond valence v and can be correlated with the Me-O distance ($R$) for instance according to $s=v\ (R/R^*)^{-n}$ (23) in which $n$ is a coefficient and $R^*$ is a distance parameter, giving the Pauling bond valence v if $R=R^*$. In practice, one has used slightly different expressions like $s=(R/R_1)^{-N}$ (24) where $N$ and $R_1$ are element specific constants. More recently the expression:

$$s = e^{\frac{(R-R_0)}{b}} \qquad [2]$$

has been proposed (25) in which $R_0$ is an element specific distance and $b$ a constant ($b$=0.37Å). The value of $R_0$ has been obtained by analysis of the bond valence structure of many crystals, such that the sum of the actual bond valences $\Sigma s_j$ around an oxygen, based on the known distances $R$, is equal to the valence $V$ of the oxygen. This model is astonishingly powerful, and can even be used to predict mineral structures with corresponding distances accurately (20, 27). Equation [2] will be used in this paper.

## Proton affinity

Pauling (6) has pointed out that the basic rules determining the structure of ionic minerals result from electrostatic considerations in which valence and distance play a role. On this basis Yoon et al. (3) combined the Pauling bond valence concept (v) with Coulomb's law in order to evaluate PZC values of metal (hydr)oxides, improving the earlier Coulombic approach of Parks (1, 2), who used the valence z of the metal ion as parameter. In both PZC models a distance parameter $L$ was introduced, as an expression of Coulomb's law.

With the introduction of the MUSIC model (5) a first attempt was made to predict the proton affinity of individual surface groups, differing in the number n of coordinating Me ions. It was also the first attempt to predict the affinity of the first and second proton that binds to the same reactive group. In this model we applied the Pauling bond valence concept and related the proton affinity to the parameter $n$ v/$L$. As illustrated above and pointed out by Bleam (28), distance dependency is already present in the actual bond valence $s$ and the use of $L$ in these proton affinity models therefore may be excessive.

The use of the actual bond valences $s$ in proton affinity modelling originates from Brown (20), who calculated on this basis the neutralisation of oxygen charge and applied this concept to organic bases. Later the bond valence concept of Brown was applied to the protonation of oxo and hydroxo solution complexes by Bleam (28). He calculated the neutralization of the charge ($\Sigma s_j$) on the basis of the Pauling bond valence v of the Me ion and the number of bound protons.

In the MUSIC model the proton affinity was evaluated on the basis of a hypothetical unit charge binding to the surface oxygen. It has the advantage that proton af-

finity, surface protonation and surface charge can easily be combined in one framework. However, it has been pointed out that the actual proton charge, positioned at the ligand, is less than 1 because of the formation of H bonds (28). The charge distribution in a hydrogen bond expressed in the bond valence of donating (O-H) or an accepting (O...H) H bond, can be related to the O-O distance $d$ (25), as given in Fig. 3.

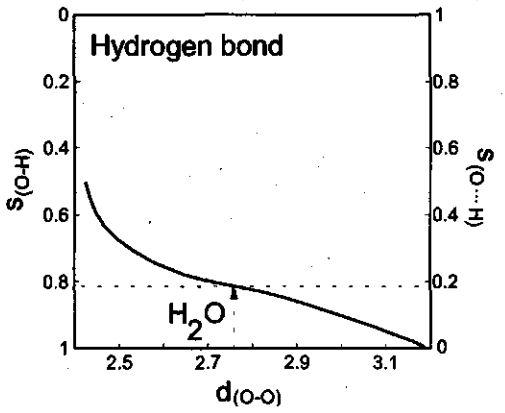


Fig. 3 Bond valences $s$ of the proton donating H-O bond and the proton accepting bond H...O as function of the O-O distance $d$, using the data of Brown and Altermatt (25). Based on the mean distance of O-O in water (2.76 Å), the bond valence of the donating and of the accepting H bond will be about 0.81 valence unit and 0.19 valence unit respectively.

The donating H bond valence in water is about 0.8 valence unit (v.u.) and this value was used by Bleam (28). This value is far too large to explain the difference in proton affinity of oxo and hydroxo solution complexes on the basis of the approach of Bleam (28). In can be shown that the correct H-H interaction can only be explained with his application of the bond valence model assuming an unusually low apparent charge of about 0.6 unit valences for a proton ($s_{O-H}$).

Based on the Pauling bond valence sum rule, it can be shown that in stable ionic structures the undersaturation of the oxygen valence is less than about 0.05 valence units (20). An apparently higher value in the mineral lattice is usually due to unaccounted protons and H bonds. It has been presumed (28) that such a high degree of neutralization also prevails for surface oxygens. It should however be remembered that in mineral interfaces high electrostatic potentials (17, 19, 29, 30) and proton

adsorption (31, 32, 33, 34, 35, 36) are measured, which can only be explained by accumulation of charge and therefore by valences considerably different from near zero for surface groups.
Based on the above considerations, the MUSIC model is redefined.

## MUSIC model

Our approach starts with the bond valence sum rule, which states that the valence $V$ of an oxygen in a mineral structure is neutralized by the bonds, each contributing to the sum of the actual bond valences, yielding:

$$V = -\Sigma s_j \qquad [3]$$

In the bond valence model of Brown (20) the proton affinity has been related to what he calls the available valence, which can be defined as the undersaturation of the oxygen valence, i.e. the difference between valence $V$ of the oxygen and the neutralisation by coordinating cations: $V + \Sigma s_j$. This concept will be the basis of our new approach and can be applied to ligands of dissolved charged solution complexes and also to charged oxygens present in the interface of metal (hydr)oxides. The major problem in the application of the Brown bond valence model is the contribution of charge by the hydrogen bonds. For solution complexes Brown (20) has suggested that an oxygen ligand will accept three hydrogen bonds, while an OH ligand accepts one and donates one hydrogen bond, and an $OH_2$ ligand will only donate two hydrogen bonds. In his calculation of the available valence, however, he omitted the presence of oxygen-proton bond acceptors (O<....H). This was followed by Bleam (28) who only used donating H bonds on ligands. In the present approach we will develop a concept for donating and accepting H bonds. In this concept the structural environment of oxygens present in solution complexes may differ from the situation of a surface oxygen in the interface.

The neutralization by protons can be most clearly analyzed focussing on a water molecule in an aqueous solution, as depicted in Fig. 4. The oxygen ions have four $sp^3$ orbitals in a tetrahedral configuration.

Two of the four orbitals of O of the water molecule are occupied by protons. Both others are unoccupied. Hydrogen bond formation occurs between H occupied and

unoccupied orbitals. About 0.2 v.u. charge is transferred in such a hydrogen bond (Fig. 3). We may apply this model approach to the neutralization of the O in oxo and hydroxo solution complexes.

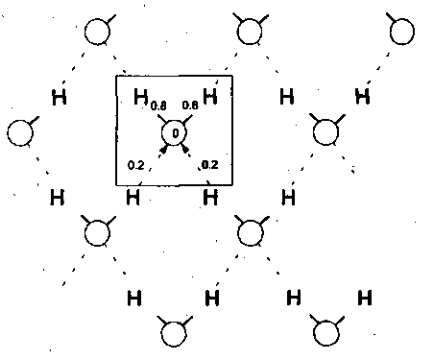


Fig. 4 The schematic structural arrangement of water molecules in an aqueous solution with H bonding, transferring part of the proton charge from one to another oxygen. In a hydrogen bond between water molecules about 0.2 v.u. are transferred. The H bond is formed between the H occupied orbital and an empty one. Both H occupied orbitals transfers each 0.2 v.u., but both other unoccupied orbitals of the same water molecule receive each 0.2 v.u. The water molecule as a whole remains uncharged.

The actual bond valences in solution complexes are unknown. In the present approach we will use the simplification that on the average the charge of the central ion (Me) is distributed equally over the ligands, i.e. we apply the Pauling bond valence to the Me-O bond as we did before (5). The neutralization of the oxygen charge can be calculated from the contributions s by the Me ion ($s_{Me}$= v ≡ $z$ / $CN$]), the H occupied ($m$) and the unoccupied ($n$) orbital(s), according to:

$$V \neq -\Sigma s_j = -[s_{Me} + ms_H + n(1-s_H)] \qquad [4]$$

in which $s_H$ is the bond valence of the H donating bond and $(1-s_H)$ the bond valence of the accepting one. In our approach the charge of the surface oxygens and the charge of oxygen ligands of solution complexes ($V$) is a priori not fully neutralised, i.e. $V \neq \Sigma s_j$. In an oxocomplex one orbital is occupied by a Me ion and three empty orbitals are able to form hydrogen bonds i.e. $m$=0, $n$=3 and in a hydroxo complex one donating and two accepting hydrogen bonds are present, i.e. $m$=1, $n$=2. Note that in both cases for solution complexes the sum $m$+$n$ equals 3.

The intrinsic proton affinity constant, log $K$, can be related to the undersaturation of the oxygen valence of the reactant which is defined as - ($\Sigma s_j + V$). In solution chemistry the intrinsic proton affinity of complexes is formulated with the Brönsted proton donor and acceptor concept in which the proton affinity of the donating reac-

tion is defined relatively to the protonation reaction of water. The protonation reaction of water $H^+ + H_2O <=> H_3O^+$ has by definition an intrinsic log $K$ value of log $K \equiv 0$ ($K \equiv 1$), and the undersaturation valence of the oxygen of the reactant (water) is zero, i.e. $-(\Sigma s_j + V)=0$ (Fig. 4). It implies that the relation between log $K$ and the actual oxygen charge, $\Sigma s_j + V$, is of the kind:

$$[\log]K = -A\ (\Sigma s_j + V) \qquad [5]$$

in which A is a constant.

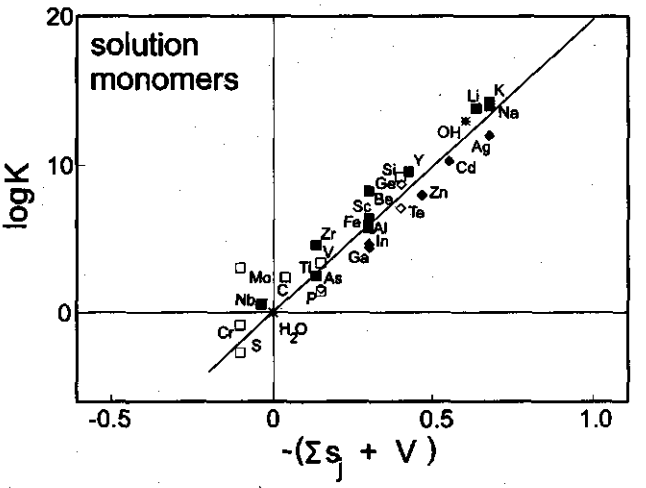


Fig. 5 The intrinsic log $K_{intr}$ values for the protonation of hydroxo and oxo complexes versus the undersaturation of charge on the oxygen ligand $-(\Sigma s_j + V)$. The solid squares indicate the log $K_{intr}$ values of the proton adsorption reaction of neutral hydroxo complexes, having a central cation with an electron configuration of rare gases. The corresponding open squares indicate the intrinsic log $K_{intr}$ for the protonation of negatively charged oxo complexes with a similar electron configuration. The log $K_{intr}$ of negatively charge oxo complexes has been corrected for the electrostatic work related to the discharging of the negative ion by the proton. The log $K_{intr}$ for the protonation of hydroxo and oxo complexes of cations with 10-d electrons are indicated with solid and open diamonds respectively. The log $K_{intr}$ values were taken from Baes and Mesmer (37). For C(arbon) the true intrinsic logK for the reaction $H_2CO_3 <=> H^+ + HCO_3^-$ of log $K$=3.8 was used (38).

We have tested the relation of eq.[5], as given in Fig. 5. The value of A equals +19.8. The best fit in our approach was achieved if we choose for a donor H bond the valence sH of 0.80 v.u., close to the value for water (Fig. 3). According to the analysis of Brown and Altermatt (25), we know that this value is not too strongly

influenced over a relatively broad range of O-O distances in minerals (Fig. 3), justifying the use of one value throughout. Calculation shows that if the O-O distance varies with ± 0.1 Å around the mean value in water, the value of the actual oxygen charge ($\Sigma s_j + V$) changes with only about 0.03 v.u., equivalent with about 0.5 log $K$ unit. As shown in Fig. 5 some deviation from the line exists, which may be due to the oversimplification of the use of the Pauling bond valence. An important point is the value of the undersaturation of the oxygen charge. In minerals this value is nearly zero (eq.[3]). In our approach much larger values are allowed in ion complexes, and in this respect we differ from the bond valence concept as applied to charged ions by Brown (20), where all ligands and the whole ion species are assumed to be uncharged, leading to large variations in the bond valence of protons and ions.

## Interfaces

The above sketched approach can be applied to reactive groups in interfaces. In our previous approach (5) we found that surface groups in general had a higher proton affinity than the corresponding groups in solution (about 4 log $K$ units) with silica as an exception. The difference has been interpreted as due to "a different arrangement of -OH(H) species and solute molecules in a flat surface structure compared with the spatial arrangement for the monomer" (5). In the redefined model it can be quantified on the basis of a difference in the number of H bonds between surface oxygens and water in the interface compared to the situation in solution. In solution monomers we have used three H bonds ($m+n=3$). However, it may be assumed for steric reasons that singly coordinated groups at surfaces often will interact with solute molecules with only two donating or accepting hydrogens bonds, i.e. $m+n=2$. For triply coordinated surface groups only one orbital is available for proton interaction, i.e. $m+n=1$. In case of a doubly coordinated surface group one may find one or two orbitals interacting with water ($m+n=1$ or 2).

It is of interest to notice that surface groups with one donating and one accepting H bond are in the model approach insensitive for a variation in the hydrogen bond valence, because the individual contributions cancel in the sum of both bonds, i.e. $s_H+(1-s_H)=1$. In our new approach we do not account for effects of surface relaxation. At present we assume that the relaxation, changing distances in the structure, does not lead to an important redistribution of charge. It should be kept in mind that

the Me ions coordinating with surface groups, still have to neutralize simultaneously also oxygens deeper in the structure, which implies that the bond valence of these oxygen bonds can not change, even if distances increase in the coordination environment as a whole. Only redistribution of charge over surface groups via common Me ions is likely, if distances are unequally changed. The new approach in the MUSIC model will be applied, as we did before (Hiemstra et al.1989b), to various oxides: $Al(OH)_3$, $TiO_2$, FeOOH and $SiO_2$.

### *Gibbsite*

Minerals with well defined simple surfaces with one type of reactive group may allow us to determine unequivocally the experimental proton affinity constant. The mineral gibbsite can be a good candidate. The hexagonal mineral particles have two types of crystal faces, a dominant planar 001 face and edge faces parallel to the c-axis (39). The planar 001 face has only doubly coordinated surface groups $Al_2OH$. It has been pointed out that these doubly coordinated $Al_2OH$ groups are not proton reactive in the normal pH range (pH=4-10) (7, 40). This has been recently reconfirmed by comparing well crystallized gibbsite preparations with a large variation in edge/planar face ratios, where the charging is directly related to the availability of the edge surface area and not to the total surface area (41). The reaction responsible for the charging is due to protonation of the singly coordinated hydroxyl surface groups:

$$AlOH^{+(s-1)} + H^+ \rightleftharpoons AlOH_2^{+s} \qquad [6]$$

In view of our new approach the proton affinity in reaction [6] will be determined by the value of the actual bond valence s. Based on the detailed structure of $Al(OH)_3$ (42), we know that the Al-OH distances R may vary quite significantly, which will lead, according to eq.[2], to a large variation in the bond valence $s$ and therefore in log $K$ (eq.[5]). Fortunately, this will not hinder a simplified evaluation, because one can show that, if for gibbsite all edge faces contribute equally to the charging behaviour, the mean value of the actual bond valence $s$ is equal to the Pauling bond valence v which has a value of v=0.5, the value used for solution monomers (Fig. 5). It implies that the experimental mean log $K$ value found for the surface protonation (eq.[6]) is valid for a mean actual bond valence $s$=0.5. Experiments show that the log $K$ of the $Al\text{-}OH^{-½}$ protonation reaction equals 10 ± 0.5 (7, 40, 43, 44). As pointed out above this value differs from the corresponding log $K$

value of the protonation of the monomer in solution ($\Delta \log K \approx 4$) because $m+n=2$. Application of our redefined MUSIC model predicts for protonation of singly coordinated surface groups a mean log $K$ of 9.9 (Fig. 8). It should be noticed that in our previous approach gibbsite was used to calibrate the log $K$ of surface reactions while here it is derived on the basis of a different number of hydrogen bridges.

## *Rutile and anatase ($TiO_2$)*

The basic unit of two $TiO_2$ polymorphs is a $Ti^{4+}$ filled oxygen octahedron ($CN$=6), linked together by two (rutile) or four (anatase) common edges (6), having only relatively small differences in Ti-O distances. The oxygen in the solid is triply coordinated ($Ti_3O^0$), receiving from each Ti a Pauling bond valence of +⅔. Based on the number of coordinating $Ti^{4+}$ ions to surface oxygens, the mineral surfaces of $TiO_2$ may have in principle three different surface groups, namely singly, doubly and triply coordinated surface groups. The surface groups with a lower coordination of $Ti^{4+}$ than the oxygens in the solid may compensate the missing charge by the uptake of one ($Ti_2O(H)$) or two protons (TiOH(H)).

There are small differences in distances in the $TiO_6$ octahedron of rutile and anatase. The triply coordinated oxygens in rutile as well as anatase are bound by two short and one slightly longer Ti-O bonds as indicated in Table 1, which leads to different bond valences $s_{Me}$.

Table 1 Me-O distances (29) and related bond valences (sMe) in two polymorphs of TiO2, rutile and anatase. Both structures are characterised by two ($n_{bond}$=2) short distances (a) and one slightly longer TiO distance (b). In order to calculate the bond valence $s$ the $R_0$ parameter of eq.[2] has to be slightly adjusted ($R_0$=1.808 and 1.795 Å for respectively rutile and anatase) in order to fulfil the sum valence rule for local neutralization in the structure $\Sigma s_j+V = 2$ (eq.[3]).

| | Rutile | | | Anatase | | |
|---|---|---|---|---|---|---|
| Group | $n_{bond}$ | distance | $s_{Me}$ | $n_{bond}$ | distance | $s_{Me}$ |
| TiO(a) | 2 | 1.946 | 0.69 | 2 | 1.937 | 0.68 |
| TiO(b) | 1 | 1.984 | 0.62 | 1 | 1.964 | 0.63 |

Based on the Ti-O distances two types of singly coordinated TiOHs-1 surface groups can be distinguished in the interface, indicated as TiO(a) and TiO(b) in Table 2 & 3. Also two types of doubly coordinated $Ti_2O^{\Sigma s-2}$ can be found, having a combination of a short (a) and a long (b) Ti-O distance (ab) or two short (a) dis-

tances (2a). The above defined MUSIC model can be applied, taking into account the actual bond valence *s*. The singly coordinated surface groups are assumed to have two solution oriented orbitals able to become part of a H bond, i.e. $m+n=2$. The same is assumed for the doubly coordinated surface groups. The calculated affinity of the different types of surface groups on the faces of rutile and anatase are given in Table 2 and 3 respectively.

Table 2 and 3 The affinity constants for rutile (Table 2) and anatase (Table 3) predicted with the MUSIC model for two types of singly coordinated TiO (a and b) and two types of doubly coordinated $Ti_2O$ groups (2a and ab), taking into account effects of redistribution of charge in the coordination sphere of Ti (actual bond valence s). The log *K* values referring to the expected actual proton transfer reaction in the normal pH range (pH=2-12) are written italic. The same is done for the actual oxygen charge of the corresponding reactant ($\Sigma s_j + V$). Note that the site density for rutile differs with a factor two from earlier reported values (7).

| Table 2 Group | $N_s$ nm$^{-2}$ | log *K* (oxo) | log *K* (hydr) | Charge $\Sigma s_j + V$ (oxo) | Charge $\Sigma s_j + V$ (hydr) | Crystal face index |
|---|---|---|---|---|---|---|
| TiO(a) | 8 | +18.0 | *+6.1* | -0.91 | *-0.31* | 101 |
| TiO(b) | 5.2&7.4 | +19.4 | *+7.5* | -0.98 | *-0.38* | 110&100 |
| $Ti_2O$(ab) | 8.0 | *+5.8* | -6.1 | *-0.29* | +0.31 | 101 |
| $Ti_2O$(2a) | 5.2&7.4 | *+4.4* | -7.5 | *-0.22* | +0.38 | 110&100 |
| $Ti_3O$ | - | -4.0 | - | +0.20 | - | 110 |

| Table 3 Group | $N_s$ nm$^{-2}$ | log *K* (oxo) | log *K* (hydr) | Charge $\Sigma s_j + V$ (oxo) | Charge $\Sigma s_j + V$ (hydr) | Crystal face index |
|---|---|---|---|---|---|---|
| TiO(a) | 5.6&5.2 | +18.2 | *+6.3* | -0.92 | *-0.32* | 010&011 |
| TiO(b) | 7 | +19.1 | *+7.2* | -0.97 | *-0.37* | 001 |
| $Ti_2O$(ab) | 5.6&5.2 | *+5.6* | -6.3 | *-0.28* | +0.32 | 010&011 |
| $Ti_2O$(2a) | 7 | *+4.7* | -7.2 | *-0.23* | +0.37 | 001 |
| $Ti_3O$ | - | -4.0 | - | +0.20 | - | all |

With the predicted values it must be possible to estimate the PZC of rutile and anatase. The 110 and 100 faces of rutile are considered as dominant ones (45). On these surfaces the singly and doubly coordinated surface groups are present in a 1:1 ratio. The expected PZC value can be calculated on the basis of the log *K* values

for the groups present, taking the mean of the log $K$ of both groups (log $K$=7.5 and 4.4), which leads to PZC=5.9 (Fig. 8). The 1:1 ratio is also found at the 101 face (Table 2). This face has the same PZC value. The PZC value is in accordance with reported PZC values for rutile of 5.8±0.2 (10, 34, 46, 47, 48). Although the Ti-O distances in anatase are slightly different from those of rutile, the calculated PZC for the faces mentioned (Table 3) is the same and in accordance with reported values (34, 48, 49). It is possible to explain a slightly higher or lower PZC value assuming a larger proportion of respectively singly or doubly coordinated surface groups in the Ti oxide interface. Very recently the bond valence concept have been applied in combination with our original MUSIC approach, leading to partly similar results (50).

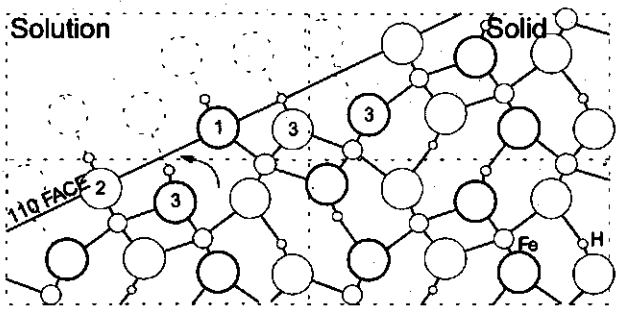


Fig. 6 A schematic representation of the cross-section of goethite perpendicular to the c-axis showing the surface structure of the 110 face. In the solid, the oxygens (large circles) are triply coordinated with $Fe^{+3}$ (only two Fe-O bonds are shown). The bold circles indicate a raised position in the lattice. Half of the oxygens have a proton attached (OH). At the interface a lower coordination number (*CN*) is found. The *CN* is indicated by the numbers 1, 2 or 3 which identify the singly, doubly or triply coordinated oxygens, respectively. The singly coordinated surface groups are assumed to have rotated to avoid overlapping orbitals, breaking the hydrogen bond with the backwards laying triply coordinated $Fe_3OH$, which orients its H bond to a water molecule in the interface. The arrow indicates the reorientation of the H bond of $Fe_3OH$ towards H2O in solution (dashed circles).

## *Goethite (α-FeOOH)*

The basic groups in the mineral structure of goethite have been discussed above. Monodomainic goethite crystals have predominantly 110 faces with 4 different types of surface groups. For the formation of a singly coordinated surface group two common Fe ions are removed, which may lead to a repulsive interaction of the former Fe oriented oxygen orbitals. This can be minimized in general if a singly coordinated oxygen rotates around the Me-O bond. In goethite this is probably only

possible in the absence of a H bond between the surface oxygen and a $Fe_3OH$ group present more backwards in the structure. It implies that the H bond of the $Fe_3OH$ is reoriented to a water molecule in the interface (Fig. 6).

Table 4 The predicted intrinsic proton affinity constants (logKintr) for the 4 types of surface groups present at the 110 face using the goethite structure with lattice parameters of Hazeman et al. (51). The logK values of the protonation reactions determining pH dependent charge are written in italic.

| Group | $N_s$ $nm^{-2}$ | log $K$ (oxo) | log $K$ (hydr) | $s_{Me}$ | $m+n$ |
|---|---|---|---|---|---|
| $Fe_1O_{II}$ | 3 | 19.6 | 7.7 | 0.61 | 2 |
| $Fe_2O_{II}$ | 3 | 12.3 | 0.4 | 0.59+0.59 | 1[a)] |
| $Fe_3O_I$ | 6 | 11.7 | | 0.40+0.40+0.40 | 1 |
| $Fe_3O_{II}$ | 3 | 0.2 | | 0.60+0.60+0.60 | 1 |

[a)] If $m+n=2$ the log $K$(oxo) value would be 8.3.

Based on the situation sketched, the log $K$ values can be calculated. In Table 4 we present the predicted protonation constants. As indicated in Table 4, the log $K$ for the protonation of doubly coordinated oxo groups is high, leading to $Fe_2OH$ groups which will not react with an additional proton in the normal pH range, i.e. the groups can be considered as inert. The protonation constant of the $Fe_3O_{II}$ groups is predicted to be very low. It implies that this group will remain unprotonated as suggested previously (11). As will be discussed later, calculation shows that the PZC of the 110 face with the given groups equals about 9.5 (Fig. 8). This value is in the range of PZC values reported for most well crystallized goethites, being PZC=9-9.6 (7, 14, 52, 53, 54, 55, 56, 57, 58). A lower PZC value could be achieved if the 021 faces at the end of the goethite needles have a lower PZC. This is discussed in Venema et al. (58).

### *Silica SiO2*

The charging curves of silica are quite different from what is usually found for Me (hydr)oxides. One aspect concerns the slopes of the charging curves in the PZC which are extremely low. It can be understood on the basis of the MUSIC approach as due to the specific bond valence in silica (5). In the PZC all reactive surface groups are protonated ($\theta_H$=1) and uncharged ($SiOH^0$) while for many Me (hydr)oxides like gibbsite, goethite and Ti oxides in the PZC only part of the individual reac-

tive groups have reacted with a proton ($\theta_H \neq 1$) and the surface groups remain charged. For details we refer to Hiemstra et al.(5).

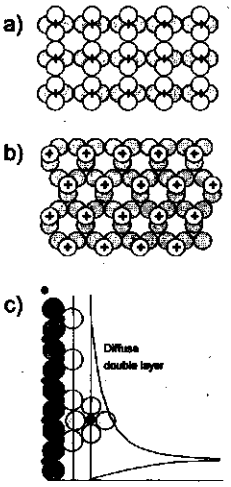


Fig. 7a The schematic representation of the 100 face of cristobalite being a good starting model for understanding the surface structure of amorphous silica. The surface groups are present in isolated pairs, protruding the surface, creating a penetrable surface. The oxygens indicated with open circles protrude the surface. A similar situation is found at the 0001 face of trydimite (Fig.7b). The Si ions, indicated as a cross, are present sandwiched between the oxygen layers. In Fig.7c a schematic cross section of the interface is depicted, comprising protruded surface groups and a double layer.

It has been suggested (59) that the 100 face of cristobalite is a good starting model for understanding the surface structure of silica. At this face singly coordinated surface groups are present in isolated pairs (Fig. 7a). The SiOH groups protrude the surface. Also in other surface configurations, like the 0001 face of tridymite (Fig. 7b), SiOH groups protrude the surface (46). This typical type of surface structure is responsible for the relatively high charging of silicas, which is expressed in the high electrostatic capacitance $C$ where $C$=3-4 F/m$^2$ (7, 11), resulting from a relatively small separation of surface and counter charge (Fig. 7c). The surface layer is penetrable for water molecules and this suggests that the possibilities for the formation of H bonds between the singly coordinated surface groups and water is larger than what is usually found on close-packed surface structures, i.e. the number of $m+n$=3 instead of 2. Using this approach the calculated log $K_{1,1}$ value for the singly coordinated surface groups is 7.9, being quite close to the value of 7.5 used in describing the charge of fully hydrated non porous siliça (7). We have assumed in this calculation an actual bond valence $s_{Si}$ of 1. The predicted log $K_{1,2}$ value for the protonation of SiOH is -4.0. Combination of both log $K$ values gives the prediction of the PZC (Fig. 8), being about PZC=1.9 very close to values reported for silica and quartz PZC = 2±0.3 (60, 61).

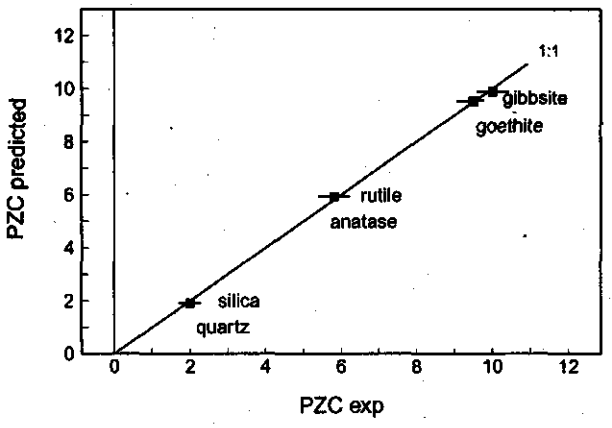


Fig. 8 Experimental PZC values for various (metal) hydroxides in relation with the calculated PZC values. The values are based on predicted individual proton affinity constants of the various types of surface groups in the interface.

## Modelling surface charge

The new MUSIC approach in terms of surface charge modelling needs some discussion. In the previous MUSIC model the proton was in all aspects treated as a unit charge, which has the advantage that *per definition* all proton charge present, is attributed to the surface. However in case of the presence of hydrogen bonds, it is possible that some charge is leaking to an adjacent adsorbed water, i.e. transfer of charge may occur. In principle it is possible to take these details into account, but considerable detailed information at the atomic scale about the positioning and charge distribution of the ions in the interface is needed in relation to the hypothetical electrostatic planes. In the present study we will simplify the approach assuming one electrostatic plane for the various types of surface groups to which all proton charge is attributed. It implies the use of a Basic Stern (BS) approach for charging curves, as we did before (7), where the proton charge is attributed to 0-plane and where the counter- and co-ions are present in the 1 plane (ion pairs) or in the diffuse double layer. This approach has the advantage that the definition of surface charge (0-plane) remains equivalent with H adsorption, measured with acid/base titration, in contrast to the case of transfer of proton charge from one electrostatic plane to another.

Table 5 The bookkeeping of charge for the surface groups at the 110 interface of goethite on the basis of the actual bond valence *s* and the Pauling bond valence v, attributing in both cases all proton charge to the surface group. Note that in case of the use of the actual bond valences the charge of surface species is often lower than what is found in the Pauling bond valence approach.

| Group | charge $\Sigma s_j + V$ | charge $\Sigma s_j + V$ |
|---|---|---|
| $Fe_IO_{II}H$ | -0.39 | -0.5 |
| $Fe_2O_{II}H$ | +0.18 | 0 |
| $Fe_3O_IH$ | +0.21 | +0.5 |
| $Fe_3O_{II}H$ | +0.21 | +0.5 |
| $Fe_3O_{II}$ | -0.21 | -0.5 |
| Sum | 0 | 0 |

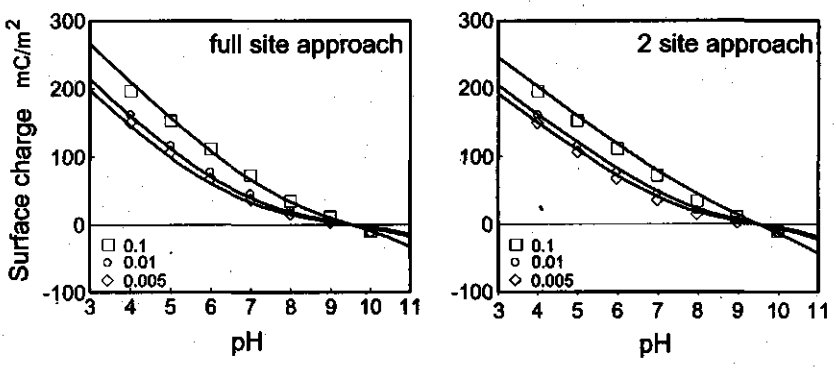


Fig. 9a The calculated surface charge at the 110 face of goethite versus pH at three different electrolyte concentrations taking into account all surface groups with the appropriate predicted proton affinity constants of Table 4 and using cation and anion pair formation constants (log $K_c$= log $K_a$=-1) and $C$=1.35 F/m$^2$. In Fig.9b the calculated surface charge is given for the simplified case (11) of the presence of two proton reactive surface groups with an equal proton affinity log $K_{FeOH}$= log $K_{Fe3O}$= 9.5 and log $K_c$= log $K_a$=-1 with $C$=0.9 F/m2. The data points indicate the experimental charge of goethite (11).

In the modelling the surface charge results from the presence of oxygens and protons and in addition also coordinating Me ions contribute charge. A logical suggestion in view of the new approach is the use of the actual bond valence s as written in for instance eq.[6]. However, for the proper bookkeeping of charges at a sur-

face (illustrated in Table 5 for the goethite interface) all reactions can also be written in terms of the Pauling bond valence, yielding the same results in terms of bookkeeping of charge. This can be understood realising that the actual bond valence can be interpreted as the result of only a relative redistribution of charge within the structure, not affecting the overall charge.

The advantage of the use of the Pauling bond valence for the calculation of the surface charge is that the formulation of the species and reactions are independent from the actual bond valence which may include some uncertainty due to uncertainties in distances in crystal structures. Furthermore the notation of the species is simpler and with the use of the Pauling bond valence for bookkeeping of charge we keep the connection with our previous work in terms of the MUSIC model and CD--MUSIC model. Another advantage is that for a proper bookkeeping some inert species types can be omitted. For instance, based on the log $K$ values predicted for a doubly coordinated $Fe_2OH$ surface group, it will be shown later that in the pH range pH 2-12 this group will be not protonated nor deprotonated. Based on this phenomenon, the group can be considered as inert. In case of the use of Pauling bond valences $\nu$ for surface groups the charge of the group $Fe_2OH$ is zero (Table 5), i.e. it is written as $Fe_2OH^0$ and it therefore does not have to be used in the calculation scheme. However, if the actual bond valence $s$ of this group is used, the group is not uncharged, i.e. it is written as $Fe_2OH^{0.18}$ and it is necessary to take it into account for a proper calculation of the surface charge.

In conclusion, we will use the actual bond valence and the H bonds to predict the log $K$ values of the individual surface groups, and we will use at present the Pauling bond valence for a proper bookkeeping of charges in the interface, attributing all proton charge to the electrostatic surface plane. In a recent previous approach of the charging of the interface of goethite (Hiemstra and VanRiemsdijk 1996), the interfacial behaviour in terms of proton adsorption and charging has been simplified to the use of two proton reactive groups ($FeOH^{-½}$ and $Fe_3O^{-½}$). It is of interest to analyse the charging behaviour of goethite in view of the new approach and compare the calculated surface speciation with the simplified approach with 2 surface groups (11). In Fig. 9 the calculated charge of the 110 face is given together with the experimental surface charge of goethite (data Hiemstra and Van Riemsdijk (11)). The curves of Fig. 9a have been calculated using a BS approach with a Stern

layer capacitance of 1.35 F/m$^2$. The ion pair formation constants are set equal to the value previously used (log $K_c$=log $K_a$=-1) (11). Description of the data with a simplified approach with 2 surface groups (Fig. 9b) yields a lower value for the capacitance of the Stern layer ($C$=0.9 F/m$^2$).

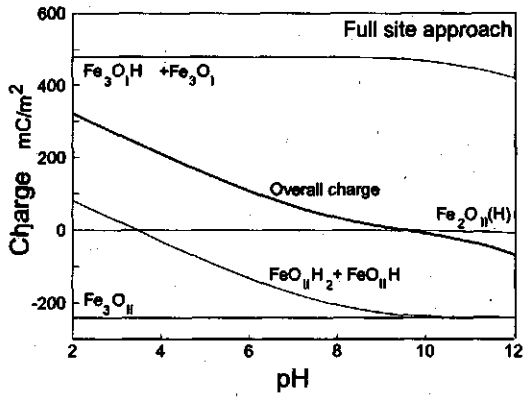


Fig. 10 The calculated contribution of the various surfaces groups to the charge development as function of pH in 0.1 M $NaNO_3$ for a full site approach. The site density of each site is $N_s$=3 nm$^{-2}$. In all cases symmetrical ion pair formation is assumed (log $K_c$= log $K_a$= -1). The capacitance is 1.35 F/m$^2$. The overall charge is indicating by the dashed line.

The speciation of the surface groups corresponding to the full site approach (Fig. 9a) is given in Fig. 10. As shown in the figure, the variation in surface charge is mainly due to variation in the speciation of two groups. This is in accord with the hypothesis of Hiemstra and VanRiemsdijk (11) in which the proton reactive groups are singly coordinated surface groups and triply coordinated surface groups of type I. In case of the full site approach the contribution of both species to the change in surface charge is strongly pH dependent. At low pH (pH<PZC) it is determined by the changes in speciation of the singly coordinated surface group, while at high pH the charge is due to deprotonation of the $Fe_3O_IH$ group (Fig. 10). It is of interest to note that in the standard pH range (pH=4-10), the triply coordinated surface groups mainly act as a permanent negative charge ($Fe_3O_{II}$), or permanent positive charge ($Fe_3O_IH$).

The above given speciation can be compared with the speciation in the case of the simplified 2 site approach (Fig. 11a). As shown, the speciation is now fully dif-

ferent. Both sites in the simplified approach contribute equally in the change of surface charge. This is mainly caused by the choice of one log $K_H$ value for both groups which was the result of the lack of information about the precise log $K$ for both reactions. Based on the predicted difference in log $K$, it is possible to simulate in a two site approach the effect of a pH dependent contribution as found in the full site approach. This is indicated in Fig. 11b, using the predicted values of log $K_{FeOH}$=7.7 and log $K_{Fe3O}$=11.7. In this case the speciation of the proton reactive groups is nearly identical with the full site approach.

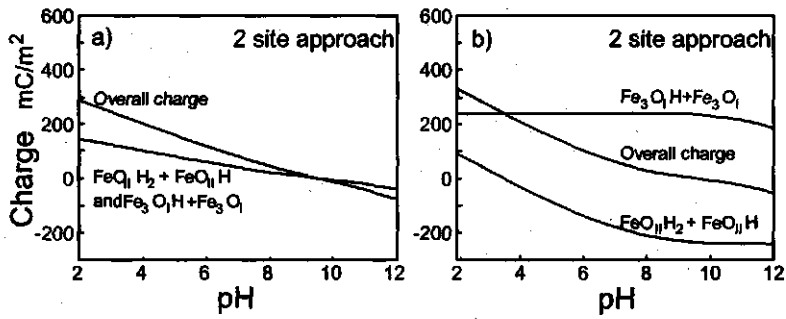


Fig. 11 The calculated contribution of the various surfaces groups to the charge development as function of pH in 0.1 M NaNO3 for a simplified 2 site approach with one proton affinity constant log $K_{FeOH}$= log $K_{Fe3O}$= 9.5, as used by Hiemstra and VanRiemsdijk (11), and a 2 sites approach using the predicted constants for log $K_{FeOH}$= 7.7 and log $K_{Fe3O}$= 11.7. The site density of each site is $N_s$=3 nm$^{-2}$. In all cases symmetrical ion pair formation is assumed (log $K_c$= log $K_a$= -1). The capacitances are respectively 0.9 F/m$^2$ and 1.5 F/m$^2$. The overall charge is indicating by the dashed line in both figures.

It should be noticed that the difference in log $K$ ($\Delta$log $K$= 0 or 4) for the reactive groups (Fig. 11a,b) is the main reason for apparent difference in the electrostatic capacitance $C$, needed to describe the same experimental data. A difference in $\Delta$log $K$ between two single protonation reactions might also be part of the explanation for the quite different charging behaviour observed for different Ti oxide preparations. Hiemstra and VanRiemsdijk (14) reported that the experimental capacitance (slope charging curve) of the rutile preparation of Yates (46) is considerably lower than those of the preparations of Bérubé and DeBruyn (34) and Fokkink et al.

(47). Similar observations can be made for the anatase preparations of Bérubé and DeBruyn (34) and Sprycha (49) and that of Foissy et al. (62). Recently Spanos et al. (48) have interpreted the difference in charging behaviour of a rutile and an anatase in terms of a difference in the $\Delta\log K$ for the classical 2 step protonation reaction assuming one type of surface group. In view of the above approach, part of the difference in behaviour may be due to the presence of different crystal faces in the preparations. The 101 face of rutile and the 010+011 face of anatase are typical examples of a surface with a very small difference in log $K$ between two surface groups, while the 100+110 face of rutile and the 001 face of anatase have a large difference ($\Delta\log K \approx 3$) in proton affinity of the singly and doubly coordinated surface group (Table 2&3). This leads to a quite different surface speciation, similar as illustrated in Fig. 10 and Fig. 11b, and a different surface charge in case of the same electrostatic capacitance for the compact part of the double layer.

Table 6 The actual charge of the important (Fig.10) surface oxygen species at the 110 face of goethite, calculated using actual bond valence contributions $s_{Me}$, $s_H$ and $(1\text{-}s_H)$ (eq.[4]), assuming charge transfer by hydrogen bonds. The sum of the charge of the surface oxygen and the charge transferred is attributed to the electrostatic surface plane given in the third column (see also Table 5). The actual charge of most surface oxygens is quite close to zero except the values of the proton reactive singly coordinated group, changing from FeOH to $FeOH_2$ with a corresponding change of surface charge.

| Group | Actual Oxygen | Charge Transferred | Charge sum |
|---|---|---|---|
| $Fe_1O_{II}H$ | -0.39 | +0.00 | -0.39 |
| $Fe_1O_{II}H_2$ | +0.21 | +0.40 | +0.61 |
| $Fe_2O_{II}H$ | -0.02 | +0.20 | +0.18 |
| $Fe_3O_IH$ | +0.01 | +0.20 | +0.21 |
| $Fe_3O_I$ | -0.59 | -0.20 | -0.79 |
| $Fe_3O_{II}$ | -0.01 | -0.20 | -0.21 |

Finally we want discuss the actual charge of surface oxygens present in the interface. Therefore let's return to the speciation of the 110 face of goethite (Fig. 10). In Table 6 the dominant surface species present in the pH range pH=4-10 are given. For the surface oxygen of the given species we have calculated the actual charge, the amount of charge transferred by H bonds and the overall charge (sum) attributed to the electrostatic surface plane (0-plane). The latter ones are equal to the values given in Table 5. Looking to the actual charge of the dominant species, one finds

that most of the species are nearly uncharged. The increase of the surface charge below the PZC value (Fig. 10) is mainly due to protonation of the surface group with the largest undersaturation of the oxygen, the singly coordinated surface group. In the reaction $FeO_{II}H + H^+ <=> FeO_{II}H_2$ the charge of the reactant changes with 0.6 v.u., as result of the change of an accepting H bond ($1-s_H$) into a proton donating H bond ($s_H$). The charge resulting from charge transfer in the H bond changes from 0.0 to +0.4 v.u. The sum of both changes is equal to the unit proton charge. At high pH the development of negative surface charge is mainly due to deprotonation of the nearly uncharged $Fe_3O_1H$ (+0.01 v.u), leading to $Fe_3O_1$ with an actual charge of -0.59 v.u. on the surface oxygen. The charge resulting from charge transfer by the H bond changes from +0.20 v.u. into -0.20 v.u.

Low actual oxygen charges of surface species are also found for Ti oxides (Table 2 and 3). For silica also such an observation can be made, where the overall charge of the SiO species is only -0.4 v.u. using the actual bond valence $s$ ($s_{Me}$=1) and three accepting hydrogen bonds ($1-s_H$=0.2), whereas the use of the Pauling bond valence $v$ leads to a charge of -1 v.u. It illustrates that the present MUSIC model not fully but partly realises Bleam's suggestion of a low undersaturation of charge of surface oxygens (28).

## Conclusions

Based on the above presented refined MUSIC model several conclusions can be drawn:

- The proton affinity of oxygens originates from the degree of undersaturation of the valence.
- The saturation of oxygen valence is determined by the number of coordinating Me ions and the number of proton donating and also accepting H bonds.
- The charge attribution of the Me ions can be found from the Pauling bond valence ($v=z_{Me}/CN$) in case of a symmetrical distribution of charge in the coordination environment or from the actual bond valence $s$ (Brown1978), being related to the actual difference in the MeO distances in the coordination environment (asymmetric distribution).
- The charge attribution of protons results from H bridge formation. The charge attribution depends on the number of donating ($m$) and accepting H bonds ($n$). In monomeric oxo and hydroxo solution complexes the total number of donating

and accepting H bonds equals 3 ($m+n=3$).

- The number of donating ($m$) and accepting H bonds ($n$) in surface groups depends on the number of coordinating Me ions and the surface structure. The sum of donating and accepting H bonds $m+n$ is generally 2 (or 3) for singly (Me) coordinated surface oxygens, 1 or 2 for doubly coordinated oxygens and 1 for triply coordinated ones.
- The charge distribution in a hydrogen bond of solution complexes and of hydrated interfaces is relatively close to the value of 0.8 and 0.2 v.u. for respectively a donating and an accepting H bond.
- The actual charge of the surface groups in the pH range pH=2-12 is often less than 0.5 v.u.
- The different behaviour of silica in terms of proton affinity is due to the open surface structure with protruded reactive SiOH groups, which may lead to a larger number of H bonds ($m+n=3$ in stead of 2 as found for a close packed surface).
- The presence of a proton accepting bond decreases the proton affinity with about 4 log $K$ units.
- The MUSIC model predicts on the basis of the individual proton affinity constants the correct PZC of Me hydroxides, oxohydroxides and oxides, like gibbsite, goethite, rutile, anatase and silica and quarz.
- Bookkeeping of surface charge on the basis of Pauling bond valences v for Me ions is equivalent with a bookkeeping using actual bond valences of Me ions ($s_{Me}$).

## References


1 Parks,G.A., *Chem. Rev.* **65**, 177 (1965).

2 Parks,G.A., *Adv.Chem.Ser.* **67**, 121 (1967).

3 Yoon,R.H., Salman,T. and Donnay,G., *J.Colloid Interface Sci.* **70**, 483 (1979).

4 Sverjensky,D.A., *Geochim Cosmochin Acta* **58**, 3123 (1994)

5 Hiemstra, T., Van Riemsdijk, W.H., and Bolt, G.H., *J. Colloid Interface Sci.* **133**, 91 (1989).

6 Pauling,L., *J.Am.Chem.Soc.* **51**, 1010 (1929).

7 Hiemstra,T., De Wit,J.C.M., and Van Riemsdijk,W.H., *J. Colloid Interface Sci.* **133**, 105 (1989).

8 Nabavi,M., Spalla,O. and B. Cabane, *J. Colloid Interface Sci.* **160**, 459 (1993).

9 Contescu,C., Contescu,C., and J.A. Schwarz, *J. Phys. Chem.* **98**, 4327 (1994).

10 Giacomelli,C.E., Avena, M.J., and De Pauli, C.P., *Langmuir* **11**, 3483 (1995).

11 Hiemstra,T., and Van Riemsdijk,W.H., *J. Colloid Interface Sci.* **179**, 488 (1996).

12 Venema,P., Hiemstra, T., and Van Riemsdijk,W.H., *J. Colloid Interface Sci.*, submitted (1996).

13 Cornell,R.M., Posner,A.M., and Quirk,P.J., *J.Inorg.Nucl.Chem.* **36**, 1937 (1974).

14 Hiemstra, T., and W.H. Van Riemsdijk, *Colloid Surf.* **59**, 7 (1991).

15 Schwertmann,U., and Cornell,R.M., "Iron Oxides in the Laboratory. Preparation and Characterization", Chap.5, VCH verlag, Weinheim, Germany, 1991.

16 Barrón,V., J. Torrent, *J.Colloid Interf. Sci.* **177**, 407 (1996).

17 Bousse,L., DeRooij,N.F., and P. Bergveld, *Surf.Sci.* **135**, 479 (1983).

18 Bousse,L., Mostarshed,S., VanDerSchoot,B., DeRooij,N.F., Gimmel, P., and W. Göpel, *J.Colloid Interface Sci.* **147**, 1991.

19 Van Hall ,R.E.G., Thesis, University Twente, Enschede, The Neterhlands (1995)

20 Brown, I.D., *Chem. Soc. Rev.* **7**, 359 (1978).

21 Newham,R.E., and De Haan, Y.M., *Z. Kristall.* **B117**, 235 (1962).

22 Schwertmann, U., in "Minerals in Soil Environment", Dixon and Weed (eds), chap.5, SSSA Madison (1989)

23 Brown, I.D., and Shannon, R.D., *Acta Cryst.* **A32**, 266 (1973).

24 Brown, I.D., and Wu, K.K., *Acta Cryst.* **B32**, 1957 (1976).

25 Brown, I.D., and Altermatt, K.K., *Acta Cryst.* **B41**, 244 (1976).

26 Brown, I.D., in Structure and bonding in Crystals, M.O'Keeffe and A. Navrotsky (eds), Vol.2, New York, Academic Press 1981.

27 O'Keeffe, M., *Struct. Bonding* **71**, 162 (1989)

28 Bleam, W.F., *J.Colloid Interf. Sci.* **159**, 312 (1993).

29 Cromer, D.T., and K. Herrington, *J.Am.Chem.Soc.* **77**, 4708 (1955).

30 J.Lyklema, and J.Th.G.Overbeek, *J.Colloid Interface Sci.* **16**, 595 (1961)

31 Bolt,G.H., *J.Phys.Chem.* **61**, 1166 (1957).

32 Parks,G.A., and P.L. DeBruyn, *J.Phys. Chem.* **66**, 967 (1962)

33 Atkinson,R.J., Posner,A.M., and J.P.Quirk, *J. Phys.Chem.* **71**, 550 (1967).

34 Bérubé Y.G., and P.L. DeBruyn, *J.Colloid Interf. Sci.* **27**, 305 (1968)

35 P. Schindler and H.R. Kamper, *Helv. Chim. Acta* **51**, 1781 (1968)

36 W. Stumm, C.P. Huang and S.R. Jenkins, *Croat. Chem. Acta*, **42** 223 (1970)

37 Baes,C.F., Mesmer,R.E., Hydrolysis of Cations, John Wiley & Sons, New York, 1976.

38 Stumm, W. and J.J.Morgan, Aquatic Chemistry, Chap 3, John Wiley & Sons, New York, 1981.

39 Bragg,L.,and Claringbull,G.F.,in "The Crystalline State" (L.Bragg,Ed.) Vol.IV, Bell and Sons, London. 1965

40 Hiemstra, T., Van Riemsdijk,W.H., and Bruggenwert,M.G.M., *Neth.J.Agric.Sci.* **35**, 281 (1987).

41 Hiemstra, T., Han Yong, Van Riemsdijk,W.H., *J. Colloid Interface Sci.* in preparation.

42 Saalfeld,H., and M.Wedde, Z. Kristall. **139**, 129 (1974)

43 Hingston,F.J., Posner,A.M., & Quirk,P.J., *J. Soil Sci.* **23**, 177 (1972)

44 Kavanagh,B.V., Posner,A.M., and Quirk,P.J., *Disc. Farad. Soc.* **59**, 242 (1975)

45 Jones,P., and Hockey,J.A., *Trans.Faraday Soc.* **67**, 2679 (1971).

46 Yates,D.E., The structure of the oxide/aqueous electrolyte interface. Ph.D.thesis, University of Melbourne, Melbourne, 1975.

47 Fokkink,L.G.J., De Keizer,A., and J.Lyklema, *J. Colloid Interface.Sci.* **127**, 116 (1989).

48 Spanos, N., Georgiadou,I. and A. Lycourghiotis, *J. Colloid Interface.Sci* **172**, 374 (1995).

49 Sprycha,R., *J. Colloid Interface Sci.* **102**, 173 (1984)

50 Contescu,C.,Popa,V.T. and J.A.Schwarz, *J. Colloid Interf. Sci.* **180**, 149 (1996)

51 Hazeman,J.L., Brerar,J.F., and A.Manceau, *J. Mat. Sci. Forum* **79**, 821 (1991)

52 Evans,T.D., Leal,J.R. and Arnold,P.W., *J. Electroanal. Chem* **105**, 161 (1979).

53 Bloesch,P.M., Bell,L.C., and Hughes,J.D.,Aust.J.Res. 25, 377 (1987).

54 Jung,R.F., James,R.O., and Healy,T.W., *J. Colloid Interface Sci.* **118**, 463 (1987).

55 Zeltner,W.A., and Anderson,M.A., *Langmuir* **4**, 469 (1988)

56 Johnson, B.B., *Environ. Sci. Technol.* **24**, 112 (1990).

57 Tejedor-Tejedor,M.I., and Anderson,M.A., *Langmuir* **6**, 602 (1990).

58 Venema,P., Hiemstra T., and W.H. VanRiemsdijk (in preparation).

59 Peri,J.B., and Hensley,A.L., *J.Phys.Chem.* **72**, 2926 (1968).

60 Iler,R.K., "The Chemistry of Silica". Wiley, New York, 1979

61 Sposito,G., "The Surface Chemistry of Soils". Oxford Univ.Press, New York, 1984.

62 Foissy,A.M., Pandou,A., Lamarche J.M., and N. Jaffizic-Renault, *Colloids Surf.* **5**, 363 (1982).

# 6

# Intrinsic proton affinity of reactive surface groups of Metal (hydr)oxides: Application to Iron (hydr)oxides

Peter Venema, Tjisse Hiemstra, Peter G. Weidler and Willem H. van Riemsdijk

Geochimica et Cosmochimica Acta, submitted, 1996

## Abstract

*Recently an improved method was developed for the calculation of proton affinities of individual surface groups of metal (hydr)oxides. The method is a refinement of the MUlti SIte Complexation (MUSIC) model. In the MUSIC model, Pauling bond valences are used for the prediction of the individual proton affinities of surface groups of metal (hydr)oxides. One of the major changes in the refined MUSIC model is that the Pauling bond valences are redefined with a method in which the bond valence is related to the bond length.*

*In this paper, the refined MUSIC model is applied to three different iron (hydr)-oxides (goethite, lepidocrocite and hematite). The resulting proton affinities can be combined with the crystal structure and morphology in order to describe the experimental charging curves. The charging curves could be described very well for minerals with a well known (goethite) or reasonably well known (lepidocrocite) crystal morphology. For crystals of which the morphology is less well known (hematite), the refined MUSIC model can be a powerful support for a suggested morphology.*

## Introduction

The charging of metal (hydr)oxides is very important for the adsorption behaviour of other ions (1, 2). The surface charge of metal (hydr)oxides can be positive, zero or negative. This variable charging can be explained by adsorption and desorption reactions of protons with surface groups of the metal (hydr)oxide surface (1). The corresponding proton affinity constants are therefore of major importance for a good understanding of surface speciation.

A relationship is expected between the proton affinity and the PZC of metal (hydr)-oxides. A correlation between PZC and affinity can only result in a singly proton affinity constant (3, 4, 5), whereas one needs for each type of surface group one or two proton affinity constants. Few attempts have been made to predict proton affinity constants of individual surface groups for metal (hydr)oxides. Hiemstra and van Riemsdijk were the first to predict the proton affinities for different types of surface groups. In this so called MUSIC model a relation is found between the proton affinity of a surface group and the summation of all bond valences of the bonds with underlying metal ions (6, 7).

In the model it is assumed that the charge of a central ion is equally distributed over its ligands which implies the use of Pauling bond valences (8). This prerequisite, however, is only met for a few metal (hydr)oxides. In this study the actual bond valences will be used, which can be calculated from a relationship between the bond length and the bond valence of a particular bond (9, 10). The new method will be applied to three different iron (hydr)oxides namely; Goethite, Lepidocrocite and Hematite. For the prediction of the individual proton affinity constants, the exact metal - oxygen distances in the iron(hydr)oxide crystals are obtained from literature. Goethite will be used to discuss the calculation method and therefore the crystal structure will be discussed in detail.

The predicted proton affinities for the individual surface groups, combined with the surface composition are used to predict the charging curves of the three different iron(hydr)oxides. In the calculations a Basic Stern model will be used as model for the water/solid interface.

## The MUSIC approach

### *The Classical MUSIC model*

The work of Pauling (8) may form the basis for a new vision on surface complexation. In a metal (hydr)oxide crystal, the metal ion with valence ($+z$) is surrounded by several (hydr)oxide groups. The number of surrounding ligands is indicated as the coordination number ($CN$). In Paulings concept, the charge of this central ion is distributed evenly over its surrounding ligands leading to the so called bond strength or reduced valence ($s$):

$$s = \frac{z}{CN} \qquad [1]$$

In the MUSIC model, the proton affinity of a surface group is directly related to the summation of the Pauling bond valences of its coordinating metal ions:

$$\log K_H = f(n \cdot s) \qquad [2]$$

in which $n$ is the number of metal ions that are coordinated with the surface (hydr)-oxide group (6), leading to predictions as given in table 1.

Table 1. Values of log $K_H$ as predicted by the "classical" MUSIC model (7). It can be seen that the model predicts that a singly coordinated group will be protonated (log $K_H$ = 24.4). Further it is predicted that doubly coordinated surface groups are mainly uncharged.

| Surface group | Formal charge | Log *K* |
|---|---|---|
| $FeO^{-1/2}$ | -1.5 | 24.4 |
| $FeOH^{-1/2}$ | -0.5 | 10.6 |
| $Fe_2O^{-1}$ | -1.0 | 13.6 |
| $Fe_2OH^{0}$ | 0.0 | -0.2 |
| $Fe_3O^{-1/2}$ | -0.5 | 4.3 |

The predicted values can be used in model calculations. It can be shown that only two protonation reactions are of relevance for the prediction of the charging behaviour namely the protonation of $FeOH^{-1/2}$ and $Fe_3O^{-1/2}$ (7, 11). This implies that the predicted PPZC (Pristine Point of Zero Charge) of an iron (hydr)oxide is determined by the site densities of the singly coordinated $FeOH^{-1/2}$ and the triply coordinated $Fe_3O^{-1/2}$ groups.

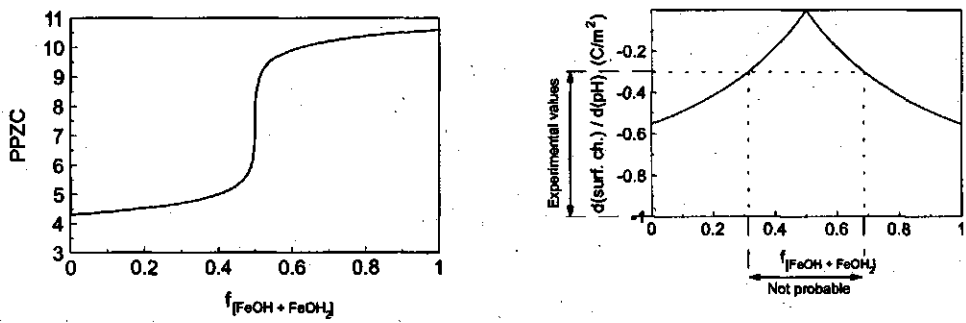


Fig. 1 The log *K* values and the charge of the singly coordinated (hydr)oxide group and the triply coordinated oxide group (Table. 2) are used for the calculation of the predicted PPZC (a) and the slope of the predicted charging curve (b) as a function of the fraction singly coordinated surface groups. Experimental values of the slopes indicate that fractions between 0.3 and 0.7 are not probable. This indicates that the model must predict either a low PPZC or a high PPZC.

In the appendix, a relationship between the fraction of one of the sites and the proton activity in the PPZC is derived (Eq. [A. 4]). Application of this equation to the FeOH(H)-$Fe_3O$(H) system yields Fig. 1a. For high fractions of singly coordinated surface groups, the predicted PPZC values are high (above pH 9.5) while for low

fractions these values are very low (below pH 5). For fractions close to a ratio of about 1:1, PPZC values of between 5 and 9.5 are found. For this fraction, however, the slope of the charging curve in the PPZC (eq. [A.5]) approaches zero which means that the surface does not charge at al (Fig. 1b). The experimental slopes for goethite can vary between values of -0.3 and -1, which indicates that surface fractions between 0.3 and 0.7 are improbable (Fig. 1b). This indicates that the experimental charging curves of goethite cannot be described with the constants given in Table 1.

The above conclusion has led to the refinement of the MUSIC model approach taking into account more structural details (11). In the following section, the method of calculating the actual bond valences will be explained.

## *Actual Bond Valences*

In the Pauling bond valence concept, charge is equally distributed over the ligands, which is equivalent with the assumption of equal distances in the coordination environment (12). The relation between the actual bond valence $s_{i-j}$ and the bond length $R_{i-j}$ is according to Brown (13):

$$s_{i-j} = e^{\frac{(R_{i-j} - R_{0\,i-j})}{0.37}} \qquad [3]$$

in which $R_{0\,i-j}$ is an ion dependent parameter and the value of 0.37 is found empirically as the best parameter for all the different kinds of bonds. In this article only iron(hydr)oxides will be considered for which $R_{0\,Fe\text{-}O} = 1.759$ (10, 13). This value of $R_{0\,Fe\text{-}O}$ is optimized for a broad range of environments and can therefore deviate from the optimal value for an individual iron (hydr)oxide. In this paper, the values of $R_{0\,Fe\text{-}O}$ are optimized for each individual crystal structure so that the sum of bond valences equals the charge of the central ion.

For structural H-bonds we applied a relation between the crystal O-O distance and the bond valence $s_H$ given by Brown and Altermat (13) in stead of using eq. [3]. The bond valence for a proton bond to a surface oxygen $s_H$ is set at 0.8 (14, 15, 16) the remaining 0.2 valence units are the bond valence of a donating hydrogen bridge to an adsorbed water.

## *Prediction of log $K_H$*

The actual bond valence theory can be applied to surface groups. The formal charge of a surface oxygen $V_s$ is given by the summation of its valence (= -2) and the bond valences of all its ligands ($s_i$ ):

$$V_s = -2 + \sum_{i=1}^{n_i} s_i \qquad [4]$$

in which $s_i$ can be the bond valence of the Fe-O bonds ($s_{Fe\text{-}O}$) but also the bond valence of donating ($s_H$) and accepting ($1\text{-}s_H$) H-bonds. In interfaces, the undersaturation of the surface oxygens ($V_s$) can be related to the proton affinity.

Hiemstra et al. (16) found a linear relationship between the log $K_H$ values and the actual oxygen charge for both dissolved and surface species according to:

$$\mathrm{Log}K_H = A\ (-2 + \sum_{i=1}^{n_i} s_i) \qquad [5a]$$

or

$$\mathrm{Log}\ K_H = -19.8\ (-2 + m\ s_H + n\ (1-s_H) + \sum_{i}^{n_{st.}} s_{i\ st.}) \qquad [5b]$$

in which $m$ is the number of donating H-bridges with adsorbed water, $n$ is the number of accepting H-bridges with adsorbed water, $n_{st.}$ the total number structural bonds, $s_{i\ st.}$ is the bond valence of an structural Me-O or H-O bond while $s_H$ is the bond valence for an adsorbed proton (donating H-bridge).

Eq. [5b] applies to the proton affinity constants for complexes in solution as well as for surface groups. The difference in affinity for the surface groups compared to the solution complexes is in this model due to a difference in the number of hydrogen bonds with adsorbed water.

In solution complexes, oxygen ligands normally have four orbitals of which one is metal ion oriented and the three others are able to form donating and/or accepting H-bonds (i.e. $n+m = 3$) (16). The number of possible H-bonds that can be formed

by a surface ligand is less if it has more than one structural bonds (Me-O and H-O) and may also be less due to steric reasons. For singly coordinated surface oxygens, the value for $n+m$ normally equals 2 (16). Doubly coordinated surface oxygens may have a maximum of two hydrogen bridges with adsorbed water. For triply coordinated surface oxygens only one ligand is available ($m+n = 1$).

The model predictions with the revised MUSIC model will be compared with experimental charging curves. In the following sections first the experimental methods will be discussed and next the new model will be applied to respectively goethite, lepidocrocite and hematite.

## Experimental

The hematite and lepidocrocite used in this study was prepared in the lab of Prof Schwertmann, the preparation method is described elsewhere (17). The goethite was prepared in our lab, the method of preparation is also described elsewhere (7, 18).

For storage of solutions and for the experiments, plastic bottles were used. In the experiments, demineralized, distilled water (DD water) was used. For the adsorption experiments, stocks were prepared of all the solutions.

The NaOH stock solution was made by dissolving 25 gr of NaOH (Merck p.a.) in 25 ml DD water. This was cooled down, centrifuged and 7.5 ml of the supernatant was pipetted in 1 L pre-boiled d.d. water. The stock was calibrated by titration with 0.1000 HCl (Titrisol) and f.f. as indicator.

The $HNO_3$ stock was made by diluting app. 12 ml of $HNO_3$ in 1 L d.d. water. The acid was later calibrated with the stock base and f.f. as indicator.
The background electrolyte stock was made by weighing 255 gr NaNO3 in 1 L d.d. water. All suspensions were titrated at three salt concentrations (0.005 M, 0.01 M and 0.1 M). The reversibility was checked at every salt concentration by titrating with base and with acid. The base (NaOH), acid ($HNO_3$) and salt ($NaNO_3$) solutions were prepared from their stock solutions. For the base and the salt solutions pre boiled DD water was used.

At the beginning of a measurement, the sample was brought to the lowest salt level

and left one night over at a pH of about 5 in a nitrogen atmosphere. The titration was carried out in a nitrogen atmosphere with a computer directed titration stand (19). With the stand three salt levels could be titrated automatically. The outer junction of the reference electrode (a double junction saturated KCl electrode) was filled with a mixture of $NaNO_3$ (0.125 N) and $KNO_3$ (0.875 N) (20). For this solution, the mobility of the positive and negative ions are about the same, so that the diffusion potential over the outer junction is salt independent (21). The electrodes were calibrated with pH 7 and pH 4 buffers before and after the experiment. The calibration of the electrode and the base and acid solutions were checked with a blank titration.

For the model description of the charging curves for the metal(hydr)oxides an interface model is needed. In this study a simple Basic Stern model is used as an interface model. This model is described in detail elsewhere (22, 23, 24).

In the next section, the resulting charging curves will be discussed. The curves will be compared with the predicted values as discussed in the former sections. For the calculations, the log $K_H$ values and the site densities are fixed on the values that result from the crystal structure. This fitting procedure is done by trial and error.

## Results and discussion for Goethite

In this section, the revised MUSIC model will be applied to goethite. For this application the crystal structure and morphology must be known and these crystal properties will therefore be discussed first. Surface relaxation is not considered for the calculations, although it may play a role for the Fe-O bond lengths at the crystal surface (25, 26). However, surface relaxation may be of less importance in terms of charge distribution because the charge of a central iron ion must always be neutralized by its bonds. This implies that the bond valences of the surface oxygens have a very small degree of freedom.

The predicted charging behaviour will be discussed and compared to the data. For all calculations the log $K$ value for pair forming ions (Na and $NO_3$) is assumed to be -1. The capacitances of the stern layer is treated as adjustable parameter for the different materials.

## *Crystal structure and morphology*

In the goethite structure, a central iron ion with six surrounding (hydr)oxide ligands can be considered as an octahedron. These octahedra are partly linked by H-bridges (Fig. 2). Two types of oxide ligands can be distinguished in goehtite, having different Fe-O and H-O distances: 1) an protonated oxygen, with a high proton affinity ($O_I$) and 2) an unprotonated oxygen, with a hydrogen bridge and a low proton affinity ($O_{II}$) (Fig. 2). In this study, the crystal structure as determined by Hazemann et al. (27) is used. On the basis of the distances in the crystal structure, the bond valences can be calculated using a value for $R_{0,Fe\text{-}O}$ of 1.7631 (Fig. 3).

In the calculations, a distinction has been made between internal H-bridges of a surface ligand and H-bridges between a surface ligand and adsorbed water. Internal H-bridges are a part of the crystal structure, so they cannot be considered as free orbitals and therefore they do not contribute to the value of $n+m$.

Table 2 The surface compositions and predicted proton affinities for the different surface groups of the 110 face of goethite. Underlined numbers in the columns for the bond lengths and valences refer to structural hydrogen bonds. The resulting log $K_{intr}$ are shown in the last column, the upper value is the first protonation constant and the lower value the second protonation constant. The values of log $K_{intr}$ are calculated with the assumption that structural hydrogen bridges do not persist, the underlined numbers in this column refer to calculations in which the structural hydrogen do bridges persist.

Goethite 110 Face

| Type of group | $N_S$ (sites/nm$^2$) | Bond lengths (Å) | | | $s$ | | | m | | n | | log $K_{H1}$ log $K_{H2}$ |
|---|---|---|---|---|---|---|---|---|---|---|---|---|
| $Fe_1O_{II}$ | 3.03 | 1.946 | <u>1.767</u> | | 0.610 | <u>0.194</u> | | 0 | <u>0</u> | 2 | <u>2</u> | 19.6 |
| | | | | | | | | 1 | <u>1</u> | 1 | <u>1</u> | 7.7 |
| $Fe_2O_{II}$ | 3.03 | 1.958 | 1.958 | | 0.591 | 0.591 | | 0 | | 1 | | 12.3 |
| | | | | | | | | 1 | | 0 | | 0.4 |
| $Fe_3O_{II}$ | 3.03 | 1.958 | 1.946 | 1.946 | 0.591 | 0.610 | 0.610 | 0 | | 1 | | -0.2 |
| $Fe_3O_I$ | 6.06 | 2.092 | 2.103 | 2.103 | 0.411 | 0.399 | 0.399 | 0 | | 1 | | 11.7 |

For the prediction of the charging behaviour, the surface composition in terms of surface groups must be known. This surface composition is determined by the crystal faces that occur at the crystal. For goethite, the dominant crystal faces are the (110) face and the (021) face (28, 29, 30). The (110) face is the most important

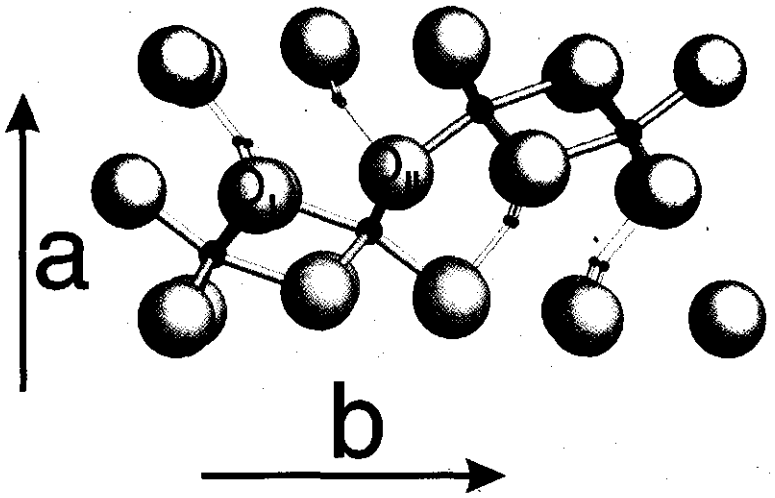


Fig. 2 The unity cell of goethite with four "full" and four "empty" octahedra. The large spheres represent oxygens, the intermediate spheres are the central iron ions and the small spheres represent the protons. An iron ion with six surrounding oxygens can be considered as an octahedron. In the picture it can be seen that both iron-filled and empty octahedra occur. Note that oxygen atoms can be protonated (short O-H distance) or unprotonated (long O-H distance).

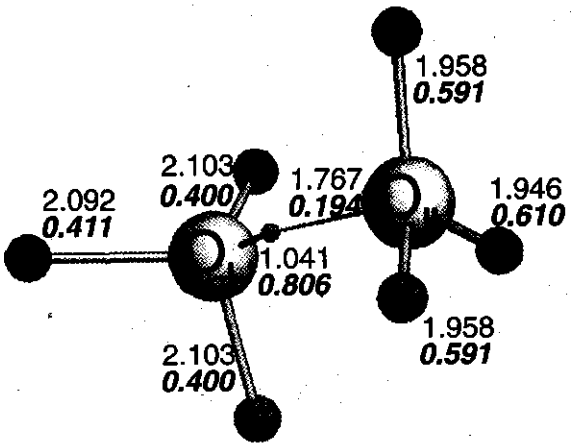


Fig. 3 The two different oxygens that occur in goethite with all bond lengths (upper numbers) and bond valences (italic, bolt lower numbers). The large spheres represent the oxygens, the smaller dark spheres the iron while the proton is the smallest sphere.

plane of these two, normally the reactive surface of goethite consists for about 80-95 percent of the (110) face.

At the (110) face, two triply coordinated $O_I$ groups, one doubly coordinated $O_{II}$ group and one singly coordinated $O_{II}$ group occurs per unit cell (Table 2). The singly coordinated $O_{II}$ groups may have an internal hydrogen bridge to one of the triply coordinated $O_I$ groups (11, 16).

The bond valences for the different surface groups can be found from the crystal structure and the H-bridges to adsorbed water molecules. For the application of eq. [5], the values for $m$ and $n$ are of major importance, because different choices can be made. The major results of the different options will be discussed in detail.

For the formation of singly coordinated $O_{II}$ groups at the (110) interface, two structural Fe ions have to be removed (Fig. 3). This leads to the coordination with one Fe ion and the presence of a structural H-bond with an $O_I$ oxygen. The corresponding calculated bond valences are resp. 0.610 and 0.194. In case of the formation of two H bonds with adsorbed water molecules, the calculated proton affinity for the first protonation step ($n$ = 2) equals
$\log K_{H1}$ = -19.8 (-2+2* 0.2 +0.610+0.194) = 15.8

This high value results in protonation forming FeOH under normal pH conditions. The actual oxygen charge of FeOH is now due to one donating H-bond ($m$=1) and one accepting H-bond ($n$=1), leading to: $\sum s_i$ = +1*0.8+1*0.2 +0.610+0.194, corresponding with $\log K_{H2}$ = 3.9 (second protonation step). It is also possible that the internal hydrogen bridge between the singly coordinated $O_{II}$ and the triply coordinated $O_I$ group does not persist. In this case the two predicted proton affinities are 19.6 and 7.7 respectively.

The doubly coordinated surface groups at the (110) face may form one or two H bonds with adsorbing water. The next calculation example will be given for the doubly coordinated $O_{II}$ group. For this group also two different options are possible. In the first option, two H-bonds are formed in the interface ($n$+$m$ = 2), the proton affinities for this case are then $\log K_{H1}$ = 8.3 and $\log K_{H2}$ = -3.6. In case one H-

bond is formed ($n+m = 1$) the proton affinities are log $K_{H1}$ = 12.2 and log $K_{H2}$ = 0.4.

Table 3 The surface composition and predicted proton affinities for the different surface groups of the 021 face of goethite. The underlined values in the column for the bond lengths and bond valence represent structural hydrogen bridges. The resulting log $K_{intr}$ are shown in the last column the upper value is the first protonation constant and the lower value the second protonation constant. The values of log $K_{intr}$ are calculated with the assumption that structural hydrogen bridges do not persist, the underlined numbers in this column refer to calculations in which the structural hydrogen do bridges persist.

Goethite 021 Face

| Type | $N_s$ | Bond lengths | | | $s$ | | | m | | n | | log $K_{H1}$ | |
|---|---|---|---|---|---|---|---|---|---|---|---|---|---|
| $FeO_{II}$ | 3.75 | 1.958 | <u>1.767</u> | | 0.591 | <u>0.194</u> | | 0 | <u>0</u> | 2 | <u>2</u> | 20.0 | <u>16.1</u> |
| | | | | | | | | 1 | <u>1</u> | 1 | <u>1</u> | 8.1 | <u>4.2</u> |
| $FeO_I$ | 3.75 | 2.103 | <u>1.041</u> | | 0.399 | <u>0.806</u> | | 0 | <u>0</u> | 2 | <u>2</u> | 23.8 | <u>7.9</u> |
| | | | | | | | | 1 | <u>1</u> | 1 | <u>1</u> | 11.9 | <u>-4.0</u> |
| $Fe2O_{II}$ | 3.75 | 1.958 | 1.946 | <u>1.767</u> | 0.591 | 0.610 | <u>0.194</u> | 0 | <u>0</u> | 2 | <u>1</u> | 11.9 | <u>8.0</u> |
| | | | | | | | | 1 | | 1 | | 0.0 | |
| $Fe2O_I$ | 3.75 | 2.103 | 2.092 | <u>1.041</u> | 0.399 | 0.411 | <u>0.806</u> | 0 | <u>0</u> | 2 | <u>1</u> | 19.6 | <u>3.7</u> |
| | | | | | | | | 1 | | 0 | | 7.7 | |

The calculation method for the triply coordinated surface groups is straightforward. In Table 2, the crystal parameters and the calculated log $K_H$ values are shown. At the (021) face, doubly coordinated and singly coordinated surface groups occur of both the $O_I$ and the $O_{II}$ type (Table 3). The site density for each of these types of groups is 3.75 sites/nm$^2$. Each singly coordinated $O_I$ resp. $O_{II}$ surface group has an structural H-bridge with a doubly coordinated $O_{II}$ resp. $O_I$ surface group. For the calculations it can be assumed that the structural hydrogen bridges do not persist at the (021) interface (table 3) or that they do persist at the (021) interface (table 3 underlined values).

The calculated proton affinities can now be used for calculating charging curves. Before the results of the calculations will be shown, we will first give some explanation about the influence of the formal charges of the surface groups on the

model predictions. In the "classical" MUSIC theory, the formal charges of surface (hydr)oxides could have broken values (e.g. -½, +½ ). In the revised model, the formal charges can have real values (e.g. -0.735, -0.398). The question arises which influence the formal charges of individual surface groups will have on the overall charging description. To answer this question, we consider a unit cell at a crystal face. For this unit cell, all charges of the surface groups must add to an integer value because otherwise the surface charge cannot be neutralized by adsorbing ions. This implies that if a surface group exists with a formal charge of -0.7, there must be another surface group with a formal charge of -0.3 (or +0.7). The description of the charging behaviour with these two surface groups is the same as the description of the charging behaviour of two surface groups with formal charge -0.5. So for the description of the charging behaviour of a metal (hydr)oxide, the formal charges calculated with the ("classical") pauling distribution approach will give the same description as the "new" formal charges. Therefore for all calculations in this article, only the "classical" formal charges are used.

### *Experimental Data compared with predicted charging behaviour*

The goethite, used in this study consists of about 90% (110) face and 10% (021) face. This implies that the charging behaviour of the goethite surface is mainly determined by the (110) face, so the model description of this surface must be in accordance with the data.

If we assume that the structural hydrogen bridge in the (110) interface does not persist, there are still two options left. For the first option, the doubly coordinated surface groups have two solution oriented orbitals ($m+n = 2$). In this case the model predicts a PPZC of 8 for the (110) face (Fig. 4a). A higher PPZC is found if the doubly coordinated surface groups at the (110) face only have one reactive orbital ($m+n=1$) (Fig 4b). For this case, the predicted PPZC is 9.5.

The (021) face may also influence the overall description of the charging behaviour. For the predicted charging behaviour of the (021) face, one may assume that the hydrogen bridges for the surface groups do not persist (Fig. 5a), resulting in a predicted PPZC of about 10. The option in which the hydrogen bridges do persist (Table 3, underlined values), results in a predicted PPZC of 8 (Fig. 5b).

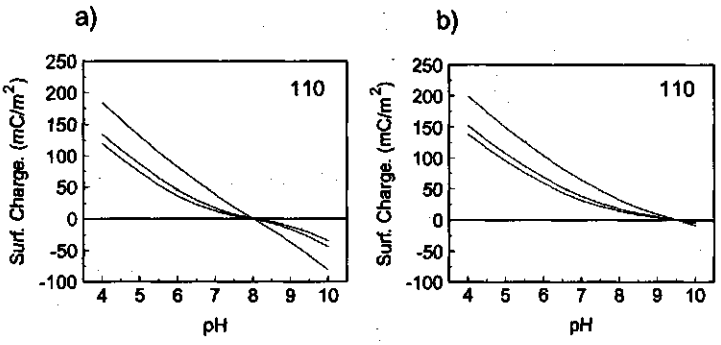


Fig. 4 The charging curves for the three background salt concentrations (0.005, 0.01 and 0.1 mol/l) for the (110) face as predicted with the model if the internal hydrogen bridge not persists while $m+n=2$ for the doubly coordinated surface group (a) and $m+n=1$ for the doubly coordinated surface groups (b). For the Stern layer capacitance see Fig. 6.

From the experimental charging curves of goethite a PPZC of 9.3 is found (Fig 6). This PPZC is in agreement with values found before (31, 32, 33, 34, 35). The goethite sample that is used in this study has a high surface area (95 $m^2/g$) and electron micrographs show that the crystals are well defined monodomainic. It was mentioned already that the (110) face dominates the charging behaviour. Considering the experimental data and regarding the results shown in Fig. 1, it is not likely that the internal hydrogen bridge in the (110) face will persist. The predicted PPZC for the (110) face becomes too low for this option. The best description of the data is obtained if it is assumed that the internal hydrogen bridge does not persist and that the doubly coordinated surface group has one ligand that can form a hydrogen bridge ($m+n=1$) (Fig. 4a). For reasons of consistence it is assumed that on the (021) face also the internal hydrogen bridges do not persist (Fig. 5a). The overall description of the charging behaviour is very good although the predicted PPZC is slightly too high (lines in Fig. 6).

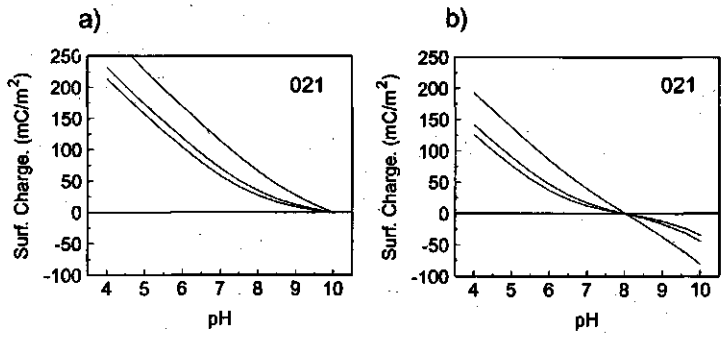


Fig. 5 The charging curves at the three background salt concentrations for the (021) face as predicted with the model if the hydrogen bridges for the surface groups do not persist (a) and the same calculations if they do persist (b). For the Stern layer capacitance see Fig. 6.

However the assumption that the doubly coordinated groups at the (110) face can only form one hydrogen bridge with adsorbed water does not seem to be logical. This may be a point for future research.

The predicted proton affinities for goethite do not harmonize with values found by Rustad et al. (36). A remarkable part of our model prediction (see Table 2) is that all reactive surface groups of the 110 face are almost completely neutralized and stable over a wide pH range. Only the singly coordinated surface groups show a relatively high local charge and are also the most important groups that are predicted to be reactive during the titration. In the work of Rustad et al. relatively small differences (± 2 log $K$ units) are found between proton affinities of $O_I$ and $O_{II}$ groups with the same metal coordination. Our calculations, however showed much higher differences (up to 12 log $K$ units) between the proton affinities of these two types of surface oxygens. According to Rustad et al (36), the large differences in log $K$ values between surface groups with different coordination by metal ions are smoothed out if surface relaxation is considered.

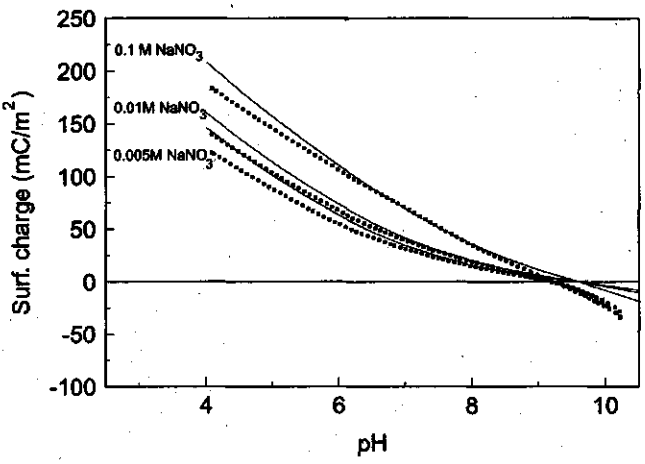


Fig. 6 Charging behaviour of goethite for three different salt concentrations. The lines represent the model calculations, while the dots represent the data. The charging curves are measured with three different background salt concentrations. The Stern layer capacitance used was 1.25 F/m$^2$.

The most striking difference is that Rustad et al. find a difference ($\Delta$ log $K_H$) of about 2 log $K_H$ units between the proton affinities of the first and the second protonation step for the doubly coordinated surface groups. In this study we find a difference of 11.9 log $K_H$ units. The relatively low $\Delta$log $K_H$ value that is found by Rustad et al. is also not in accordance with experimental evidence that shows the interaction between protons bound to neighbouring groups increases tremendously with decreasing separation (37). In that study, an extrapolated value can be derived that shows a difference of about 15 log $K$ units if the protons would react on the same site. This experimental result strongly supports the idea that the difference between consecutive protonation steps on the same surface groups of solids should also be large. The $\Delta$log $K_H$ value found by Rustad et al. is not consistent with this idea.

The finding of Rustad et al. that singly coordinated oxo surface groups are instable is in accordance with the high protonation constants for these groups found in this study. The high protonation constant found with the MUSIC model implies that the oxo group will always be protonated at normal pH values.
If the proton affinity and acidities of Rustad et al. are interpreted as log $K_{H\,int}$ values, the predicted PPZC for goethite with 90% (110) face and 10% (021) face is about 8.9. This value is in reasonable accordance with the data and the model pre-

diction of this study. The method to calculate the PPZC mentioned by Rustad et al. is not in accordance with the findings of this study (appendix). A PPZC can in general not be obtained by a single average of the log $K_H$ values of the different surface groups.

## Results and discussion for Lepidocrocite

### *Crystal structure and morphology*

Lepidocrocite has the same chemical composition as goethite (FeOOH) (Fig. 7) but the crystal structure is different (38). The structure that is used in this study has been determined by Christensen and Christensen (38). In the lepidocrocite crystal also two different types of oxygens can be distinguished (Fig. 7). The structural environment of both types of oxygen differ from the types in goethite; Oxygen $O_{II}$ is surrounded by four iron atoms and therefore unprotonated, $O_I$ is surrounded by two iron atoms and two protons (Fig. 8). For the calculation of the bond valences (eq. [5]), the value of $R_{0\ Fe\text{-}O}$ has been optimized to 1.7694. The crystal is not perfectly electroneutral with this value. The iron centred octahedra have a charge deficit of 0.4 % while the tetrahedra have a deficit of 0.9 % ($O_I$ centred) and an excess of 1.5 % ($O_{II}$ centred). The crystal structure that was determined more recently by Christensen et al. (39) gave less perfect results with the bond valence method. Better results were obtained with a structure that was calculated with molecular statics (25). Because this last structure was not originally determined from x-ray analysis, the crystal structure of Christensen and Christensen (38) is used here.

Table 4 The surface composition and predicted proton affinities for the surface groups of the 010 face of lepidocrocite. The resulting log $K_{int}$ are shown in the last column the upper value is the first protonation constant and the lower value the second protonation constant.

Lepidocrocite 010 Face

| Type of group | $N_S$ (sites/nm$^2$) | Bond lengths (Å) | | $s$ | | m | n | log $K_{H1}$<br>log $K_{H2}$ |
|---|---|---|---|---|---|---|---|---|
| $Fe_2O_I$ | 8.4 | 2.019 | 2.019 | 0.509 | 0.509 | 0 | 2 | 11.5 |
| | | | | | | 1 | 1 | -0.4 |

The most probable crystal faces are the (010), (100) and (001) faces (17, 29). It can be expected that the (010) and the (001) face are the dominant crystal faces (40%-60% of the surface) (17).

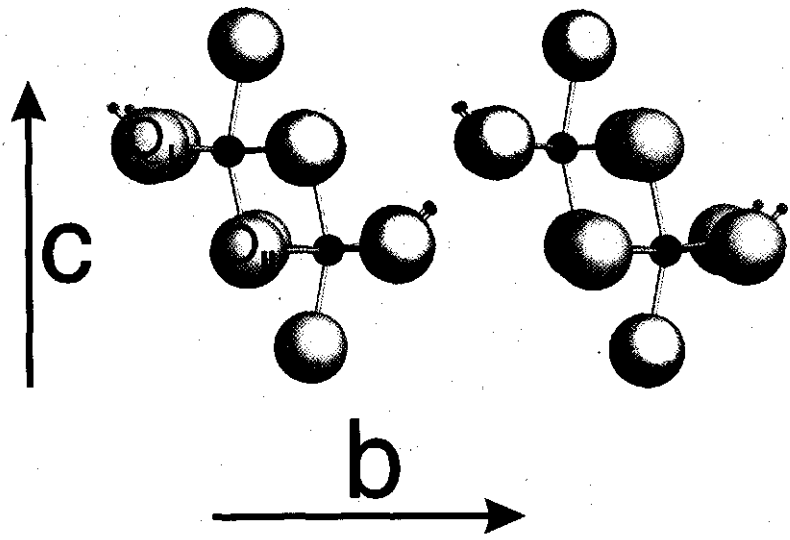


Fig. 7 The unity cell of lepidocrocite with four "filled" octahedra. The large spheres represent oxygens, the intermediate spheres are the central iron ions and the small spheres represent the protons. An iron ion with six surrounding oxygens can be considerd as an octahedron. In the picture it can be seen that only iron-filled octahedra occur. Note that oxygen atoms can be protonated (two O-H bonds) or unprotonated.

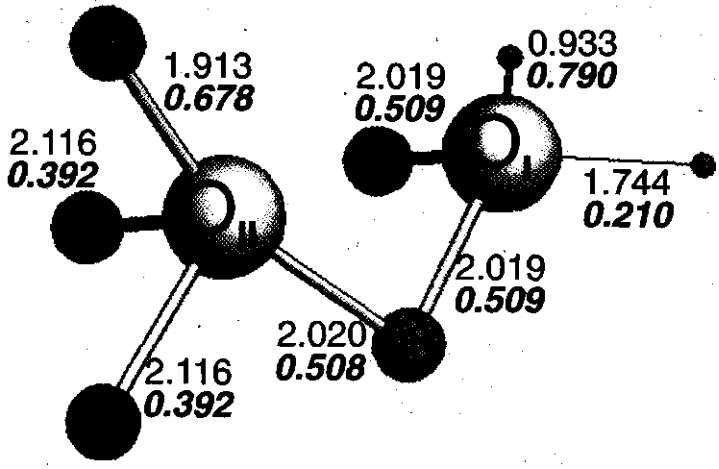


Fig. 8 The two different oxygens that occur in lepidocrocite with all bond lengths in Å (upper numbers) and bond valences (bolt, italic, lower numbers).

The surface composition of the (010) face is simple; just doubly coordinated surface groups occur with $m+n=2$ (Table 4). In lepidocrocite, the octahedra are asymmetric in the c-direction, this asymmetry results in different Fe-$O_{II}$ bond lengths for the (001) face (1.913 Å) and the 00$\bar{1}$ face (2.020 Å). At both the (001) and the 00$\bar{1}$ face, singly coordinated $O_{II}$, triply coordinated $O_{II}$ and doubly coordinated $O_I$ surface groups occur in a ratio 1:1:1 (Table 5). For all $O_{II}$ groups one Fe-O bond length differs for the two crystal faces. The doubly coordinated $O_I$ surface group has the same Fe-O bond lengths for both crystal faces (Table 5) and they have a structural hydrogen bridge. These hydrogen bridges will probably persist because their structural environment at the crystal face is the same as in the bulk.

Table 5 The surface composition and predicted proton affinities for the different surface groups of the 001 face of lepidocrocite. The underlined values in the column for the bond lengths and bond valence represent structural hydrogen bridges. The resulting log Kintr are shown in the last column the upper value is the first protonation constant and the lower value the second protonation constant. The underlined values in the columns for $m$, $n$ and log $K$ represent values if the structural hydrogen bridges would persist.

| Type of group | $N_S$ (sites/nm$^2$) | Bond lengths (Å) | $s$ | m | n | log $K_{H1}$ log $K_{H2}$ |
|---|---|---|---|---|---|---|
| **Lepidocrocite 001 Face** | | | | | | |
| $Fe_IO_{II}$ | 5.2 | 1.913 | 0.678 | 0 | 2 | 18.2 |
| | | | | 1 | 1 | 6.4 |
| $Fe_2O_I$ | 5.2 | 2.019 2.019 <u>0.933</u> | 0.509 0.509 <u>0.790</u> | 0 <u>0</u> | 2 <u>1</u> | 15.5 |
| | | | | 1 | 1 | 3.6 |
| $Fe_3O_{II}$ | 5.2 | 2.116 2.116 1.913 | 0.392 0.392 0.678 | 0 | 1 | 6.7 |
| **Lepidocrocite 00$\bar{1}$ Face** | | | | | | |
| $Fe_IO_{II}$ | 5.2 | 2.020 | 0.508 | 0 | 2 | 21.6 |
| | | | | 1 | 1 | 9.7 |
| $Fe_2O_I$ | 5.2 | 2.019 2.019 <u>1.744</u> | 0.509 0.509 <u>0.210</u> | 0 <u>0</u> | 2 <u>1</u> | 15.5 |
| | | | | 1 | 0 | 3.6 |
| $Fe_3O_{II}$ | 5.2 | 2.116 2.116 2.020 | 0.392 0.392 0.508 | 0 | 1 | 10.1 |

The surface composition of the (100) face is different, here singly coordinated $O_I$, singly coordinated $O_{II}$ and triply coordinated $O_{II}$ surface groups occur in a ratio 2:1:1 (Table 6). The singly coordinated $O_I$ oxygens have two internal hydrogen

bridges. The two internal hydrogen bridges may not persist because their structural environment is distorted. If they do persist, this surface group will behave as a triply coordinated surface group (table 6, underlined values).

Table 6 The surface composition and predicted proton affinities for the different surface groups of the 100 face of lepidocrocite. The underlined values in the column for the bond lengths and bond valence represent structural hydrogen bridges. The resulting log Kintr are shown in the last column the upper value is the first protonation constant and the lower value the second protonation constant. The underlined values in the columns for $m$, $n$ and log $K$ represent values if the structural hydrogen bridges would persist.

Lepidocrocite 100 Face

| Type of group | $N_s$ (sites/nm$^2$) | Bond lengths (Å) | | | $s$ | | | m | n | | log $K_{H1}$ log $K_{H2}$ |
|---|---|---|---|---|---|---|---|---|---|---|---|
| $Fe_tO_I$ | 8.24 | 2.019 | <u>0.933</u> | <u>1.767</u> | 0.509 | <u>0.210</u> | <u>0.790</u> | 0 | 2 | <u>1</u> | 21.6 |
| | | | | | | | | | | | 9.7 |
| $Fe_tO_{II}$ | 4.12 | 2.116 | | | 0.392 | | | 0 | 2 | | 23.9 |
| | | | | | | | | 1 | 1 | | 12.0 |
| $Fe_3O_{II}$ | 4.12 | 2.116 | 2.020 | 1.913 | 0.392 | 0.508 | 0.678 | 1 | | | 4.4 |

### *Experimental Data compared with predicted charging behaviour*

According to literature (29, 40), the (010) and the (001) face are the dominant crystal faces with about 10% of the area occupied by (100) crystal faces. Because at the (010) face only doubly coordinated surface groups occur, which are inert according to MUSIC, it is expected that lepidocrocite is relatively inert.

The lepidocrocite, used in this study, is porous so that the crystal faces all may have imperfections. It is very well possible that steps and pores occur at the different crystal faces, causing a different composition in terms of surface sites (28). The relative amount of the different crystal faces is therefore not easy to estimate.

As expected, the model predicts that the (010) face is inert, only for high pH values the surface charge is slightly negative (Fig. 9a). The predicted charging of the (001) faces is shown in Fig. 9b. The (001) and (00$\bar{1}$) face will occur in a ratio 1:1, so the overall charging behaviour is the resultant of these both faces. In Fig 9b this resultant is shown as a solid curve.

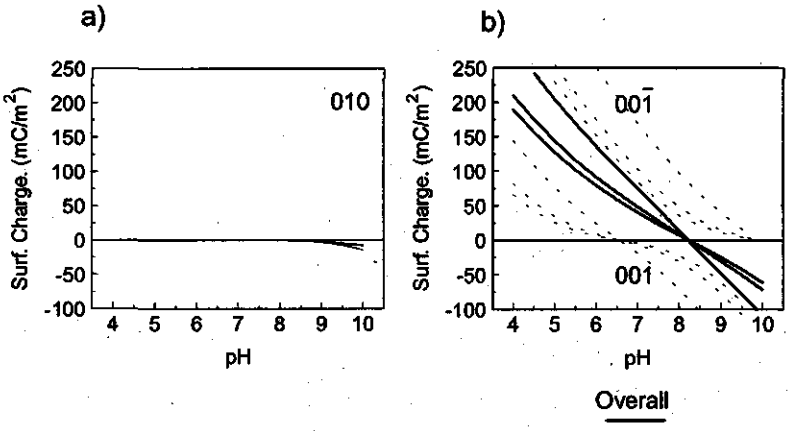


Fig. 9 The charging curves at three background salt concentrations (0.005, 0.01 and 0.1 mol/l) for the perfect (010) face (a) and the (001) and 00$\bar{1}$ face, these faces probably exist in a ratio 1:1 so the overall curve is a resultant of both faces, represented by the solid line (b).

The charging behaviour of the (100) head face can be calculated with the assumption that the hydrogen bridges persist (Fig. 10a). For this option the singly coordinated $O_t$ groups have a low log $K_H$. The PPZC of the surface is much higher if the hydrogen bridges are assumed not to persist (Fig. 10b).

The surface area of Lepidocrocite is quite high (73 $m^2/g$), but the crystals are less well defined as the goethite crystals (17). The PPZC is 8 and the surface charges as high as goethite (Fig 11) which is surprising because the inert (010) face must be an important face. The charging curves are in agreement with curves measured by Madrid and Diaz-Barrientos (41).

The overall charge is calculated with 50% (001) + 00$\bar{1}$ face, 10% (100) face and 40% (010) face (lines in Fig. 11). For the (100) face the internal hydrogen bridges are assumed to persist. The predicted PPZC is slightly too low (0.1 log $K_H$ value). The model description is quite good. The high charging indicates a high porosity which can be described with a high stern layer capacitance. The capacitance used for the calculations is 1.85 $F/m^2$ which is indeed high. The salt effect predicted by

the model in the PPZC is too low in comparison with the data. This is due to the use of different crystal faces with a different PPZC.

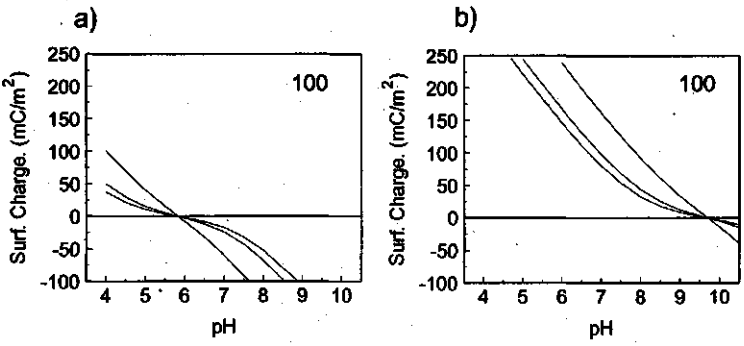


Fig. 10 The predicted charging curves at three background salt concentrations for the (100) face if the hydrogen bridges of the singly coordinated $O_1$ surface group persist (a) and if they not persist (b)

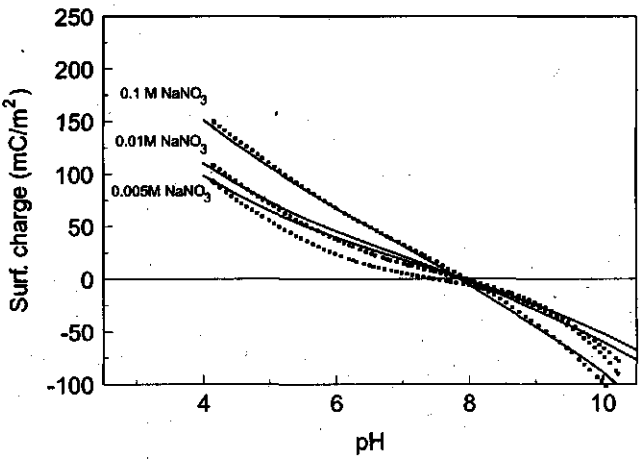


Fig. 11 The experimental charging curves for lepidocrocite for three salt concentrations. The lines represent the model predictions. The used Stern layer capacitance is 1.85 F/m$^2$.

A similar description of the charging behaviour can be obtained with 82% (001) +

00$\bar{1}$ face and 18% (100) face with a stern layer capacitance of 1.0 F/m$^2$. This may be a realistic option because the (010) face can have imperfections and the surface composition in terms of surface sites may in that case resemble the (001) and (100) face.

## Results and discussion for Hematite

### *Crystal structure and morphology*

Hematite is an iron oxide, the chemical formula is $\alpha$-$Fe_2O_3$. The crystal structure is described in detail elsewhere (42, 43). A cross section of the unit cel in (110) direction is shown in Fig. 12. All oxygens in the structure are surrounded by four iron atoms. Two different Fe - O bond lengths occur in the crystal, a short bond of 1.944 Å and a long bond of 2.113 Å. In the structure, each oxygen has two long and two short bonds with iron (Fig. 13). For an electroneutral crystal the values of $R_{0\ Fe\text{-}O}$ (eq. [5]) is optimized to 1.7625.

The crystal morphology of hematite is less well known as for goethite or lepidocrocite, the surface composition in terms of surface sites is therefore difficult to determine (30). Therefore, the surface composition is not considered in too much detail here.

Table 7 The predicted proton affinities for the different surface groups that may exist on Hematite. The resulting log $K_{intr}$ are shown in the last column the upper value is the first protonation constant and the lower value the second protonation constant.

| Hematite 001 face | | | | | | |
|---|---|---|---|---|---|---|
| Type of group | $*N_s$ (sites/nm$^2$) | Bond lengths (Å) | $s$ | m | n | log $K_{H1}$<br>log $K_{H2}$ |
| $Fe_tO_t$ | 4[1] | 2.113 | 0.388 | 0 | 2 | 24.0 |
| | | | | 1 | 1 | 12.1 |
| $Fe_tO_s$ | 1[1] | 1.944 | 0.612 | 0 | 2 | 19.6 |
| | | | | 1 | 1 | 7.7 |
| $Fe_2O_{ls}$ | 8.7 | 2.113 1.944 | 0.388 0.612 | 0 | 2 | 11.9 |
| | | | | 1 | 1 | 0.0 |

[1] These sites do not occur at the 001 face that is perfectly crystallized. In this study it is assumed that the sites arise at a 001 face with imperfections.

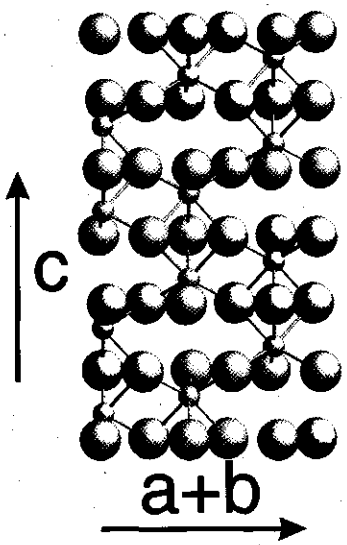


Fig. 12 The unit cel of Hematite, viewed perpendicular to the 110 face. The large spheres represent the oxygens, the smaller spheres the iron.

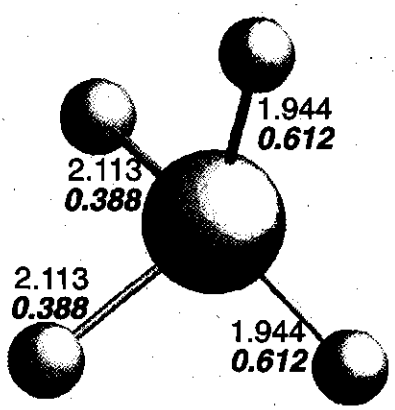


Fig. 13 The different Fe-O bond lengths and valences that occur in the hematite crystal. The large sphere represents an oxygen while the smaller spheres represent the iron. The bond lengths (upper numbers) are given in Å and the bond valences are the bolt italic lower numbers.

The hematite crystals, used in this study, are platy shaped. The dominant crystal face for these crystals is probably the (001) face (17). At the perfect (001) face, all surface groups are doubly coordinated groups with one long and one short bond (Table 7). So, like lepidocrocite, the hematite can be expected to be relatively inert. The (001) face, however, may have imperfections (26), leading to a different composition in terms of surface sites than a perfect (001) face. For the calculations it is assumed that at several positions underlying Fe atoms are missing. Here two options are possible:

a) A deep lying iron ion is missing in the surface so that three singly coordinated surface groups with a short Fe-O bond arise

b) A higher lying iron ion is missing in the surface so that three singly coordinated surface groups with a long bond arise

So at an imperfect (001) face, two types of singly coordinated surface groups and one type of doubly coordinated groups may occur (table 7).

Table 8 The predicted proton affinities for the different surface groups that may exist on Hematite. The resulting log $K_{int}$ are shown in the last column the upper value is the first protonation constant and the lower value the second protonation constant.

Hematite 110 face

| Type of group | $N_s$ (sites/nm$^2$) | Bond lengths (Å) | $s$ | m | n | log $K_{H1}$ log $K_{H2}$ |
|---|---|---|---|---|---|---|
| $Fe_1O_s$ | 5 | 1.944 | 0.612 | 0 | 2 | 19.6 |
| | | | | 1 | 1 | 7.7 |
| $Fe_2O_{II}$ | 1.7 | 2.113 2.113 | 0.388 0.388 | 0 | 2 | 7.4 |
| | | | | 1 | 1 | -4.4 |
| $Fe_2O_{ss}$ | 3.3 | 1.944 1.944 | 0.612 0.612 | 0 | 2 | 16.3 |
| | | | | 1 | 1 | 4.4 |
| $Fe_3O_{IIs}$ | 5 | 2.113 2.113 1.944 | 0.388 0.388 0.612 | 0 | 1 | 8.2 |

Other probable crystal surfaces are the (110) and (120) faces (30). The surface site composition of these two faces is similar; a singly, doubly and triply coordinated surface group in a ratio 1:1:1. All singly coordinated surface groups have a short bond and all triply coordinated surface groups have two long and one short bond (table 8). The doubly coordinated surface groups can be separated in two different types: groups with two short bonds and groups with two long bonds, occurring in a

ratio 2:1 (table 8). The above mentioned crystal faces are probable to occur at this crystal and they will be used for the description of the charging behaviour. The site densities are here used as a fit parameter.

*Experimental Data compared with predicted charging behaviour*

A platy hematite crystal consists for about 40-60% of (001) face. The rims of the plate may have a constitution like the (110) or (210) face (30). Because about 10% of the crystals had a globular shape (17) other crystal faces will probably occur too. With only the (110) and imperfect (001) face, however, the charging behaviour can be described satisfactory.

The PPZC of the (110) face is about 8. The only surface groups that can give a PPZC higher than 9 are the singly coordinated surface groups with a long Fe-O bond. As discussed before, these groups may exist at the (001) face if some structural iron atoms that coordinate to surface ligands are missing.

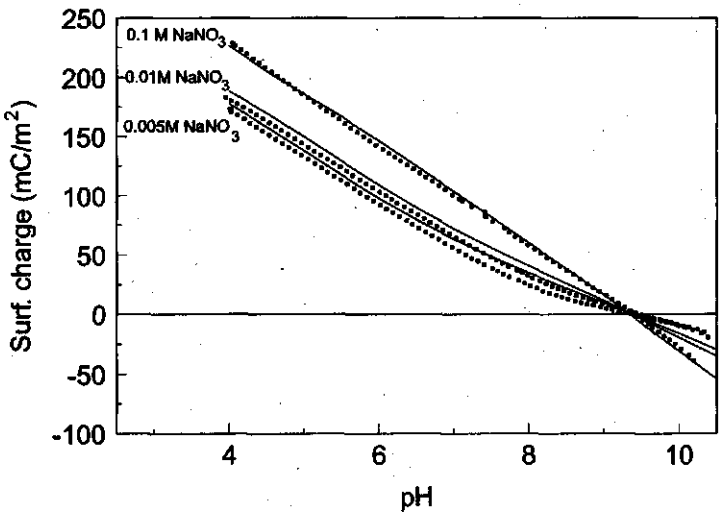


Fig. 14 The experimental charging curves of hematite for three salt concentrations represented by the dots. The lines represent the model calculation. The used stern layer capacitance is 1.4 F/m$^2$

The hematite used in this study has a relatively low surface area (36,5 m$^2$/g) and a cilindrical crystal shape (17), dominated by the (001) crystal face. The experimental PPZC is 9.4 which is in accordance with values found by Penners (44). In case of a

perfect crystallisation of the (001) face, we predict that the crystal is quite inert. However, our hematite develops a high surface charge (Fig.14). As explained by the charging behaviour of goethite, a steeper charging curve indicates that the crystal faces are imperfect. The shape of the charging curves can be described well if the log $K$ value of the pair forming ions (Na and $NO_3$) are relatively high (log $K_{pf}$=0) (45). This choice for relatively strong pair formers does not seem to be very plausible. A good alternative is the use of two different faces with a different PPZC.

A good description of the charging behaviour is obtained if it assumed that the total site density of singly coordinated surface groups at the imperfect (001) face is 5 sites/nm$^2$. In the calculations 80% of these singly coordinated surface groups at the imperfect (001) face have a long Fe-O bond (High PPZC) and 20% a short Fe-O bond (low PPZC). The combination of the imperfect (001) face (50%) and the (110) face (50%) gives a reasonable description of the experimental charging curves (lines Fig. 14). The stern layer capacitance for the model description is 1.4 F/m$^2$. The predicted salt dependency near the PPZC is sightly too low in comparison with the data.

The description can be slightly improved if two planes with a ratio 1:1 are used with only singly coordinated surface groups. The PPZC of these planes is then 8 and 11 whith a stern layer capacitance is 1.15 F/m$^2$. This simplified model describes the data very good although the protonation constant and surface composition do not fully harmonize with the values found with the MUSIC approach.

## Conclusions

The refined MUSIC model can give a good prediction of a PPZC that is the net effect of different crystal planes and different reactive groups having different log $K_H$ values. For a good description, the exact surface morphology of the crystal must be known.

The chemical heterogeneity according to the MUSIC model originates from differences in undersaturation of the surface oxygens due to differences in the number and length of metal bonds and hydrogen bonds.

The predicted individual log $K_H$ values for goethite are not in accordance with

results of Rustad et al. (36). The overall predicted PPZC value of both studies, however, are in reasonable accordance.

Based on the low reactivity of the (010) plane of lepidocrocite, this crystal face can not be dominant because of the high surface charge that was measured. If the (010) face occurs, it will have many imperfections.

For lepidocrocite, the model can be simplified to a model in which two different crystal faces are used, the (001) + (00$\bar{1}$) face and the (100) face. This option may be realistic for the porous lepidocrocite.

The charging behaviour of hematite can be described with two reactive faces with a different surface composition. This model is in good accordance with the crystal morphology of the hematite that is used in this study. The charging behaviour can also be described with one crystal plane and strong pair formers (log $K_{pf}$=0) (45). The assumption of two crystal planes with a different PPZC seems to be more realistic than the choice for strong pair formers.

The PPZC of hematite can only be predicted if singly coordinated surface groups with a long Fe-O bond are of importance. These surface groups are not dominant on the probable crystal faces, suggested by Barron and Torrent (30).

## Literature


1. Parks, G.A., and de Bruyn, P.L., The zero point of charge of oxides, *J. Phys. Chem.*, **66**, 967, (1962)
2. Atkinson R.J.; Posner A.M., and Quirk J.P.; *J. Phys. Chem.* **71**, 550-558 (1967)
3. Parks, G.A., "The iso electric points of solid oxides, solid hydroxides and aqueous hydroxo complex systems, *Chem. rev.*, **65**, 177 (1965)
4. Yoon R.H., Salman T., and Donnay G., Predicting Points of Zero Charge of Oxides and Hydroxides, *J. Colloid Interface Sci.*, **70**, 483 , (1979)
5. Sverjenski D.A., Zero-point-of-charge prediction from crystal chemistry and solvation theory, *Geochim. Cosmochim. Acta*, **58**, 3123-3129, (1994)
6. Hiemstra, T, vanRiemsdijk, W.H., and Bolt, G.H., Multisite Proton Adsorption Modeling at the Solid/Solution Interface of (Hydr)oxides: A New Approach, I. Model Description and Evaluation of Intrinsic Reaction Constants, *J. Colloid Interface Sci.* **133**, 91-104 (1989)
7. Hiemstra, T, de Wit J.C.M., and vanRiemsdijk W.H., Multisite Proton Adsorption Modeling at the Solid/Solution Interface of (Hydr)oxides: A New Approach, II. Application to various Important (Hydr)oxides, *J. Colloid Interface Sci.* **133**, 105-117 (1989)
8. Pauling L., The principles determining the structure of complex ionic crystals, *J. Am. Chem. Soc.*, **51**, 1010-1926, (1929)
9. Brown, I.D., and Shannon, R.D., Empirical Bond-Strength-Bond-Length Curves for Oxides, *Acta Cryst.*, **A 29**, 266-282, (1973)
10. Brese, N.E., and O'Keefe, M., Bond-Valence Parameters for Solids, *Acta Cryst.*, **B 47**, 192-197, (1991)
11. Hiemstra, T, and van Riemsdijk, W.H., A surface structural approach to ion adsorption: The Charge Distribution (CD) model, *J. Colloid Interface Sci.* **179**, 488-508 (1996)
12. Brown, I.D., Bond Valences-A Simple Structural Model for Inorganic Chemistry, *Chem. Soc. Rev.*, **7**, 359-376, (1978)
13. Brown, I.D., and Altermatt, D., Bond-Valence parameters Obtained from a Systematic Analysis of the Inorganic Crystal Structure Database, *Acta cryst.*, **B 41**, 244-247, (1985)
14. Brown, I.D., and Wu, K. K., Empirical Parameters for Calculating Cation-Oxygen Bond Valences, *Acta Cryst.*, **B 32**, 1957-1959, (1976)
15. Bleam W.F., On modeling proton affinity at the oxide/water interface, *J. Colloid Interface Sci.* **159**, 312-318, (1993)
16. Hiemstra T, Venema P., vanRiemsdijk W.H., Intrinsic proton affinity of reactive surface groups of Metal (hydr)oxides: The bond valence principle, *J. colloid Int. Sci.*, **184**, 680-692 (1996)
17. Weidler P.G., Oberflächen und Porositäten synthetischer Eisenoxide, Phd. thesis T.U. München dept. Soil Science, (1994)
18. Venema, P., Hiemstra, T., and van Riemsdijk, W.H., Multisite adsorption of cadmium on goethite, *J. Colloid Interface Sci.* **183**, 515-527 (1996)
19. Kinniburgh D.G., Milne C.J., Venema P., Design and Construction of a Personal-Computer-Based Automatic Titrator, *Soil Sci. Soc. Am. J.*, **59** (2), 417-422, (1995)
20. de Keizer, A., "Electrosorption of tetraalkylammonium ions on silver iodide", Phd. thesis dept. Fys. and Coll. Chemistry W.A.U., Wageningen, 1981
21. Mc Innes, D.A., *in* "The principles of electrochemistry", Dover publications Inc., New York, 1961
22. Stern O. (1924) Zur theorie der elektrolitischen doppelschicht, *Z. Elektrochem.* **30**, 508-516
23. Bolt, G.H., The ionic distribution in the diffuse double layer; *In*: "Soil chemistry; B. physico chemical models", (Bolt G.H., Ed.). Elsevier scientific publishing comp. Amsterdam, 1982
24. Venema, P., Hiemstra, T., and van Riemsdijk, W.H., Comparison of different site binding models for cation sorption: Description of pH dependency, Salt dependency and Cation-Proton exchange, *J. Colloid Interface Sci.* **181**, 45-59 (1996)

25. Rustad, J.R., Felmy, A.R., and Hay, B.P., Molecular statics calculations for iron oxide and oxyhydroxide minerals: Towards a flexible model of the reactive mineral-water interface, *Geochimica et cosmochimica acta*, **60(9)**, 1553-1562, (1996)
26. Eggleston C.M., Hochella M.F., Jr.,The structure of the hematite (001) surface by by scanning tunneling microscopy Image interpretation, surface relaxation and step structure, *Amer. Mineral.* **77**, 4843-4850
27. Hazemann J.L., Berar J.F., Manceau A., Rietveld studies of the aluminium-iron substitution in synthetic goethite, *J. Mat. Sci. Forum*, **79**, 821-826, (1991)
28. Weidler P.G., Schwinn T. and Gaub H.E., Vicinal Faces on Synthetic Goethite Observed by Atomic Force Microscopy, *Clays and Clay Minerals*, accepted (1995)
29. Schwertmann U., Cornell R., Iron Oxides in the laboratory., VCH Weinheim, New York, Basel, Cambridge, 1991
30. Barron, V, and Torrent, J, Surface hydroxyl configuration of various crystal faces of hematite and goethite, *J. Colloid Interface Sci.*, **177**, 407-410, (1996)
31. Johnson, B.B., Effect of pH temperature and concentration on the adsorption of cadmium on goethite, *Environ. Sci. Technol.* **24**, 112-118 (1990)
32. Spark, K.M., Johnson, B.B., and Wells, J.D., Characterizing heavy-metals adsorption on oxides and oxyhydroxides, *Europ. J. of Soil Sci.* **46**, 621 (1995)
33. Lumdson, L.G., and Evans, L.J., Surface complexation model parameters for goethite, *J. Colloid Interface Sci.* **164**, 119 (1994)
34. vanGeen, A., Robertson, A.P., and Leckie, J.O., Complexation of carbonate species at the goehtite surface: Implications for adsorption of metal ions in naturals waters, *Geochim. Cosmochim. Acta*, **58**, 2073-2086 (1994)
35. Mesuere, K, and Fish, W, Chromate and oxalate adsorption on Goethite. 1. Callibration of surface complexation models, *Environ. Sci. Technol.* **26**, 2357-2364 (1992)
36. Rustad, J.R., Felmy, A.R., and Hay, B.P., Molecular statics calculations of proton binding to goethite surfaces: A new approach to estimation of stability constants for multisite surface complexation models, *Geochimica et cosmochimica acta*, **60(9)**, 1563-1576, (1996)
37. Borkovec M, and Koper J.M. Ising Models of Polyprotic Acids and Bases, *J. Physical Chemistry*, **98**, 6038-6045 (1994)
38. Christensen, H., and Christensen A.N., Hydrogen bonds of gamma-FeOOH, *Acta Chem. Scand.* **A32**, 87-88, (1978)
39. Christensen A.N., Lehman M.S., and Convert P. (1982) Deuteration of crystalline hydroxides. Hydrogen bonds of γ-AlOOH (H,D) and γ-FeOOH (H,D). *Acta Chem. Scand.*, **A36**, 303-308
40. Lewis, D.G., and Farmer, V.C., Infrared adsorption of surface hydroxyl groups and lattice vibrations in lepidocrocite (γ-FeOOH) and boehmite (γ-AlOOH), *Clay minerals*, **21**, 93-100, (1986)
41. Madrid L, and Diaz-Barrientos, E., Description of titration curves of mixed materials with variable and permanent surface charge by a mathematical model. 2. Application to mixtures of lepidocrocite and monmorillonite, *J. Soil Sci.* **39**, 215-225, (1988)
42. Newnham R.E., and de Haan Y.M., Refinement of the α $Al_2O_3$ , $Ti_2O_3$ , $V_2O_3$ , $Cr_2O_3$ structures, *Zeits. Krist.*, **117**, 235, (1962)
43. Antipin M.Y., Tzirelson, V.G., Flugge, M.P., Gerr, R.G., Struchov, Y.T., Ozerov, R.P., The electron density distribution in hematite, Fe2O3 alpha, from precision X-ray diffraction data, *Jrnl Doklady Akademii Nauk SSSR (Journal of soviet physics)*, **281**, 854-857, (1985)
44. Penners J.H.G., The preparation and stability of homodisperse coloidal hematite (α-$Fe_2O_3$), PhD thesis, dept. Phisical and Colloid Chemistry, Wageningen Agricultural University, (1985)
45. Hiemstra, T, van Riemsdijk, W.H., and Bruggenwert, M.G.M., *Neth. J. Agriculture*, **35, 281 (1987)**

# 7

# Comparison of different iron (hydr)oxides with respect to their charging, cat- and anion adsorption behaviour

# Comparison of different iron (hydr)oxides with respect to their charging, cat- and anion adsorption behaviour


## Abstract

*Five iron (hydr)oxides that differ in crystal structure and/or morphology are compared with respect to their chemical behaviour. Cadmium and phosphate adsorption and the charging behaviour are measured and modelled. For the modeling, the CD-MUSIC approach is used. It is tried to keep the models as simple as possible, with a minimum of parameters. Further it is tried to choose parameters which are in accordance with the crystal structure and morphology.*
*The results are split in two parts: the first part treats three goethites that differ in crystal structure and morphology and the second part treats goethite, lepidocrocite and hematite.*

*The two goehtites with a high surface area but a different crystal morphology showed no difference in their chemical behaviour. This is peculiar because it was expected that these goethites would have a different surface site constitution. The goethite with a low surface area showed higher surface charging and phosphate adsorption than the other two goethites. This chemical behaviour could be described well with a higher Stern layer capacitance and a higher site density.*

*Investigation of the influence of model parameters on the description showed that a higher Stern layer capacitance results in a higher charging but in a lower adsorption of cadmium and in a lesser extent lower phosphate adsorption. A higher site density on the other hand hardly influences the charging behaviour but results in a higher phosphate and cadmium adsorption.*

*These findings are also used for the description of the data of hematite and lepidocrocite. For these two iron (oxyhydr)oxides, the crystal morphology is less well known. This means that the choice for the model parameters has a higher degree of freedom.*


## Introduction

Iron (hydr)oxides are one of the most abundant (hydr)oxides in nature. In soil systems, iron (hydr)oxides of different crystal structure and morphology occur. It has

been shown that different iron (hydr)oxides can have a different charging behaviour (1). These differences in charging behaviour are related to differences in crystal structure and morphology (1,2), which will influence the adsorption of other ions too (3).

The influence of differences in crystal morphology, on the chemical behaviour of three iron oxyhydroxides with the same crystal structure (goethite), will be discussed first. Two of these goethites have monodomainic crystals, one of them has long needles (gt. A) and the other has relatively short needles (gt. B). The other goethite (gt. C) has large crystals with an irregular shape. Goethite is used because for this iron oxyhydroxide the crystal morphology is best known. The challenge in this study is to choose model parameters that both lead to a good description of the data and are in accordance with the crystal structure and morphology. For goethite the crystal morphology as discussed by Hiemstra and van Riemsdijk (4) and Venema et al. (1) is used. For the comparison of the data, the Charge Distribution - MUlti SIte Complexation (CD-MUSIC) model for metal (hydr)oxides as discussed by Hiemstra and van Riemsdijk (4) will be used. Attention will be paid to the influence of the Stern layer capacitance and the site density on the model description of the adsorption data.

In addition we will compare the chemical behaviour of two iron (hydr)oxides with a different crystal structure. For these two iron (hydr)oxides, the crystal morphology is not as well known as for goethite. Therefore the crystal morphology cannot be used to find model parameters. Here the crystal morphologies as discussed by Venema et al. (1) are used. The model results should here be considered to be a "first" approach. The number of variable parameters will be minimized as much as possible.

## Model description

The adsorption model that will be used, the CD-MUSIC model, is discussed in detail elsewhere (4, 5). The CD-MUSIC model comprises an electrostatic interface model with two charge free layers and a diffuse double layer, separated by three electrostatic planes. In this paper, we will index the surface plane with 0, the intermediate plane with 1 and the plane at the head end of the diffuse double layer with d. Details about this electrostatic part of the model can be found elsewhere (4). The

capacitance of the outer charge free layer ($C_2$) is fixed for all (hydr)oxides to a value of 5 F/m$^2$ (4).

### *Charging behaviour*

At a (hydr)oxide/solution interface, surface groups are present as either O, OH or $OH_2$ and can have a different coordination to underlying structural metal ions. On iron (hydr)oxides, singly, doubly and triply coordinated surface groups exist (5,6). The neutral doubly coordinated $Fe_2OH^0$ groups can be considered as chemically inert according to the MUSIC model (1, 4, 6, 7). So in this study, only the singly and triply coordinated surface groups are used for the description of surface charging. The protonation of these surface groups can be described in general according to:

$$S^{-½} + H^+ \leftrightarrows SH^{+½} \qquad K_H \qquad [1]$$

in which S is here a singly coordinated (FeOH) or a triply coordinated ($Fe_3O$) group. For the description of the charging behaviour, the log $K_H$ values that were found with the revised MUSIC model (Venema et al.) are averaged to one log $K_H$ value. For goethite this results in the model parameters as used by Hiemstra and van Riemsdijk (4). The averaged values of log $K_H$ are in some cases adapted slightly (some thenths of log $K$ units) to describe the experimental PPZC. In the interface model, the charge of an adsorbed proton is placed in the surface (the 0-plane).

### *Phosphate adsorption*

In addition to proton binding, also pair formation is assumed according to (4):

$$\begin{aligned} S^{-½} + Na^+ &\leftrightarrows S^{-½}Na^+ \qquad K_{pf} \\ S^{-½} + H^+ + NO_3^- &\leftrightarrows SH^{+½}NO_3^- \qquad K_H \cdot K_{pf} \end{aligned} \qquad [2]$$

in which S represents again a singly coordinated FeOH or a triply coordinated $Fe_3O$ group. The value of log $K_{pf}$ is set at -1 in all calculations. The charge of the adsorbed Na or $NO_3$ is placed in the d-plane at the head end of the diffuse double layer.

For specific adsorption of cat- and anions, only singly coordinated surface groups are assumed to be reactive (4, 8). This choice is in accordance with the classical

view on the behaviour of iron (hydr)oxides. It is based on observations of phosphate adsorption (4, 8).

Adsorption of phosphate has been described in detail by Hiemstra and van Riemsdijk (4). The adsorption is dominated by bidentate complex formation. Therefore we will, if possible, only consider the formation of bidentate surface complexes according to:

$$2\ FeOH^{-\frac{1}{2}} + PO_4^{-3} + 2\ H^+ \leftrightarrows Fe_2O_2^{p}PO_2^{q} + 2\ H_2O \qquad K_p \qquad [3]$$

$$2\ FeOH^{-\frac{1}{2}} + PO_4^{-3} + 3\ H^+ \leftrightarrows Fe_2O_2^{p}PO_2H^{q+1} + 2\ H_2O \qquad K_{PH} \qquad [4]$$

In which $p+q= -2$. In the CD-MUSIC model, the charge of the adsorbed phosphate ion is divided over the 0 and the 1-plane. The fraction of charge of the central $P^{5+}$ that is attributed to the surface plane is indicated with $f$. The total amount of charge that must be attributed to the 0-plane is given by the summation of the fraction $f$ of the valence of the central ion ($z$) and the number of protons that co-adsorb or desorb ($n_p$):

$$\Delta z_0 = f\,z + n_p \qquad [5]$$

in which F is the Faraday constant in C/eq. The charge of the adsorbing ion that must be attributed to the 1-plane is given by the summation of the other fraction (1-$f$) of the central ion valence ($z$) and the charge of its solution oriented ligands ($c_L$):

$$\Delta z_1 = (1-f)\,z + \sum c_L \qquad [6]$$

For phosphate $z$ equals +5 and for the bidentates the number of adsorbed protons $n_p$ equals -2, the minus sign indicates desorption. The sum of the charge of the solution oriented ligands, $c_L$ for the non protonated and the protonated surface complex is -4 and -3 respectively.

### *Cadmium adsorption*

The adsorption of cadmium is described with a simple monodentate reaction:

$$FeOH^{-½} + Cd^{+2} \leftrightarrows FeOH^{p}Cd^{q} \qquad K_{Cd} \qquad [7]$$

in which $p+q=1½$. The charge distribution for an adsorbed cadmium can be calculated with eq. [5] and eq. [6]. The number of co-adsorbed protons ($n_p$) and the sum of the charge of the solution oriented ligands ($c_L$) is zero. It implies that the charge attribution follows directly from the distribution of the cadmium charge over the 0- and 1-plane. For a good description of an extended cadmium data set, a high affinity site is needed (5). In this study only the low affinity sites will be used because no extended data sets of cadmium are available for all (hydr)oxides.

All log $K$ values have been calculated on basis of activities. The model calculations are done with the chemical equillibrium program ECOSAT. In ECOSAT, activity coefficients are calculated with the Davis equation:

$$\gamma_i = -0.5\ z_i^2\ \left(\frac{\sqrt{I}}{1+\sqrt{I}} - 0.2\ I\right) \qquad [8]$$

in which $I$ is the ionic strength and $z_i$ the valence of ion $i$.

## Experimental

The lepidocrocite, hematite and goethites (gt. B and gt. C) (courtesy P.Weidler and S. Glasauer) were produced in Munich, the production is described elsewhere (9, 10, 11). The method to produce goethite A can be found in chapter 3 (5). The BET surface area was measured by $N_2$ gas adsorption (courtesy of P.Weidler, S. Glasauer and A. Korteweg).

All experiments were done in plastic vessels and all chemicals were stored in plastic bottles to avoid silica contamination. For the experiments distilled, demineralized water (DD water) was used.

For the measurement of the charging curves and the cadmium adsorption attention was paid to avoid contamination of $CO_2$. During these experiments air was excluded by a continuous flow of $N_2$ through the vessel and the base solution (NaOH) was stored in an exsiccator.

The experimental methods for the measurement of the charging behaviour are described in detail in Venema et al. 1996 (5). The charging curves were measured with the help of a personal computer controlled titrator (12) at three salt concentrations (0.005, 0.01 and 0.1 mol/l $NaNO_3$). At each salt concentration, first a titration with base and then with acid was done to check reversibility.

Cadmium adsorption isotherms were measured at pH 6 and pH 7 in 0.1 M $NaNO_3$. The method, used to measure the isotherms is described in detail elsewhere (5). The suspension was brought to the appropriate salt level with $NaNO_3$ and left overnight at pH 5 in a nitrogen atmosphere to exclude $CO_2$. Next, it was brought to the desired pH with NaOH and cadmium was then added while the pH was kept at the target value (± 0.05 pH units) by adding NaOH. A sample was taken after equilibrating for 4 hours and a new cadmium dose was added. Six or seven samples were taken for each experiment (one pH). An experiment lasted 2.5 days. Duplicate experiments for Goethite C at pH 7 in a salt concentration of 0.1 M showed good agreement.

Cadmium analysis was performed for solution samples which had been filtered through 0.025 µm micropore membrane filters (PH70, Schleicher & Schuell). The first 1 to 2 ml of filtered solution were discarded to prevent loss of cadmium by adsorption on the filter. The loss of cadmium by the filter was not detected for a concentration of $10^{-5}$ mol/l solution. The filtered solution was analyzed for cadmium by flame AAS and/or GFAAS.

Phosphate adsorption edges were measured at a constant suspension density of 150 $m^2/l$ and an initial P. concentration of 0.5 mmol/l for all metal (hydr)oxides. No $CO_2$ was excluded for these experiments. For lepidocrocite and hematite an extra data set was measured, the suspension densities were 83 $m^2/l$ (lepidocrocite) and 290 $m^2/l$ (hematite). The experiments are done in plastic bottles. The suspensions in the bottles were first brought to a salt concentration of 0.1 mol/l ($NaNO_3$), then acid ($HNO_3$) or base (NaOH) was added depending on the desired pH. If the bottles were at the right salt level and pH, $NaH_2PO_4$ was added to reach the initial P. concentration of 0.5 mmol/l. Next, the bottles were put in an end over end shaker for 24 hours after which part of the suspension was centrifuged at 20.000 rpm. The

phosphate concentration was measured in the supernatant colorimetrically after colouring with molybdate. The pH was measured in the suspension.

## Results and discussion for goethites with a different morphology

### *Crystal structure and morphology*

The three different goethites that are used in this study, differ in their crystal morphology. The two monodomainic goethites differ in particle size and therefore specific surface area. Goethite A has long needle shaped crystals while goethite B has short needle shaped crystals. The goethite with the long needles (Gt. A) is a reference material because many experiments were done with this material in our lab. Finally, the goethite with the low surface area (goethite C) has very large crystals. The model parameters for the reactive sites of goethite as given by Venema et al. (1) are shown in Table 1. These values are the basis for the simplified model that is used in this study.

Table 1 The morphology and surface composition for goethite (1) that forms the basis for the model used in this study. For the 021 face, the two types of singly coordinated surface groups are not considered separately but are treated as one type of surface group. For the 110 face, the $Fe_3O_{110}$ and one $Fe_3O^{-}_{110}$ are considered to form an inert pair.

| 021 Face (10%) | | | 110 Face (90%) | | |
|---|---|---|---|---|---|
| Surface-group | $N_s$ (sites/nm$^2$) | Log $K_H$ | Surface group | $N_s$ (sites/nm$^2$) | Log $K_H$ |
| $FeOH_{021}$ | 3.75 | 8.1 | $FeOH_{110}$ | 3 | 7.7 |
| $FeOH^{-}_{021}$ | 3.75 | 11.9 | $Fe_3O_{110}$ | 3 | -0.2 |
| | | | $Fe_3O^{-}_{110}$ | 6 | 11.7 |

The goethite model as discussed by Hiemstra and van Riemsdijk (4) and Venema et al. (5) is used. In this model, two crystal faces are of importance, the 110 and the 021 face (10, 13). The ratio 110 : 021 for goethite A is about 9:1 (4, 5). For goethite B, this ratio is expected to be 8:2, based on interpretation of electron micrographs. This ratio may differ for goethites with a different geometry. In the following sections attention will be paid to the choice for the ratio in crystal faces. In the model only one plane is used that has the averaged site density of the 021 and 110 crystal face.

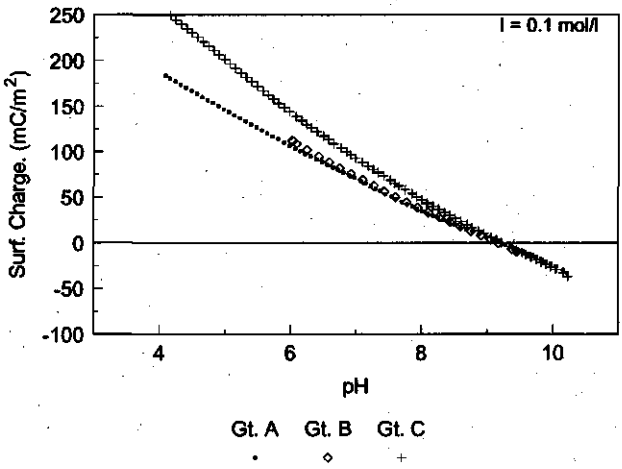


Fig. 1 Charging curves of the different metal (hydr)oxides for a background salt concentration ($NaNO_3$) of 0.1 mol/l.

## *Comparison of the data*

The specific surface area of the goethites was measured with $N_2$ adsorption yielding: 95 $m^2/g$ (Gt. A), 136 $m^2/g$ (Gt. B) and 27 $m^2/g$ (Gt. C).

In Fig. 1, the charging curves of the goethites are shown for a background salt concentration of 0.1 mol/l $NaNO_3$. The values of the PPZC were nearly equal for the different goethites, Goethite A and Goethite B (9.3), Goethite C (9.2). The PPZC values are in good accordance with values found before for Goethite (14, 15, 16, 17). It is striking that the two monodomainic goethites (Gt. A and Gt. B) have a similar charging behaviour. The surface of goethite C charges significantly higher than the other two goethites. This is in accordance with a relationship between the specific surface area of goethite and its experimental charging capacity at a fixed salt concentration found by Hiemstra et al. (7). In that study, a significantly higher surface charge density was found for the surface of metal (hydr)oxides with a lower specific surface area.

Cadmium adsorption isotherms are measured at pH 6 for all materials and at pH 7 for Goethite A and Goethite C only (Fig. 2). It should be noted that the data for all

goethites coincide quite well. It is stressed here that goethite C charges much higher than the other two goethites while the cadmium adsorption is nearly the same. The cadmium adsorption data are in accordance with data found in literature for Goethite (14, 15, 18, 19). It is interesting to see that the two monodomainic goethites (Gt. A and Gt. B) show the same cadmium adsorption at pH 6. The goethite with the short needles (Gt. B) is expected to have a relatively higher fraction of 021 face. In a previous study to cadmium adsorption on goethtite (5) a model is used in which high affinity sites for cadmium occur at the 021 face. This model predicts a higher cadmium adsorption for goethite B. Because the cadmium adsorption on the monodomainic goethites is the same, it is suggested that the ratio of the 110 and 021 face is not different for these two goethites (5).

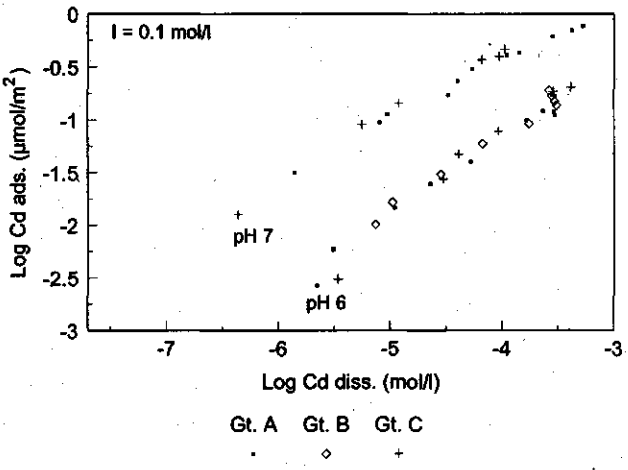


Fig. 2 Cadmium adsorption on the five iron (hydr)oxides at pH 6 and pH 7. The background salt concentration ($NaNO_3$) is 0.1 mol/l.

For the adsorption of phosphate on the different goethites, adsorption edges were measured (Fig. 3). The monodomainic goethites (Gt. A and Gt. B) have the same phosphate adsorption for low pH values (Fig. 3). For the higher pH values, goethite A shows a higher adsorption. This result may indicate that the site density, corresponding to the ratio [110 face : 021 face], is different for both monodomainic goethites. Compared to the other goethites, the large crystal goethite (Gt. C) shows a somewhat higher phosphate adsorption. So both the surface charging and the

phosphate adsorption of goethite C is higher than that of the other two goethites. The cadmium adsorption, however, is the same for all goethites.

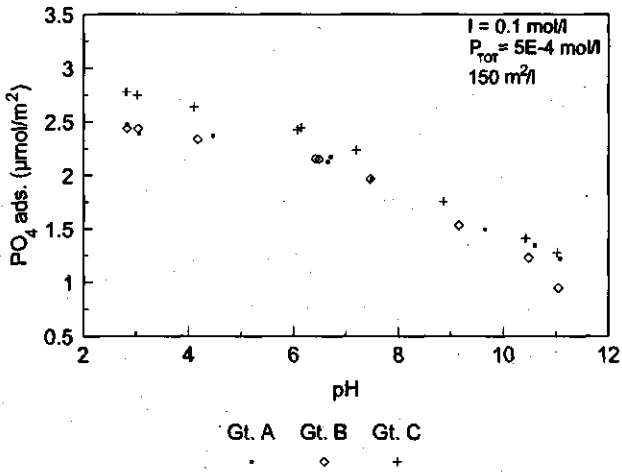


Fig. 3 Adsorption edges for phosphate adsorption on the three different goethites. The suspension density is 150 $m^2/l$, the initial phosphate concentration 5E-4 mol/l and the salt concnetration ($NaNO_3$) is 0.1 mol/l.

The phosphate data in literature can differ for (hydr)oxides that have a different shape or porosity (20, 21), especially for longer reaction times. The adsorption time in this study is limited to 1 day. Longer adsorption times may result in considerably higher phosphate surface loadings (22, 23). It is beyond the scope of this study to consider longer reaction times for phosphate adsorption.

## *Model descriptions of the data*

Goethite A.

The goethite with the long needle morphology has a surface area of 95 $m^2/g$. Its surface charges to about 180 $mC/m^2$ at pH 4 and a salt concentration of 0.1 mol/l (Fig. 1). In the model, the averaged value of log $K_H$ is reduced with 0.2 log $K$ unit to 9.3 so that the predicted PPZC and the experimental PPZC coincide.

The surface composition in terms of crystal faces of goethite A is according to former studies 90% 110 face and 10% 021 face (4, 5). The needles of goethite B have a composition with 80% 110 and 20% 021 face (5). The charging and adsorption

behaviour of these two different goethites, however, does not show a significant difference. It can therefore be concluded that both goethites must have the same surface compostition. For these two goethites, the choice for the surface composition with the highest amount of 021 face is the most logical. A lower amount of 021 face on the short needle crystals is not possible because of the crystal morphology. A higher amount of 021 face on the long needle crystals (goethite A), however, may exist because of imperfections or the existence of vicinal faces (13). In our model calculations, therefore, a model with 80% 110 face and 20% 021 face is used. According to the explanation above, this is the most logical choice. The choice for a surface composition with 90% 110 face and 10% 021 face for goehtite A, that was made before (5) is physically less realistic.

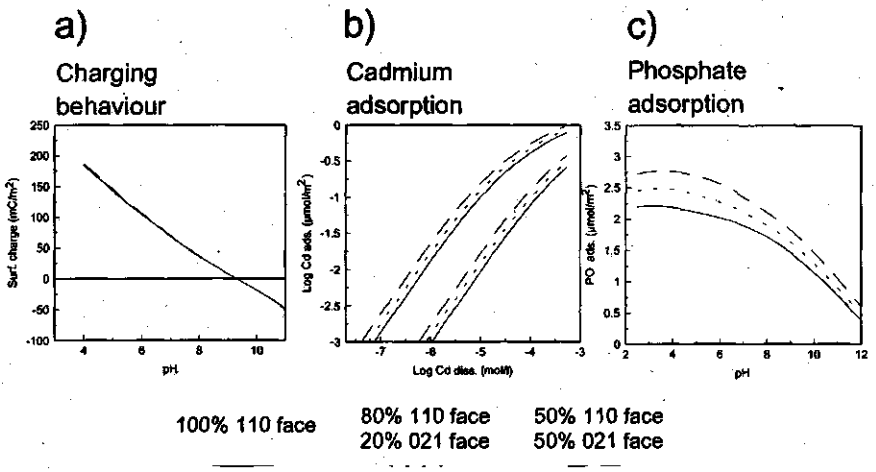


Fig. 4 The influence of the surface composition on the model description. The log $K$ values as shown in Table 4 are used. In the calculations, one face is used with an averaged site density of the goethite 110 face and 021 face (Table 1). The used compositions are: 100% 110 face: singly coordinated (3 sites/nm$^2$), triply coordinated (3 sites/nm$^2$) (solid lines), 80% 110 face, 20 % 021 face: singly coordinated (3.9 sites/nm$^2$), triply coordinated (2.4 sites/nm$^2$) (dashed lines), 50% 110 face, 50% 021 face: singly coordinated (5.25 sites/nm$^2$), triply coordinated (1.5 sites/nm$^2$) (striked lines).
With these surface compositions calculations are done at a background salt concentration of 0.1M $NaNO_3$ for the charging behaviour (a), cadmium adsorption (b) and phosphate adsorption at 0.5 mmol P./l and 150m$^2$ goethite/l

Before we will discuss the model descriptions, we will first investigate the influence of the surface composition on the model descriptions. To illustrate this influence, model calculations have been done with three different surface constitutions. For the

calculations, only one face is used with an averaged site density of the 110 and 021 face, three surface ratios of 110-021 are used; 100% 110 face, 80% 110 face - 20% 021 face and 50% 110 face - 50% 021 face. The site densities for the singly and triply coordinated surface groups in sites/nm$^2$ for these options are respectively: singly 3, triply 3, (100% 110 face), singly 3.9, triply 2.4 (80% 110 face), singly 5.25, triply 1.5 (50% 110 face). The calculations show that an increase in site density for the singly coordinated surface groups results in an increase of cat- and anion adsorption (Fig. 4).

For the calculations of this study, the charging behaviour is not very sensitive to small variations in the site density (Fig. 4a). The sensitivity of the adsorption of cadmium and phosphate to the site density follows directly from the chemical equilibria (eq. [3], eq. [4] and eq. [7]). The surface potential will hardly differ between the different goethites, so an increase in reactive surface groups ($FeOH^{-½}$) will directly result in an increase of the adsorption for both cadmium and phosphate.

The use of a surface composition that has the averaged site densities for 80% 110 face and 20% 021 face leads to one crystal face with the site densities shown in Table 2. For the description of the charging behaviour, an interface model with one Stern layer is used. The description of the data with this model is very good (Fig. 5a). The capacitance of the Stern layer (overall capacitance) for this description is 0.85 F/m$^2$.

Table 2 Model parameters for both goethite A and B. The overall capacitance is fitted on the charging behaviour. The log $K$ values are related to eq. [4] (log $K_H$) and eq. [5] (log $K_P$). The surface groups can be singly coordinated (FeOH) or triply coordinated ($Fe_3O$). The original crystal face for each surface group is indicated with their miller indices. The site densities used in the model are indicated.

| Overall capacitance of the interface (F/m$^2$) | | 0.85 | | | | | | |
|---|---|---|---|---|---|---|---|---|
| | | Surface Parameters | | | | | | |
| Group | $N_s$ | log $K_H$ | log $K_{Cd}$ | $f_{Cd}$ | log $K_P$ | $f_P$ | log $K_{PH}$ | $f_{PH}$ |
| $FeOH_{110/021}$ | 3.9 | 9.3 | 6.9 | 0.3 | 29.7 | 0.46 | 35.9 | 0.56 |
| $Fe_3O_{110}$ | 2.4 | 9.3 | ------ | ------ | ------ | ------ | ------ | ------ |

The adsorption of cadmium can be described reasonably with the monodentate surface complex (Fig. 5b). The slope of the adsorption isotherms, however is slightly too high. The scope of this study is to compare the adsorption behaviour of different metal (hydr)oxides. This is the reason why in this study, no high affinity or bidentate surface complexes are used as in a previous study (5). Using a detailed model makes a comparison between the different metal (hydr)oxides more complicated.

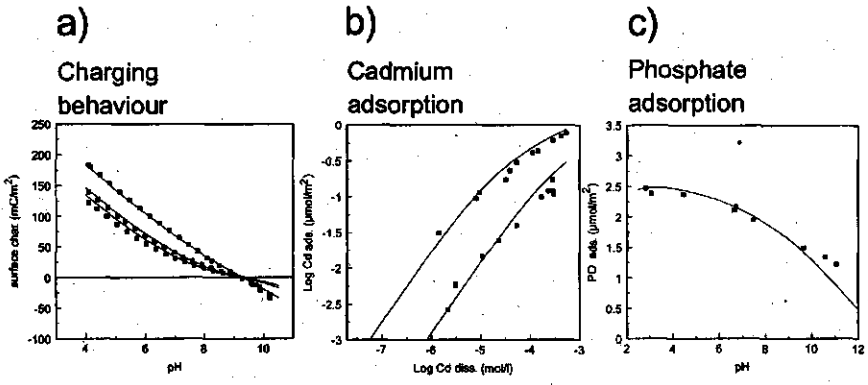


Fig. 5 Model description of the data for goethite A, the model calculations are represented by the lines. The charging behaviour (a) is shown for three salt concentrations, 0.005, 0.01 and 0.1 mol/l $NaNO_3$. The cadmium adsorption (b) is measured at pH 6 and 7 at a salt concentration of 0.1 mol/l $NaNO_3$. Phosphate adsorption (c) was measured with a total amount of phosphate of 0.000495 mol/l and a suspension density of 150 $m^2$/l.

For the description of the phosphate data, the parameters for the phosphate surface complexes as used by Hiemstra and van Riemsdijk (4) are adapted slightly. The binding constants for phosphate adsorption are the same, however, if the adsorption equillibria are expressed as:

$$2\ FeOH_2^{+½} + PO_4^{-3} \leftrightarrows Fe_2O_2{}^pPO_2{}^q + 2\ H_2O \qquad K_{P'} \qquad [9]$$

$$2\ FeOH_2^{+½} + PO_4^{-3} + H^+ \leftrightarrows Fe_2O_2{}^pPOOH^q + 2\ H_2O \qquad K_{PH'} \qquad [10]$$

The affinities for phosphate surface complexation of eq. [3] and eq. [4] are now related to the phosphate affinities of eq. [9] and eq. [10] according to:

$$\mathbf{Log}K_{\mathbf{P}} = \mathbf{Log}K_{\mathbf{P}'} + 2\ \mathbf{Log}K_{\mathbf{H}} \qquad [11]$$

$$\mathbf{Log}K_{\mathbf{PH}} = \mathbf{Log}K_{\mathbf{PH}'} + 2\ \mathbf{Log}K_{H} \qquad [12]$$

So the phosphate affinity for the two goethites is the same, in case the value of log $K_H$ shifts 0.1 log $K$ units, the value of log $K_P$ shifts 0.2 log $K$ units.

The $f$ factors are slightly lower in comparison with the values used by Hiemstra and van Riemsdijk resulting in a lower pH dependency. This difference in $f$ may be due to the different capacitance of the Stern layer. The description of the phosphate data with these parameters is very good (Fig. 5c).

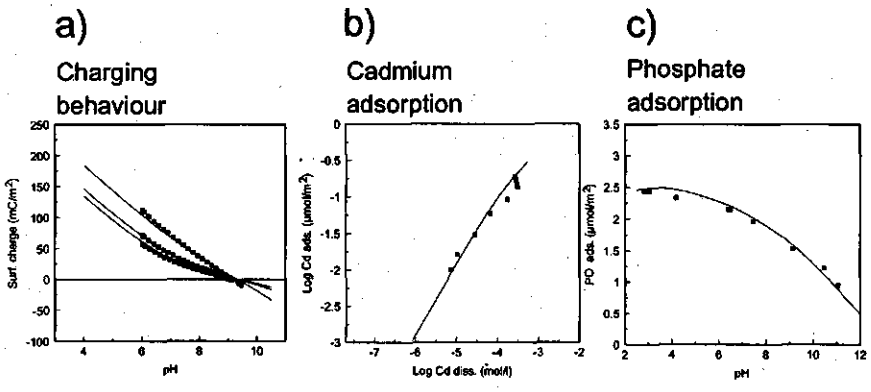


Fig. 6 Model description of the data for goethite B, the model calculations are done with the same parameters as used for goethite A and they are represented by the lines. The charging behaviour (a) is shown for three salt concentrations, 0.005, 0.01 and 0.1 mol/l $NaNO_3$. The cadmium adsorption (b) is measured at pH 6 at a salt concentration of 0.1 mol/l $NaNO_3$. Phosphate adsorption (c) was measured with a total amount of phosphate of 0.000495 mol/l and a suspension density of 150 $m^2$/l.

Goethite B.

As discussed in the previous section, the chemical behaviour of goethite A and goethite B do not show significant difference. The same model parameters are

therefore used for these two goethites (see Table 2). The model descriptions are shown in Fig. 6, the overall description of the data is very good. This confirms the idea that the overall surface composition of both goethites is the same. A similar result was found before for the study of cadmium adsorption (5).

Goethite C.
The goethite with the large crystals has a much lower surface area than the other two goethites (27 $m^2/g$). The surface charges higher than the surface charge of the other goethites (Fig. 1). This observation is in accordance with the relationship between the slope of the charging curve and the surface area found by Hiemstra et al. (7). Another difference between the behaviour of the large crystal and the mono-domainic goethites is the large phosphate adsorption at low pH in comparison to the other goethites (Fig. 3). The PPZC of the goethite is 9.2, which is slightly lower than the PPZC of the other two goethites. The values of log $K_H$ are therefore adapted to a value of 9.2.

A large H-charging capacity of a mineral may be explained in terms of a high surface roughness. A high surface roughness means that adsorbed pair forming ions can partly penetrate the surface so that they in an extreme case would occupy the same electrostatic plane as adsorbing protons. This implies that the distance between the outer plane, in which the pair formers are placed (d-plane), and the surface plane, for the protons (0-plane), decreases with increasing surface roughness (24, 25). A smaller distance between the 0-plane and the d-plane results in a higher Stern layer capacitance.

In order to understand the influence of the capacitance on the model descriptions, three calculations have been done with three different capacitances (Fig. 7). The outer layer capacitance ($C_2$) is fixed to the value of 5 $F/m^2$ for the calculations. The predicted surface charge increases with increasing capacitance (Fig. 7a). Both the adsorbed amount of cadmium and phosphate, however, decreases with increasing capacitance. This influence of the increase of the Stern layer capacitance on the adsorption is mainly due to a change in the potential profile of the interface. The change in the potential profile for a positively charged surface is schematically shown in fig. 8. The surface potential ($\psi_0$) does almost not change with changing

capacitance. The potential in the Stern layer ($\psi_1$), however, increases with increasing Stern layer capacitance.

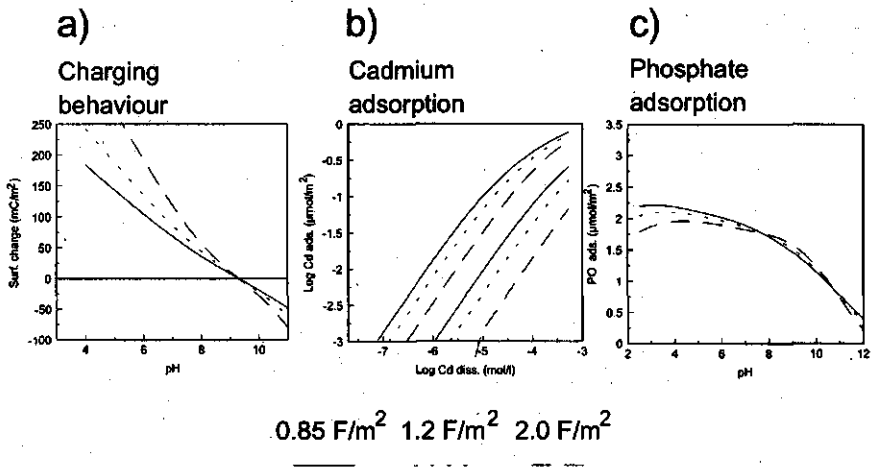


Fig. 7 The influence of the capacitance on the charging behaviour (a), cadmium adsorption at pH 6 and 7 (b) and phosphate adsorption (c) for the model prediction. All calculations are done with a background salt concentration ( $NaNO_3$) of 0.1 mol/l and an outer layer capacitance ($C_2$) of 5 F/m$^2$. For phosphate, the suspension density is 150 m$^2$/l at a phosphate concentration of 0.5 mmol/l.

The increase in Stern layer potential results in an increasing repulsion of cadmium ions and attraction of phosphate ions. So for cadmium, both the electrostatic effect and the effect on the surface speciation cause a decrease of the adsorption. For cadmium adsorption, the electrostatic effect is the most important effect. The overall effect of an increase in the capacitance will therefore result in a decrease of cadmium adsorption (Fig. 7b).

Because of the high adsorption of negative phosphate ions at low pH values, the overall surface charge becomes negative. Therefore, for low pH values, the electrostatic effect of a change in the capacitance for phosphate is similar to that for cadmium. In Fig. 7c is shown that for pH values between 8 and 10, the effect of the capacitance on the adsorption is inverted. This is caused by a decrease in the phosphate adsorption so that the overall surface charge becomes positive again. For the pH values above the PZC, the surface charge is always negative so that the influence of the capacitance is similar to that for the low pH values again. Summarized it can be concluded that the effect of an increasing inner layer capacitance on the

adsorption of an ion is negative in case the ion charge and the surface charge have the same sign.

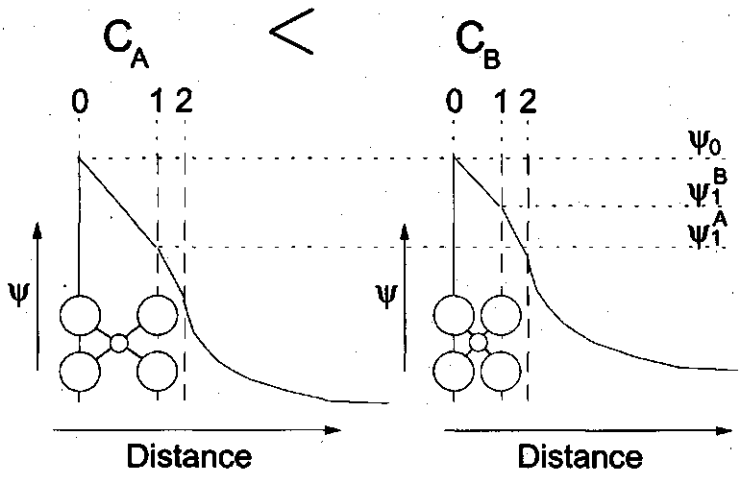


Fig. 8 The influence on the capacitance on the potential profile in the interface of an (hydr)oxide. The value of $C_A$ is smaller than the value of $C_B$ so the thickness of the inner charge free Stern layer for $C_A$ is larger. The decrease of the potential with the distance is equal for both capacitances. A thicker Stern layer results therefore in a larger decrease of the potential so that the value of $\psi_{1,A}$ is lower than the value of $\psi_{1,B}$.

A good description of the charging behaviour of goethite C is obtained with a Stern layer capacitance of 1.2 F/m$^2$. The increase of the Stern layer capacitance, however, will result in an decrease of the predicted cadmium adsorption (Fig. 7b). So the model would predict a lower cadmium adsorption for goethite C in comparison to goethite A, which is not in accordance with the data. Also the higher capacitance does not explain the higher phosphate adsorption at low pH for goethite C. The model gives a correct description if a higher site density is assumed (Fig. 4c).

This may imply that the ratio 110:021 is different in comparison with the other goethites. Such an option seems to be plausible for a crystal on which many imperfections occur. On this goethite, other crystal faces may also occur so that different site densities can occur. In Table 3, the model parameters that are used for the description of the data are shown.

The site density that is used for this goethite is 7.4 sites/nm$^2$. This site density, combined with the ratio singly:triply coordinated surface groups can not be explained with only the 110 and 021 crystal face. The reason for the choice for these model parameters will be discussed in the paragraph for the phosphate adsorption.

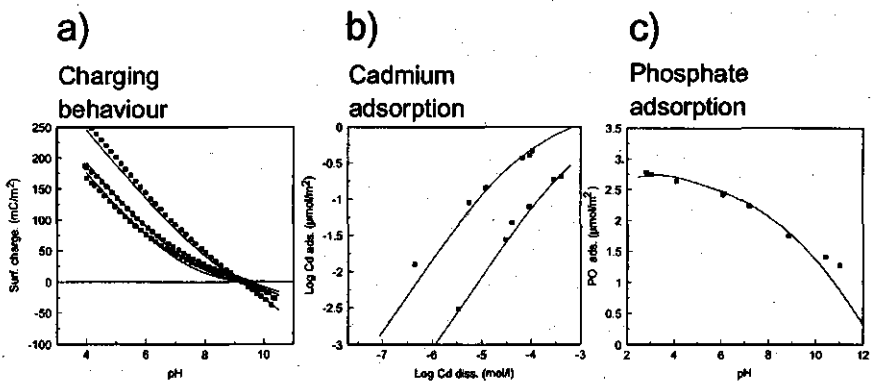


Fig. 9 Model description of the data for goethite C, the model calculations are represented by the lines. The charging behaviour (a) is shown for three salt concentrations, 0.005, 0.01 and 0.1 mol/l $NaNO_3$. The cadmium adsorption (b) is measured at pH 6 and 7 at a salt concentration of 0.1 mol/l $NaNO_3$. Phosphate adsorption (c) was measured with a total amount of phosphate of 0.000495 mol/l and a suspension density of 150 m$^2$/l.

The higher site density compensates the effect of the higher Stern layer capacitance on the adsorption of cadmium. The predicted level of cadmium adsorption remains therefore constant using the same log $K_{Cd}$ and $f$ as for goethite A and B. The model description is in good accordance with the data (Fig. 9b).

For phosphate adsorption, a higher capacitance causes just a slight decrease in comparison to the model parameters for goethite A and B. The increasing site density therefore results in a much higher phosphate adsorption which is in good accordance with the data (Fig. 9c). The phosphate data cannot be described with a model in which the 021 face is more important (see Fig. 4c). If the 021 face is more important, then the amount of singly coordinated surface groups would increase while

the amount of triply coordinated surface groups would decrease. For a proper description of the phosphate adsorption, however, the ratio singly: triply coordinated surface groups can not be altered too much.

Table 3 Model parameters for goethite C. The overall capacitance is fitted on the charging curves. The log $K$ values are related to eq. [4] (log $K_H$) and eq. [5] (log $K_P$). The surface groups can be singly coordinated (FeOH) or triply coordinated ($Fe_3O$). The original crystal face for each surface group is indicated with their miller indices. The site densities are the site densities, used in the model.

| Overall capacitance of the interface ($F/m^2$) | | | | 1.05 | | | | |
|---|---|---|---|---|---|---|---|---|
| | Surface Parameters | | | | | | | |
| Group | $N_s$ | log $K_H$ | log $K_{Cd}$ | $f_{Cd}$ | log $K_P$ | $f_P$ | log $K_{PH}$ | $f_{PH}$ |
| $FeOH_{110/021}$ | 4.1 | 9.2 | 6.9 | 0.3 | 29.5 | 0.48 | 35.7 | 0.58 |
| $Fe_3O_{100}$ | 3.4 | 9.2 | ------ | ------ | ------ | ------ | ------ | ------ |

The phosphate affinities used are in good accordance with the affinities of the monodomainic goethites. For the calculations, the same phosphate affinity (if adapted with 2 $\Delta$ log $K_H$) and a slightly higher $f$-factor (more inner sphere) is used.

## Results and discussion for metal (hydr)oxides with a different morphology and crystal structure

In the previous sections, the influence of the model parameters on the description is investigated. For goethite it is possible to choose model parameters that are in accordance with the crystal structure and morphology. For hematite and lepidocrocite the crystal morphology is not well known. This implies that for these two materials, less information is available about the surface composition in terms of reactive sites. In this section, a first approach is made to model the chemical behaviour of hematite and lepidocrocite.

### *Crystal structure and morphology*

Lepidocrocite

The lepidocrocite (Lepi.) that is used in this study is probably porous (1). The morphology of lepidocrocite is not well known because the crystals are not well

defined. Three crystal faces are probably dominant on lepidocrocite: the 010, the 001 and the 100 face. Based on interpretation of electron micrographs, the lepidocrocite of this study has a ratio of the crystal faces 010:001:100 of about 4:4:1 (1) in case of monodomainic crystals.

It was found before that the description of the charging behaviour of lepidocrocite was not improved if more planes were used in the model (1). Therefore, we will use for lepidocrocite only one plane with an averaged site density of the reactive singly and triply coordinated surface groups. The values used to calculate these averages are shown in Table 4.

Table 4 The morphology and surface composition for lepidocrocite (1) that form the basis for the model used in this study. The singly coordinated surface group $FeOH^{*}_{100}$ has two internal hydrogen bridges and will therefore behave like a triply coordinated surface group. For this study, the $FeOH^{*}_{100}$ and the $Fe_3O$ surface group are not considered separately but are treated as one type of surface group. For the 001 face, both the two types of singly coordinated and the two types of triply coordinated surface groups are also treated as one type of singly coordinated surface group and triply coordinated surface group respectively.

| 100 Face (20%) | | | 001 Face (80%) | | |
|---|---|---|---|---|---|
| Surface-group | $N_s$ (sites/nm$^2$) | Log $K_H$ | Surface group | $N_s$ (sites/nm$^2$) | Log $K_H$ |
| $FeOH_{100}$ | 4.1 | 9.7 | $FeOH_{001}$ | 2.5 | 6.4 |
| $FeOH^{*}_{100}$ | 8.2 | 12.0 | $Fe_3O_{001}$ | 2.5 | 6.7 |
| $Fe_3O_{100}$ | 4.1 | 4.4 | $FeOH_{00\bar{1}}$ | 2.5 | 9.7 |
| | | | $Fe_3O_{00\bar{1}}$ | 2.5 | 10.1 |

The 010 face has only doubly coordinated surface groups and it is therefore considered to be inert. For an imperfect crystal it is likely that the 010 crystal face has imperfections so that singly and triply coordinated surface groups will arise at this crystal face. In the study of Venema et al. (1) it was found that a model with only the 001 and 100 face could describe the charging behaviour very well. In this study, therefore, a model is used with only the 001 and 100 face in a ratio 4:1.

The averaged log $K_H$ value for all singly and triply coordinated surface groups at the 001 face and $00\bar{1}$ face is 8.2, which is the log $K_H$ that is used for all surface

groups at this surface. At the 100 face, two types of singly coordinated surface groups occur. The surface groups indicated as $FeOH^{"}_{100}$ have two internal hydrogen bonds and will therefore behave as triply coordinated surface groups.

Hematite

For the hematite (Hema.), used in this study, the 001 face is probably a dominant crystal face because 90% of the crystals have a platy shape (9). The composition of the rims of the platy crystals is unknown. We chose the 110 face as a representative crystal face here. The ratio 110:001 in the model is 6:4. In Table 5, the surface composition in terms of the reactive surface sites is shown (1). This surface composition forms the basis for the model.

Table 5 The crystal morphology and site densities for hematite (1) that are the basis for the model of this study. For the 001 face, only the dominant singly coordinated surface group is considered in the model.

| 110 Face (60%) | | | (imperfect) 001 Face (40%) | | |
|---|---|---|---|---|---|
| Surface-group | $N_s$ (sites/nm$^2$) | Log $K_H$ | Surface group | $N_s$ (sites/nm$^2$) | Log $K_H$ |
| $FeOH_{110}$ | 4.1 | 7.7 | $FeOH_{001}$ | 2.5 | 12.1 |
| $Fe_3O_{110}$ | 8.2 | 8.2 | $FeOH^{"}_{001}$ | 2.5 | 7.7 |

The 001 face is a crystal face with only doubly coordinated surface groups. Venema et al. (1) found that the charging behaviour could be described only if it was assumed that the 001 face had imperfections. From the crystal structure it could be concluded that singly coordinated surface groups probably exist at the imperfect 001 face. For the singly coordinated groups, the site density used is 4.5 sites/nm$^2$. The 110 face has an overall site density of 15 sites/nm$^2$. At the crystal face singly, doubly and triply coordinated surface groups occur in a ratio 1:1:1.

For a good description of the charging behaviour, two separate planes were needed in the model (5). These two planes will therefore be used in this study too. In the calculations, the 001 face is assumed to have only singly coordinated surface groups with a high log $K_H$ (12.0) as reactive groups. At the 110 face, the log $K_H$ values of the singly and triply coordinated surface groups are averaged. The average value of log $K_H$ is 7.95 which is the value used for the surface groups at this crystal face.

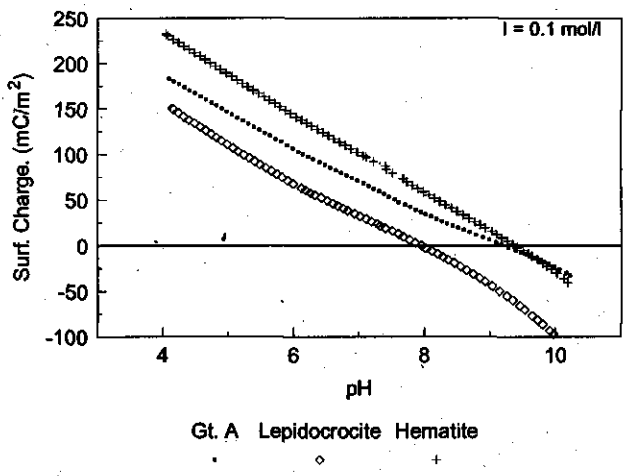


Fig.10 Charging curves of three different iron (hydr)oxides for a background salt ($NaNO_3$) of 0.1 mol/l.

## *Comparison of the data*

The charging behaviour of lepidocrocite and hematite differ from the charging behaviour of goethite A (Fig. 10). Lepidocrocite has a much lower PPZC than the other oxides and the slope of the charging curve is similar to that of hematite. The experimental PPZC for lepidocrocite is in accordance with results of Madrid and Diaz Barrientos. The charging behaviour shows assymmetry with respect to the PPZC, this assymmetry was also found by Madrid and Diaz-Barrientos (26). This assymmetry is not predicted with the new MUSIC model (1). The surface charges found in this study, are much higher than the values found by Madrid and Diaz Barrientos. The hematite used in this study has a PPZC that is similar to the PPZC of goethite A, but the surface charge is much higher (Fig. 10). The experimental PPZC value is in accordance with values found before (27).

For cadmium, the adsorption behaviour of lepidocrocite differs slightly from the adsorption on goethite (Fig. 11). For pH 7 the adsorption is higher while for pH 6 the adsorption level is about the same, this means that the pH dpendency is different. For hematite, the cadmium adsorption is significantly lower for both pH 6 and pH 7 in comparison to goethite. These experimental data are in reasonable accordance with cadmium adsorption data from literature for hematite (28, 29).

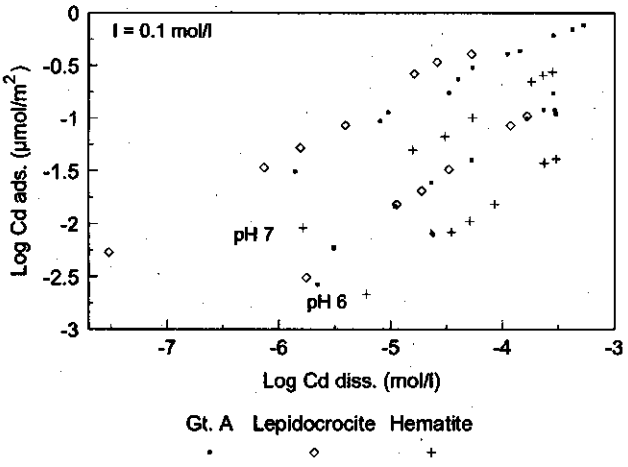


Fig. 11 Cadmium adsorption isotherms at a background salt concentration of 0.1 mol/l ($NaNO_3$) and two different pH values for goethite A, lepidocrocite and hematite.

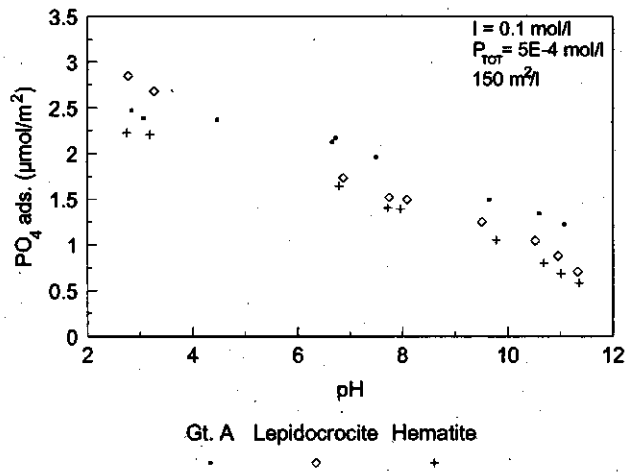


Fig. 12 Phosphate adsorption isotherms for backround salt concentration 0.1 mol/l ($NaNO_3$), a suspension density of 150 $m^2$/l and 0.5 mmol/l P.

For lepidocrocite, the phosphate adsorption per $m^2$ is considerably higher than values found by Madrid and Arambarri (30). For low pH, the phosphate adsorption

for lepidocrocite is higher than for goethite (Fig. 12). The lepidocrocite in this study has both a higher surface charge and a higher phosphate adsorption in comparison to the lepidocrocite data from literature. This result is comparable with the higher charging and phosphate adsorption that was found for goethite C in comparison to goethite A. Like for these two goethites, the lepidocrocite of this study may have a higher surface roughness in comparison to the lepidocrocite from literature.
Hematite shows a low phosphate adsorption in comparison to goethite A. This is peculiar, especially considering the high surface charging of hematite (Fig. 10). The high surface charging can be explained with a high surface roughness (high Stern layer capacitace, see Fig. 8) in combination with a relatively low surface site density of singly coordinated surface groups (Fig. 5).

### *Model descriptions of the data*

Lepidocrocite

It was found before (1) that the charging behaviour could be described well if about 40% of the surface is inert (010 face) while the overall capacitance is high. With this option, however, the high phosphate adsorption at low pH (Fig. 12) can not be described. The same charging curve could be obtained without 010 face and a much lower capacitance. In this case, the overall site density for the reactive sites (singly + triply) is much higher. Using a surface composition with 20% 001 face and 80% 100 face leads to an average surface site density of 11.2 sites/nm$^2$ of which 72% are sites of the 001 face and 28% of the 100 face (see Table 6). A higher site density, however, is needed for a good description of the data. This may imply that other crystal faces are present. For the description of the phosphate data, a site density of 12.5 leads to a good description for low pH values. This site density would correspond with a model for which the surface would consist for about 40% of 001 face. The surface site composition for the model, however, does not correspond with this crystal face composition. A more detailed description of the phosphate model will follow later.

The description of the charging behaviour with the model is in reasonable accordance with the data (Fig. 13a). However, the assymmetry of the charging behaviour is not described well with the model. This assymmetry may be due to experimental errors. The only way to describe this assymmetry in the charging behaviour is to assume that the doubly coordinated surface groups are reactive (1). The proton affi-

nity for the first protonation step ($Fe_2O^{-1} + H^+ \leftrightarrows Fe_2OH^0$) of these groups, however, must in this case be much lower than the predicted value with the refined MUSIC model. Another option to describe the assymmetry is the use of assymetric pair formers. The Stern layer capacitance for this model description is 0.97 F/m$^2$.

Table 6 Model parameters for lepidocrocite. The overall capacitance is fitted on the charging curves. The log $K$ values are related to eq. [4] (log $K_H$) and eq. [5] (log $K_P$). At The surface groups can be singly coordinated (FeOH) or triply coordinated ($Fe_3O$). The original crystal face for each surface group is indicated with their miller indices. The site densities are the site densities, used in the model.

| Overall capacitance of the interface (F/m$^2$) | 0.97 |
|---|---|

Surface Parameters

| Group | $N_s$ | log $K_H$ | log $K_{Cd}$ | $f_{Cd}$ | log $K_P$ | $f_P$ | log $K_{PH}$ | $f_{PH}$ |
|---|---|---|---|---|---|---|---|---|
| $FeOH_{001/00i}$ | 4.50 | 8.2 | 6.1 | 0.5 | 27.4 | 0.46 | 33.8 | 0.56 |
| $Fe_3O_{001/00i}$ | 4.50 | 8.2 | ------ | ------ | ------ | ------ | ------ | ------ |
| $FeOH_{100}$ | 0.88 | 12.0 | 9.6 | 0.5 | 27.5[a] | 0.26 | ------ | ------ |
| $\{Fe_3O\}''_{100}$[b] | 2.62 | 5.8 | ------ | ------ | ------ | ------ | ------ | ------ |

[a] At this surface component only phosphate monodentate groups can exist
[b] This type of surface groups consists of singly coordinated surface groups with two internal hydrogen bridges (66.67%) and triply coordinated surface groups (33.33%).

The cadmium adsorption can be described well (Fig. 13b), if a higher fraction of the charge of adsorbed cadmium is attributed to the 0-plane (higher $f$-factor) in comparison to the model for goethite. This higher $f$-factor results in a higher pH dependency. The experimental slope of the adsorption isotherm is higher than the predicted slope. This slope indicates that surface heterogeneity is important for cadmium adsorption. The introduction of the high affinity $FeOH_{100}$ cadmium complex can not explain the low experimental slope.

The log $K$ values for phosphate adsorption for the singly coordinated surface groups at the 001 face are consistent with the values found for goethite A. Also the $f$-factors for lepidocrocite are in good accordance with the $f$-factors for Goethite A.

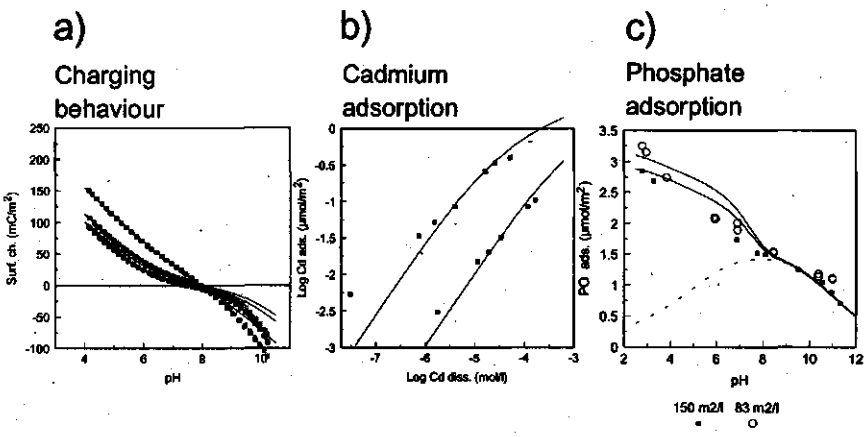


Fig. 13 Model description of the data for lepidocrocite, the model calculations are represented by the lines. The charging behaviour (a) is shown for three salt concentrations; 0.005, 0.01 and 0.1 mol/l $NaNO_3$. The cadmium adsorption (b) is measured at pH 6 and 7 at a salt concentration of 0.1 mol/l $NaNO_3$. Phosphate adsorption (c) was measured with a total amount of phosphate of 0.000495 mol/l and suspension densities of 83 $m^2$/l and 150 $m^2$/l, the dashed line represents the adsorption of the monodentate surface complex.

The phosphate data show a high adsorption at high pH values for both suspension densities (Fig. 10c). This can be described only with a high affinity surface complex. In the model, the singly coordinated surface groups at the 100 face are assumed to form these high affinity complexes. These singly coordinated surface groups are not positioned in pairs at the surface so that they cannot form bidentate complexes. Therefore a monodentate complex is used for these groups, according to:

$$FeOH^{-½} + PO_4^{-3} + H^+ \approx FeO\,{}^{p}PO_3^{q} + H_2O \qquad K_P \qquad [13]$$

This monodentate has an extremely high affinity compared to the monodentate phosphate surface complex used by Hiemstra and vanRiemsdijk (4). The use of a bidentate complex for this group is not only physically not desirable but it would also lead to a worse description. The values for $f$ for the different phosphate complexes are in reasonable accordance with values for respectively mono and bidentate surface complexes. The overall description of the phosphate data is reasonable with the current assumptions (Fig. 13c). The bend in the model description is caused by

the fact that the monodentate phosphate complex (dashed lines) becomes dominant for high pH values.

Table 7 Model parameters for hematite. The overall capacitance is calculated as a function of the log $K$ values are related to eq. [4] (log $K_H$) and eq. [5] (log $K_P$)

| Overall capacitance of the interface ($F/m^2$) | | | | | 1.20 | | | |
|---|---|---|---|---|---|---|---|---|
| Surface Parameters 110 face (60%) | | | | | | | | |
| Group | $N_s$ | log $K_H$ | log $K_{Cd}$ | $f_{Cd}$ | log $K_P$ | $f_P$ | log $K_{PH}$ | $f_{PH}$ |
| FeOH | 5.0 | 7.95 | 4.9 | 0.3 | 27.0 | 0.54 | 33.2 | 0.64 |
| $Fe_3O$ | 5.0 | 7.95 | ------ | ------ | ------ | ------ | ------ | ------ |
| Surface Parameters inperfect 001 face (40%) | | | | | | | | |
| Group | $N_s$ | log $K_H$ | log $K_{Cd}$ | $f_{Cd}$ | log $K_P$ | $f_P$ | log $K_{PH}$ | $f_{PH}$ |
| FeOH | 4.0 | 12.1 | 9.1 | 0.3 | 35.3 | 0.54 | 41.5 | 0.64 |

## Hematite

It is difficult to describe the hematite titration curves without the assumption of strong pair formers (in this case log $K_{pf} = 0$) or the assumption of two different crystal faces. The latter option seems physically more attractive than the use of strong pair formers. In this study therefore the model with two different crystal faces is used. It was discussed before that the hematite that is used in this study has a cilindrical shape. The cilinders of the hematite have a height that is of the same order of magnitude as the diameter.

For a good description of the data, the value of log $K_{Cd}$ for the singly coordinated surface groups at the 110 face is 2 log $K$ units lower than the value of log $K_{Cd}$ for goethite A. The values of log $K_H$ differ 1.35 log $K$ units for the same groups. The differences in log $K_{Cd}$ and log $K_H$ for the singly coordinated surface groups of the 001 face in relation to goethite A are 2.2 and 2.8 respectively. So the values of log $K_{Cd}$ for hematite are relatively low in comparison to goethite A. The cadmium data are described well with the model parameters shown in Table 4 (Fig. 14b).

The log $K$ values for phosphate on hematite are slightly in better accordance with the log $K$ for phosphate on goethite A. The value for the $f$-factor is slightly higher than the value used for goethite A. In the model, both planes have a higher density of singly coordinated surface groups than in the goethite A model. The predicted phosphate adsorption, however, is slightly lower than for goethite which is in accordance with the data for both suspension densities (Fig. 14c). This lower phosphate adsorption is caused by the higher Stern layer capacitance (Fig. 8c).

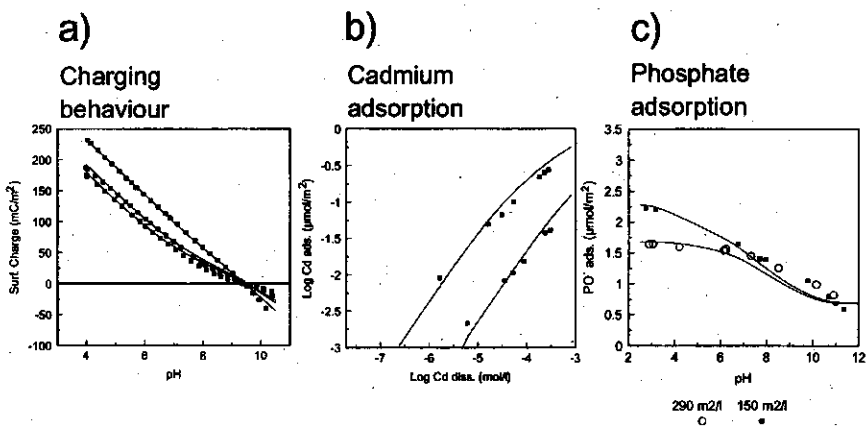


Fig. 14 Model description of the data for hematite, the model calculations are represented by the lines. The charging behaviour (a) is shown for three salt concentrations, 0.005, 0.01 and 0.1 mol/l $NaNO_3$. The cadmium adsorption (b) is measured at pH 6 and 7 at a salt concentration of 0.1 mol/l $NaNO_3$. Phosphate adsorption (c) was measured with a total amount of phosphate of 0.000495 mol/l and suspension densities of 150 $m^2/l$ and 290 $m^2/l$.

## Conclusions

The charging behaviour of the different goethites can be described well with simplified models that are consistent with the parameters found by Venema et al. (1). For the imperfect goethite (gt. C), a higher capacitance is needed for the description of the higher surface charge.

A higher Stern layer capacitance in the model leads to a higher predicted surface charge at constant pH and salt concentration. For the description of the adsorption of phosphate and cadmium, however, a higher Stern layer capacitance leads to a lower predicted adsorption. Especially the description of the adsorption of cadmium

is very sensitive for the chosen Stern layer capacitance.

The adsorption of phosphate and cadmium on the different goethites can be described well with the simplified models. For goethite with an imperfect surface, a higher site density is needed to describe the higher phosphate adsorption. The predicted cadmium adsorption with these model parameters is the same as the predicted adsorption for the other two goethites. So, for cadmium, the effect of a higher site density is compensated by the effect of the higher capacitance. This is in good accordance with the data.

For the description of the chemical behaviour of hematite and lepidocrocite, more assumptions have to be made because the crystal morphologies are not well known. For lepidocrocite, a monodentate surface complex is needed for a reasonable description of the phosphate data. For hematite, a high Stern layer capacitance is needed, combined with a high site density.

According to the most probable crystal morphology for both hematite and lepidocrocite, crystal faces with only inert surface groups are dominant. It has to be assumed that these inert crystal faces have imperfections and are therefore not chemically inert.

## References


1. Venema, P., Hiemstra, T., van Riemsdijk, W.H., *Geochimica et Cosmochimica Acta*, submitted
2. Hiemstra, T., Venema, P., and van Riemsdijk, W.H., *J. Colloid Interface Sci.* **184**, in press
3. Barrow, N.J., Brummer, G.W., and Strauss, R., Effects of Surface Heterogeneity on Ion Adsorption by Metal Oxides and by Soils, *Langmuir*, **9**(10), 2606-2611, (1993)
4. Hiemstra, T, and van Riemsdijk, W.H., A surface structural approach to ion adsorption: The charge distribution (CD) model, *J. Colloid Interface Sci.* **179**, 488-508, (1996)
5. Venema, P., Hiemstra, T., vanRiemsdijk, W.H., Multi site adsorption of cadmium on goethite, *J. Colloid Interface Sci.* Submitted 1996
6. Hiemstra, T., Riemsdijk, W.H. van, and Bolt, G.H., Multisite Proton Adsorption Modeling at the Solid/Solution Interface of (Hydr)oxide: A New Approach, I. Model Description and Evaluation of Intrinsic Reaction Constants, *J. Colloid Interface Sci.* **133**, 91-104 (1989)
7. Hiemstra, T., de Wit, J.C.M., and van Riemsdijk, W.H., Multisite Proton Adsorption Modeling at the Solid/Solution Interface of (Hydr)oxide: A New Approach, II. Application to Various Important (Hydr)oxides, *J. Colloid Interface Sci.* **133**, 105-117 (1989)
8. Parfitt, R.L., Atkinson, R.J., and Smart, R.St.C., The mechanism of phosphate fixation by iron oxides, *Soil Sci. Soc. Am. Proc.*, **39**, 837-841 (1975)
9. Weidler, P.G., Oberflächen und Porositäten synthetischer Eisenoxide, PhD thesis T.U.M, Munich, 1995
10. Schwertmann,U., and Cornell,R.M., "Iron Oxides in the Laboratory. Preparation and Characterization", Chap.5, VCH verlag, Weinheim, Germany, 1991.
11. Morup, S., Madsen, M.B., and Franck, J., A new interpretation of Moessbauer spectra of microcrystalline goethite: super-ferromagnetic or super-spin-glass behavior?, *J. Magnet. Mag. Mat.* **40**, 163-174 (1983)
12. Kinniburgh, D.G., Milne, C.J., Venema, P., Design and construction of a Personal-Computer based automatic titrator, *Soil Sci. Soc. Am. J.* **59** (2), 417-422 (1995)
13. Weidler, P.G., Schwinn, T., Gaub, H.E., Vicinal faces on synthetic goethite observed by atomic force microscopy, *Clays Clay Miner.*, **44**, (in press), (1996)
14. Johnson Bruce B., Effect of pH, Temperature, and Concentration on the Adsorption of Cadmium on Goethite, *Environ. Sci. Technol.*, **24**(1), 112-118, (1990)
15. Spark, K.M., Johnson, B.B., Wells, J.D., Characterizing heavy metal adsorption on oxides and oxyhydroxides, *Europ. J. Soil Sci.*, **46**, 621-631, (1995)
16. Mesuere, K, and Fish, W, Chromate and oxalate adsorption on goethite 1. Calibration of Surface complexation models, *Environ. Sci. Technol.* **26**, 2357-2370 (1992)
17. Lumdson, L.G., and Evans, L.J., Surface complexation model parameters for goethite (α-FeOOH), *J. Colloid Interface Sci.* **164**, 119-125 (1994)
18. Gunneriusson Lars, Composition and stability of Cd(II)-Chloro and -Hydroxo Complexes at the Goethite (α-FeOOH)/Water interface, *J. Colloid Interface Sci.* **163**, 484-492, (1994)
19. Hayes K.F., Leckie J.O., Modeling Ionic Strength Effects on Cation Adsorption at Hydrous Oxide/Solution Interfaces, *J. Colloid Interface Sci.* **115**(2), 564-572,(1987)
20. Colombo C., Barron V., and Torrent J., Phosphate adsorption and desorption in relation to morphology and crystal properties of synthetic hematites, *Geoch. et cosmoch. acta*, **58**(4), 1261-1269, (1993)

21. Torrent J., Schwertmann U., and Barron V., Phosphate sorption by natural hematites, *Europ. J. Soil Sci.*, 45, 45-51, (1994)
22. Cabrera, F., De Arambarri, P., Madrid, L., and Toca, C. G., Desorption of phosphate from iron oxides in relation to equilibrium pH and porosity, *Geoderma*, **26**(3), 203-216, (1981)
23. Torrent, J., Barron, V., and Schwertmann, U., Phosphate Adsorption and Desorption by Goethites Differing in Crystal Morfology, *Soil Sci. Soc. Am. J.*, **54**, 1007-1012, (1990)
24. Yates '75 (PhD thesis)
25. Bowden, J.W., Posner, A.M., Quirk, J.P., Ionic Adsorption on Variable charge Mineral Surfaces. Theoretical-Charge Development and Titration Curves, *Aust. J. Soil Res.*, **15**, 121-136, (1977)
26. Madrid, L., and Diaz-Barrientos, E.D., Description of mixed materials with variable and permanent surface charge by a mathematical model. 1. Theory. 2. Application to mixtures of lepidocrocite and monmorillonite, *J. Soil Sci.*, **39**, 215-225, (1988)
27. Penners, N.H.G., PhD thesis W.A.U., Wageningen 1985
28. vanRiemsdijk, W.H., de Wit, J.C.M., Koopal, L.K., and Bolt, G.H., Metal Ion Adsorption on Heterogeneous Surfaces: Adsorption Models, *J. Colloid Interface Sci.*, **116**, 511-522, (1987)
29. Fokkink, L.G.J., Ion adsorption on oxides, Surface charge formation and cadmium binding on rutile and hematite, PhD thesis W.A.U., Wageningen 1987
30. Madrid L., and De Arambarri P., Adsorption of phosphate by two iron oxides in relation to their porosity, *J. Soil Sci.*, **36**, 523-530, (1985)

# Summary

An important part of the reactive surface of many soils are metal (hydr)oxide surfaces. Cations and anions can adsorb specifically to the metal (hydr)oxide surface. It can be expected that metal (hydr)oxides that have different physical properties (crystal structure and porosity) also have a different chemical behaviour (ion adsorption and charging).

In the first chapter, the chemical properties of metal (hydr)oxides and the principles of modelling their chemical behaviour are explained briefly. An important property of metal (hydr)oxides is the variation of their surface charge with the pH. This variable surface charge is caused by adsorption and desorption of protons. The adsorption and desorption of protons is classically modelled with a two step protonation, a 2 p$K$ model. A new vision on the protonation of the surface is developed by Hiemstra and van Riemsdijk with their MUlti SIte Complexation (MUSIC) model. This model predicts that the $\Delta$p$K$ between the first and second proton that binds to the same surface oxygen is very large, which leads to the fact that in practice only one proton affinity constant per reactive site type is of relevance. This lead to a surface charging model in which only one protonation step is needed.
The charge of the surface causes an electrostatic potential difference between the surface and the solution. The adsorption of cat- and anions is strongly influenced by this potential difference. The description of the electrostatic potential profile depends on the choice of the interface model. So, for a good description of adsorption data, the model choice is essential. The interface models, used in this thesis all comprise a Diffuse Double Layer (DDL) in which ions are concentrated that compensate the surface charge. The interface model is often extended with one or two charge free Stern layers. The introduction of two charge free layers results in an interface with three planes. One plane is the surface plane, an intermediate plane is the border between the two charge free layers and the outer plane is the start of the DDL. In this thesis, a new approach for the interface, the Charge Distribution (CD) model is used. In this CD approach, an interface with two Stern layers (three planes) is used. In the model, the charge of adsorbing ions is divided over the two inner planes (the surface plane and the intermediate plane). For this charge distribution, a parameter $f$ is introduced that indicates the fraction of the charge of an adsorbing ion that is attributed to the surface. The CD-MUSIC model is a combination of this CD model with the MUSIC complexation model. The description of

charge distribution in inner sphere complexes in the CD-MUSIC model is an logical and consistent extension of the charge distribution as used in the MUSIC model.

In the second chapter, five surface complexation models are used to systematically compare their description of the basic charging behaviour and cation adsorption phenomena using an extended data set for proton and cadmium adsorption on goethite. The scope and limitations of the models are discussed. The models comprise different combinations of a surface complexation model and an interface model. None of the models can describe all the data satisfactory. Especially the release of protons upon cadmium adsorption appears to be a difficult phenomenon to describe accurately. The best results are obtained with a model that is a combination of a 1 pK surface complexation model and an interface model with three planes (two Stern layers). This model is able to describe the pristine charging behaviour, the pH dependency of cadmium adsorption and the salt dependency of cadmium adsorption, using 5 adjustable parameters. The predicted H/Cd exchange ratio, however, is significantly less than the observed ratio.

The CD-MUSIC model is applied to cadmium adsorption on the goehtite surface in the third chapter. In this model, the charge of an central ion of an adsorption complex is distributed over its ligands which are present in two different electrostatic planes. The adsorption of cadmium and the cadmium-proton exchange ratio were measured as function of metal ion concentration, pH and ionic strength. The data could be described well, using cadmium surface complexes that are in accordance with recent EXAFS data. EXAFS is a modern spectroscopic technique that can be used to characterise surface complexes. In the model two different crystal planes (the dominant 110 face and the minor 021 face) were used in a ratio 9:1. The fraction of 10% for the 021 plane is also used for the description of phosphate adsorption and is considered to be a material property of our goethite crystals. The only adjustable parameters for the CD-MUSIC modeling are the inner layer capacitance ($C_1$), two cadmium surface complexation constants with corresponding charge distribution factors $f$ for cadmium. The charge distribution factors $f$ can be compared with the theoretical value that results from applying the Pauling concept of equal charge distribution over the surrounding ligands. This comparison shows that the fitted $f$ values are in good accordance with the Pauling charge distribution values. The assumption that high affinity complexes occur on the 021 face was

investigated with a goethite having a different geometry, namely shorter needles compared to our goethite. The 021 face is expected to be more important for this goethite (about 20% of the surface), hence it might be expected that this goethite would have a relatively high affinity for cadmium. However, in adsorption experiments at pH 6, no significant difference in cadmium adsorption, compared to our goethite was found. The reason why this result was not found may be the presence of imperfections at the 110 face, which results in a higher relative abundance of the edge binding groups than expected from the idealized crystal morphology. The fact that both goethite samples show similar chemical behaviour suggests that a model with only one electrostatic plane should be sufficient to describe the data. To test this hypothesis, calculations were done with the high and the low cadmium affinity surface complex present on the same face. This model showed no significant difference from the model in which the high and the low cadmium surface complex were placed on separate crystal planes, where each plane developed its own surface potential.

The CD-MUSIC model is successful in describing extended data sets of cadmium adsorption and phosphate adsorption on goethite. In the fourth chapter, the parameters of these studies are combined to study the interaction between phosphate and cadmium on goehtite. With the extra information that can be obtained from the interaction experiments, the cadmium adsorption model is refined. From the model calculations it can be concluded that cadmium carbonate precipitates for high cadmium concentrations and pH values above 6. A very good description of the data is obtained with a model in which the singly coordinated surface groups at the 110 face of goethite are assumed to form both monodentate and bidentate surface species with cadmium. It is concluded that the CD-MUSIC model is able to describe data sets of both simultaneous and single adsorption of cadmium and phosphate with the same parameters. The model calculations confirmed the idea that for goethite only singly coordinated surface groups are reactive for specific ion binding.

The MUSIC model predicts the proton affinities of individual surface groups. In the model the proton affinity of a surface group is related to the number of structural bonds with underlying metal ions. In the fifth chapter, a refined MUSIC model is presented. According to the refined MUSIC model, different proton affinities ori-

ginate from differences in undersaturation of the surface oxygens due to differences in the number and length of metal bonds and hydrogen bonds. The factors valence and coordination number, which are the basis of Pauling definition of bond valence, in combination with the number of coordinating (Me and H) ions, are dominant in determining the proton affinity. The neutralization of an oxygen by Me ion(s) is calculated on the basis of the actual bond valence, which accounts for structural details, resulting from an asymmetrical distribution of charge in the coordination environment. An important role in the new version of the MUSIC model is given to the hydrogen bonds. The model shows that the proton affinity is not only determined by the number of donating hydrogen bonds but also by the number of accepting hydrogen bonds.
The proton affinity of surface groups and that of solution complexes can be understood in one theoretical framework, on the basis of a different number of donating and accepting H bonds. The MUSIC model predicts on the basis of the individual proton affinity constants the correct PZC of Me hydroxides, oxohydroxides and oxides, like gibbsite, goethite, rutile, anatase and silica and quarz.

In chapter six, the application of the refined MUSIC model, is described in more detail for three different iron (hydr)oxides (goethite, lepidocrocite and hematite). The resulting proton affinities can be combined with the crystal structure and morphology in order to describe the experimental charging curves. The charging curves are described very well for minerals with a well known (goethite) or reasonably well known (lepidocrocite) crystal morphology. For crystals of which the morphology is less well known (hematite), the refined MUSIC model can be a powerful support for a suggested morphology.

In the last chapter, five iron (hydr)oxides that differ in crystal structure and/or morphology are compared with respect to their chemical behaviour. Cadmium and phosphate adsorption and the charging behaviour are measured and modelled. For the modeling, the CD-MUSIC approach is used. It is tried to keep the models as simple as possible, with a minimum of parameters. Further it is tried to choose parameters which are in accordance with the results that are presented in chapter six. The final results are split in two parts: the first part treats three goethites that differ in crystal structure and morphology and the second part treats goethite, lepidocrocite and hematite.

The two goehtites with a high surface area but a different crystal morphology showed no difference in their chemical behaviour. This is peculiar because it was expected that these goethites would have a different surface site constitution. The goethite with a low surface area showed higher surface charging and phosphate adsorption than the other two goethites. This chemical behaviour could be described well with a higher Stern layer capacitance and a higher site density.

Investigation of the influence of model parameters on the description showed that a higher Stern layer capacitance results in a higher charging but in a lower adsorption of cadmium and in a lesser extent lower phosphate adsorption. A higher site density on the other hand hardly influences the charging behaviour but results in a higher phosphate and cadmium adsorption.

These findings are also used for the description of the data of hematite and lepidocrocite. For these two iron (oxyhydr)oxides, the crystal morphology is less well known. This means that it is not possible to determine the model parameters unequivocaly.

# Samenvatting

Een belangrijk deel van het reactieve oppervlak van de bodem bestaat uit metaal-(hydr)oxide oppervlakken. Kationen (zoals zware metalen) en anionen (zoals fosfaat of sulfaat) kunnen een chemische binding aangaan met het metaal(hydr)oxide oppervlak. Het is te verwachten dat verschillende metaal(hydr)oxiden verschillen vertonen in chemisch adsorptiegedrag.

In het eerste hoofdstuk worden de basisprincipes van het oppervlakte chemisch gedrag van metaal(hydr)oxides en de methoden die gebruikt worden om dit gedrag te modelleren uitgelegd. Een belangrijke eigenschap van metaal(hydr)oxiden is de variatie van de oppervlaktelading met de pH. Deze variabele oppervlaktelading wordt veroorzaakt door de adsorptie en desorptie van protonen. De adsorptie en desorptie van protonen wordt vaak gemodelleerd met een twee-staps protonatie (2 p$K$) model. Een nieuwe visie op protonadsorptie door metaal(hydr)oxiden is ontwikkeld door Hiemstra en van Riemsdijk met het MUliti SIte Complexation (MUSIC) model. Dit model voorspelt dat de protonaffiniteiten voor de twee protoneringsstappen ver uit elkaar liggen zodat onder normale omstandigheden, slechts één protonerings stap van belang is. Met dit model kan de variabele lading van het oppervlak met één protoneringsstap per type reactieve oppervlaktegroep worden gemodelleerd.

De oppervlaktelading veroorzaakt een elektrisch potentiaalverschil tussen het oppervlak en de oplossing. De adsorptie van kat- en anionen wordt sterk beinvloed door dit potentiaal verschil. De beschrijving van het verloop van de elektrostatische potentiaal als functie van de afstand tot het oppervlak is sterk afhankelijk van de keuze van het grensvlakmodel. Hieruit blijkt dat de keuze van het model essentieel is voor een goede beschrijving van adsorptiedata. De grensvlakmodellen, die in deze studie worden gebruikt hebben allemaal een Diffuse Dubbellaag (DDL) waarin ionen zijn geconcentreerd die de oppervlaktelading neutraliseren. Het grensvlakmodel wordt vaak uitgebreidt met één of twee ladingsvrije zones tussen het oppervlak en de DDL. In dit proefschrift wordt een model met twee ladingsvrije zones gebruikt. Door de introductie van twee ladingsvrije zones in het model ontstaan drie denkbeeldige vlakken; één vlak is het oppervlak, een tweede vlak is de scheiding tussen de eerste en de tweede ladingsvrije zone en het derde vlak is de scheiding tussen de tweede ladingvrije zone en de DDL. In dit proefschrift wordt een nieuwe benadering voor het grensvlak gebruikt, het zogenaamde ladingverdelings model

(Charge Distribution Model, CDM). In deze benadering wordt de lading van een ion, dat bindt via liganduitwisseling met oppervlaktegroepen, verdeeld over het oppervlak en het middelste vlak. Voorheen werd een ion als een puntlading beschouwd en werd de lading in zijn geheel in één van de vlakken geplaatst. In het ladingverdelings model wordt een factor *f* geïntroduceerd die de fractie van de lading aangeeft die in het oppervlak wordt geplaatst. Het ladingverdelings model van het grensvlak is gecombineerd met het MUSIC oppervlakte adsorptiemodel in het CD-MUSIC model. De beschrijving van de ladingsverdeling in een geadsorbeerd complex (een geadsorbeerd ion met omringend water of zuurstof), is een logische en consistente uitbreiding van de ladingsverdeling zoals die in het MUSIC model wordt gehanteerd.

In het tweede hoofdstuk worden vijf verschillende gangbare modellen gebruikt om een systematische vergelijking te maken tussen hun mogelijkheden om simultaan het ladingsgedrag en de adsorptie van kationen aan goethiet te kunnen beschrijven. De beperkingen en mogelijkheden van de verschillende modellen worden besproken. De modellen omvatten verschillende combinaties van een oppervlakte complexatiemodel en een grensvlakmodel. Geen van de bestaande modellen kon een bevredigende simultane beschrijving geven van de verschillende data sets. Vooral de desorptie van protonen door adsorptie van cadmium (omwisseling) geeft problemen voor de modelbeschrijvingen. De beste resultaten worden verkregen met een model met twee ladingsvrije zones en een DDL gecombineerd met het MUSIC oppervlakte complexatiemodel. Dit model is een vereenvoudigde versie van het CD-MUSIC model. Het model is in staat om simultaan het ladingsgedrag van goethiet en zowel de pH als de zoutafhankelijkheid van cadmium adsorptie aan goethiet te beschrijven met vijf aanpasbare parameters. De voorspelde proton/cadmiumomwisseling met dit model is lager dan de gevonden experimentele waarde.

In het derde hoofdstuk wordt het CD-MUSIC model toegepast op de adsorptie van cadmium aan goethiet. De lading van het geadsorbeerde cadmium ion wordt hierin verdeeld over de liganden (water moleculen en OH groepen) die het ion omringen. Voor het model komt dit neer op het verdelen van de lading over de twee binnenste vlakken. De adsorptie van cadmium en de cadmium-proton uitwisseling zijn gemeten als functie van de pH en zoutconcentratie. Deze data worden goed beschreven met adsorptiecomplexen die overeenstemmen met recente EXAFS data. EXAFS is

een moderne spectroscopische techniek die gebruikt wordt om oppervlakte complexen te karakteriseren. In het model worden twee verschillende kristalvlakken onderscheiden. De verhouding van de verschillende vlakken is in overeenstemming met de verhouding die is gebruikt voor het beschrijven van fosfaatadsorptie en wordt beschouwd als een materiaal eigenschap van onze goethietkristallen. De enige aanpasbare parameters zijn de Sternlaag capaciteit (maat voor de dikte van de ladingsvrije zone), twee cadmium affiniteiten en twee ladingverdeling factoren *f*. De ladingverdeling factoren *f* kunnen worden vergeleken met de theoretische ladingsverdeling. Deze theoretische waarden komen voort uit een theorie over ladingverdeling in kristallen die is ontwikkeld door Pauling. Deze theoretische waarden en de waarden, gevonden met het CD-MUSIC model komen goed overeen.
In het model worden oppervlaktegroepen met een hoge affiniteit voor cadmium voorondersteld op één van de kristalvlakken. Deze aanname is gecontroleerd met adsorptie metingen aan een goethiet met een andere geometrie. Een andere geometrie betekent een andere verhouding in kristalvlakken en dus een andere relatieve hoeveelheid van oppervlakte groepen met een hoge cadmium affiniteit. Dit zou betekenen dat de twee verschillende goethieten een verschillende adsorptie karakteristiek voor cadmium hebben. De metingen aan de twee verschillende goethieten lieten echter geen verschil zien. Dit resultaat doet vermoeden dat het model vereenvoudigd zou kunnen worden naar een model waarin slechts één vlak wordt gebruikt.

Het CD-MUSIC model is met succes toegepast op het beschrijven van uitgebreide datasets van zowel cadmium als fosfaat aan goethiet. In het vierde hoofdstuk worden de parameters van deze modellen verenigd om de interactie tussen cadmium en fosfaat aan goethiet te bestuderen. Met de extra informatie die verkregen wordt met de interactie experimenten is het cadmium adsorptiemodel verbeterd. Uit de berekeningen blijkt dat cadmiumcarbonaat neerslaat voor hoge cadmium concentraties en pH waarden. Een goede beschrijving van de data wordt verkregen als een extra cadmium oppervlaktecomplex wordt gebruikt. Met dit uitgebreide cadmium model wordt de beschrijving van de cadmium data, zoals besproken in hoofdstuk 3, niet slechter. De beschrijving van de cadmium fosfaat interactie met het model is zeer goed. Het CD-MUSIC model kan dus goed worden gebruikt om interactie processen bij adsorptie van verschillende ionen te beschrijven. Dit is van groot belang voor het begrijpen van processen in natuurlijke systemen.

Het MUSIC model voorspelt protonaffiniteiten van individuele oppervlakte groepen. In dit model wordt een relatie gelegd tussen het aantal bindingen met onderliggende metaal ionen en de protonaffiniteit van een oppervlakte zuurstof groep. In het vijfde hoofdstuk wordt een verbeterde versie van het MUSIC model gepresenteerd. In dit verbeterde model vinden verschillen in protonaffiniteit hun oorsprong in verschillen in onderverzadiging van de lading van oppervlaktegroepen. Deze onderverzadiging van de lading van de verschillende oppervlaktegroepen wordt weer veroorzaakt door verschillen in aantal en lengte van bindingen met onderliggende metaalionen. Vooral de valentie en het aantal bindingen (coordinatienummer), die de basis vormen voor de bindingsvalentie volgens de definities van Pauling, zijn van belang voor het bepalen van de protonaffiniteit. De neutralisatie van de valentie van een oppervlaktezuurstof wordt in het vernieuwde model berekend met de actuele bindingsvalentie. Deze actuele bindingsvalentie is gerelateerd aan de exacte kristalstructuur. Het model laat zien dat de protonaffiniteit mede wordt bepaald door interne waterstof bruggen.
De protonaffiniteiten van oppervlakte groepen en van opgeloste stoffen kan binnen een theoretisch raamwerk begrepen worden. Het verbeterde MUSIC model voorspelt op basis van de individuele protonaffiniteits constanten de correcte PZC van metaaloxiden, hydroxiden en oxohydroxiden, zoals gibbsiet, goethiet, rutiel, anatase, silica en kwarts.

In het zesde hoofdstuk, wordt de toepassing van het verbeterde MUSIC model op drie verschillende ijzer(oxohydr)oxiden in detail beschreven. De resulterende protonaffiniteiten kunnen worden gecombineerd met de kristalstructuur en morfologie om het ladingsgedrag van het materiaal te voorspellen. Voor kristallen met een goed bekende of redelijk goed bekende kristalstructuur zoals goethiet en lepidocrociet, kan het experimentele ladingsgedrag goed worden beschreven. Als de kristalstructuur minder goed bekend is, kunnen de uitkomsten van het MUSIC model, gecombineerd met experimentele ladingscurves, een ondersteuning zijn voor een vooronderstelde kristalmorfologie.

In het laatste hoofdstuk wordt het chemisch adsorptiegedrag van vijf ijzer(hydr)oxiden met een verschillende kristalstructuur en/of morfologie vergeleken. Voor de vijf verschillende (hydr)oxiden is het cadmium en fosfaat adsorptie gedrag en het ladingsgedrag gemeten en gemodelleerd. Het CD-MUSIC model is gebruikt voor de

modellering van de data. De modellen voor de verschillende oxiden zijn zo eenvoudig mogelijk gehouden met een minimum aan parameters. Daarnaast is geprobeerd om de modellen zoveel mogelijk in overeenstemming te houden met de resultaten uit hoofdstuk 6. De uiteindelijke resultaten kunnen in twee delen worden gesplitst: het eerste deel behandelt drie goethieten met een verschillende morfologie en het tweede deel behandelt lepidocrociet en hematiet.

Twee goethieten met een hoog specifiek oppervlak maar een verschillende kristalmorfologie laten geen verschil in chemisch adsorptiegedrag zien. Dit is een opvallend resultaat omdat verwacht wordt dat de twee goethieten een verschillende compositie van reactieve groepen hebben. Een goethiet met een relatief laag reactief oppervlak heeft, onder gelijke omstandigheden, een hogere oppervlaktelading en een hogere fosfaat adsorptie per $m^2$ oppervlak dan de twee goethieten met het hoge specifieke oppervlak. Dit verschil in chemisch gedrag van het goethiet met het lage specifieke oppervlak kan goed beschreven worden met een hogere Stern capaciteit en sitedichtheid.

Onderzoek naar de invloed van model parameters op de beschrijving laat zien dat een hogere Stern laag capaciteit resulteert in een hogere oppervlaktelading, maar in een lagere cadmium en, in mindere mate, lagere fosfaat adsorptie. Een hogere site dichtheid heeft daarentegen nauwelijks invloed op de oppervlaktelading maar resulteert wel in een hogere cadmium en fosfaat adsorptie.

Deze resultaten kunnen ook worden gebruikt voor het beschrijven van de data van hematiet en lepidocrociet. Voor deze twee ijzer(oxyhydr)oxiden is de kristalstructuur minder goed bekend dan van goethiet. Dit betekent dat het niet mogelijk is om de model parameters eenduidig vast te stellen aan de hand van de kristalstructuur en morfologie.

## Levensloop

Peter Venema werd geboren op 17 November 1962 te Enschede. In 1980 behaalde hij zijn HAVO diploma aan het Kottenpark College te Enschede. Vervolgens behaalde hij in 1984 het diploma Technische Natuurkunde aan de Hogere Technische School te Enschede. In 1985 begon hij met de studie Bodemkunde aan de Landbouw Universiteit Wageningen om zich meer te kunnen richten op de milieuproblematiek. Aanvankelijk lag zijn belangstelling vooral bij maatschappelijk georienteerde vakken. Na een aantal jaren kwam hij terug bij zijn oude liefde, in 1991 behaalde hij zijn bul met afstudeervakken Numerieke Wiskunde, Bodemscheikunde en Bodemvruchtbaarheid. Vanaf 1991 tot 1996 heeft hij bij de vakgroep Bodemkunde en Plantenvoeding van de Landbouwuniversiteit Wageningen gewerkt aan dit proefschrift. Vanaf januari 1997 is hij werkzaam als toegevoegd docent bij de vakgroep informatica van de Landbouwuniversiteit.